BEILSTEIN JOURNAL OF ORGANIC CHEMISTRY

Reactive intermediates – carbocations

Edited by Dean J. Tantillo and Stephanie R. Hare

Imprint

Beilstein Journal of Organic Chemistry
www.bjoc.org
ISSN 1860-5397
Email: journals-support@beilstein-institut.de

The *Beilstein Journal of Organic Chemistry* is published by the Beilstein-Institut zur Förderung der Chemischen Wissenschaften.

Beilstein-Institut zur Förderung der Chemischen Wissenschaften
Trakehner Straße 7–9
60487 Frankfurt am Main
Germany
www.beilstein-institut.de

BEILSTEIN JOURNAL OF ORGANIC CHEMISTRY

Stereochemical investigations on the biosynthesis of achiral (*Z*)-γ-bisabolene in *Cryptosporangium arvum*

Jan Rinkel and Jeroen S. Dickschat*

Letter

Open Access

Address:
Kekulé-Institute for Organic Chemistry and Biochemistry, University of Bonn, Gerhard-Domagk-Str. 1, 53121 Bonn, Germany

Email:
Jeroen S. Dickschat* - dickschat@uni-bonn.de

* Corresponding author

Keywords:
biosynthesis; carbocation chemistry; enzyme mechanisms; nerolidyl diphosphate; terpenes

Beilstein J. Org. Chem. **2019,** *15,* 789–794.
doi:10.3762/bjoc.15.75

Received: 31 January 2019
Accepted: 21 March 2019
Published: 27 March 2019

This article is part of the thematic issue "Reactive intermediates – carbocations".

Guest Editor: S. R. Hare

Abstract

A newly identified bacterial (*Z*)-γ-bisabolene synthase was used for investigating the cyclisation mechanism of the sesquiterpene. Since the stereoinformation of both chiral putative intermediates, nerolidyl diphosphate (NPP) and the bisabolyl cation, is lost during formation of the achiral product, the intriguing question of their absolute configurations was addressed by incubating both enantiomers of NPP with the recombinant enzyme, which resolved in an exclusive cyclisation of (*R*)-NPP, while (*S*)-NPP that is non-natural to the (*Z*)-γ-bisabolene synthase was specifically converted into (*E*)-β-farnesene. A hypothetical enzyme mechanistic model that explains these observations is presented.

Introduction

Given the enormous impact of chirality within biomolecules for all forms of life, it is fascinating to see how nature is able to maintain and reproduce stereochemical information. This concept largely involves the introduction of stereocentres to achiral starting materials by the action of enzymes. While reactions fulfilling this category are still challenging within synthetic chemistry, and methods managing to reach this goal are desperately desired, in the enzymatic world with its completely chiral environment these transformations are ubiquitous, which diminishes the hard border between achiral and chiral. One intriguing example for this kind of reactivity is represented by terpene synthases (TSs), arguably building up the class of natural products with the highest density of stereochemical information, the terpenes. By providing a defined cavity including its molecular coating together with binding and activation of the diphosphate (OPP) moiety, these enzymes convert simple achiral oligoprenyl diphosphates into often complex, polycyclic hydrocarbons or alcohols with introduction of multiple stereocentres in just one enzymatic step [1-3]. With this approach, nature makes perfect use of the versatile chemistry of carboca-

tions with its hydride or proton shifts and Wagner–Meerwein rearrangements leading to a large variety of possible structures. Among terpenoid natural products, achiral compounds are rarely found, but still present. In this group, there are acyclic compounds like the linear sesquiterpene (*E*)-β-farnesene (**1**, Figure 1), which is known as an alarm pheromone in aphids [4,5], but also monocyclic terpenes like α-humulene (**2**), a widely occurring sesquiterpene in many essential oils [6,7]. Whereas the stereochemical imprint of a TS on achiral products is not directly visible, there still can be a chiral cyclisation cascade behind these terpenes. This is true as well for examples featuring a mirror plane like the monoterpene 1,8-cineol (eucalyptol, **3**), for which the absolute configuration of the intermediary terpinyl cation has been investigated using deuterium labelling, demonstrating different stereochemical courses in the plant *Salvia officinalis* [8,9] and in the bacterium *Streptomyces clavuligerus* [10]. Also the highly unusual methylated sesquiterpene sodorifen (**4**) possesses a mirror plane [11] making any labelling experiment hard to interpret and is nevertheless most likely biosynthesised through chiral intermediates [12]. For these cases, it is a particular challenge to uncover the stereochemical information hidden behind the achiral product structure. In this study, we addressed the chiral intermediates in the biosynthesis of the achiral sesquiterpene (*Z*)-γ-bisabolene (**5**) by a TS from a soil bacterium.

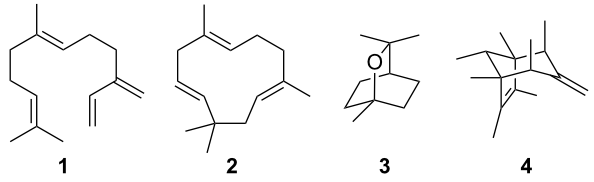

Figure 1: Structures of achiral terpenes: (*E*)-β-farnesene (**1**), α-humulene (**2**), 1,8-cineol (**3**) and sodorifen (**4**).

Results and Discussion

Functional characterisation of a bacterial (*Z*)-γ-bisabolene synthase

Within our efforts to characterise bacterial TSs with new functions and mechanisms, a TS (WP_035857999) from the soil actinomycete *Cryptosporangium arvum* DSM 44712 was cloned into the *E. coli* expression vector pYE-express [13] (Table S1, Supporting Information File 1), because of its phylogenetic distance to characterised TSs (Figure S1, Supporting Information File 1). The amino acid sequence of the enzyme features known conserved motifs both for binding [14] and activation [15] of the diphosphate moiety together with structurally important residues [16,17] (Figure S2, Supporting Information File 1). For in vitro activity testing, the enzyme was expressed in *E. coli* BL21(DE3), purified (Figure S3, Supporting Information File 1) and incubated with the common terpene precursors geranyl- (GPP, C_{10}), farnesyl- (FPP, C_{15}), geranylgeranyl- (GGPP, C_{20}) and geranylfarnesyl (GFPP, C_{25}) diphosphate. With hexane extraction and GC–MS analysis, only the incubation with FPP yielded a terpene product (Figure 2) that was isolated and identified by one- and two dimensional NMR spectroscopy (Table S2, Supporting Information File 1), EIMS databases and GC retention index as the known sesquiterpene (*Z*)-γ-bisabolene (**5**). Because the two olefinic carbon atoms of its quaternary double bond could not be unambiguously assigned from HMBC data, labelling experiments with (6-^{13}C)- and (7-^{13}C)FPP [18] were also conducted (Figure S4, Supporting Information File 1). These results characterise the TS from *C. arvum* as a (*Z*)-γ-bisabolene synthase (BbS).

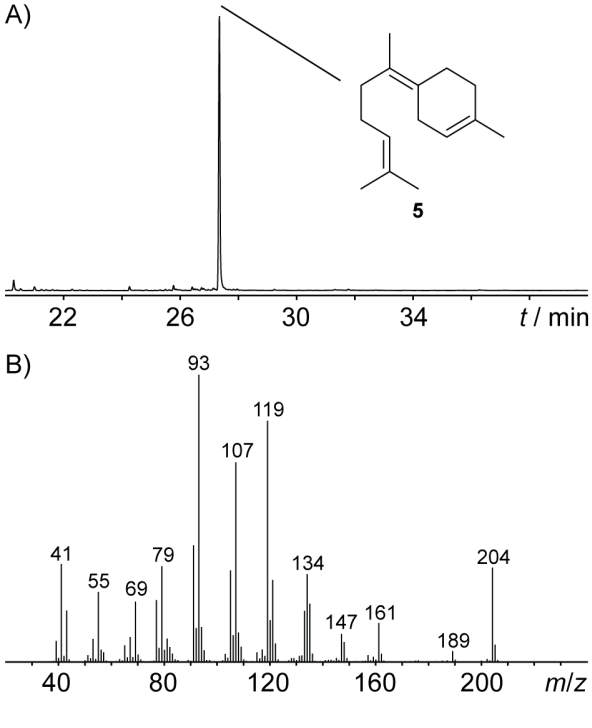

Figure 2: A) Total ion chromatogram of a hexane extract from the incubation of FPP with BbS and B) EI mass spectrum of the main product identified as (*Z*)-γ-bisabolene (**5**).

The achiral, monocyclic sesquiterpene **5** is abundant in many essential oils and was reported from different sources such as the liverwort *Dumortiera hirsuta* [19]. Its (*Z*)-configured exocyclic double bond has also attracted the attention of synthetic chemistry for a diastereoselective total synthesis [20-22]. The wide occurrence of **5** is likely connected to the simple biosynthesis from FPP featuring the common bisabolyl cation (**A**) as an intermediate after 1,6-cyclisation (Scheme 1). For this cyclisation, a formal isomerisation of the (*E*)-configured double bond in FPP to the (*Z*)-configured double bond in **A** is needed.

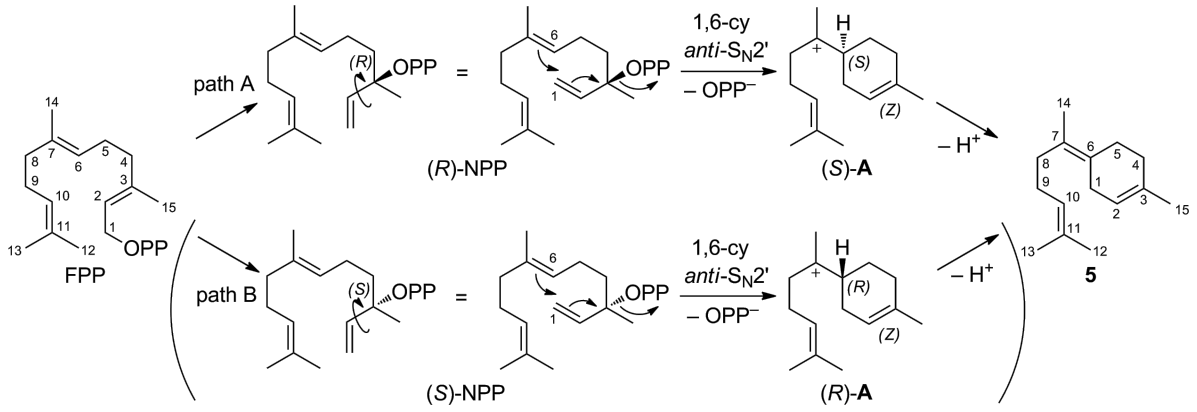

Scheme 1: Cyclisation mechanism to **5** involving either the intermediates (*R*)-NPP and (*S*)-**A** (path A) or (*S*)-NPP and (*R*)-**A** (path B). Numbering of carbons in **5** reflect their origin in FPP.

To address this problem, a 1,3-suprafacial transposition of OPP to nerolidyl diphosphate (NPP) is usually assumed [23]. This tertiary allylic diphosphate can undergo 1,6-cyclisation after a rotation around the C-2,C-3 single bond. Both NPP and **A** are chiral which raises the question of the active enantiomers in the BbS-catalysed reaction. This problem is challenging since the stereoinformation is destroyed in the final deprotonation step, which prevents any conclusion at the product stage, e.g., by use of enantioselectively labelled substrates [8-10]. If the nucleophilic attack of the C-6,C-7 double bond at the allylic system proceeds with an *anti* stereochemistry (*anti*-S_N2' reaction), which is favoured for a concerted process and is also discussed for other cyclisation mechanisms [24-26], the four theoretically possible options for the BbS cyclisation mechanism are narrowed down to two possibilities: Either the reaction takes place via (*R*)-NPP resulting in (*S*)-**A** after ring closure (Scheme 1, path A) or via (*S*)-NPP, which would suggest involvement of (*R*)-**A** (Scheme 1, path B). This stereochemical link between NPP and **A** was also observed in a theoretical docking study with *epi*-isozizaene synthase suggesting (*S*)-NPP and (*R*)-**A** to be included in its cyclisation mechanism [27].

The absolute configuration of the intermediates nerolidyl diphosphate and the bisabolyl cation

To address this question experimentally, (*R*)- and (*S*)-NPP were synthesised following a known route for enantioselective preparation of nerolidol [28] by Sharpless epoxidation of farnesol in analogy to the reported synthesis of geranyllinaloyl diphosphates [29] (Scheme S1, Supporting Information File 1). Aiming for an easy and unambiguous interpretation of the incubation experiments, the synthesised nerolidol samples (showing moderate to good ee values as judged by Mosher ester analysis of the preceeding epoxides, Figure S5, Supporting Information File 1) were purified by preparative HPLC on a chiral stationary phase to >99% ee for both samples (Figure S6, Supporting Information File 1), before converting them into the NPPs. For comparison, also racemic NPP was synthesised by a Grignard reaction of geranylacetone with vinylmagnesium bromide. The two NPP samples featuring a well-defined stereocentre, and (*rac*)-NPP, were incubated with recombinant BbS, the experiments were extracted with hexane and analysed by GC–MS (Figure 3). A selective product formation was observed for the two enantiomers of NPP, which is surprising in the light of the fact that these reactive tertiary allylic diphosphates were often found to result in a complex mixture of terpene cyclase products and Mg^{2+}-catalysed spontaneous hydrolysis products for other TSs [29,30]. While the reaction with (*R*)-NPP leads to BbS's native product **5**, for (*S*)-NPP formation of the acyclic elimination product (*E*)-β-farnesene (**1**) was observed, which was identified by EI mass spectral library and GC retention index (I = 1460 (HP-5MS), lit: I = 1459 (HP-5MS) [31]). Incubation with (*rac*)-NPP resulted in a nearly 1:1 mixture of both products, showing that both enantiomers of NPP were converted with similar efficiency.

These results clearly rule out (*S*)-NPP, but rationalise (*R*)-NPP as an intermediate in the cyclisation mechanism of BbS, and are in favour of the (*S*)-bisabolyl cation (**A**) to be deprotonated to **5** within the cascade reaction (Scheme 1, path A) [24-26], although the stereochemical link between NPP and **A** could not be demonstrated experimentally in this study. The formation of (*R*)-NPP from FPP as a 1,3-*syn*-allylic rearrangement can be rationalised in a binding mode of FPP, in which OPP is located on a defined face of the C-2,C-3-double bond by the enzyme's active site (e.g., on top of it, Figure 4A). This migration of OPP to C-3 results in a reorganisation of the resulting structure to a cisoid conformation for the follow up 1,6-ring closure. To

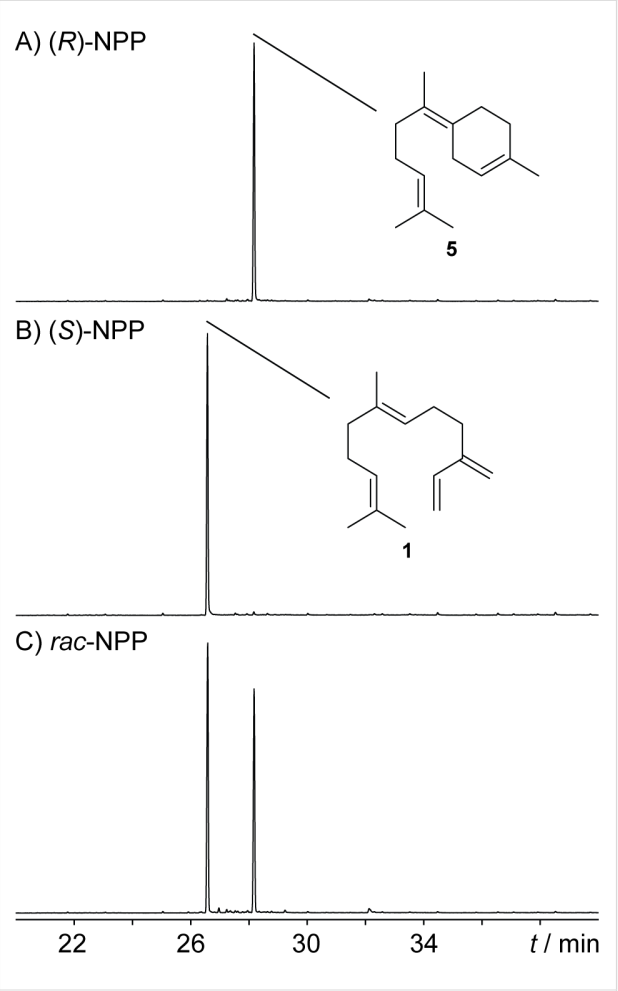

Figure 3: Total ion chromatograms of hexane extracts from incubation experiments with BbS and A) (*R*)-NPP, B) (*S*)-NPP and C) (*rac*)-NPP.

explain the astonishing selectivity between the two NPP enantiomers by BbS, different NPP conformations inside the chiral environment of the active site in BbS have to be assumed (Figure 4B + 4C). The architecture of the active site may stay the same in both cases, so a fixed OPP moiety with binding by the trinuclear Mg^{2+} cluster and a comparable folding of the isoprenoid chain in both cases is reasonable. Therefore, the two smallest substituents at the stereocentre formally change their places for the two enantiomers of NPP, representing a minor structural change of the substrate that can be tolerated in the active site. While the binding of (*R*)-NPP leads to a productive conformation that exhibits a close proximity between C-6 and C-1 for ring closure to (*S*)-**A** initiated by OPP abstraction, (*S*)-NPP cannot occupy this conformation for its different stereocentre. Instead, abstraction of the OPP moiety leads to an allylic cation with an unproductive conformation for further ring closure and is thus quenched by abstraction of a proton, presumably by participation of the diphosphate nearby, to give **1**.

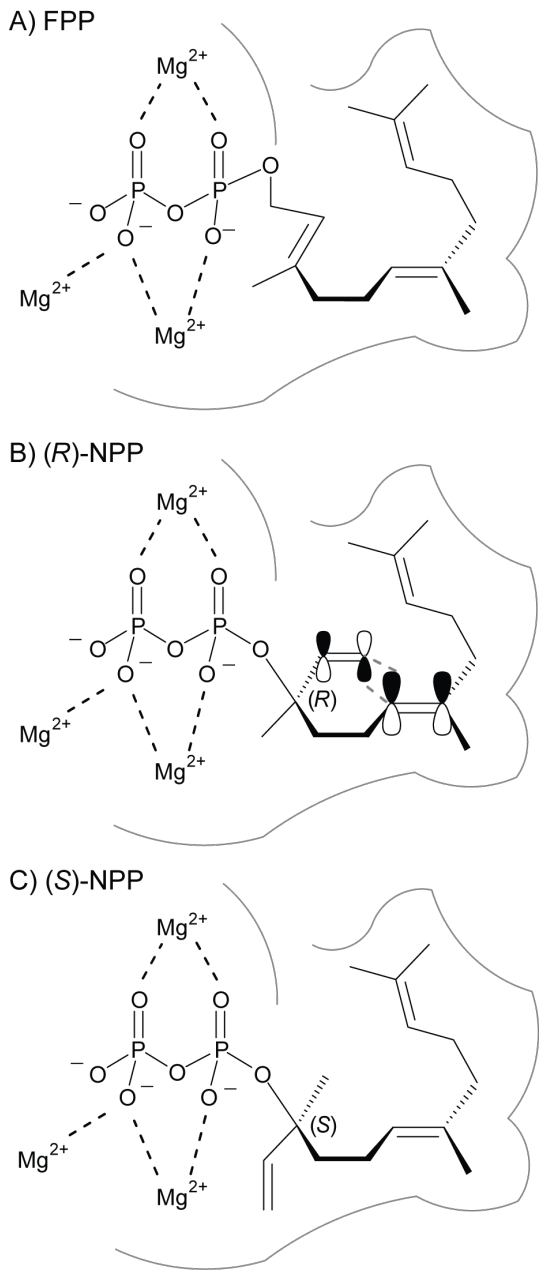

Figure 4: Hypothetical BbS active site comparable conformational folds of A) FPP, B) (*R*)- and C) (*S*)-NPP explaining the selective formation of **5** from (*R*)-NPP by ring closure via (*S*)-**A** and of **1** from (*S*)-NPP by hampering ring closure leading to elimination.

Conclusion

During the course of this work, a new TS from *C. arvum* was characterised as a (*Z*)-γ-bisabolene (**5**) synthase (BbS). Despite its monocyclic achiral structure, the biosynthesis of **5** proceeds via two chiral intermediates, NPP and the bisabolyl cation (**A**), whereas the absolute configuration of the first was addressed experimentally by the synthesis and in vitro incubation of both enantiomers of NPP. These experiments clearly showed the

involvement of (*R*)-NPP in the BbS-catalysed reaction, whereas diphosphate was selectively eliminated from (*S*)-NPP by BbS to yield **1**. The selectivity is understandable by the fixed, chiral active site architecture of BbS promoting ring closure only for (*R*)-NPP. In future studies, this experimental approach will not only provide insights into the stereochemical identity of intermediates in cases of achiral terpenes inhibiting any conclusion from the product structure as shown here, but will also deepen our knowledge of general NPP utilisation by sesquiterpene synthases. The chirality of this tertiary diphosphate is currently largely underinvestigated in the characterisation of TSs, even for cascades requiring its involvement.

Supporting Information

Experimental details of culture conditions, gene cloning, protein purification, incubation experiments, isolation of **5** and HPLC purifications, the amino acid sequence of BbS, a phylogenetic tree with the location of BbS, SDS-PAGE analysis, listed NMR data of **5**, labelling experiments for NMR assignment, synthetic procedures for the NPPs, Mosher ester analysis of epoxides, and chiral GC analysis of nerolidols.

Supporting Information File 1

Experimental part.
[https://www.beilstein-journals.org/bjoc/content/supplementary/1860-5397-15-75-S1.pdf]

Acknowledgements

This work was funded by the Deutsche Forschungsgemeinschaft (DI1536/7-1). We thank Andreas J. Schneider for HPLC purifications.

ORCID® iDs

Jeroen S. Dickschat - https://orcid.org/0000-0002-0102-0631

References

1. Christianson, D. W. *Chem. Rev.* **2017,** *117,* 11570–11648. doi:10.1021/acs.chemrev.7b00287
2. Dickschat, J. S. *Nat. Prod. Rep.* **2016,** *33,* 87–110. doi:10.1039/c5np00102a
3. Tantillo, D. J. *Angew. Chem., Int. Ed.* **2017,** *56,* 10040–10045. doi:10.1002/anie.201702363
4. Bowers, W. S.; Nault, L. R.; Webb, R. E.; Dutky, S. R. *Science* **1972,** *177,* 1121–1122. doi:10.1126/science.177.4054.1121
5. Gibson, R. W.; Pickett, J. A. *Nature* **1983,** *302,* 608–609. doi:10.1038/302608a0
6. Katsiotis, S. T.; Langezaal, C. R.; Scheffer, J. J. C. *Planta Med.* **1989,** *55,* 634. doi:10.1055/s-2006-962205
7. Bouajaj, S.; Benyamna, A.; Bouamama, H.; Romane, A.; Falconieri, D.; Piras, A.; Marongiu, B. *Nat. Prod. Res.* **2013,** *27,* 1673–1676. doi:10.1080/14786419.2012.751600
8. Wise, M. L.; Savage, T. J.; Katahira, E.; Croteau, R. *J. Biol. Chem.* **1998,** *273,* 14891–14899. doi:10.1074/jbc.273.24.14891
9. Wise, M. L.; Urbansky, M.; Helms, G. L.; Coates, R. M.; Croteau, R. *J. Am. Chem. Soc.* **2002,** *124,* 8546–8547. doi:10.1021/ja0265714
10. Rinkel, J.; Rabe, P.; zur Horst, L.; Dickschat, J. S. *Beilstein J. Org. Chem.* **2016,** *12,* 2317–2324. doi:10.3762/bjoc.12.225
11. von Reuß, S. H.; Kai, M.; Piechulla, B.; Francke, W. *Angew. Chem., Int. Ed.* **2010,** *49,* 2009–2010. doi:10.1002/anie.200905680
12. von Reuss, S.; Domik, D.; Lemfack, M. C.; Magnus, N.; Kai, M.; Weise, T.; Piechulla, B. *J. Am. Chem. Soc.* **2018,** *140,* 11855–11862. doi:10.1021/jacs.8b08510
13. Dickschat, J. S.; Pahirulzaman, K. A. K.; Rabe, P.; Klapschinski, T. A. *ChemBioChem* **2014,** *15,* 810–814. doi:10.1002/cbic.201300763
14. Christianson, D. W. *Chem. Rev.* **2006,** *106,* 3412–3442. doi:10.1021/cr050286w
15. Baer, P.; Rabe, P.; Fischer, K.; Citron, C. A.; Klapschinski, T. A.; Groll, M.; Dickschat, J. S. *Angew. Chem., Int. Ed.* **2014,** *53,* 7652–7656. doi:10.1002/anie.201403648
16. Rinkel, J.; Lauterbach, L.; Dickschat, J. S. *Angew. Chem., Int. Ed.* **2017,** *56,* 16385–16389. doi:10.1002/anie.201711142
17. Rinkel, J.; Lauterbach, L.; Rabe, P.; Dickschat, J. S. *Angew. Chem., Int. Ed.* **2018,** *57,* 3238–3241. doi:10.1002/anie.201800385
18. Rabe, P.; Barra, L.; Rinkel, J.; Riclea, R.; Citron, C. A.; Klapschinski, T. A.; Janusko, A.; Dickschat, J. S. *Angew. Chem., Int. Ed.* **2015,** *54,* 13448–13451. doi:10.1002/anie.201507615
19. Saritas, Y.; Bülow, N.; Fricke, C.; König, W. A.; Muhle, H. *Phytochemistry* **1998,** *48,* 1019–1023. doi:10.1016/s0031-9422(97)00484-6
20. Anastasia, L.; Dumond, Y. R.; Negishi, E.-i. *Eur. J. Org. Chem.* **2001,** 3039–3043. doi:10.1002/1099-0690(200108)2001:16<3039::aid-ejoc3039>3.0.co;2-v
21. Wolinsky, L. E.; Faulkner, D. J.; Finer, J.; Clardy, J. *J. Org. Chem.* **1976,** *41,* 697–699. doi:10.1021/jo00866a023
22. Corey, E. J.; Seibel, W. L. *Tetrahedron Lett.* **1986,** *27,* 909–910. doi:10.1016/s0040-4039(00)84134-9
23. Arigoni, D. *Pure Appl. Chem.* **1975,** *41,* 219–245. doi:10.1351/pac197541010219
24. Rinkel, J.; Rabe, P.; Garbeva, P.; Dickschat, J. S. *Angew. Chem., Int. Ed.* **2016,** *55,* 13593–13596. doi:10.1002/anie.201608042
25. Cane, D. E.; Tandon, M. *J. Am. Chem. Soc.* **1995,** *117,* 5602–5603. doi:10.1021/ja00125a029
26. Hu, Y.; Chou, W. K. W.; Hopson, R.; Cane, D. E. *Chem. Biol.* **2011,** *18,* 32–37. doi:10.1016/j.chembiol.2010.11.008
27. Pemberton, R. P.; Ho, K. C.; Tantillo, D. J. *Chem. Sci.* **2015,** *6,* 2347–2353. doi:10.1039/c4sc03782k
28. Le, T. C.; Chauhan, K. R. *Nat. Prod. Commun.* **2014,** *9,* 297–298.
29. Rinkel, J.; Rabe, P.; Chen, X.; Köllner, T. G.; Chen, F.; Dickschat, J. S. *Chem. – Eur. J.* **2017,** *23,* 10501–10505. doi:10.1002/chem.201702704
30. Benedict, C. R.; Lu, J. L.; Pettigrew, D. W.; Liu, J.; Stipanovic, R. D.; Williams, H. J. *Plant Physiol.* **2001,** *125,* 1754–1765. doi:10.1104/pp.125.4.1754

31. Asuming, W. A.; Beauchamp, P. S.; Descalzo, J. T.; Dev, B. C.; Dev, V.; Frost, S.; Ma, C. W. *Biochem. Syst. Ecol.* **2005,** *33,* 17–26. doi:10.1016/j.bse.2004.06.005

License and Terms

BEILSTEIN JOURNAL OF ORGANIC CHEMISTRY

Enantioselective Diels–Alder reaction of anthracene by chiral tritylium catalysis

Qichao Zhang[1], Jian Lv*[1,2] and Sanzhong Luo*[1,3]

Full Research Paper

Open Access

Address:
[1]Key Laboratory of Molecular Recognition and Function, Institute of Chemistry, Chinese Academy of Sciences, 100190, Beijing, China, [2]State Key Laboratory Base of Eco-Chemical Engineering, College of Chemistry and Molecular Engineering, Qingdao University of Science & Technology, 266042, Qingdao, China and [3]Center of Basic Molecular Science (CBMS), Department of Chemistry, Tsinghua University, 100084, Beijing, China

Email:
Jian Lv* - lvjian@iccas.ac.cn; Sanzhong Luo* - luosz@tsinghua.edu.cn

* Corresponding author

Keywords:
anthracene; carbocation catalysis; Diels–Alder reaction; Fe(III)-based phosphate anion; tritylium salt

Beilstein J. Org. Chem. **2019,** *15,* 1304–1312.
doi:10.3762/bjoc.15.129

Received: 12 February 2019
Accepted: 24 May 2019
Published: 14 June 2019

This article is part of the thematic issue "Reactive intermediates – carbocations".

Guest Editor: S. R. Hare

Abstract

The combination of the trityl cation and a chiral weakly coordinating Fe(III)-based bisphosphate anion was used to develop a new type of a highly active carbocation Lewis acid catalyst. The stereocontrol potential of the chiral tritylium ion pair was demonstrated by its application in an enantioselective Diels–Alder reaction of anthracene.

Introduction

Carbocation Lewis acid catalysis has grown significantly over the last two decades [1-13]. The development of asymmetric carbocation catalysts has been long pursued but remains a challenging task. One strategy is to design and synthesize stabilized chiral carbocations with chirality installed onto their backbones. Pioneering efforts along this line by Kagan, Sammakia, and Chen have shown that chiral catalysis with such chiral carbocations was indeed plausible to achieve stereocontrol (Scheme 1a). [14-19]. However, the enantioselectivity was low in most cases. In addition, the synthetic efforts to access these chiral cations were generally non-trivial which limited their further development. Recently, we developed a chiral ion-pair strategy for asymmetric carbocation catalysis, with chiral trityl phosphate as the carbocation precursor [20,21]. In this latent strategy, the carbocation precursor can undergo facile ionic dissociation upon mild external stimulation such as polar substrates (such as α-ketoesters) to form a catalytically active chiral ion pair for substrate activation and chiral induction (Scheme 1b). In our further explorations, we noticed that the dissociation of trityl phosphate was generally sluggish, thus

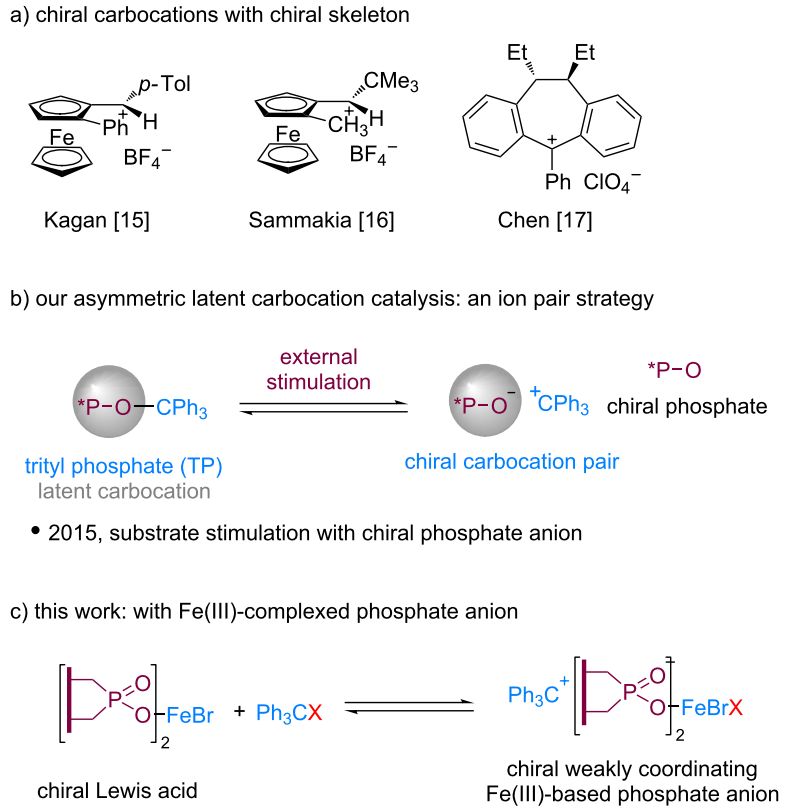

Scheme 1: Asymmetric carbocation catalysis.

limiting its applicability. To expand its utility, we report herein a metal-complexed phosphate anion for chiral carbocation catalysis.

Weakly coordinating anions [22,23] have been widely used in inorganic and organic chemistry [24-27] as well as in polymer chemistry [28-33]. Although tritylium salts with various types of these counter anions based on B(III), Al(III), Ga(III), Fe(III), Nb(III), Ta(III), Y(III) and La(III) centers and ligands have been investigated in Lewis acid catalysis over the past decades, a chiral counter anion [34,35] with metal elements as the central atom, however, was seldom reported. Typically, the tritylium salts with weakly coordinating anions can be synthesized through a simple halide abstraction from the trityl halide in the presence of strong Lewis acids [36]. We herein report the design and exploration of a new trityl carbocation that has a chiral weakly coordinating Fe(III)-based phosphate anion for the effective asymmetric catalysis in the Diels–Alder reaction of anthracenes.

Results and Discussion

In our previous work, we found that less than 6% of trityl phosphate (TP) dissociated to trityl cations in the presence of a polar substrate such trifluoropyruvate [20]. In order to improve the efficiency of the dissociation, we started by first studying the properties of tritylium salts with a weakly coordinating metal-based phosphate anion (Scheme 2). Upon in situ mixing the chiral trityl phosphate (**TP**, 0.05 mM) and different Lewis acids (0.05 mM), such as $InCl_3$, $InBr_3$, InI_3, $In(OTf)_3$, $Sc(OTf)_3$, $Hf(OTf)_3$, $GaCl_3$, and $FeBr_3$, the originally colorless solution of the chiral trityl phosphate **TP** turned orange, suggesting the formation of tritylium ions (Scheme 2a). The stimulated trityl cation generation was probed by UV–vis spectroscopy. As shown in Figure 1a, when treated with different Lewis acids, trityl phosphate **TP** showed a variable tendency to dissociate into the free tritylium ion pair with $InBr_3$ as the most active Lewis acid. An estimation based on UV absorption showed that approximately 76% of **TP** dissociated into trityl cations in the presence of $InBr_3$. On the other hand, tritylium salts with a weakly coordinating metal-based monophosphate or bisphosphate anion could also be obtained when trityl bromide was treated with the corresponding metal phosphate, which can be prepared in situ following our previously described procedure (Scheme 2b,c) [37,38]. UV analysis indicated that the indium salt **1a** or gallium salt **1b** (0.05 mM) could induce ca. 92% dissociation of trityl bromide (0.05 mM) to generate the trityl cation. Also, $FeBr_3$, a chiral Fe(III) monophosphate (M = $FeBr_2$) **1c** or even the bulky Fe(III) bisphosphate **2a**

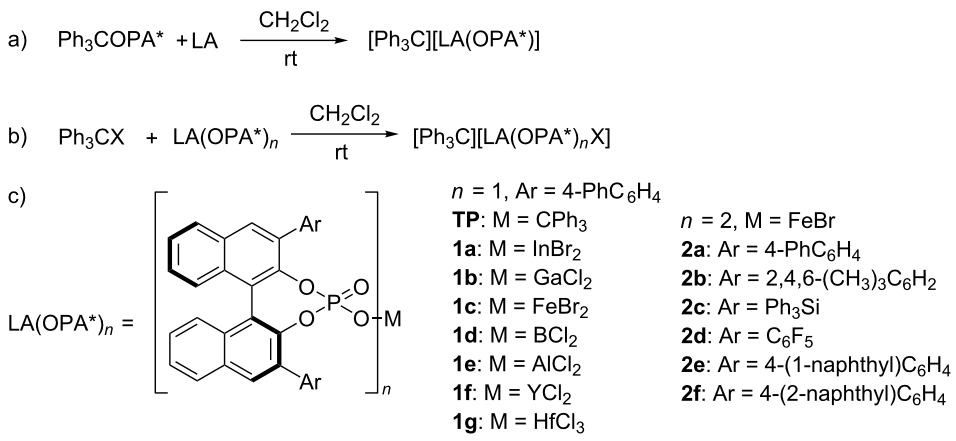

Scheme 2: Synthesis of new carbocation catalysts with weakly coordinating metal-based phosphate anion.

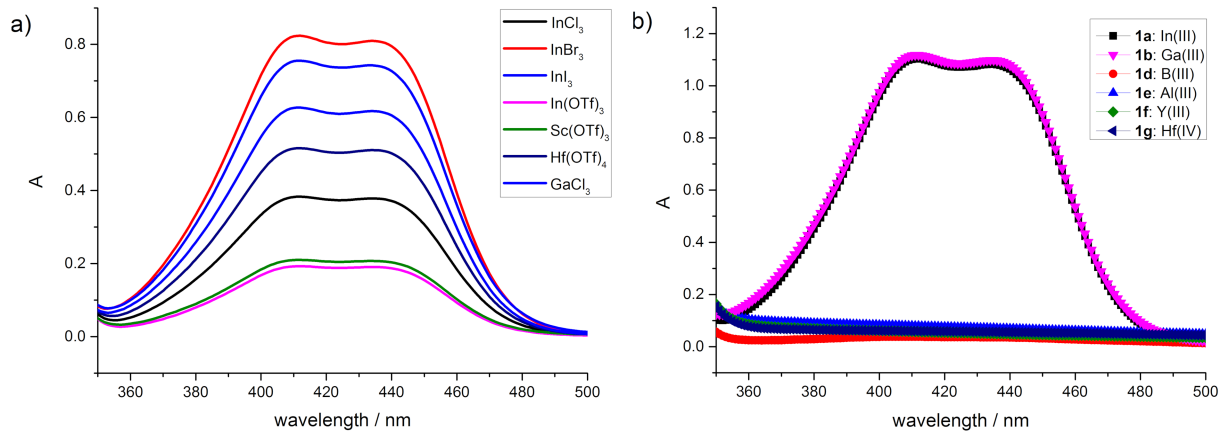

Figure 1: Dissociation of latent carbocation by the use of Lewis acids. a) UV–vis absorption spectra of **TP** (0.05 mM) upon the addition of Lewis acids (0.05 mM), such as $InCl_3$, $InBr_3$, InI_3, $In(OTf)_3$, $Sc(OTf)_3$, $Hf(OTf)_4$, and $GaCl_3$. b) UV–vis absorption spectra of trityl bromide (Ph_3CBr, 0.05 mM) upon the addition of the chiral Lewis acids (0.05 mM), such as **1a**, **b**, and **d**–**g**.

promoted the dissociation of trityl bromide. In the latter case, the dissociation was estimated to be 54% by in-situ IR spectroscopy (UV–vis spectra were not applicable due to absorption overlap; see Supporting Information File 1 for details).

We next tested the metal phosphate strategy in the Diels–Alder reaction of anthracene, for which a catalytic asymmetric version has not been achieved yet. Recently, we reported that the tritylium salt [Ph_3C][BArF], in situ generated by Ph_3CBr and NaBArF, could promote the Diels–Alder reaction with anthracenes and various unsaturated carbonyl compounds under mild conditions [13]. The use of latent carbocation catalysis with **TP** was examined in order to achieve enantioselective control. To our delight, **TP** catalyzed the asymmetric reaction affording cycloadduct **5a** in excellent enantioselectivity (97% ee), however, with only 9% yield (Table 1, entry 1). Subsequent efforts to improve the activity by enhancing the dissociation efficiency of latent carbocation through heating or photolysis did not lead to any improvement. We next investigated whether the tritylium salts with a chiral weakly coordinating metal-based phosphate anion could facilitate the asymmetric catalytic Diels–Alder reaction. To implement this strategy, different trityl phosphates or halides, Lewis acids, chiral metal phosphate and their combinations were examined in the model reaction of anthracene (**3a**) and β,γ-unsaturated α-ketoester **4a**. When **TP** was first treated with metal Lewis acid (Scheme 2a, and Table S1 in Supporting Information File 1), the reaction showed good reactivity but no enantioselectivity at all, indicating a strong background reaction (Table 1, entry 2). We next examined the second strategy in which trityl bromide was treated with preformed chiral metal phosphate to their equilibration before they were subjected to the catalytic test. When metal monophosphates **1a–c** (Table 1, entries 3–5) were applied, the reaction started showing some enantioselectivity with decent

Table 1: Screening and optimization for the asymmetric catalyzed Diels–Alder reaction of anthracene by carbocations.

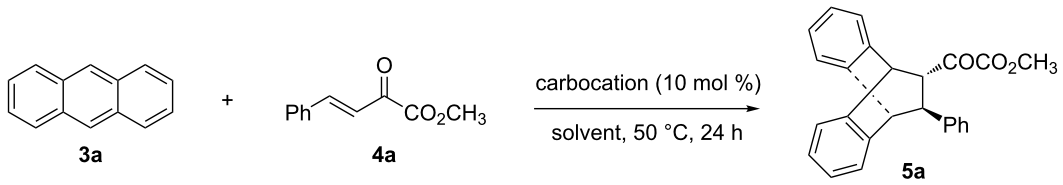

entry[a]	carbocation		solvent	yield (%)[b]	ee[c]
	TrX	Lewis acid			
1	**TP**	none	DCE	9	97
metal-based monophosphate anion					
2	**TP**	$InBr_3$	DCE	94	rac
3	Ph_3CBr	**1a**	DCE	55	14
4	Ph_3CBr	**1b**	DCE	49	−16
5	Ph_3CBr	**1c**	DCE	79	36
Fe(III)-based bisphosphate anion					
6	Ph_3CBr	**2a**	DCE	46	40
7	Ph_3CBr	**2a**	DCM	58	56
8	Ph_3CBr	**2a**	$CHCl_3$	36	42
9	Ph_3CBr	**2a**	toluene	20	46
10	Ph_3CBr	**2a**	CH_3CN	nr	–
11	Ph_3CBr	**2b**	DCM	17	14
12	Ph_3CBr	**2c**	DCM	55	28
13	Ph_3CBr	**2d**	DCM	67	26
14	Ph_3CBr	**2e**	DCM	22	68
15	Ph_3CBr	**2f**	DCM	70	74
16[d]	Ph_3CBr	**2f**	DCM	55	90
17[d]	Ph_3CCl	**2f**	DCM	57	91
18[d,e]	Ph_3CCl	**2f**	DCM	70	91
19[d]	none	**2f**	DCM	nr	–
20[d]	Ph_3CCl	none	DCM	nr	–

[a]General conditions: **3a** (0.4 mmol), **4a** (0.2 mmol), TrX (10 mol %), and Lewis acid (10 mol %) in 2 mL solvent at 50 °C. [b]Yield of isolated product. [c]Determined by HPLC analysis on a chiral stationary phase. [d]Room temperature. [e]48 h.

activity maintained. The combined use of trityl bromide and **1a** (10 mol %) led to the desired adduct **5a** with 55% yield and in 14% ee at 50 °C (Table 1, entry 3). This is in contrast to the **TP**/$InBr_3$ combination where the reaction was much faster but racemic (Table 1, entry 3 vs 2), suggesting that the preformed metal phosphate is critical to effect catalysis and chiral induction. Among the metals screened, Fe(III) phosphate gave the optimal results in terms of both activity and enantioselectivity (79% yield, 35% ee, Table 1, entry 5). Fe(III)-based bisphosphate anions were also tested. To our delight, when trityl bromide and **2a** (10 mol %) were used, the reaction gave a slightly increased enantioselectivity (Table 1, entry 6). Further improvement on activity and enantioselectivity could be achieved by conducting the reaction in DCM as the solvent (Table 1, entries 7 vs 6, 8–10). Next, we screened different chiral Fe(III) bisphosphates **2a**–**f** and the best results were obtained in the presence of **2f**, whereas others resulted in either low activity or poor enantioselectivity (Table 1, entries 15 vs 7, 11–14). Eventually, trityl chloride and chiral Fe(III) bisphosphate **2f** were identified to be the optimal combination, affording adduct **5a** in 91% ee and 70% yield at room temperature (Table 1, entries 17 and 18).

In a control experiment, we found that chiral iron salt **2f** itself turned out to be ineffective to catalyze the reaction in the absence of trityl chloride (Table 1, entry 19), indicating that the reaction is catalyzed by tritylium salts with Fe(III)-complexed bisphosphate as the chirality-inducing anion.

With the optimal reactions conditions established, the scope was next explored with Ph_3CCl/**2f** in CH_2Cl_2 (DCM) at room temperature and the results are presented in Table 2. A variety of β,γ-unsaturated α-ketoesters **4** was subjected to the reaction

Table 2: Scope for the asymmetric catalyzed Diels–Alder reaction of anthracene (**3a**) with ketoesters **4** by carbocations.

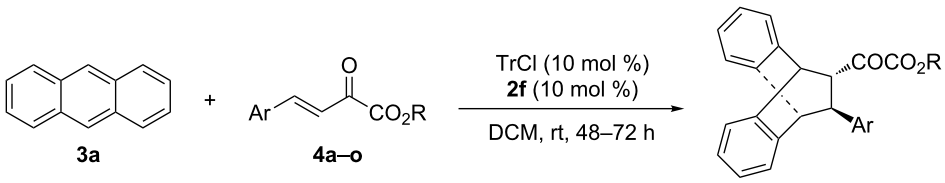

3a **4a–o** **5a–o**

entry[a]	α-ketoesters	product	yield (%)[b]	ee (%)[c]
1	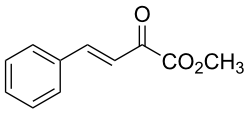 **4a**	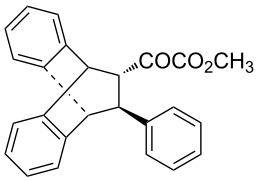 **5a**	70	91
2	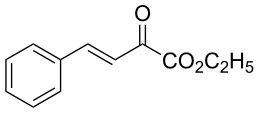 **4b**	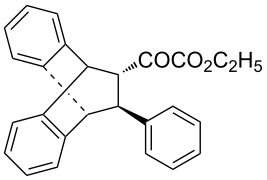 **5b**	82	74
3	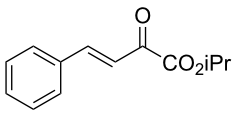 **4c**	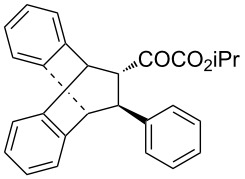 **5c**	46	55
4	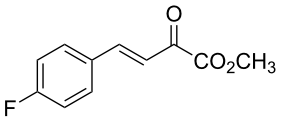 **4d**	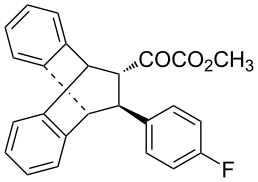 **5d**	74	80
5	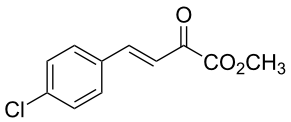 **4e**	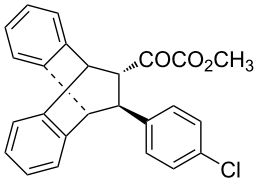 **5e**	68	75
6	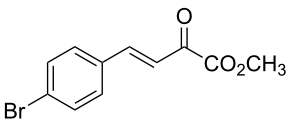 **4f**	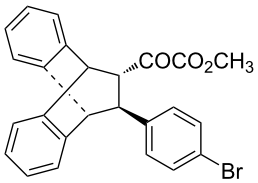 **5f**	66	81

Table 2: Scope for the asymmetric catalyzed Diels–Alder reaction of anthracene (**3a**) with ketoesters **4** by carbocations. (continued)

7	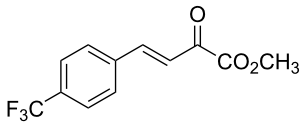 **4g**	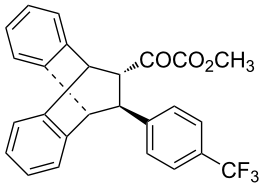 **5g**	77	76
8	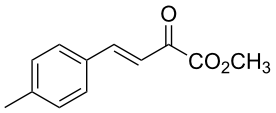 **4h**	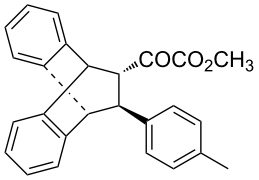 **5h**	48	80
9	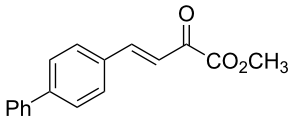 **4i**	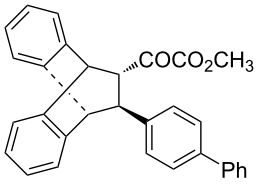 **5i**	68	93
10	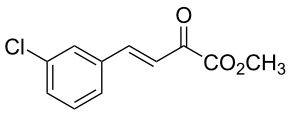 **4j**	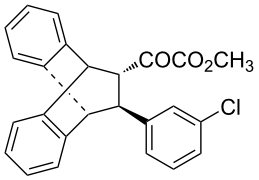 **5j**	92	91
11	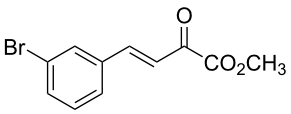 **4k**	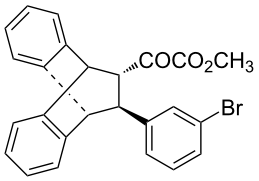 **5k**	86	87
12	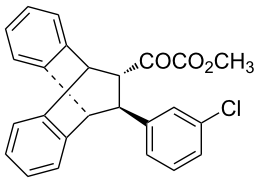 **4l**	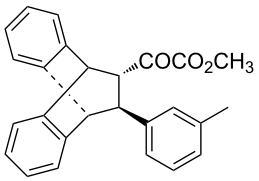 **5l**	76	89
13	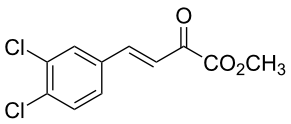 **4m**	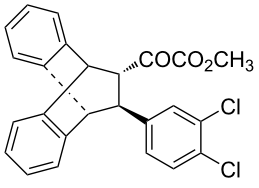 **5m**	85	73

Table 2: Scope for the asymmetric catalyzed Diels–Alder reaction of anthracene (**3a**) with ketoesters **4** by carbocations. (continued)

14	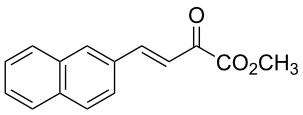 **4n**	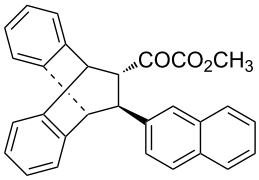 **5n**	42	83

[a]General conditions: **3a** (0.4 mmol), **4** (0.2 mmol), TrCl (10 mol %), and **2a** (10 mol %) in DCM (2 mL) at room temperature. [b]Yield of isolated product. [c]Determined by HPLC analysis on a chiral stationary phase.

with anthracene (**3a**) to give the desired cycloadducts **5a**–**n** in moderate to good yields and with up to 93% ee. The bulkier isopropyl ketoester resulted in a lower yield and enantioselectivity (Table 2, entry 3 vs 1 and 2). Variations on the aromatic group of the ketoesters were well tolerated, giving the products in decent yields and high enantioselectivities. Unfortunately, no reaction was observed when an aliphatic substituted β,γ-unsaturated α-ketoester was used (data not shown).

The Diels–Alder reaction of substituted anthracenes has been well-developed and we next examined the scope with substituted anthracenes. Unfortunately, these well-explored substrates did not work in our chiral catalysis system giving either no activity or poor enantioselectivity, particularly in cases of 9-monosubstituted anthracenes. When 9,10-dimethylanthracene (**3b**) was used, the reaction showed high yield (93% for **5o**) but low enantioselectivity (23% ee, Scheme 3a). Surprisingly, the chiral iron salt **2f** itself in the absence of trityl chloride also promoted the reaction, showing a relatively lower activity with 85% yield of **5o** but opposite chiral induction (−65% ee, Scheme 3a). The electron-rich nature of dimethylanthracene may account for catalysis with the iron salts. On the other hand, an opposite chiral induction in this case is a clear indication of distinctive carbocation catalysis instead of metal Lewis acid catalysis in the presence of trityl chloride.

In addition, we tested the current carbocation catalytic system to prepare cycloadduct **5k** in a large scale (Scheme 3b). When

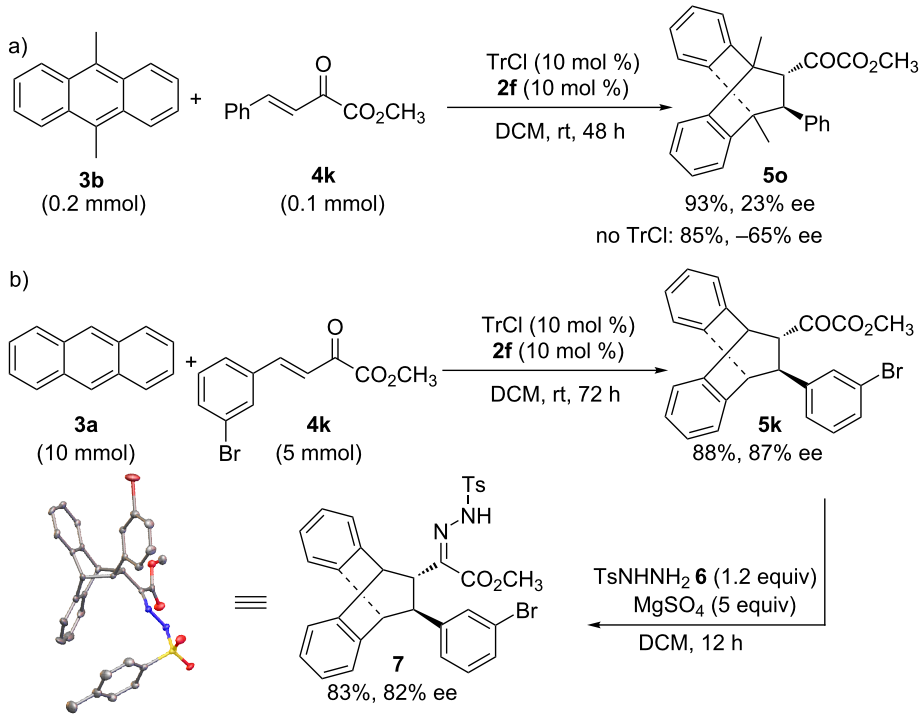

Scheme 3: a) The reaction with 9,10-dimethylanthracene (**3b**). b) Gram-scale reaction of **3a** and **4k**, and transformation of cycloadduct **5k**.

using 10 mol % Ph_3CCl/**2f**, the reaction afforded cycloadduct **5k** in 88% yield of isolated product and with 87% ee. In the presence of $MgSO_4$ (5 equiv), treatment of **5k** (1 equiv) with sulfonylhydrazine **6** (1.2 equiv) in CH_2Cl_2 led to the desired *N*-tosylhydrazone **7** in 83% yield and with 82% ee (Scheme 3b). The absolute configuration was assigned on the basis of the structure of **7**, which was confirmed unambiguously by an X-ray crystallographic study [39]. Tentative transition states to account for the observed stereoselectivity are provided in Supporting Information File 1, Figure S3.

Conclusion

In summary, we have introduced a new motif of chiral weakly coordinating Fe(III)-based bisphosphate anion for high performance asymmetric carbocation Lewis acid catalysis. The introduction of a metal-coordinated phosphonate anion with balanced association ability with tritylium ions provided a new opportunity in pursuing chiral ion pair-type carbocation catalysis. The resulted asymmetric tritylium catalysis has enabled the so-far challenging Diels–Alder reactions of unsubstituted anthracene with good activity and up to 93% ee. Further studies are currently underway to elucidate the mechanistic details and to extend the chiral tritylium salt catalysis to other reactions.

Supporting Information

Supporting Information File 1

Experimental procedures and characterization data of all products, copies of ^1H and ^{13}C NMR, IR, HRMS, and HPLC spectra of all compounds.
[https://www.beilstein-journals.org/bjoc/content/supplementary/1860-5397-15-129-S1.pdf]

Acknowledgements

We thank the Natural Science Foundation of China (21390400, 21521002, 21472193) and the Chinese Academy of Sciences (QYZDJ-SSW-SLU023) for financial support. S.L. is supported by the National Program of Top-notch Yong Professionals, and J. L. is supported by the Taishan Scholarship Project of Shandong Province.

ORCID® iDs

Jian Lv - https://orcid.org/0000-0001-7641-5411
Sanzhong Luo - https://orcid.org/0000-0001-8714-4047

References

1. Mukaiyama, T.; Kobayashi, S.; Shoda, S.-i. *Chem. Lett.* **1984,** *13,* 907–910. doi:10.1246/cl.1984.907
2. Mukaiyama, T.; Kobayashi, S.; Murakami, M. *Chem. Lett.* **1985,** *14,* 447–450. doi:10.1246/cl.1985.447
3. Kobayashi, S.; Matsui, S.; Mukaiyama, T. *Chem. Lett.* **1988,** *17,* 1491–1494. doi:10.1246/cl.1988.1491
4. Yanagisawa, M.; Mukaiyama, T. *Chem. Lett.* **2001,** *30,* 224–225. doi:10.1246/cl.2001.224
5. Roy, S. R.; Nijamudheen, A.; Pariyar, A.; Ghosh, A.; Vardhanapu, P. K.; Mandal, P. K.; Mandal, P. K.; Datta, A.; Mandal, S. K. *ACS Catal.* **2014,** *4,* 4307–4319. doi:10.1021/cs5010695
6. Bah, J.; Franzén, J. *Chem. – Eur. J.* **2014,** *20,* 1066–1072. doi:10.1002/chem.201304160
7. Bah, J.; Naidu, V. R.; Teske, J.; Franzén, J. *Adv. Synth. Catal.* **2015,** *357,* 148–158. doi:10.1002/adsc.201400609
8. Naidu, V. R.; Ni, S.; Franzén, J. *ChemCatChem* **2015,** *7,* 1896–1905. doi:10.1002/cctc.201500225
9. Moosavi-Zare, A. R.; Zolfigol, M. A.; Rezanejad, Z. *Can. J. Chem.* **2016,** *94,* 626–630. doi:10.1139/cjc-2015-0629
10. Zhang, Q.; Lü, J.; Luo, S. *Acta Chim. Sin. (Chin. Ed.)* **2016,** *74,* 61–66. doi:10.6023/a15090587
11. Lyons, D. J. M.; Crocker, R. D.; Enders, D.; Nguyen, T. V. *Green Chem.* **2017,** *19,* 3993–3996. doi:10.1039/c7gc01519d
12. Liu, J.; Xu, J.; Li, Z.; Huang, Y.; Wang, H.; Gao, Y.; Guo, T.; Ouyang, P.; Guo, K. *Eur. J. Org. Chem.* **2017,** 3996–4003. doi:10.1002/ejoc.201700634
13. Zhang, Q.; Lv, J.; Li, S.; Luo, S. *Org. Lett.* **2018,** *20,* 2269–2272. doi:10.1021/acs.orglett.8b00619
14. Riant, O.; Samuel, O.; Kagan, H. B. *J. Am. Chem. Soc.* **1993,** *115,* 5835–5836. doi:10.1021/ja00066a066
15. Taudien, S.; Riant, O.; Kagan, H. B. *Tetrahedron Lett.* **1995,** *36,* 3513–3516. doi:10.1016/0040-4039(95)00531-g
16. Sammakia, T.; Latham, H. A. *Tetrahedron Lett.* **1995,** *36,* 6867–6870. doi:10.1016/0040-4039(95)01440-s
17. Chen, C.-T.; Chao, S.-D.; Yen, K.-C.; Chen, C.-H.; Chou, I.-C.; Hon, S.-W. *J. Am. Chem. Soc.* **1997,** *119,* 11341–11342. doi:10.1021/ja970900o
18. Magdziak, D.; Pettus, L. H.; Pettus, T. R. R. *Org. Lett.* **2001,** *3,* 557–559. doi:10.1021/ol006963k
19. Pommerening, P.; Mohr, J.; Friebel, J.; Oestreich, M. *Eur. J. Org. Chem.* **2017,** 2312–2316. doi:10.1002/ejoc.201700239
20. Lv, J.; Zhang, Q.; Zhong, X.; Luo, S. *J. Am. Chem. Soc.* **2015,** *137,* 15576–15583. doi:10.1021/jacs.5b11085
21. Ni, S.; Ramesh Naidu, V.; Franzén, J. *Eur. J. Org. Chem.* **2016,** 1708–1713. doi:10.1002/ejoc.201501621
22. Krossing, I.; Raabe, I. *Angew. Chem., Int. Ed.* **2004,** *43,* 2066–2090. doi:10.1002/anie.200300620
23. Strauss, S. H. *Chem. Rev.* **1993,** *93,* 927–942. doi:10.1021/cr00019a005
24. Moss, S.; King, B. T.; de Meijere, A.; Kozhushkov, S. I.; Eaton, P. E.; Michl, J. *Org. Lett.* **2001,** *3,* 2375–2377. doi:10.1021/ol0161864
25. Anderson, L. L.; Arnold, J.; Bergman, R. G. *J. Am. Chem. Soc.* **2005,** *127,* 14542–14543. doi:10.1021/ja053700i
26. Nguyen, T.-T.-T.; Türp, D.; Wagner, M.; Müllen, K. *Angew. Chem., Int. Ed.* **2013,** *52,* 669–673. doi:10.1002/anie.201206010
27. Fischer, S.; Schmidt, J.; Strauch, P.; Thomas, A. *Angew. Chem., Int. Ed.* **2013,** *52,* 12174–12178. doi:10.1002/anie.201303045
28. Roberts, J. A. S.; Chen, M.-C.; Seyam, A. M.; Li, L.; Zuccaccia, C.; Stahl, N. G.; Marks, T. J. *J. Am. Chem. Soc.* **2007,** *129,* 12713–12733. doi:10.1021/ja0680360

29. Chen, M.-C.; Roberts, J. A. S.; Seyam, A. M.; Li, L.; Zuccaccia, C.; Stahl, N. G.; Marks, T. J. *Organometallics* **2006,** *25,* 2833–2850. doi:10.1021/om0508334
30. Metz, M. V.; Sun, Y.; Stern, C. L.; Marks, T. J. *Organometallics* **2002,** *21,* 3691–3702. doi:10.1021/om020087s
31. Mager, M.; Becke, S.; Windisch, H.; Denninger, U. *Angew. Chem., Int. Ed.* **2001,** *40,* 1898–1902. doi:10.1002/1521-3773(20010518)40:10<1898::aid-anie1898>3.0.co;2-k
32. Zhou, J.; Lancaster, S. J.; Walker, D. A.; Beck, S.; Thornton-Pett, M.; Bochmann, M. *J. Am. Chem. Soc.* **2001,** *123,* 223–237. doi:10.1021/ja002820h
33. Sun, Y.; Metz, M. V.; Stern, C. L.; Marks, T. J. *Organometallics* **2000,** *19,* 1625–1627. doi:10.1021/om990946l
34. Mahlau, M.; List, B. *Angew. Chem., Int. Ed.* **2013,** *52,* 518–533. doi:10.1002/anie.201205343
35. Phipps, R. J.; Hamilton, G. L.; Toste, F. D. *Nat. Chem.* **2012,** *4,* 603–614. doi:10.1038/nchem.1405
36. Hinz, A.; Labbow, R.; Reiß, F.; Schulz, A.; Sievert, K.; Villinger, A. *Struct. Chem.* **2015,** *26,* 1641–1650. doi:10.1007/s11224-015-0638-0
37. Lv, J.; Zhang, L.; Luo, S.; Cheng, J.-P. *Angew. Chem., Int. Ed.* **2013,** *52,* 9786–9790. doi:10.1002/anie.201304561
38. Wang, L.; Lv, J.; Zhang, L.; Luo, S. *Angew. Chem., Int. Ed.* **2017,** *56,* 10867–10871. doi:10.1002/anie.201704020
39. CCDC 1863542 (**7**) contains the supplementary crystallographic data for this paper. This data can be obtained free of charge from The Cambridge Crystallographic Data Centre.

License and Terms

BEILSTEIN JOURNAL OF ORGANIC CHEMISTRY

Cyclobutane dication, $(CH_2)_4^{2+}$: a model for a two-electron four-center (2e-4c) Woodward–Hoffmann frozen transition state

G. K. Surya Prakash* and Golam Rasul

Full Research Paper

Open Access

Address:
Loker Hydrocarbon Research Institute and Department of Chemistry, University of Southern California, University Park, Los Angeles, CA 90089-1661, USA

Email:
G. K. Surya Prakash* - gprakash@usc.edu

* Corresponding author

Keywords:
cyclobutane dication; 2e-4c bond; frozen transition state; Woodward–Hoffmann rule

Beilstein J. Org. Chem. **2019,** *15,* 1475–1479.
doi:10.3762/bjoc.15.148

Received: 01 March 2019
Accepted: 28 June 2019
Published: 03 July 2019

This article is part of the thematic issue "Reactive intermediates – carbocations".

Guest Editor: S. R. Hare

Abstract

The structures of the elusive cyclobutane dication, $(CH_2)_4^{2+}$, were investigated at the MP2/cc-pVTZ and CCSD(T)/cc-pVTZ levels. Calculations show that the two-electron four-center (2e-4c) bonded structure **1** involving four carbon atoms is a minimum. The structure contains formally two tetracoordinate and two pentacoordinate carbons. The non-classical σ-delocalized structure can be considered as a prototype for a 2e-4c Woodward–Hoffmann frozen transition state. The planar rectangular shaped structure **2** with a 2e-4c bond was found not to be a minimum.

Introduction

The protonated hydrogen cation (H_3^+, **i**) is the simplest known structure involving a two-electron three-center (2e-3c) bond (Scheme 1). The first spectroscopic detection of the H_3^+ ion was reported by Oka in 1980 [1]. Similarly, the structure of five coordinated protonated methane (CH_5^+, **ii**), a prototype of nonclassical carbocations, could not be interpreted by the classical tetravalency bonding concept [2,3] also requiring the engagement of a 2e-3c bond as suggested by Olah in 1969 [4,5]. A compelling number and huge array of carbocations involving higher coordinate carbon is by now realized by experimental studies.

Hypercarbon chemistry covers in addition to carbocations also carboranes, carbon-bridged organometallics, carbonyl clusters, along with others. The rapidly evolving field has been extensively surveyed [6]. In comparison, structures of the carbocations involving a two-electron four-center (2e-4c) bond are rare. This type of bonding could occur in rigid frameworks such as in 1,3-dehydro-5,7-adamantanediyl dication (**iii**) [7] and pagodane dication (**iv**) [8]. The question is can a 2e-4c bond exist in a molecular structure involving four atoms without any rigid frameworks such as in the diprotonated hydrogen (H_4^{2+}, **v**) and the cyclobutane dication $(CH_2)_4^{2+}$ (**vi**)?

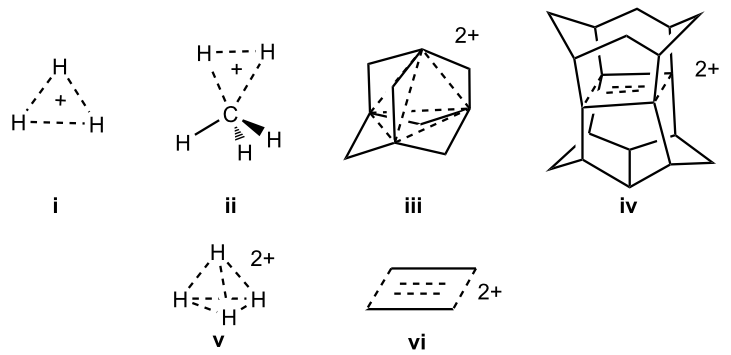

Scheme 1: Examples of 2e-3c and 2e-4c bonded structures.

The structures of H_4^{2+} (including **v**) were previously analyzed at various theoretical levels including CISD/6-311++G(d,2pd) by von Ragué Schleyer, Koch and co-workers [9]. No structure with four connected hydrogens, however, was found to be a minimum on the potential energy surface (PES) of H_4^{2+}. The structure of the rectangular shaped cyclobutane dication $(CH_2)_4^{2+}$ (**vi**) was computed by Olah, Prakash et al. [8,10] using semiempirical and ab initio methods and later by Herges, von Ragué Schleyer, Schindler and Fessner [11] using an ab initio method. The various levels of calculations including MP2/6-31G* indicated that the structure **vi** was not a minimum [11]. The 1,3-dehydro-5,7-adamantanediyl dication (**iii**) [7] with 2e-4c bonding was generated and identified by ^{13}C NMR spectroscopic and theoretical methods corresponding to a three dimensional aromaticity. The four bridge-head p-orbitals overlap inward in a tetrahedral fashion involving two electrons.

We have now extended our study to obtain information on the structure, stabilities and possible rearrangement pathways of the elusive cyclobutane dication. The species is an example of the simplest carbodication containing a 2e-4c bond and can be considered as a prototype for a frozen Woodward–Hoffmann transition state analog [12,13]. The 2e-4c delocalized σ-bishomoaromatic system is representative of a 2e-aromatic pericyclic species. This type of system may be considered as the transition state of the allowed cycloaddition of ethylene to ethylene dication. Electron delocalizations take place in the plane of the conjugated systems unlike cyclobutadiene dication (**vi**), where delocalization takes place through conventional p-type orbitals. GIAO-CCSD(T) derived ^{13}C NMR chemical shifts of the structures were also computed to probe the nature and extent of the positive charge delocalization.

Calculations

The Gaussian 09 program [14] was employed for geometry optimizations and frequency calculations. Vibrational frequencies at the MP2/cc-pVTZ//MP2/cc-pVTZ level were used to characterize stationary points as minima (NIMAG (number of imaginary frequencies) = 0 or transition state NIMAG = 1) and to compute zero point vibrational energies (ZPE), which were scaled by a factor of 0.96 [15]. CCSD(T)/cc-pVTZ optimizations and GIAO-CCSD(T) ^{13}C NMR chemical shifts calculations by the GIAO (Gauge Invariant Atomic Orbitals) method [16-19] using tzp and qzp basis sets, which were optimized by Schäfer, Horn and Ahlrichs [20,21], have been performed with the CFOUR program [22,23]. The ^{13}C NMR chemical shifts were computed using TMS (calculated absolute shift, i.e., σ(C) = 197.9 (GIAO-CCSD(T)) as a reference.

Results and Discussion

Structures of **1–4** were optimized at the MP2/cc-pVTZ and CCSD(T)/cc-PVTZ levels. CCSD(T)/cc-PVTZ structures will be discussed throughout unless otherwise stated. Dication **1** is expected to form by removal of two electrons from cyclobutane. At both MP2/cc-pVTZ and CCSD(T)/cc-PVTZ levels, the C_2 symmetric form **1** (Figure 1) was found to be a minimum for $(CH_2)_4^{2+}$. This is confirmed by frequency calculations at the corresponding levels. The ring of the structure **1** embraces a puckered conformation with a puckering angle (the angle between the two three-membered rings) of 136° as shown in Figure 1. The structure contains conventionally two tetracoordinate and two pentacoordinate carbons. It resembles a complex between two ethylene radical cations, $(CH_2)_4^{2+}$, culminating in the formation of a 2e-4c bond. Total electron density, HOMO and LUMO of the dication **1** are depicted in Figure 2. In such a small ring doubly charged system, charge–charge repulsion is certainly strong, but the bonding interactions as well as charge delocalization are good enough to counter this repulsion. The C1–C4 and C2–C3 bonds (1.968 Å) were calculated to be significantly longer than the C1–C2 and C3–C4 bonds (1.430 Å). The D_{2h} symmetric structure **2** was also computed for comparison with the structure **1**. Computed vibrational frequencies at the MP2/cc-pVTZ//MP2/cc-pVTZ level indicated that the rectangular shaped structure **2** could not be a minimum as it

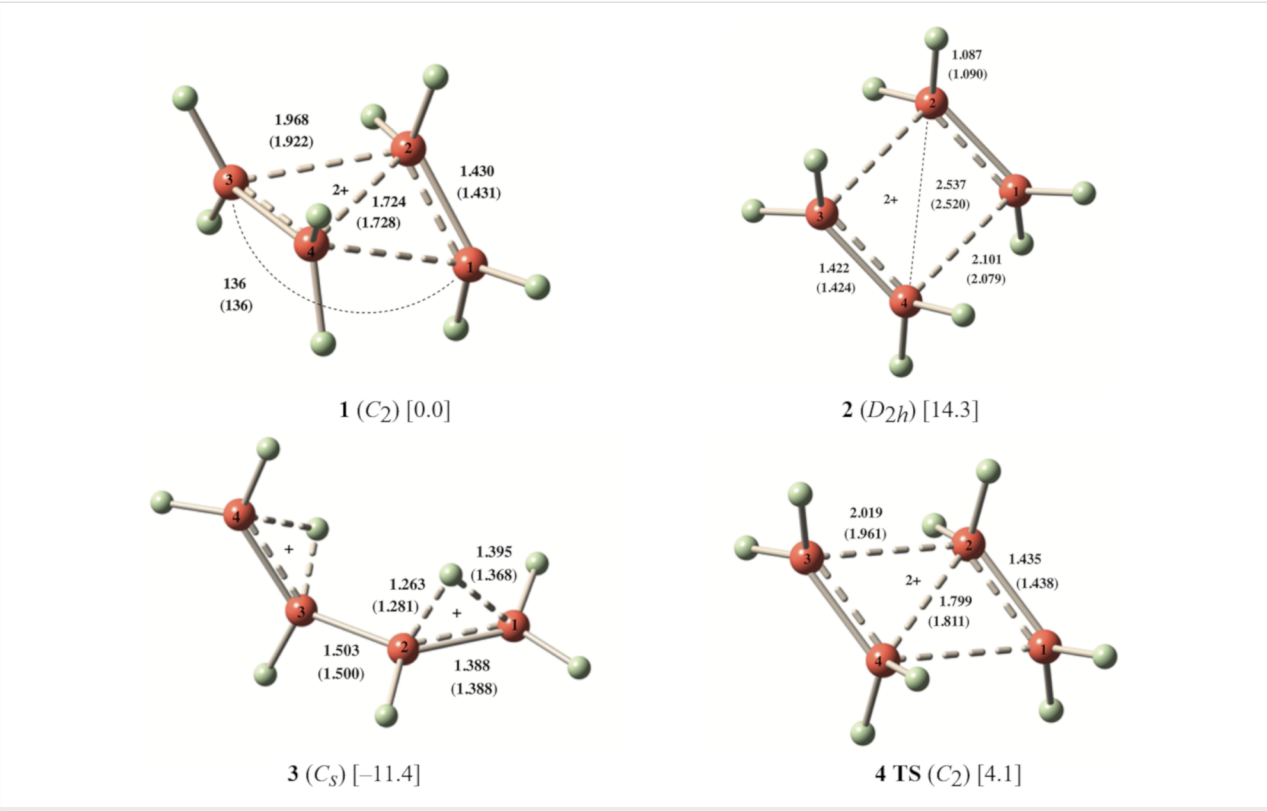

Figure 1: CCSD(T)/cc-pVTZ (MP2/cc-pVTZ) optimized structures and relative energies [in kcal/mol] of **1**–**4**.

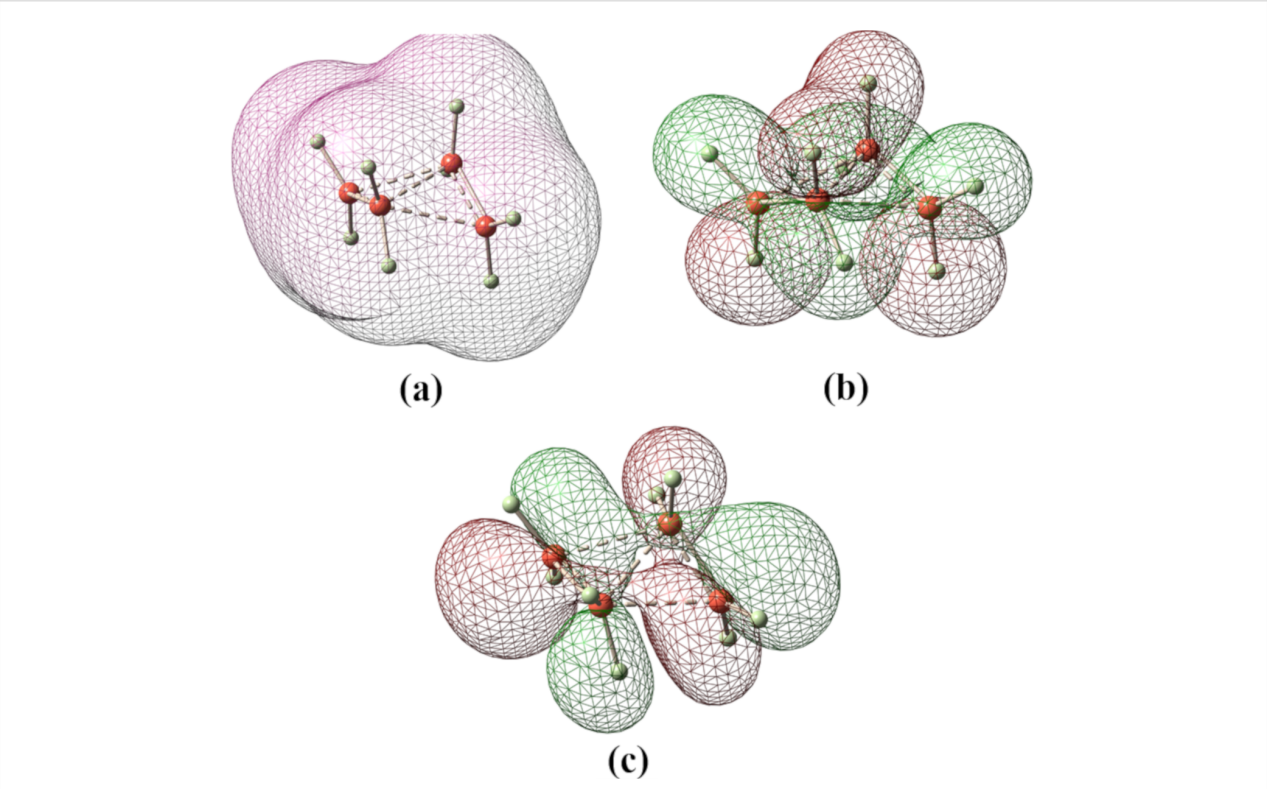

Figure 2: (a) Total electron density, (b) HOMO and (c) LUMO of the dication **1**; coefficients are calculated at the HF/6-31G* level.

contains two imaginary frequencies (NIMAG = 2, corresponding to the vibrations of the two ethylene units in plane and out of plane).

Moreover, structure **2** was also found to be notably disfavored over the structure **1** by 14.3 kcal/mol at the CCSD(T)/cc-PVTZ + ZPE level (Figure 1, Table S9 in Supporting Information File 1). Attempts to find a minimum for the open 1,4-butanediyl dication, bearing two primary carbenium centers failed due to automatic transformation to the thermodynamically more stable hydrogen-bridged structure **3** (Figure 1).

The twisted angle between the planes of the hydrogen-bridged units in **3** was found to be 91.4°. Expectedly, the structure **3** was found to be favored over the structure **1** by 11.4 kcal/mol (Figure 1, Table S9 in Supporting Information File 1). Planar parallelogram-shaped structure **4** was identified as the transition state for the transformation of **1** to **3** (Figure 1). The structure **4** lies 4.1 kcal/mol above **1**. Dissociation of **1** leading to two ethylene radical cations (CH_2=$CH_2^{\cdot+}$) was also considered. The process was found to be exothermic by 12.8 kcal/mol at the CCSD(T)/cc-PVTZ + ZPE level. We tried, but could not locate a transition state for the dissociation process at the CCSD(T)/cc-PVTZ level.

The ^{13}C NMR chemical shifts of the structures **1**–**3** were computed by employing GIAO-MP2 and GIAO-CCSD(T) methods using CCSD(T)/cc-pVTZ geometries. GIAO-CCSD(T) calculated ^{13}C NMR chemical shifts for **1** show that the C1 and C2 carbons are deshielded at δ 216.6 and 40.2 ppm, respectively, indicating a nonclassical nature of the ion in accord with its tetra- and pentacoordinate nature. Computed ^{13}C NMR chemical shifts of the structure **1** are given in Table 1. Vibrational frequencies of the structure **1** are given in Table S10 (see Supporting Information File 1).

Conclusion

The present study at the MP2/cc-pVTZ and CCSD(T)/cc-pVTZ levels shows that the cyclobutane dication, $(CH_2)_4^{2+}$ (**1**), a prototype for a 2e-4c Woodward–Hoffmann frozen transition state, is a viable minimum on its potential energy surface. The structure contains formally two tetracoordinate and two pentacoordinate carbons. It resembles a complex between two ethylene radical ions, $(C_2H_4)^{2\cdot+}$, culminating in the formation of a 2e-4c bond involving four carbon atoms. The planar rectangular shaped structure **2** with a 2e-4c bond was found to be not a minimum.

Supporting Information

Supporting Information File 1

MP2/cc-pVTZ and CCSD(T)/cc-pVTZ optimized Cartesian coordinates of **1**–**4**, energies, ZPE and relative energies of **1**–**4** (Table S9) and calculated frequencies and IR intensities of **1** (Table S10).
[https://www.beilstein-journals.org/bjoc/content/supplementary/1860-5397-15-148-S1.pdf]

Acknowledgements

Support of our work by Loker Hydrocarbon Research Institute is gratefully acknowledged.

ORCID® iDs

G. K. Surya Prakash - https://orcid.org/0000-0002-6350-8325

References

1. Oka, T. *Phys. Rev. Lett.* **1980,** *45,* 531–534. doi:10.1103/physrevlett.45.531
2. Kekulé, A. *Ann. Chem. Pharm.* **1858,** *106,* 129–159. doi:10.1002/jlac.18581060202
3. Kekulé, A. *Z. Chem. (Leipzig, Ger.)* **1867,** *3,* 217.
4. Olah, G. A.; Klopman, G.; Schlosberg, R. H. *J. Am. Chem. Soc.* **1969,** *91,* 3261–3268. doi:10.1021/ja01040a029
5. Olah, G. A. In *Chemical Reactivity and Reaction Paths;* Klopman, G., Ed.; Wiley: London, 1974.
6. Olah, G. A.; Prakash, G. K. S.; Wade, K.; Molnár, Á.; Williams, R. E. *Hypercarbon Chemistry;* John Wiley & Sons, Inc.: Hoboken, NJ, U.S.A., 2011. doi:10.1002/9781118016466
7. Bremer, M.; von Ragué Schleyer, P.; Schötz, K.; Kausch, M.; Schindler, M. *Angew. Chem., Int. Ed. Engl.* **1987,** *26,* 761–763. doi:10.1002/anie.198707611

Table 1: GIAO calculated[a] ^{13}C NMR chemical shifts using CCSD(T)/cc-pVTZ geometries.

no	atom	GIAO-MP2/tzp	GIAO-CCSD(T)/tzp
1	C1, C3	217.4	216.6
	C2, C4	39.9	40.2
2	C1, C2, C3, C4	196.6	195.8
3	C1, C4	182.0	179.5
	C2, C3	134.4	132.1

[a]The ^{13}C NMR chemical shifts were referenced to TMS, for numbering scheme please see Figure 1.

8. Prakash, G. K. S.; Krishnamurthy, V. V.; Herges, R.; Bau, R.; Yuan, H.; Olah, G. A.; Fessner, W. D.; Prinzbach, H. *J. Am. Chem. Soc.* **1986,** *108,* 836–838. doi:10.1021/ja00264a046
9. Glukhovtsev, M. N.; von Ragué Schleyer, P.; van Eikema Hommes, N. J. R.; De M. Carneiro, J. W.; Koch, W. *J. Comput. Chem.* **1993,** *14,* 285–294. doi:10.1002/jcc.540140305
10. Prakash, G. K. S.; Krishnamurthy, V. V.; Herges, R.; Bau, R.; Yuan, H.; Olah, G. A.; Fessner, W. D.; Prinzbach, H. *J. Am. Chem. Soc.* **1988,** *110,* 7764–7772. doi:10.1021/ja00231a029
11. Herges, R.; von Ragué Schleyer, P.; Schindler, M.; Fessner, W. D. *J. Am. Chem. Soc.* **1991,** *113,* 3649–3656. doi:10.1021/ja00010a003
12. Goldstein, M. J.; Hoffmann, R. *J. Am. Chem. Soc.* **1971,** *93,* 6193–6204. doi:10.1021/ja00752a034 and references cited therein.
13. Hoffmann, R.; Stohrer, W.-D. *J. Am. Chem. Soc.* **1971,** *93,* 6941–6948. doi:10.1021/ja00754a042
14. *Gaussian 09,* Revision A.02; Gaussian, Inc.: Wallingford, CT, 2009.
15. Alecu, I. M.; Zheng, J.; Zhao, Y.; Truhlar, D. G. *J. Chem. Theory Comput.* **2010,** *6,* 2872–2887. doi:10.1021/ct100326h
16. London, F. *J. Phys. Radium* **1937,** *8,* 397–409. doi:10.1051/jphysrad:01937008010039700
17. Ditchfield, R. *Mol. Phys.* **1974,** *27,* 789–807. doi:10.1080/00268977400100711
18. Wolinski, K.; Hinton, J. F.; Pulay, P. *J. Am. Chem. Soc.* **1990,** *112,* 8251–8260. doi:10.1021/ja00179a005
19. Schäfer, A.; Horn, H.; Ahlrichs, R. *J. Chem. Phys.* **1992,** *97,* 2571–2577. doi:10.1063/1.463096
20. Gauss, J. *Chem. Phys. Lett.* **1992,** *191,* 614–620. doi:10.1016/0009-2614(92)85598-5
21. Gauss, J. *J. Chem. Phys.* **1993,** *99,* 3629–3643. doi:10.1063/1.466161
22. CFOUR, a quantum chemical program package, Stanton, J. F.; Gauss, J.; Harding, M. E.; Szalay, P. G. with contributions from Auer, A. A.; Bartlett, R. J.; Benedikt, U.; Berger, C.; Bernholdt, D. E.; Bomble, Y. J.; Cheng, L.; Christiansen, O.; Heckert, M.; Heun, O.; Huber, C.; Jagau, C.; Jonsson, D.; Jusélius, J.; Klein, K.; Lauderdale, W. J.; Mathews, D. A.; Metzroth, T.; O'Neill, D. P.; Price, D. R.; Prochnow, E.; Ruud, K.; Schiffmann, F.; Schwalbach, W.; Stopkowicz, S.; Tajti, A.; Vµzquez, J.; Wang, F.; Watts, J. D.; and the integral packages MOLE-CULE (Almlçf, J and Taylor, P. R.), PROPS (Taylor, P. R.), ABACUS (Helgaker, T.; Aa, H. J.; Jensen H. J. A.; Jørgensen, P.; Olsen, J.), and ECP routines (Mitin, A. V.; Wüllen, C. van), 2010.
23. Harding, M. E.; Metzroth, T.; Gauss, J.; Auer, A. A. *J. Chem. Theory Comput.* **2008,** *4,* 64–74. doi:10.1021/ct700152c

BEILSTEIN JOURNAL OF ORGANIC CHEMISTRY

Different reactivity of phosphorylallenes under the action of Brønsted or Lewis acids: a crucial role of involvement of the P=O group in intra- or intermolecular interactions at the formation of cationic intermediates

Stanislav V. Lozovskiy[1], Alexander Yu. Ivanov[2] and Aleksander V. Vasilyev*[1,3,§]

Full Research Paper

Open Access

Address:
[1]Department of Organic Chemistry, Institute of Chemistry, Saint Petersburg State University, Universitetskaya nab., 7/9, Saint Petersburg, 199034, Russia, [2]Center for Magnetic Resonance, Research Park, St. Petersburg State University, Universitetskiy pr., 26, Saint Petersburg, Petrodvoretz, 198504, Russia and [3]Department of Chemistry, Saint Petersburg State Forest Technical University, Institutsky per., 5, Saint Petersburg, 194021, Russia

Email:
Aleksander V. Vasilyev* - aleksvasil@mail.ru

* Corresponding author
§ Tel.: 07 812 670 93 52; fax: 07 812 670 93 90; a.vasilyev@spbu.ru

Keywords:
aluminum chloride; cation; intermediate; oxaphospholium ions; phosphorylallenes; phosphoryl group; triflic acid

Beilstein J. Org. Chem. **2019,** *15,* 1491–1504.
doi:10.3762/bjoc.15.151

Received: 06 March 2019
Accepted: 28 June 2019
Published: 08 July 2019

This article is part of the thematic issue "Reactive intermediates – carbocations".

Guest Editor: S. R. Hare

Abstract

3-Methylbuta-1,2-dien-1-ylphosphonic acid derivatives (phosphorylallenes) [X_2(O=)P–CR=C=CMe_2, X = Cl, OMe, NR_2, or SAr] undergo intramolecular cyclization into the corresponding 1,2-oxaphospholium ions in the Brønsted superacid TfOH. These cations have been thoroughly studied by means of NMR spectroscopy. The hydrolysis of superacidic solutions of these species afforded cyclic phosphonic acids and other phosphorus-containing compounds. Contrary to Brønsted acids, 3-methylbuta-1,2-dien-1-ylphosphonic dichloride [Cl_2(O=)P–HC=C=CMe_2] reacted with the Lewis acid $AlCl_3$ in an intermolecular way forming noncyclic intermediates, which were investigated by NMR spectroscopy and DFT calculations. Hydrolysis of these species resulted in the formation of phosphoryl-substituted allyl alcohols and 1,3-butadienes. A strong coordination of the oxygen of the P=O group with $AlCl_3$ prevented the formation of cyclic 1,2-oxaphospholium ions and played a crucial role in the different reactivity of such phosphorylallenes under the action of Brønsted or Lewis acids. Apart from that, the reaction of dichlorophosphorylallenes with arenes and $AlCl_3$ led to products of hydroarylation of the allene system, phosphoryl-substituted alkenes and/or indanes. This is the first example of a Lewis acid-promoted intermolecular hydroarylation of allenes bearing electron-withdrawing substituents. Plausible reaction mechanisms have been proposed on the basis of the investigated reactions, and NMR analysis and DFT studies of the intermediate cationic species.

Introduction

Electrophilic reactions of allenes have been intensely explored in organic synthesis [1-3]. In particular, reports on electrophilic activation of phosphorylallenes are numerous [4-10]. Miscellaneous electrophiles, such as sulfenyl, selenyl, and telluryl chlorides, were used in reactions with these allenes. However, only a few studies have been focused on reactions of phosphorylallenes with Brønsted acids [11,12]. These reactions proceed through an intermediate formation of the corresponding 2,5-dihydro-1,2-oxaphosphol-2-ium ions. The progenitor of the oxaphospholium ion family, 2,2-dichloro-5,5-dimethyl-1,2-oxaphosphol-2-ium, was postulated for the first time in 1978 [12].

We have recently reported on the generation, NMR characterization and reactions of oxaphospholium ions bearing phenyl or phenoxy substituents at the phosphorus atom of phosphorylallenes [13-16]. These cations were intermediates in Brønsted and Lewis acid-promoted intramolecular reactions of phosphorus-containing allenes with aromatic π-nucleophiles giving rise to various (bi)cyclic phosphorus-containing compounds [13-16].

It should be especially emphasized that intermolecular reactions of phosphorylallenes with arenes have not been yet achieved. In general, intermolecular hydroarylation of allenes has been developed for reactions catalyzed by complexes of various metals [17], such as Pd [18-20], Pt [21], Au [22-25], Ir [26], Rh [27,28], and Co [29]. However, only electron-rich allenes, bearing electron-donating substituents, take part in the metal-catalyzed reactions. There are just a few examples of Brønsted acid catalyzed intermolecular hydroarylations of allenes by electron-rich arenes, indoles [30] or phenols [31]. Other arenes (benzene and its substituted derivatives) have not been involved in these reactions. Concerning electron-deficient allenes, bearing electron-withdrawing groups, there is only one example of a trifluoroacetic acid-promoted hydroarylation with indoles [30]. To the best of our knowledge, up to the moment, there are no examples for an intermolecular hydroarylation of electron-deficient allenes by benzene derivatives under the action of strong Brønsted or Lewis acids.

The main goals of this work were to study transformations of various phosphorylallenes under electrophilic activation with Brønsted or Lewis (super)acids, including reactions with arenes as π-nucleophiles, and investigation of intermediate cationic species by means of NMR and DFT calculations.

Allenes used in this study are presented in Figure 1. We explored allenes having different substituents at the phosphoryl group: chloro (**1a–d**), amino (**1e–g**), arylsulfanyl (**1h**,**i**), and methoxy (**1j**).

Results and Discussion

Reactions of allenes with Brønsted acids

Allenes **1a,b,e–j** upon dissolving in TfOH in an NMR tube at room temperature formed intensively colored solutions of the corresponding 1,2-oxaphospholium ions **A–H** (Table 1). These species are formed by protonation of the central carbon atom of the allene system that gives the corresponding allyl cations, which undergo cyclization onto the oxygen of the P=O group. These ions have similar NMR data: the signal of the new proton H4 is located in the range 6.30–8.07 ppm, the signal of vinyl carbon C4 at 166.8–171.9 ppm, and the signal of quaternary carbon C5 at 96.0–116.3 ppm. It is worth noting that 2,2-dichloro (**A**, **B**) and 2,2-diarylsulfanyl (**F**, **G**)-substituted cations exhibit down field shifted signals in the ^{31}P NMR (δ 87.82–115.37 ppm) in comparison with 2,2-diamino (**C**, **D**, **E1**) and 2,2-dimethoxy (**H**)-substituted species (δ ^{31}P 52.87–70.79 ppm). This reveals that, for amino and methoxy substituents, positive charge is delocalized onto these groups to a greater extent than in the case of chloro or arylsulfanyl ones.

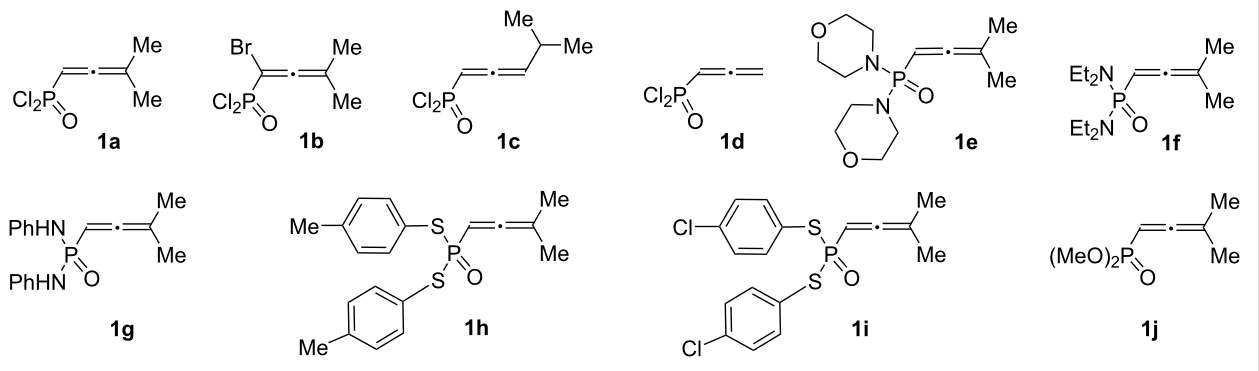

Figure 1: Allenes **1a–j** used in this study.

Table 1: Selected ^{1}H, ^{13}C and ^{31}P NMR data for cations **A–H** derived from the protonation of the corresponding allenes **1a**,**b**,**e–j** in TfOH at room temperature.

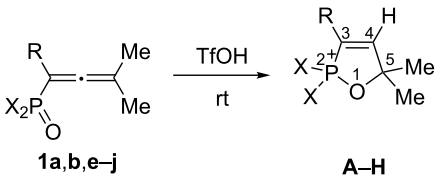

1a,**b**,**e–j** **A–H**

Allene	Cation	R	X	^{1}H NMR, δ, ppm (*J*, Hz)		^{13}C NMR, δ, ppm (*J*, Hz)			^{31}P NMR, δ, ppm
				H3	H4	C3	C4	C5	
1a	**A**	H	Cl	8.11 dd (68.3, 8.3)	7.00 dd (49.4, 8.3)	116.4 d (111.3)	169.9 d (14.3)	110.8 d (10.8)	97.04
1b	**B**	Br	Cl	–	8.07 dd (55.1)	104.9 d (137.0)	169.8 d (33.2)	113.6 d (5.4)	87.82
1e	**C**	H	$O(CH_2CH_2)_2N$	7.89 dd (49.2, 8.3)	6.45 dd (36.9, 8.3)	109.3 d (131.9)	170.3 d (14.3)	98.9 d (10.0)	64.33
1f	**D**	H	Et_2N	7.49 dd (49.3, 8.2)	6.56 dd (38.8, 8.2)	109.1 d (126.6)	170.0	102.0	70.79
1g	**E1**	H	PhNH	m (overlapping with other signals)	6.42 dd (37.1, 7.8)	111.6 d (137.5)	168.3 d (12.8)	96.0	52.87
1h	**F**	H	$4\text{-}MeC_6H_4S$	7.26 dd (54.0, 7.9)	6.33 dd (45.5, 7.9)	113.1 d (82.7)	167.1 d (10.0)	116.3 d (7.6)	115.37
1i	**G**[a]	H	$4\text{-}ClC_6H_4S$	7.41 dd (54.4, 7.9)	6.40 dd (45.9, 7.9)	111.1 d (81.0)	166.8 d (10.3)	101.8	114.56
1j	**H**	H	MeO	7.93 dd (54.6, 8.5)	6.30 dd (35.8, 8.4)	107.3 d (159.4)	171.9 d (14.4)	97.8 d (13.2)	57.82

[a]Content of cation **G** in reaction solution was ≈50% based on ^{31}P NMR data.

Cations **A–D**, and **F–H** are stable in TfOH at room temperature for a long time, they are not transformed into other species under the superacidic conditions. Unlike the others, allene **1g** undergoes consequent transformations in TfOH at room temperature (see Scheme 1 and Figure 2). First, when dissolved in the acid, allene **1g** forms oxaphospholium ion **E1** (Table 1) through an intermediate formation of allyl cation **E** (Scheme 1). Ion **E1** is transformed very fast into another species; after one minute new signals appear in the NMR spectra (see ^{31}P NMR monitoring of this process in Figure 2), and after 12 hours it is completely converted to this new cation. It is most likely that this species is 1,2-azaphosphol-2-ium ion **E2**, which is formed through allyl cation **E**.

However, cation **E2**, in turn, is further transformed into one more species during several days. The set of spectral data (see below) for this final species indicates that, most likely it should be seven-membered heterocyclic cation **E4**, which is formed through the P–N bond cleavage in **E2** and formation of intermediate cation **E3** (Scheme 1).

In the ^{31}P NMR spectra, the signal of **E4** is the most up field shifted (δ 24 ppm, see Figure 2 and Scheme 1) in comparison with signals of the species **E1** (δ 53 ppm) and **E2** (δ 43 ppm). This difference may reveal that phosphorus in cation **E4** is bound to a carbon atom, rather than to a heteroatom O or N, like in **E1** and **E2**. Structurally close six-membered ring cations, having the C–P bond, resonate at 30.5–31.9 in ^{31}P NMR [16], that is close to the spectrum for species **E4**.

Apart from that, in ^{13}C NMR spectra, the signals of quaternary carbon bearing two methyl groups in **E2** and **E4** are very close (δ 70.3–70.9 ppm, see Scheme 1). Contrary to that, the signal of this carbon for **E2** is very much down field shifted (δ 96.1 ppm). This indicates that in species **E2** and **E4** this carbon is connected to a protonated amino group, and in **E1** it is bound to oxygen. The same range of absorbance around 100 ppm for this carbon was observed previously for other oxaphospholium ions [14,16].

Then, we carried out hydrolysis of cations **A**–**H** (Scheme 2). Results of hydrolysis strongly depend on the substituent X on the phosphorus atom. Ions containing a labile P–X bond (X = Cl, O, S), namely **A**, **B**, and **F**–**H**, gave unstable adducts **2** (registered by GC–MS), which are further transformed into acids **3**. The structure of compound **3a** was confirmed by X-ray

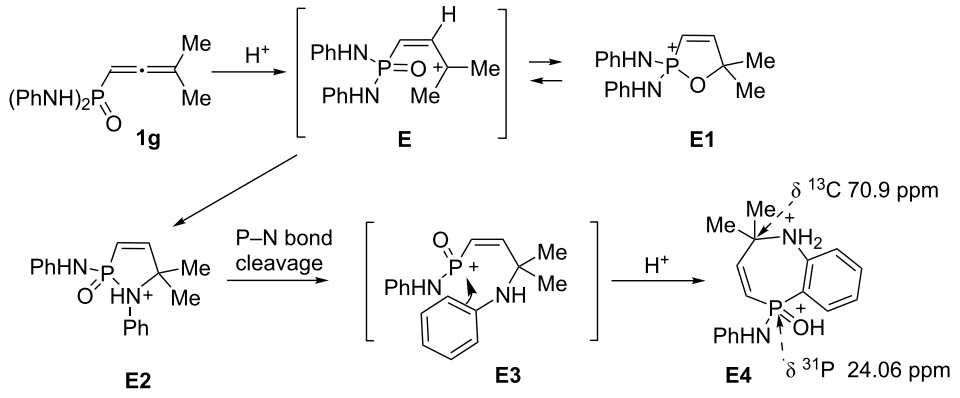

Scheme 1: Transformations of allene **1g** in TfOH leading to the formation of cations **E1**, **E2** and **E4** including selected spectral data for cation **E4**.

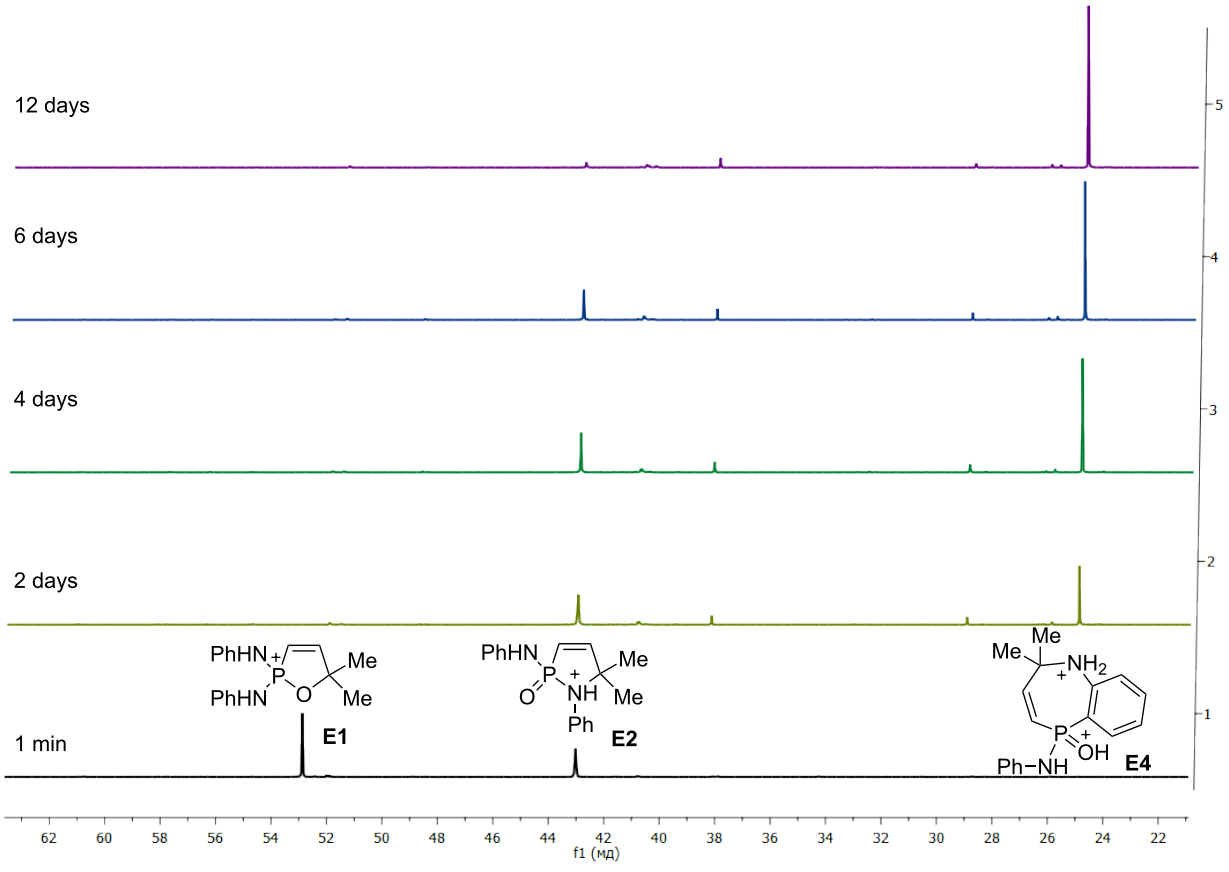

Figure 2: ^{31}P NMR monitoring of the progress of transformation of **E1** into **E2** and **E4** in TfOH at room temperature.

analysis (see Supporting Information File 1). On the other hand, hydrolysis of cations **C**,**D**, bearing a stable P–N bond, resulted in the formation of allyl alcohols **4**. Aqueous work-up of a superacidic solution of cation **E4** led to azaphosphepine-5-oxide **5**. This substance is insoluble in organic solvents, however, we were able to measure its ^{1}H NMR spectrum in D_2O at elevated temperature (80 °C, see Supporting Information File 1).

Taking into account the stability of the P–N bond against hydrolysis, we conducted reactions of the cations **A**, **B**, and

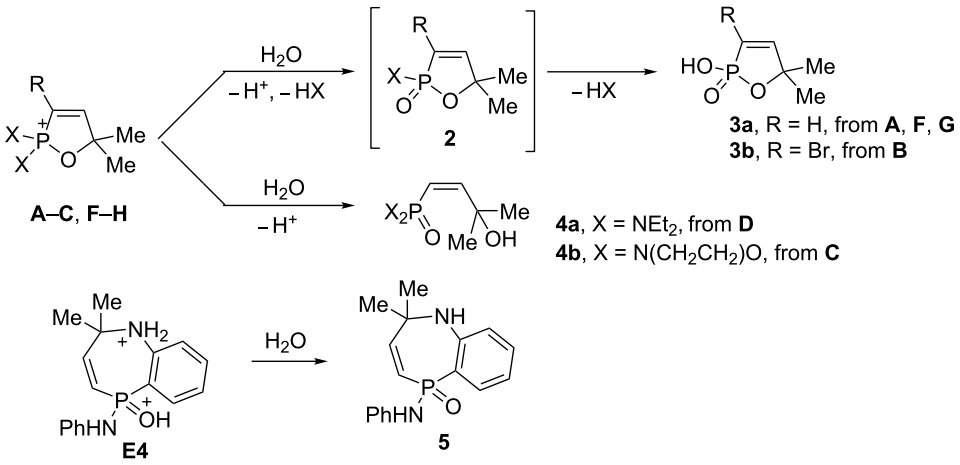

Scheme 2: Results of the hydrolysis of cations **A**–**H**.

F–**H** with morpholine (Scheme 3). Amides **6a,b** were isolated as products of these reactions in excellent yields. The plausible reaction mechanism includes at the first stage nucleophilic attack of morpholine onto the phosphorus cationic center that gives cation **I**, which is transformed into species **J**. Hydrolysis of the latter leads to cation **K** and then finally to amides **6a**,**b**.

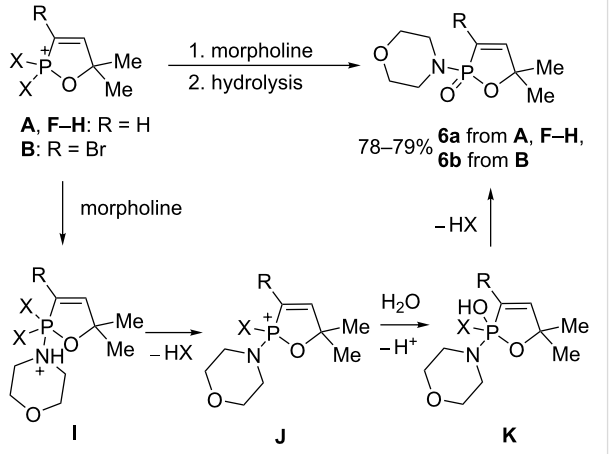

Scheme 3: Preparation of amides **6a**,**b** from cations **A**, **B**, and **F**–**H**.

We carried out a large-scale one-pot solvent-free synthesis of amides **6a**,**b** starting from propargyl alcohols **7a**,**b** at room temperature (Scheme 4). At the first step, alcohols **7a**,**b** in the reaction with PCl_3 were transformed into the corresponding allenes **1a**,**h**. Then, the addition of Brønsted acid (TfOH or H_2SO_4) gave cations **A** and **B**, respectively. The interaction of these species with morpholine followed by hydrolysis furnished the target amides **6a**,**b** in total yields of 60–90% (see procedures in Supporting Information File 1).

It should be noted that allene **1d** bearing no alkyl groups and monoalkylated allene **1c** formed complex mixtures of oligomeric products under the action of various Brønsted acids (H_2SO_4, FSO_3H, TfOH). In this case, the intermediate oxaphospholium ions are unstable and undergo consequent transformations. Apart from that, attempts to quench cations **A**–**H** with external aromatic π-nucleophiles failed. No products of intermolecular electrophilic aromatic substitution were obtained.

Reactions of allenes with Lewis acid $AlCl_3$

Then, we checked reactions of allenes **1a–j** with and without benzene under the action of the strong Lewis acid $AlCl_3$, using benzene or dichloromethane as a solvent, followed by hydroly-

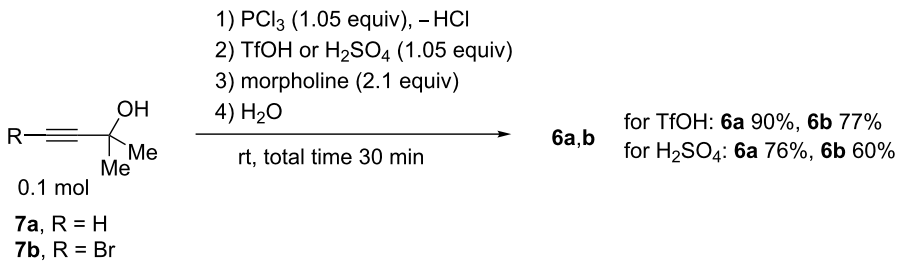

Scheme 4: Large-scale one-pot solvent-free synthesis of amides **6a**,**b** from the corresponding propargylic alcohols.

sis of the reaction mixtures. Allenes **1c–j** gave complex mixtures of oligomeric products under these conditions. However, allenes **1a**,**b** afforded the desired product of hydroarylation with benzene (vide infra).

$AlCl_3$-promoted reactions of allene **1a** were studied under various conditions (Table 2). This compound in reaction with $AlCl_3$ without benzene afforded a mixture of allyl alcohol *Z*-**9** and diene *E*-**10a** after aqueous work-up (Table 2, entries 1 and 2). The amount of 2.1 equivalents of $AlCl_3$ is sufficient for activation of this transformation (compared to the amount of $AlCl_3$ in entries 1 and 2, Table 2). On the other hand, 1 equivalent of $AlCl_3$ is not enough to activate allene **1a**; thus, under these conditions, only acid **2** was obtained as a product of the hydrolysis of starting compound **1a** (Table 2, entry 3). Methanolysis of the reaction mixture gave diene *E*-**10b** (Table 2, entry 7). The reaction of allene **1a** with benzene resulted in the formation of alkene *Z*-**11a**, as a product of intermolecular hydroarylation of the carbon–carbon double bond (Table 2, entries 4–6). This reaction required 2.1 equivalents of $AlCl_3$, 1.05 equivalents of benzene and five minutes at room temperature (Table 2, entry 4). It is worth noting, that the use of other Lewis acids, $NiCl_2$, $EuCl_3$, $FeCl_3$, CuOTf, $AgNO_3$, did not activate allene **1a**; in these reactions only the product of the hydrolysis **8** was finally isolated.

The configuration of the carbon–carbon double bond in compounds *Z*-**9**, *E*-**10b** and *Z*-**11a** was determined on the basis of the observed values of the spin–spin interaction constants for vinyl protons (13–14 Hz for *cis*-isomers and 17–18 Hz for *trans*-isomers), and using H,H-NOESY correlations for *Z*-**11a** (see Supporting Information File 1).

Having these conditions for hydroarylation of allene **1a** in hand (Table 2, entry 4), we conducted reactions with the series of arenes (Table 3). An excess of methanol was used for quenching of reaction mixtures instead of water. This treatment produced dimethoxyphosphoryl groups [$(MeO)_2P{=}O$] in the reaction products, rather than the acidic group [$(HO)_2P{=}O$] in compounds **8–11a** (Table 2). The presence of the $(MeO)_2P{=}O$ group in the structures of reaction products makes them more soluble in organic solvents and easy to isolate in preparative reactions.

Depending on the structure of the starting arene, allene **1a** gave two kinds of reaction products, *E*-/*Z*-alkenes **11** and/or indanes **12** (Table 3). Thus, in reactions with benzene, only *cis*-alkene *Z*-**11b** was obtained in 88% yield (Table 3, entry 1). The sole formation of alkenes *E*-**11g**, *Z*-**11h** and *Z*-**11i**, and *E*/*Z*-**11l** was also observed in reactions with 1,2-dimethoxybenzene (veratrole) (Table 3, entry 6), fluorobenzene (Table 3, entry 7) and

Table 2: $AlCl_3$-promoted reactions of allene **1a** at room temperature with/without benzene at various conditions.

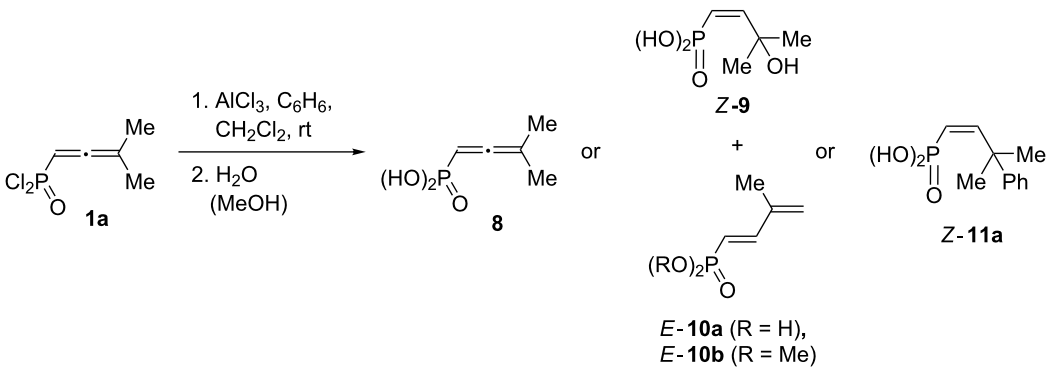

Entry	Equiv of $AlCl_3$	Equiv of benzene	Time, min	Yield of **8**, %	Yield of **9** + **10a**,**b**, %	Yield of **11a**, %
1	5	no benzene	15	–	33 (**9**) + 32 (**10a**)	–
2	2.1	no benzene	15	–	35 (**9**) + 36 (**10a**)	–
3	1	1.05	15	98	–	–
4	2.1	1.05	5	–	–	82
5	2.1	1.05	15	–	–	78
6	2.1	1.05	60	–	–	81
7[a]	2.1	no benzene	15	–	45 (**10b**)	–

[a]Reaction mixture was quenched with methanol.

Table 3: $AlCl_3$-promoted reactions of allene **1a** with arenes leading to alkenes **11** and indanes **12** at room temperature for 5 min.

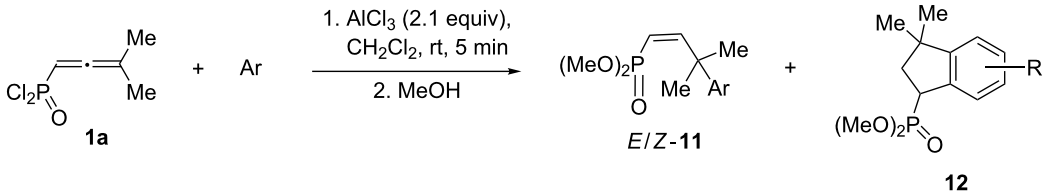

Entry	Starting arene, ArH	Reaction products **11** and **12**, yield, %
1		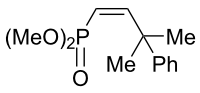 *Z*-**11b**, 88%
2	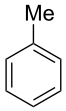	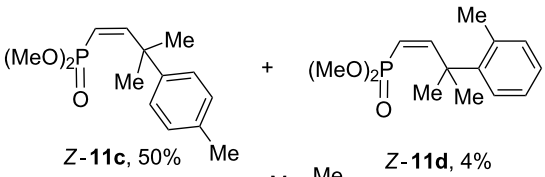 *Z*-**11c**, 50% + *Z*-**11d**, 4% 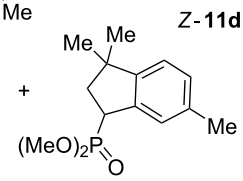 **12a**, 16%
3	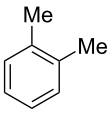	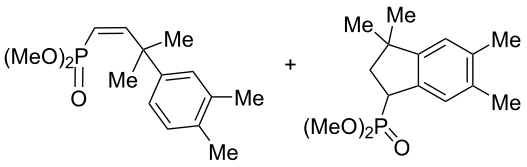 *Z*-**11e**, 50% + **12b**,16%
4	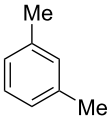	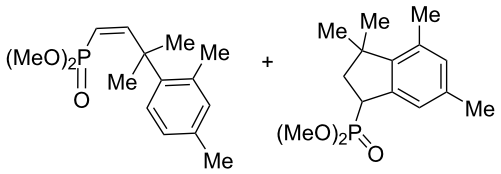 *Z*-**11f**, 4% + **12c**, 89%
5	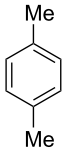	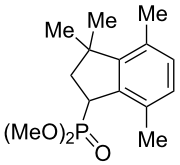 **12d**, 95%
6[a]	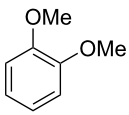	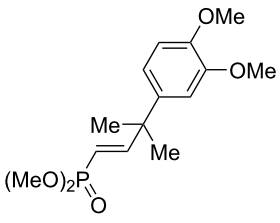 *E*-**11g**, 87%

Table 3: $AlCl_3$-promoted reactions of allene **1a** with arenes leading to alkenes **11** and indanes **12** at room temperature for 5 min. (continued)

7	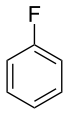	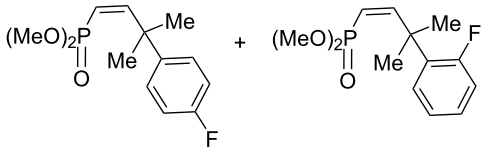 *Z*-**11h**, 53% + *Z*-**11i**, 15%
8	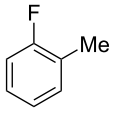	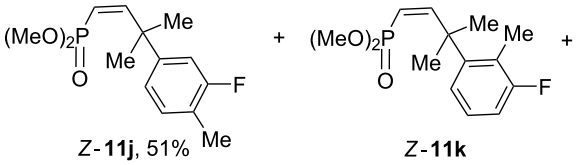 *Z*-**11j**, 51% + *Z*-**11k** + 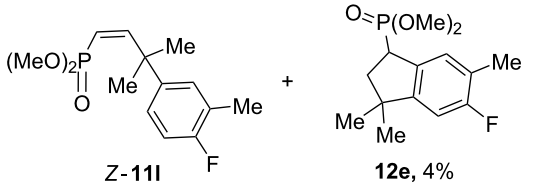 *Z*-**11l** + **12e**, 4% *Z*-**11k** + *Z*-**11l** = 30%
9	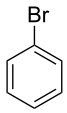	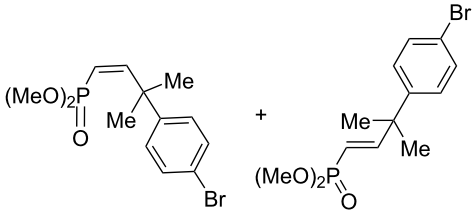 *Z*-**11m**, 40% + *E*-**11m**,40%

[a]Reaction was run with 3.1 equiv of $AlCl_3$.

bromobenzene (Table 3, entry 9), respectively. On the other hand, reactions with methylbenzenes (toluene, *o*- and *m*-xylenes, *o*-fluorotoluene) led to mixtures of alkenes **5** and indanes **6** (Table 3, entries 2–4, and 8). However, *p*-xylene gave the only reaction product, indane **6d**, in nearly quantitative yield of 95% (Table 3, entry 5).

It should be emphasized that compounds **11** and **12** were obtained as inseparable mixtures after TLC separation due to their close chromatographic retention parameters. However, *E*- and *Z*-isomers of alkenes **11** can be separated by preparative thin-layer chromatography, for instance, compounds *E*-**11m** and *Z*-**11m** (Table 3, entry 9 and Supporting Information File 1).

The *E*/*Z*-stereochemistry of compounds **11** was determined on the basis of the values of spin–spin interaction constants of vinyl protons, which were 13–14 Hz for *Z*-isomers and 17–18 Hz for *E*-isomers (see Supporting Information File 1).

Reactions of allene **1a** with strongly donating arenes, 1,3,5-trimethylbenzene (mesitylene), 1,2,4-trimethylbenzene (pseudocumene), phenol, thiophenol, 1,3-dimethoxybenzene, 1,4-dimethoxybenzene, and other arenes, such as 1,2-dichlorobenzene, 1,4-dibromobenzene, gave rise to complex mixtures of oligomeric compounds.

In the same reaction with benzene, allene **1b** afforded alkene *Z*-**11n** in high yield (Scheme 5).

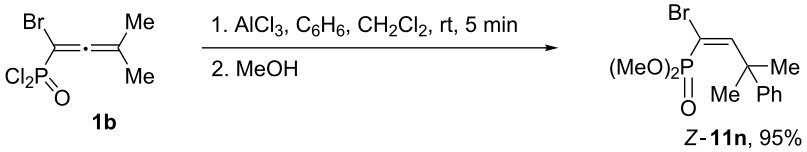

Scheme 5: $AlCl_3$-promoted hydroarylation of allene **1b** by benzene leading to alkene *Z*-**11n**.

The use of morpholine for quenching of the superacidic reaction mixture gave amide *Z*-**11o** in the reaction of **1a** with benzene (Scheme 6).

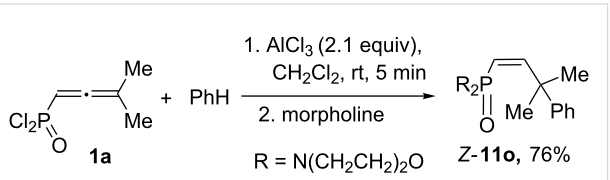

Scheme 6: Reaction of allene **1a** with benzene under the action of $AlCl_3$ followed by quenching of the reaction mixture with morpholine leading to amide *Z*-**11o**.

We also conducted a large-scale one-pot synthesis of indane **12d** starting from 2-methylbut-3-yn-2-ol (Scheme 7, see procedure in Supporting Information File 1). The first stage of this procedure gave allene **1a**, which was dissolved in CH_2Cl_2 and subjected to reaction with *p*-xylene under the action of $AlCl_3$. Finally, methanolysis of the reaction mixture resulted in the formation of indane **12d** in a total yield of 78%.

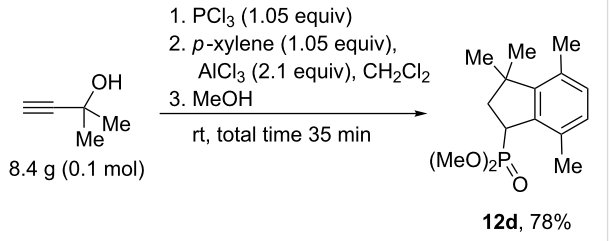

Scheme 7: Multigram-scale one-pot synthesis of indane **12d** from 2-methylbut-3-yn-2-ol.

To elucidate the reaction mechanism additional experiments were conducted. First of all, alkenes **11** were subjected to the action of five-fold excess of $AlCl_3$ at room temperature or elevated temperature. However, no formation of indanes **12** was detected. Then we carried out an NMR study to catch the reaction intermediates. Upon mixing of allene **1a** with 1 equivalent of $AlCl_3$ in CD_2Cl_2 in an NMR tube at room temperature, a yellow solution was formed, which was most likely a complex of **1a** with $AlCl_3$, which is coordinated onto oxygen of the P=O group. The comparison of ^{1}H, ^{13}C, and ^{31}P NMR spectra of starting **1a** and its complex with $AlCl_3$ **13** is presented in Figure 3 (see full spectral data in Supporting Information File 1). It is clear that the complex formation led to significant broadening of NMR spectral lines and, mainly, a downfield shift of the corresponding signals, due to large positive charge on the phosphorus atom. This solution was stable for a long time (several days) and complex **13** was not converted into other compounds. It must be reminded here, that allene **1a** did not react with benzene under the action of 1 equivalent of $AlCl_3$ (see Table 2, entry 3).

Addition of more than 1 equivalent of $AlCl_3$ (2–5 equivalents) to a solution of **1a** in CD_2Cl_2 in an NMR tube resulted in an immediate formation of diene *E*-**14** as a part of a complex mixture (Scheme 8, see Supporting Information File 1 for NMR). Compare with the same transformations of **1a** followed by hydrolysis of the reaction mixture affording a mixture of alcohol *Z*-**9** and diene *E*-**10a** (Table 2, entries 1 and 2). The formation of compound **14** in an NMR monitoring experiment may also indicate that alcohol *Z*-**9** is formed upon hydrolysis of allene **8** (Table 2, entries 1 and 2). Reaction of allene **1a** with deuterobenzene C_6D_6 (1 equivalent) under the action of $AlCl_3$ (2 equivalents) in CD_2Cl_2 in an NMR tube gave alkene **15** (Scheme 8) analogously to the formation of alkenes **11** (Table 3).

Thus, the different reactivity of these particular dichlorophosphorylallenes under the action of Brønsted or Lewis acids can be explained by involvement of the P=O group in intra- or intermolecular interactions at the formation of cationic intermediates. Strong coordination of Lewis acid $AlCl_3$ with the P=O group completely deactivates it for further intramolecular reac-

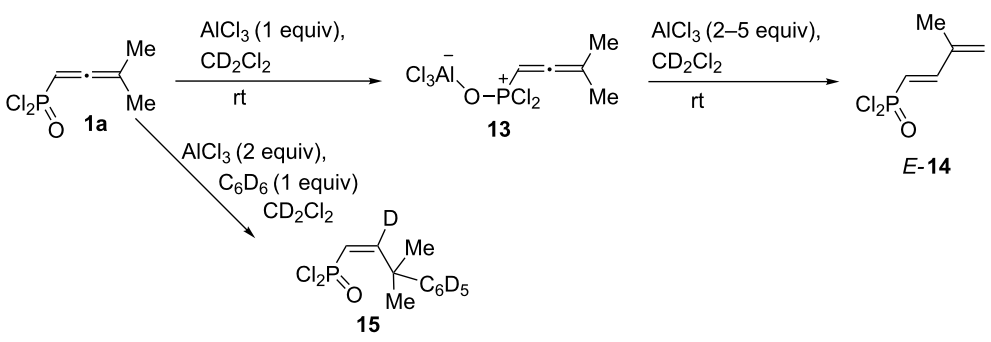

Scheme 8: ^{1}H, ^{13}C, and ^{31}P NMR monitoring of $AlCl_3$-promoted reactions of allene **1a** leading to compounds *E*-**14** or **15** at room temperature.

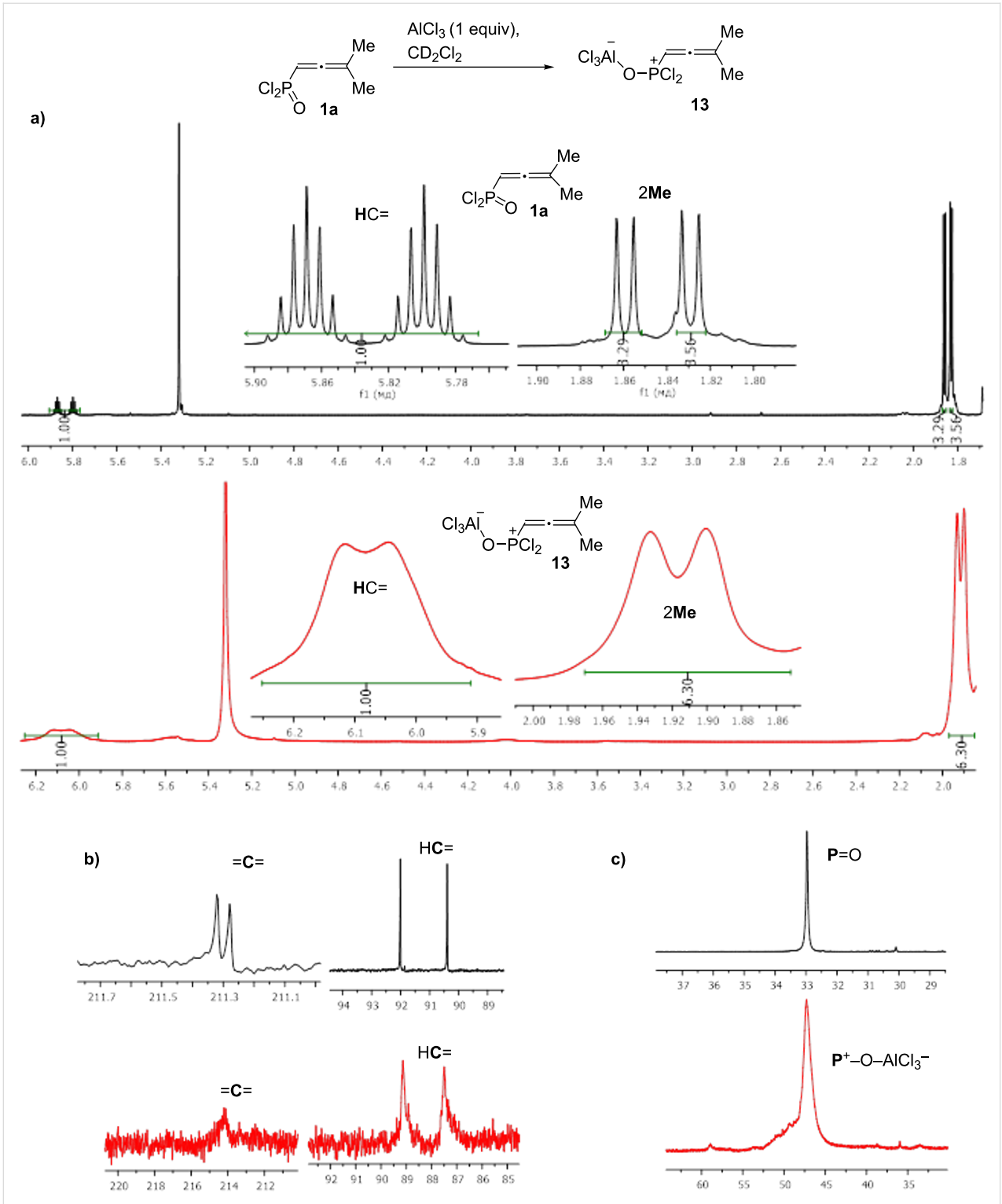

Figure 3: NMR spectra of starting allene **1a** (black) and its complex with 1 equivalent of $AlCl_3$ **13** (red) in CD_2Cl_2 at room temperature: (a) ^{1}H NMR, (b) ^{13}C NMR (selected signals, doublets due to ^{13}C–^{31}P spin–spin interaction), (c) ^{31}P NMR.

tions (Figure 3, Table 2). Despite solvation in the Brønsted superacid TfOH, the P=O group takes part in intramolecular cyclization into oxaphospholium ions (Table 1). These two different types of reaction intermediates, generated from such allenes in Brønsted and Lewis acids, lead to various reaction products.

Based on the data obtained, one may propose a plausible mechanism A for the transformation of allene **1a** in the presence of $AlCl_3$ (Scheme 9). When the first equivalent of $AlCl_3$ is added to allene **1a**, adduct **13** is formed as a result of electrophilic attack of $AlCl_3$ on the oxygen atom. The second equivalent of $AlCl_3$ is coordinated to the central atom of the allene system of the complex **13** and gives intermediate **16**. The latter, in the absence of nucleophiles (arene molecules), undergoes deprotonation from the methyl group affording butadiene **14**. Hydrolysis of the latter resulted in compounds *Z*-**9** and *E*-**10a**. Whereas, in the presence of an arene, cation **16** reacts with it leading to species **17**. The latter can be protonated with the formation of cation **18**. This species may react in two different ways. The first option is it could lead to alkene **19** and finally to compounds **11** upon methanolysis of the reaction mixture. An alternative pathway for species **18** is cyclization into indane structure **20**, which is further transformed into **21** and **12**. At the same time, an alternative mechanism B, involving the formation of the protic superacid HCl–$AlCl_3$ and its participation in the observed reaction should be considered (Scheme 10). The required catalytic amount of such superacid may be formed due to the presence of traces of HCl (byproduct in acetylene–allene rearrangement step) in the reaction mixture. Next, the protonaton of complex **13** occurs, leading to allylic cation **22**. As analogue of cation **16** (Scheme 9), the latter can interact with arenes giving hydroarylated complex **23**. Consequently, it eliminates $AlCl_3$ and is transformed into $P(O)Cl_2$ alkene **19**. The latter can further undergo a protonaton–cyclization sequence (alkene **19**→cation **24**→$P(O)Cl_2$ indane **21**). Target $P(O)OMe_2$ alkenes **11** and indanes **12** are formed during methanolysis of **19** and **21** consequently.

In accordance with both mechanisms A and B, yields of indanes **12** should be increased for substrates having electron-donating groups, Ar. Indeed, the highest yields of indanes **12** were achieved for the reactions of allene **1a** with the electron-rich arenes toluene and xylenes (Table 3, entries 2–5).

We carried out a DFT study [at the B3LYP/6-311+G(2d,2p) level of theory] for the observed $AlCl_3$-involved reactions (Scheme 9, Scheme 10, Table 4 and Supporting Information File 1 for details of DFT calculations). First, the thermochemistry (Δ*G* of reaction) for selected transformations (**1a**→**13**→**16**→**17** for mechanism A, **1a**→**13**→**22**→**23** for

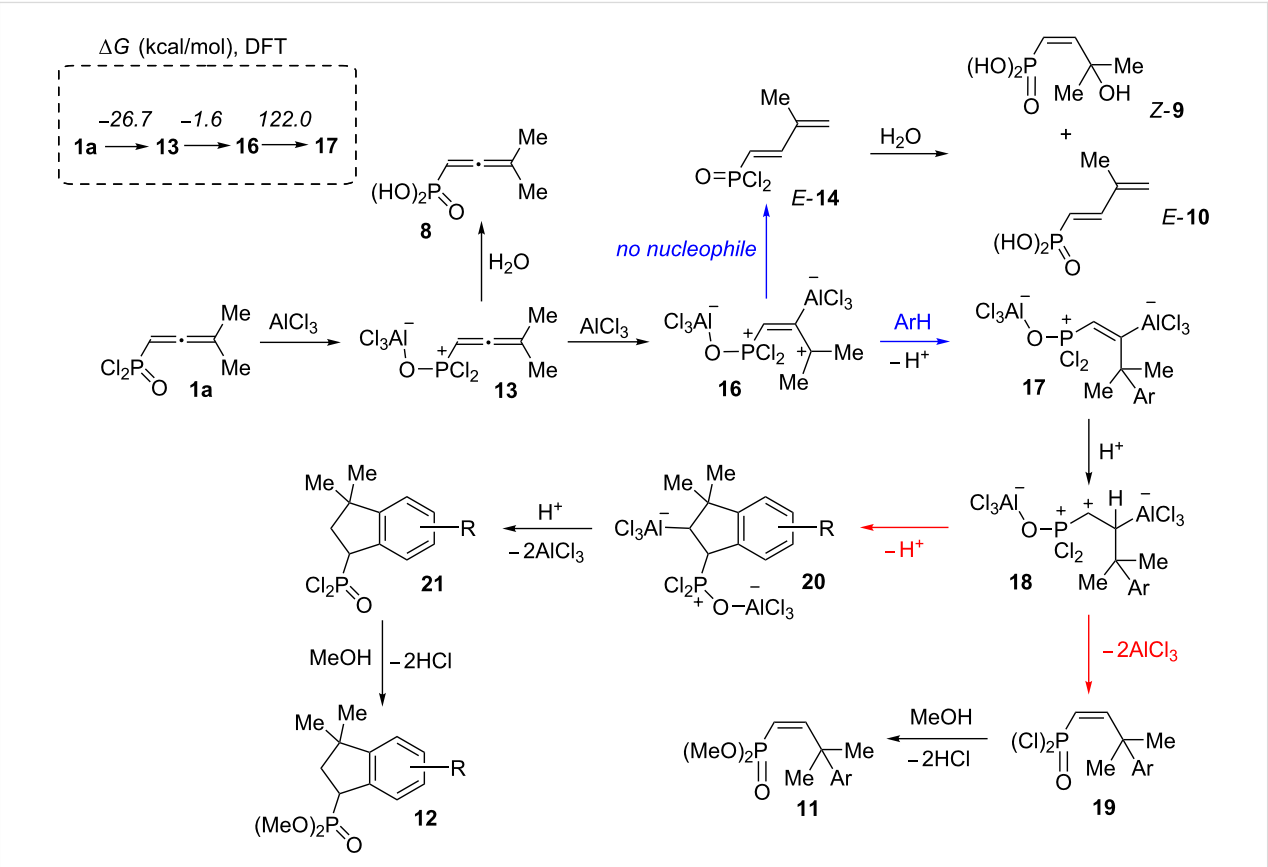

Scheme 9: Plausible reaction mechanism A for the formation of compounds **9**, **10**, **11**, **12** from aillene **1a** involving $AlCl_3$ attack on the central atom of allenic complex **13**.

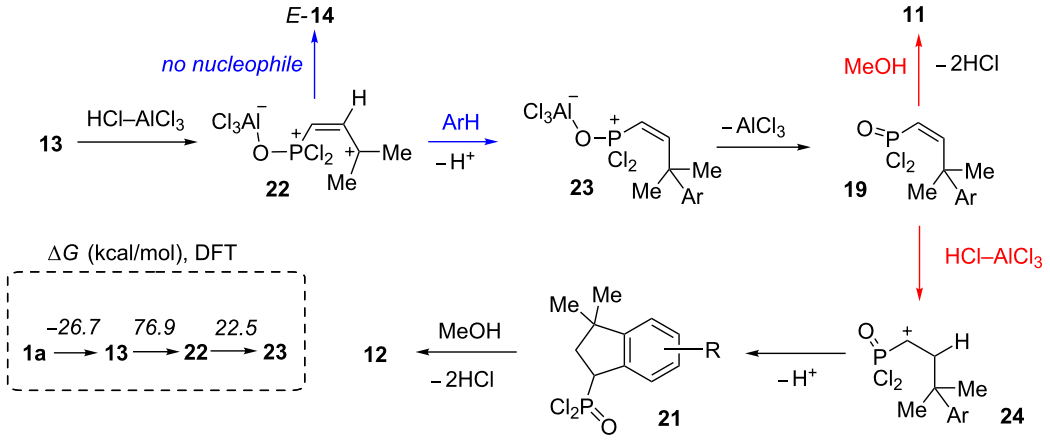

Scheme 10: Plausible reaction mechanism B of formation of compounds **11**, **12** from allene **1a** involving HCl–$AlCl_3$ attack on the central atom of allenic complex **13**.

Table 4: Comparison of selected electronic characteristics of species **16** (mechanism A) and species **22** (mechanism B) derived from allene **1a**.

mechanism A key intermediate vs *mechanism B key intermediate*

Species	ω,[a] eV	q (P),[b] e	q (C^1),[b] e	q(C^3),[b] e	k_{LUMO}(P),[c] %	k_{LUMO}(C^1),[c] %	k_{LUMO}(C^3),[c] %
16	3.42	1.78	-0.64	**0.11**	16.6	3.2	**32.1**
22	17.1	1.73	-0.52	**0.44**	0.73	7.4	**56.6**

[a]Global electrophilicity index ω = (E_{HOMO} + E_{LUMO})^2/8 (E_{LUMO} – E_{HOMO}); [b]natural charges; [c]contribution of atomic orbital into the molecular orbital.

mechanism B) was explored. Formation of complex **13** from allene **1a** and $AlCl_3$ is exergonic (−26.7 kcal/mol) and thermodynamically favorable. The arylation stage for mechanism A (**16**→**17**) is significantly less endergonic (22.6 kcal/mol) than that in mechanism **B** (**22**→**23**, 122.0 kcal/mol, Scheme 9). At the same time, formation of allylic cation **22** (mechanism B) is accompanied by positive changes in Δ*G* (76.9 kcal/mol), whereas its analogue species **16** formed with slightly negative ΔG (−1.6 kcal/mol, Scheme 10).

Next, we compared electronic characteristics (global electrophilicity indexes ω, natural charges (NBO) and atomic orbital contributions into LUMO) of species **16** and **22** as key intermediates from mechanisms A and B. The calculations reveal that both charge and orbital factors coincide in electrophilic reactivity of carbon C3 in species **16**, **22** (Scheme 9 and Scheme 10). At the same time, the carbon C3 in C-protonated intermediate **22** bears a more positive charge (0.44 e) and gives a rather big contribution into LUMO (56.6%) compared to that of **16** (0.11 e, 32.1%). Also, species **22** is five times more electrophilic than **16** according to values of ω. Visualizations of the LUMO for **16** and **22** are shown on Figure 4.

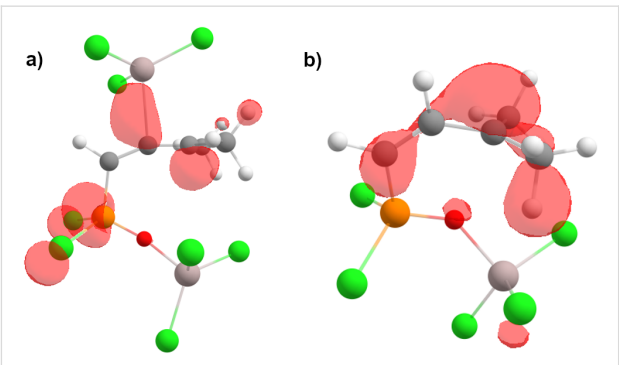

Figure 4: Visualization of LUMO, only positive values are shown, isosurface value 0.043: (a) species **16**, (b) species **22**.

Conclusion

Transformations of various phosphorylallenes under the action of strong Brønsted or Lewis acids were studied. These allenes showed different reactivity depending on the type of the acid. In the Brønsted superacid TfOH, the allenes were transformed into oxophospholium cations. Hydrolysis (or morpholinolysis) of these species afforded a series of phosphorous-containing compounds, cyclic phosphoric acids and their derivatives, and other substances. Contrarily, reactions of dichlorophosphorylallenes with the Lewis acid $AlCl_3$ proceeded through the formation of non-cyclic intermediates. Hydrolysis of the latter afforded phosphorylallyl alcohols and butadienes. For the first time, the intermolecular hydroarylation of the allene system of dichlorophosphorylallenes by arenes under the action of $AlCl_3$ was achieved. This reaction gave rise to phosphoryl-substituted alkenes and indanes. The intermediates of these reactions were investigated by means of NMR and DFT calculations, that shed light on the reaction mechanisms.

Supporting Information

Supporting Information File 1

Experimental part.
[https://www.beilstein-journals.org/bjoc/content/supplementary/1860-5397-15-151-S1.pdf]

Acknowledgement

This work was supported by the Russian Scientific Foundation (grant no. 18-13-00008). Spectral studies were performed at the Center for Magnetic Resonance, Center for Chemical Analysis and Materials Research, and Research Center for X-ray Diffraction Studies of Saint Petersburg State University, Saint Petersburg, Russia.

ORCID® iDs

Stanislav V. Lozovskiy - https://orcid.org/0000-0001-7035-0557
Alexander Yu. Ivanov - https://orcid.org/0000-0002-4228-1248
Aleksander V. Vasilyev - https://orcid.org/0000-0003-3628-1492

References

1. Krause, N.; Hashmi, A. S. K., Eds. *Modern Allene Chemistry;* Wiley-VCH: Weinheim, Germany, 2004.
2. Back, T. G.; Clary, K. N.; Gao, D. *Chem. Rev.* **2010,** *110,* 4498–4553. doi:10.1021/cr1000546
3. Yu, S.; Ma, S. *Angew. Chem., Int. Ed.* **2012,** *51,* 3074–3112. doi:10.1002/anie.201101460
4. Essid, I.; Laborde, C.; Legros, F.; Sevrain, N.; Touil, S.; Rolland, M.; Ayad, T.; Volle, J.-N.; Pirat, J.-L.; Virieux, D. *Org. Lett.* **2017,** *19,* 1882–1885. doi:10.1021/acs.orglett.7b00648
5. Berton, J. K. E. T.; Salemi, H.; Pirat, J.-L.; Virieux, D.; Stevens, C. V. *J. Org. Chem.* **2017,** *82,* 12439–12446. doi:10.1021/acs.joc.7b02227
6. Ismailov, I. E.; Ivanov, I. K.; Christov, V. C. *Molecules* **2014,** *19,* 11056–11076. doi:10.3390/molecules190811056
7. Angelov, C. M.; Enchev, D. D. *Phosphorus Sulfur Relat. Elem.* **1988,** *37,* 125–128. doi:10.1080/03086648808079026
8. Enchev, D. D. *Phosphorus, Sulfur Silicon Relat. Elem.* **2000,** *165,* 273–284. doi:10.1080/10426500008076346
9. Ivanov, I. K.; Christov, V. C. *Synth. Commun.* **2013,** *43,* 800–809. doi:10.1080/00397911.2011.609957
10. Yuan, J.; Ruan, X.; Yang, Y.; Huang, X. *Synlett* **2007,** 2871–2874. doi:10.1055/s-2007-991082
11. Macomber, R. S. *J. Org. Chem.* **1977,** *42,* 3297–3298. doi:10.1021/jo00440a021
12. Mikhailova, T. S.; Skvortsov, I. K.; Ignatiev, V. M.; Ionin, B. I.; Petrov, A. A. *Dokl. Akad. Nauk. SSSR* **1978,** *241,* 1095.
13. Lozovskiy, S. V.; Bogachenkov, A. S.; Dogadina, A. V.; Vasilyev, A. V. *Tetrahedron Lett.* **2016,** *57,* 3167–3170. doi:10.1016/j.tetlet.2016.06.026
14. Lozovskiy, S. V.; Ivanov, A. Y.; Bogachenkov, A. S.; Vasilyev, A. V. *ChemistrySelect* **2017,** *2,* 4505–4510. doi:10.1002/slct.201700637
15. Bogachenkov, A. S.; Dogadina, A. V.; Boyarskiy, V. P.; Vasilyev, A. V. *Org. Biomol. Chem.* **2015,** *13,* 1333–1338. doi:10.1039/c4ob02269f
16. Bogachenkov, A. S.; Dogadina, A. V.; Boyarskaya, I. A.; Boyarskiy, V. P.; Vasilyev, A. V. *Org. Biomol. Chem.* **2016,** *14,* 1370–1381. doi:10.1039/c5ob02143j
17. Widenhoefer, R. A. Transition metal-catalyzed hydroarylation of allenes. In *Catalytic Hydroarylation of Carbon-Carbon Multiple Bonds;* Ackermann, L., Ed.; Wiley-VCH: Weinheim, Germany, 2017; pp 361–388. doi:10.1002/9783527697649.ch9
See for a review.
18. Fang, Z.; Fu, C.; Ma, S. *Chem. – Eur. J.* **2010,** *16,* 3910–3913. doi:10.1002/chem.200903012
19. Suresh, R. R.; Swamy, K. C. K. *J. Org. Chem.* **2012,** *77,* 6959–6969. doi:10.1021/jo301149s
20. Miller, Z. D.; Montgomery, J. *Org. Lett.* **2014,** *16,* 5486–5489. doi:10.1021/ol502766q
21. Muñoz, M. P.; de la Torre, M. C.; Sierra, M. A. *Chem. – Eur. J.* **2012,** *18,* 4499–4504. doi:10.1002/chem.201103337
22. Skouta, R.; Li, C.-J. *Can. J. Chem.* **2008,** *86,* 616–620. doi:10.1139/v08-067
23. Toups, K. L.; Liu, G. T.; Widenhoefer, R. A. *J. Organomet. Chem.* **2009,** *694,* 571–575. doi:10.1016/j.jorganchem.2008.11.058
24. Tarselli, M. A.; Liu, A.; Gagné, M. R. *Tetrahedron* **2009,** *65,* 1785–1789. doi:10.1016/j.tet.2008.10.110
25. Sutherland, D. R.; Kinsman, L.; Angiolini, S. M.; Rosair, G. M.; Lee, A.-L. *Chem. – Eur. J.* **2018,** *24,* 7002–7009. doi:10.1002/chem.201800209
26. Zhang, Y. J.; Skucas, E.; Krische, M. J. *Org. Lett.* **2009,** *11,* 4248–4250. doi:10.1021/ol901759t
27. Zeng, R.; Fu, C.; Ma, S. *J. Am. Chem. Soc.* **2012,** *134,* 9597–9600. doi:10.1021/ja303790s
28. Ye, B.; Cramer, N. *J. Am. Chem. Soc.* **2013,** *135,* 636–639. doi:10.1021/ja311956k
29. Nakanowatari, S.; Mei, R.; Feldt, M.; Ackermann, L. *ACS Catal.* **2017,** *7,* 2511–2515. doi:10.1021/acscatal.7b00207
30. Fang, Z.; Fu, C.; Ma, S. *Eur. J. Org. Chem.* **2011,** 1227–1231. doi:10.1002/ejoc.201001661
31. Jin, H. J.; Kim, J. H.; Kang, E. J. *Synthesis* **2017,** *49,* 3137–3144. doi:10.1055/s-0036-1589004

BEILSTEIN JOURNAL OF ORGANIC CHEMISTRY

Superelectrophilic carbocations: preparation and reactions of a substrate with six ionizable groups

Sean H. Kennedy, Makafui Gasonoo and Douglas A. Klumpp*

Full Research Paper

Open Access

Address:
Department of Chemistry and Biochemistry, Northern Illinois University, DeKalb, IL 60178, USA

Email:
Douglas A. Klumpp* - dklumpp@niu.edu

* Corresponding author

Keywords:
cation; Friedel–Crafts; heterocycle; superacid; superelectrophile

Beilstein J. Org. Chem. **2019,** *15,* 1515–1520.
doi:10.3762/bjoc.15.153

Received: 08 March 2019
Accepted: 21 June 2019
Published: 09 July 2019

This article is part of the thematic issue "Reactive intermediates – carbocations".

Guest Editor: S. R. Hare

Abstract

A substrate has been prepared having two triarylmethanol centers and four pyridine-type substituent groups. Upon ionization in the Brønsted superacid CF_3SO_3H, the substrate undergoes two types of reactions. In the presence of only the superacid, the highly ionized intermediate(s) provide a double cyclization product having two pyrido[1,2-*a*]indole rings. With added benzene, an arylation product is obtained. A mechanism is proposed involving tetra-, penta-, or hexacationic species.

Introduction

During the 1970s and 80s, Olah and co-workers described the novel chemistry of highly-charged organic cationic species. This work lead to the concept of superelectrophilic reactivity [1-5]. Examples of superelectrophiles include the nitronium dication (**1**) and the acetylium dication (**2**, Scheme 1). Both of these species have been proposed as superelectrophilic intermediates in the reactions of nitronium (NO_2^+) and acetylium (CH_3CO^+) salts in superacids. In sufficiently acidic media, cationic electrophiles such as the nitronium ion may undergo protonation, leading to the nitronium dication (**1**), and a greatly enhanced electrophilic reactivity. In superacidic solutions, nitronium salts have been shown to react with deactivated arenes and saturated hydrocarbons (including methane) [6-9].

Numerous studies from our group and others have shown that relatively stable cationic centers – such as ammonium, phosphonium, and pyridinium groups – may also be part of superelectrophilic systems [10]. Recently, we described the chemistry of tri-, tetra-, and pentacationic electrophiles based on the triarylmethyl cation scaffold (**3–5**, Scheme 1) [11,12]. These systems utilized pyridyl rings to produce increasing amounts of positive charge adjacent to the carbocation center. Both theoretical calculations and experimental results indicated that the carbocation center undergoes a high degree of delocalization into the neighboring phenyl group. Both the trication **3** and the tetracation **4** were directly observed from FSO_3H–SbF_5 solution using low temperature NMR. Experimental observations

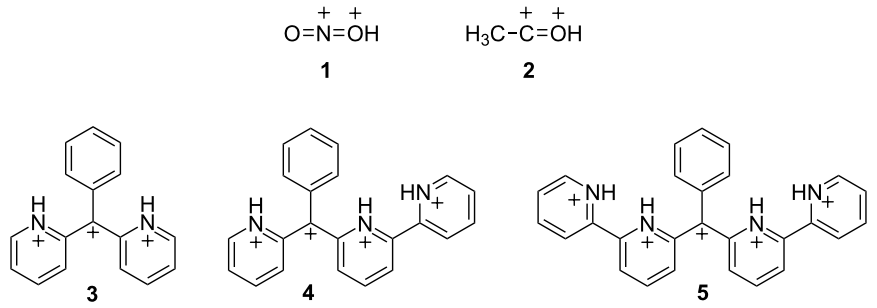

Scheme 1: Superelectrophilic species.

also revealed an exceptionally high acidity of the pyridinium N–H bonds. Here, we describe the preparation and chemistry of a substrate with six ionizable groups – four pyridyl rings and two carbinol centers.

Results and Discussion

The desired substrate was prepared in four steps from 2,6-dibromopyridine (Scheme 2). Utilizing 2-lithio-6-bromopyridne, product **6** is formed in modest yield by reaction with benzaldehyde. A nickel-catalyzed procedure gives the dipyridyl intermediate **7** [13]. This is easily oxidized to the diketone **8** and reaction of this substance with 2-lithiopyridine gives the precursor **9**. The diol **9** is a substrate with six ionizable groups.

Upon ionization in superacidic CF_3SO_3H (triflic acid), compound **9** undergoes two types of reactions. When the substrate is ionized in the presence of benzene and CF_3SO_3H, the arylation product **10** is formed as the major product (Scheme 3). Presumably, compound **10** is formed as a mixture of *meso* and *dl* stereoisomers. Similar reaction products were observed in our studies of tri-, tetra-, and pentacationic systems [11,12]. This product, **10**, is the result of charge migration involving the carbocation center and the phenyl group (vide infra). When compound **9** is treated with only superacid, the bis(pyrido[1,2-*a*]indole) **11** is formed as the major product. Likewise, the tri-, tetra-, and pentacationic systems **3**–**5** provide the pyrido[1,2-*a*]indole ring system. Interestingly, there was no evidence of the cyclization product **11** (NMR analysis) when compound **9** reacts with superacid in the presence of benzene – product **10** is formed as the major product.

These products may be explained by mechanisms involving highly ionized intermediates. It is proposed that compound **9** initially reacts in excess superacid to give the tetracationic species **12** (Scheme 4). Protonation of the hydroxy groups leads to immediate ionization and formation of the carbocation centers. For related conversions, computational and experimental data indicated that the protonated hydroxy groups (oxonium ions) are not persistent intermediates, but rather cleavage of the carbon–oxygen bond is almost instantaneous [12]. It is assumed that ionization to the carbocations occurs in a stepwise process, first providing pentacation **13** then the hexacation **14**. The product forming steps occur through either **13** or **14**. For the arylation product **10**, charge delocalization at the carbocation leads to nucleophilic attack at the *para*-position of the phenyl group. This S_EAr step is followed by protonation at the methine posi-

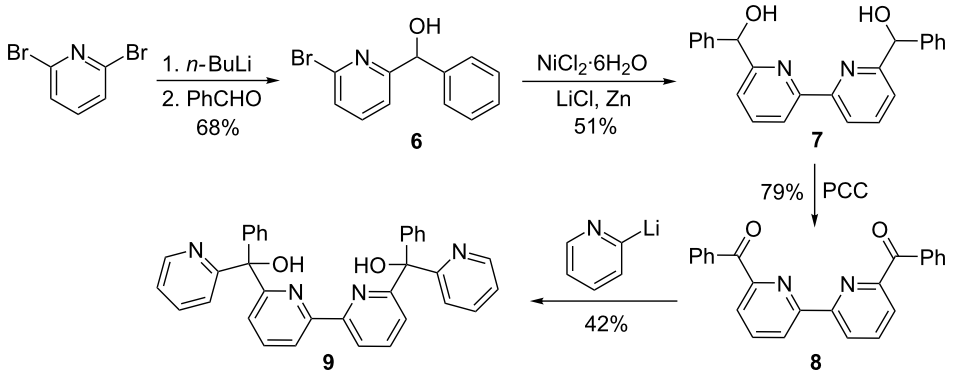

Scheme 2: Synthesis of diol substrate **9**.

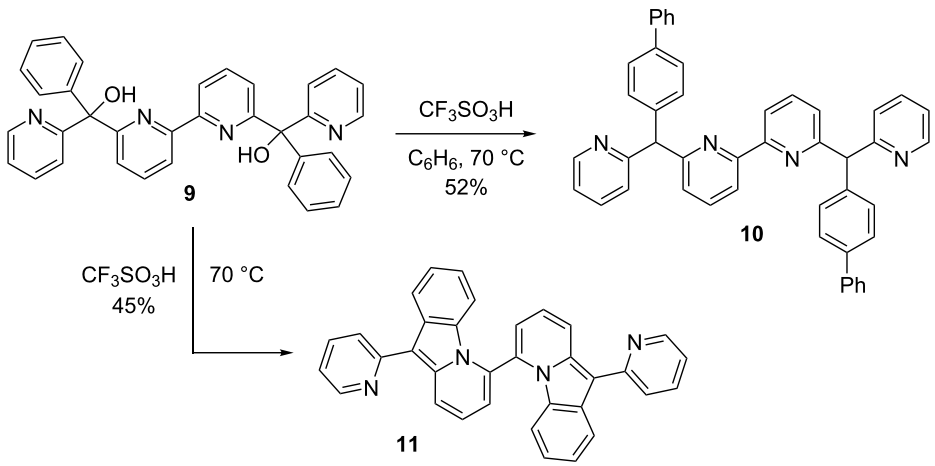

Scheme 3: Isolated yields of products from diol **9**.

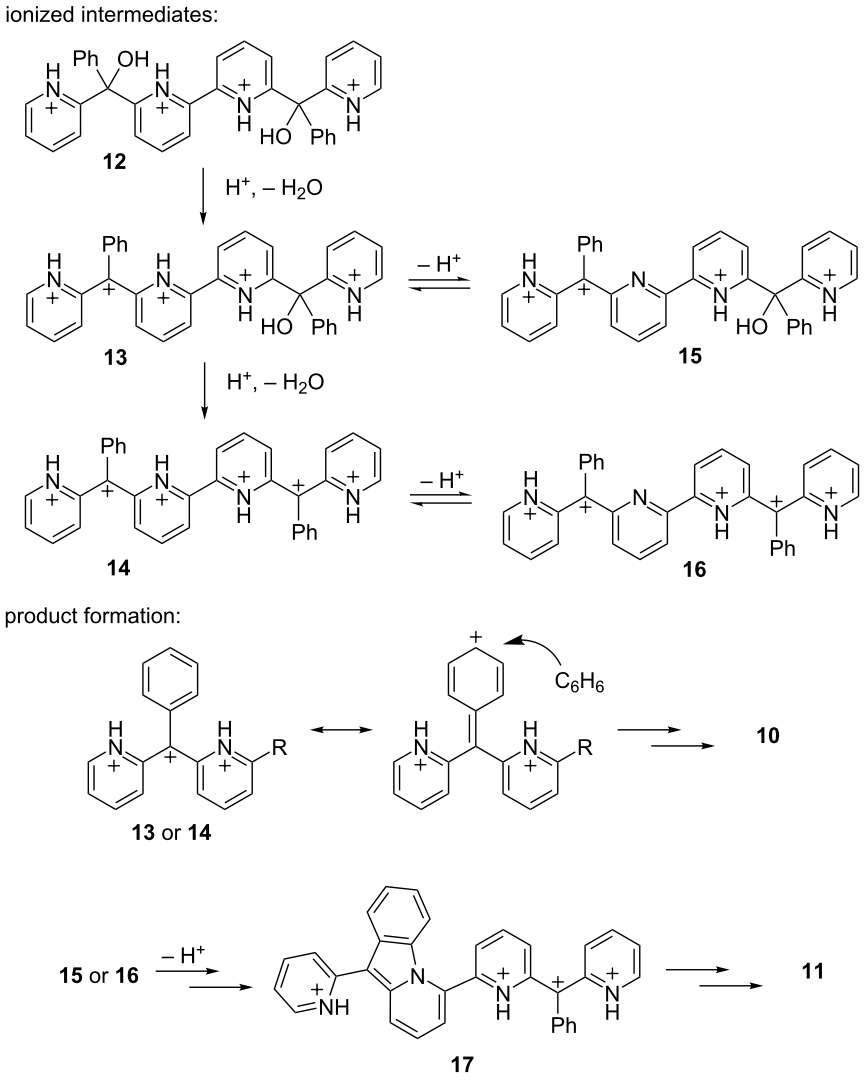

Scheme 4: Proposed mechanisms leading to products **10** and **11**.

tion and deprotonation of the *para*-carbon to complete the arylation step. For the cyclization product **11**, theoretical calculations indicate that cyclization requires deprotonation at the pyridinium ring [11]. Thus, either the tetracation **15** or the pentacation **16** is the likely precursor to the pyrido[*1,2-a*]indole ring system. The conversion to product **11** also involves a stepwise process – initially forming compound **17** then a second cyclization gives the final product **11**.

As noted above, no cyclization product **11** was observed when the chemistry was done in the presence of benzene. Only product **10** was obtained. This observation is in stark contrast to our earlier results involving both the tetracation **4** and pentacation **5**. When these highly charged ions are generated in CF_3SO_3H and C_6H_6, significant quantities of the cyclization products are formed with the respective arylation products. For example, alcohol **18** provides a mixture of products **19** and **20** in a 32:68 ratio, presumably through the pentacation **5** (Scheme 5). Even with the use of the stronger Brønsted acid, CF_3SO_3H–SbF_5, significant quantities of the cyclization product **20** are observed. This raises an obvious question: why does substrate **9** provide exclusively the arylated product **10** in the presence of benzene, while substrate **18** leads to a significant proportion of cyclization product **20**?

Our proposed mechanism of cyclization involves deprotonation of an N–H bond at the pyridinium ring. Although pyridinium deprotonation is not generally expected in a Brønsted superacid, it can occur in these systems because of the large amount of cationic charge on these structures. In comparing the chemistry of compounds **9** and **18**, compound **9** can lead to the hexacationic intermediate **14** while compound **18** can lead to the pentacationic intermediate **5**. Examination of these two structures suggests that the phenyl groups have a profound effect on stabilizing the ions. Thus, the hexacationic system **14** is stabilized by two phenyl groups, while the pentacationic system **5** has one stabilizing phenyl group (Scheme 6). The ratio of charges is 2:1 (pyridinium/benzylic carbocation) for the hexacation **14**, while the ratio of charges is 4:1 (pyridinium/benzylic carbocation) for the pentacation **5**. Similarly, we previously reported good chemoselectivity for trication **3** – no cyclization product observed in the presence of benzene – but poor chemoselectivity for the tetracation **4**. The ratio of charges in these systems are consistent: a charge ratio of 2:1 shows good chemoselectivity (trication **3**), while a charge ratio of 3:1 shows poor chemoselectivity (tetracation **4**). As we previously reported, a reaction of tetracation **4** with benzene in CF_3SO_3H leads to a mixture of arylated product (52%) and cyclization product (48%). Thus, we observed clean arylation chemistry when the

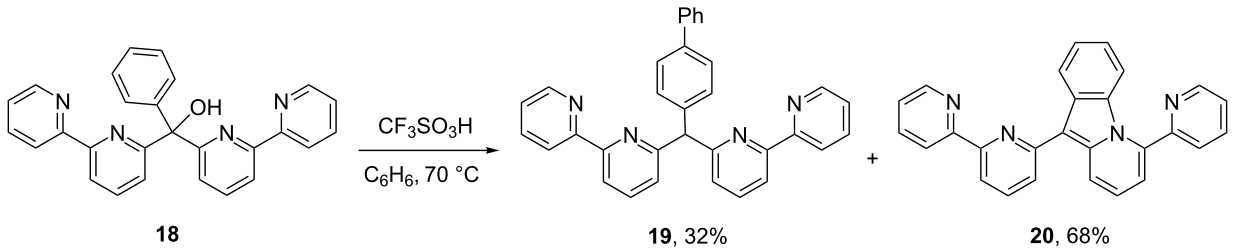

18 **19**, 32% **20**, 68%

Scheme 5: Products and relative yields from the reaction of alcohol **18** with CF_3SO_3H and C_6H_6 [12].

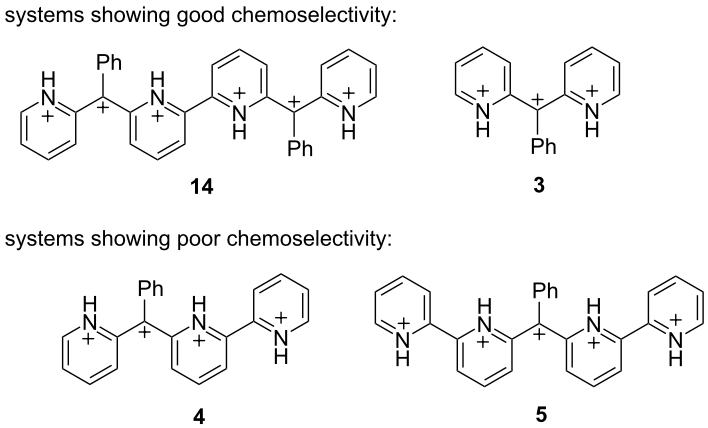

Scheme 6: Comparison of superelectrophilic carbocations (**3–5** and **14**) and their chemistry.

carbocation sites are flanked by not more than two pyridinium groups. This also means that increasing the number of adjacent pyridinium groups destabilizes the system as a whole and leads to greater N–H deprotonation. Tetracation **4** and pentacation **5** tend to undergo N–H deprotonation more readily, and consequently, this leads to rapid cyclization reactions.

Regarding the site of deprotonation, hexacation **14** could potentially undergo N–H deprotonation at the inside pyridinium ring (**16**) or the outside pyridinium ring (**21**, Scheme 7). While inside deprotonation should give the observed cyclization product **11**, outside deprotonation would give an entirely different product, one having the pyrido[1,2-*a*]indole ring at the end of the structure. Compound **11** is the only major product observed from the superacid-promoted reaction of diol **9**. This suggests outside deprotonation – and formation of ion **21** – does not occur.

The preference for inside deprotonation may be understood to be a consequence of charge–charge repulsive effects. In the case of **21**, the five cationic charges are on neighboring positions, while in the case of **16**, the five cationic charges are separated into groups of three and two charges. The increased stability of the separated cationic charge is evident in the DFT calculated energies of the ions. At the B3LYP 6-311G (d,p) level, ion **16** is calculated to be 32.7 kcal·mol^{-1} more stable than ion **21** [8]. Thus, highly charged organic ions may benefit by having groups of charges separated into smaller clusters rather than having all of the charges grouped together.

Conclusion

We have prepared a substrate with six ionizable sites. Reaction of the substrate in superacidic CF_3SO_3H leads to cyclization or arylation products, depending on the presence or absence of benzene. A mechanism is proposed involving tetra-, penta-, and hexacationic reactive intermediates. Most notably, this system shows remarkably good chemoselectivity in its reaction with benzene (only arylation product is observed). This is attributed to the presence of two carbocationic sites stabilized by benzylic-type resonance. Thus, molecular structures having a very large overall charge may be viable if stabilizing groups are incorporated into the structure.

Experimental

General. All reactions were performed using oven-dried glassware under an argon atmosphere. Trifluoromethanesulfonic acid (triflic acid) was freshly distilled prior to use. All commercially available compounds and solvents were used as received. ^{1}H and ^{13}C NMR were done using either 300 MHz or 500 MHz spectrometer; chemical shifts were made in reference to NMR solvent signals. Mass spectra were obtained from a commercial analytical laboratory. The synthesis of compound **9** is detailed in Supporting Information File 1.

Preparation of 6,6'-bis([1,1'-biphenyl]-4-yl(pyridin-2-yl)methyl)-2,2'-bipyridine (10): In a pressure tube at 25 °C, compound **9** (52.2 mg, 0.10 mmol) was dissolved in benzene (1 mL, 11.2 mmol), stirred for 5 min before triflic acid (1 mL, 11 mmol) was slowly added and the tube was then tightly closed. Following 24 h of stirring at 60–70 °C, the reaction was cooled to room temperature, poured on about 10 g of ice and then neutralized with 10 M NaOH solution. The resulting aqueous solution was then partitioned between chloroform and distilled water in a separatory funnel. The aqueous fraction was subjected to two further extractions after which the organic fractions were combined, washed with brine, dried over anhydrous sodium sulfate and filtered. The solvent was removed by rotary evaporation and the product purified by column chromatography (R_f 0.21, hexane/ethyl acetate 1:1). Compound **10** was isolated in 52% yield as oil. ^{1}H NMR (300 MHz, $CDCl_3$) δ 5.85 (s, 1H), 7.17–7.21 (m, 1H), 7.30–7.51 (m, 9H), 7.53–7.60 (m, 4H), 7.64–7.70 (m, 1H), 8.61 (d, J = 4.02 Hz, 1H); ^{13}C NMR (75 MHz, $CDCl_3$) δ 60.7, 121.9, 123.1, 124.3, 126.1, 127.1, 127.28, 127.33, 128.8, 129.6, 136.8, 138.8, 139.9, 140.2, 140.7, 141.4, 149.3, 161.1, 163.4; low-resolution ESIMS *m*/*z*: 643 [M + 1], 553, 477, 475, 401, 324, 323; high-resolution CIMS *m*/*z*: [M + 1] calcd for $C_{46}H_{35}N_4$, 643.2862; found, 643.2856.

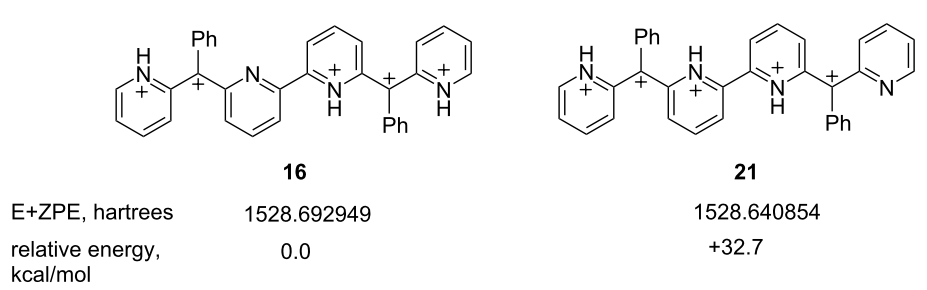

Scheme 7: DFT calculated relative energies of pentacations **16** and **21** [14].

Preparation of 10,10'-di(pyridin-2-yl)-6,6'-bipyrido[1,2-a]indole, (11): In a pressure tube at 25 °C, compound **9** (200.1 mg, 0.481 mmol) was dissolved in triflic acid (1 mL, 11 mmol) and the tube was then tightly closed. Following 24 h of stirring at 60–70 °C, the reaction was cooled to room temperature, poured on about 10 g of ice and then neutralized with 10 M NaOH solution. The resulting aqueous solution was then partitioned between chloroform and distilled water in a separatory funnel. The aqueous fraction was subjected to two further extractions after which the organic fractions were combined, washed with brine, dried over anhydrous sodium sulfate and filtered. The solvent was removed by rotary evaporation and the product purified by column chromatography (R_f 0.30, hexane/ethyl acetate 1:1). The product **11** was isolated in 45% yield as brown oil. ^{1}H NMR (300 MHz, $CDCl_3$) δ 6.81–6.88 (m, 2H), 7.19 (t, J = 4.65 Hz, 1H), 7.35–7.40 (m, 1H), 7.51 (t, J = 7.50 Hz, 1H), 7.75– 7.82 (m, 2H), 8.24–8.29 (m, 2H), 8.81 (d, J = 2.55 Hz, 1H), 9.15 (d, J = 8.79 Hz, 1H); ^{13}C NMR (75 MHz, $CDCl_3$) δ 107.2, 116.0, 116.1, 116.7, 118.1, 119.2, 120.20, 120.28, 123.3, 123.6, 124.2, 128.3, 131.9, 136.4, 138.1, 149.7, 154.4; low-resolution ESIMS m/z: 487 [M + 1], 397, 353, 320, 319, 279, 244; high-resolution CIMS m/z: [M + 1], calcd for $C_{34}H_{23}N_4$, 487.1923; found, 487.1917.

Supporting Information

Supporting Information File 1

Experimental procedures, compounds characterization, and NMR spectra; computational methods and results.
[https://www.beilstein-journals.org/bjoc/content/supplementary/1860-5397-15-153-S1.pdf]

Acknowledgements

This work was supported by the National Science Foundation (1300878). We gratefully acknowledge this support.

ORCID® iDs

Douglas A. Klumpp - https://orcid.org/0000-0001-5271-699X

References

1. Olah, G. A.; Germain, A.; Lin, H. C.; Forsyth, D. A. *J. Am. Chem. Soc.* **1975,** *97,* 2928–2929. doi:10.1021/ja00843a067
2. Olah, G. A.; Prakash, G. K. S.; Donald, P.; Loker, K. B.; Lammertsma, K. *Res. Chem. Intermed.* **1989,** *12,* 141–159. doi:10.1163/156856789x00104
3. Olah, G. A. *Angew. Chem., Int. Ed. Engl.* **1993,** *32,* 767–788. doi:10.1002/anie.199307673
4. Olah, G. A.; Klumpp, D. A. *Acc. Chem. Res.* **2004,** *37,* 211–220. doi:10.1021/ar020102p
5. Olah, G. A.; Klumpp, D. A. *Superelectrophiles and Their Chemistry;* John Wiley and Sons: Hoboken, NJ, 2008. doi:10.1002/9780470185124
6. Olah, G. A.; Lin, H. C. *J. Am. Chem. Soc.* **1974,** *96,* 549–553. doi:10.1021/ja00809a035
7. Olah, G. A.; Lin, H. C. *Synthesis* **1974,** 444–445. doi:10.1055/s-1974-23344
8. Olah, G. A.; Orlinkov, A.; Oxyzoglou, A. B.; Prakash, G. K. S. *J. Org. Chem.* **1995,** *60,* 7348–7350. doi:10.1021/jo00127a048
9. Olah, G. A.; Wang, Q.; Orlinkov, A.; Ramaiah, P. *J. Org. Chem.* **1993,** *58,* 5017–5018. doi:10.1021/jo00070a049
10. Klumpp, D. A. Activation of Electrophilic Sites by Adjacent Cationic Groups. In *Recent Developments in Carbocation and Onium Ion Chemistry;* Laali, K., Ed.; ACS Symposium Series 395; American Chemical Society: Washington, DC, 2007; pp 144–159. doi:10.1021/bk-2007-0965.ch008
11. Naredla, R. R.; Zheng, C.; Nilsson Lill, S. O.; Klumpp, D. A. *J. Am. Chem. Soc.* **2011,** *133,* 13169–13175. doi:10.1021/ja2046364
12. Gasonoo, M.; Naredla, R. R.; Nilsson Lill, S. O.; Klumpp, D. A. *J. Org. Chem.* **2016,** *81,* 11758–11765. doi:10.1021/acs.joc.6b02220
13. Newkome, G. R.; Joo, Y. J.; Evans, D. W.; Pappalardo, S.; Fronczek, F. R. *J. Org. Chem.* **1988,** *53,* 786–790. doi:10.1021/jo00239a018
14. *Gaussian 09,* Revision E.01; Gaussian, Inc.: Wallingford, CT, 2009.

License and Terms

BEILSTEIN JOURNAL OF ORGANIC CHEMISTRY

Transient and intermediate carbocations in ruthenium tetroxide oxidation of saturated rings

Manuel Pedrón[1], Laura Legnani[2], Maria-Assunta Chiacchio[2], Pierluigi Caramella[3], Tomás Tejero[4] and Pedro Merino[*1]

Full Research Paper

Open Access

Address:
[1]Instituto de Biocomputación y Física de Sistemas Complejos (BIFI), Campus San Francisco, Universidad de Zaragoza, 50009 Zaragoza, Spain, [2]Dipartimento di Scienze del Farmaco, University of Catania, V.le A. Doria 6, 95125 Catania, Italy, [3]Dipartimento di Chimica, Università di Pavia, Via Taramelli, 12, 27100, Pavia, Italy and [4]Instituto de Síntesis Química y Catálisis Homogénea (ISQCH), Campus San Francisco, Universidad de Zaragoza-CSIC, 50009 Zaragoza, Spain

Email:
Pedro Merino[*] - pmerino@unizar.es

* Corresponding author

Keywords:
alkanes; carbocations; DFT; oxidations; ruthenium tetroxide

Beilstein J. Org. Chem. **2019,** *15,* 1552–1562.
doi:10.3762/bjoc.15.158

Received: 02 March 2019
Accepted: 02 July 2019
Published: 11 July 2019

This article is part of the thematic issue "Reactive intermediates – carbocations".

Guest Editor: S. R. Hare

Abstract

The ruthenium tetroxide-mediated oxidation of cyclopentane, tetrahydrofuran, tetrahydrothiophene and *N*-substituted pyrrolidines has been studied computationally by DFT and topological (analysis of the electron localization function, ELF) methods. In agreement with experimental observations and previous DFT calculations, the rate-limiting step of the reaction takes place through a highly asynchronous (3 + 2) concerted cycloaddition through a single transition structure (one kinetic step). The ELF analysis identifies the reaction as a typical one-step-two-stages process and corroborates the existence of a transient carbocation. In the case of pyrrolidines, the carbocation is completely stabilized as an energy minimum in the form of an iminium ion and the reaction takes place in two steps.

Introduction

Ruthenium-catalyzed oxidations [1,2] and, in particular, those involving ruthenium tetroxide [3,4] occupy a privileged position among the modern oxidation methods due to their versatility regarding functional groups that can be oxidized and formed [5]. Alkane functionalization continues to be a current challenge in organic synthesis [6] and oxidation with ruthenium tetroxide allows to introduce an oxygenated functionality (alcohol or carbonyl) into a saturated carbon skeleton [7]. Moreover, if oxygen or nitrogen atoms are present, the reaction leads to the formation of esters [8,9] or amides [10,11], respectively (Scheme 1). The reaction is typically performed by preparing ruthenium tetroxide in situ from ruthenium species in

lower oxidation states ($RuCl_3$ or RuO_2) and an oxidant such as $NaIO_4$ [8]. Under these conditions RuO_4 reacts with the alkane to form intermediate species **I** that evolves to the alcohol and RuO_3, which is re-oxidized to re-start the catalytic cycle (Scheme 1) [12]. Depending on the substrates and reaction conditions (re-oxidant, solvent, temperature) the alcohol can be oxidized to the corresponding carbonyl derivative [13,14].

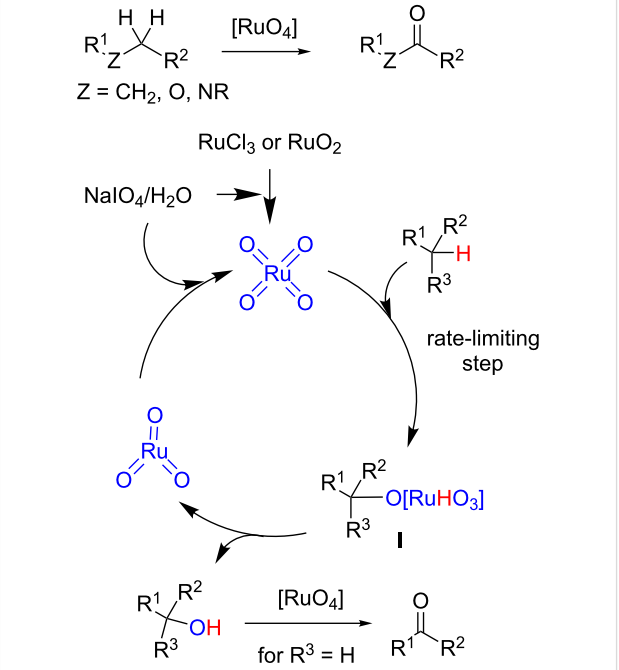

Scheme 1: Oxidation of alkanes with RuO_4.

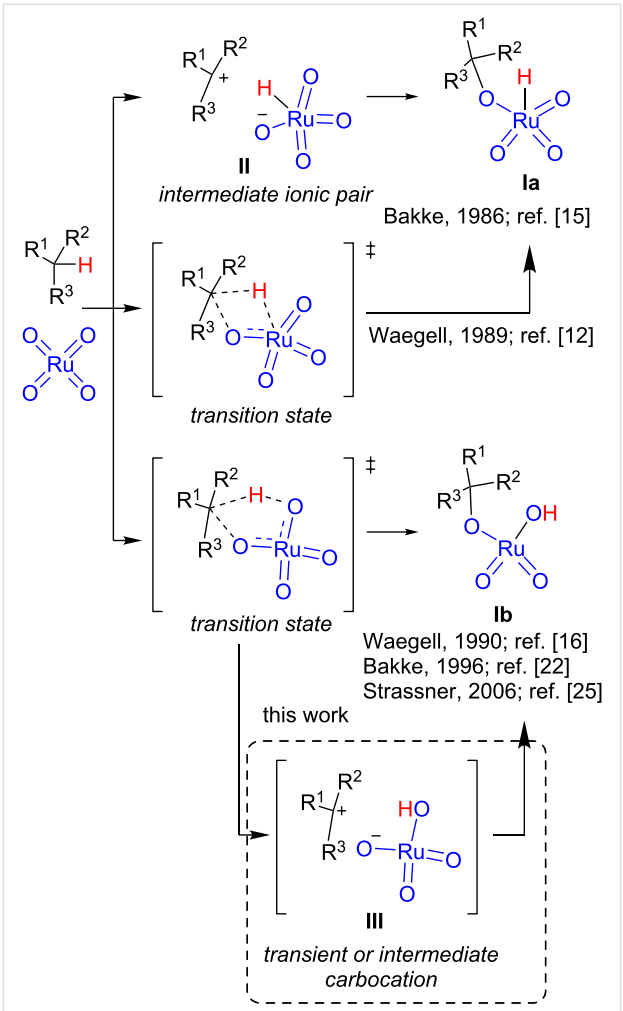

Scheme 2: Mechanisms for RuO_4 oxidation of alkanes.

The rate-limiting step of the catalytic cycle illustrated in Scheme 1 is the initial reaction between RuO_4 and the alkane, and it has been studied both experimentally and computationally having some initial controversy. The first studies were reported by Bakke et al. in 1986 who suggested the formation of intermediate ionic species on the basis of kinetic isotopic effects and solvent and substituents effects (Scheme 2) [15]. Three years later, Waegell et al. proposed a (2 + 2) concerted mechanism [12], although the intimate nature of the organometallic intermediates was not completely elucidated [16]. After some discussion in which Bakke et al. confirmed their initial proposal [17,18] and Waegell et al. proposed a new (3 + 2) asynchronous concerted mechanism [19,20], both groups converged to the latter proposed mechanism when Bakke et al. changed the interpretation of their kinetic isotopic experiments [21-24].

The (3 + 2) concerted mechanism was further confirmed by DFT calculations [25] which were also in agreement with the earlier experiments of Bakke et al. [15]. The computational study also confirmed the hydroxide adduct **Ib** as the active intermediate formed in the reaction. However, Petride et al. have demonstrated that iminium cations are intermediates in the RuO_4-mediated oxidation of tertiary amines [26] by trapping them with cyanide anion [27,28]. These results point out the formation of transient carbocations **III** that can be stabilized by the presence of heteroatoms in the alpha position. The formation of transient carbocations do not contradict, necessarily, the proposed asynchronous concerted mechanism. A deeper analysis of the full path of the reaction using MD calculations [29] would be needed in order to assess *the synchronicity* and life time of transient species [30]. The recent use of MD simulations has demonstrated that a single transition state can lead to different products in a ratio that depends on reaction dynamics [31-33]. The study of molecular dynamics trajectories has allowed characterization of ambimodal transition states in reactions involving carbocations [34,35].

We have demonstrated computationally the presence of transient carbocations in reactions taking place in one kinetic step

including asynchronous concerted cycloadditions [36] and SN_2-type reactions [37]. Moreover, the real existence of transient carbocations – which are not energy minima – predicted computationally has also been recently proven experimentally in a reaction with an only transition state in which a planar transient species is developed during the reaction [38]. The formation of transient carbocations developed along the reaction course cannot be detected by the calculation of stationary points alone. The use of topological methods, in particular the analysis of the electron localization function (ELF) [39,40] is an excellent approach to evaluate the synchronicity of organic reactions [41,42] and consequently, to predict the formation of transient carbocations [43].

In this work, we report a computational study of the RuO_4-mediated oxidation of cyclopentane, tetrahydrofuran, tetrahydrothiophene, and *N*-methyl- and *N*-benzylpyrrolidine to evaluate the extension in which transient carbocations can be formed (and whether they can become energy minima) during the rate-limiting step (Scheme 3). The RuO_4 oxidation of cyclopentane [44] and tetrahydrofuran [45] have been experimentally reported as well as the oxidation of *N*-acylpyrrolidines to the corresponding lactams [46]. Admittedly, the oxidation of tetrahydrothiophene has been approached only computationally since in that case the sulfur atom would be more easily oxidized. Since the general mechanism consisting of a (3 + 2) transition state has been confirmed as the preferred one [25], we restricted the study to this approach.

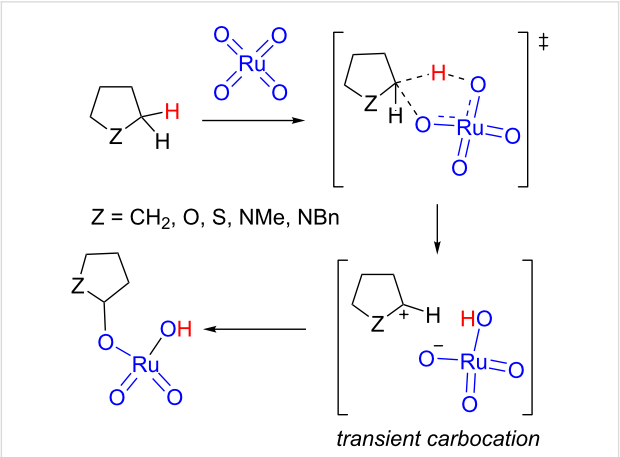

Scheme 3: Oxidation of saturated five-membered (hetero)cyclic compounds.

Computational Methods

The procedures are analogous to those previously reported [43]. All of the calculations were performed using the Gaussian 09 program [47]. Computations were done using the B3LYP functional [48,49] in conjunction with Grimme's dispersion correction [50,51] (henceforth referred to as B3LYP-d3bj). The standard basis set Def2SVP was employed [52,53]. For the purpose of comparison optimizations at gas phase and considering solvent effects (both acetonitrile and water, CPCM [54,55]) were carried out. The optimizations were carried out using the Berny analytical gradient optimization method [56]. Minimum energy pathways for the reactions studied were found by the corresponding IRC analysis [57], using the Hratchian–Schlegel algorithm [58]. The individual reactions involved in the study are bimolecular processes. In order to avoid errors due to entropic effects when comparing all stationery points in an only energy diagram, a correction to free energy was made by substracting Strans contribution and considering a 1 M concentration [59]. Single point calculations at the 3ξ level of theory, using the Def2TZVP basis set and considering solvent effects, were carried out over optimized geometries to obtain more accurate energy values. The electronic structures of stationary points were analyzed by the topological analysis of the gradient field of electron localization function (ELF) [39,40,60-66]. The ELF study was performed with the TopMod program [67] using the corresponding monodeterminantal wavefunctions of all the structures of the IRC. Structural representations were generated using CYLView [68]. The models used for calculations are those indicated in Scheme 3.

Results and Discussion

We first studied the oxidations of cyclopentane (**R1**), tetrahydrofuran (**R2**) and tetrahydrothiophene (**R3**, Scheme 4). The geometries of all stationary points were optimized at the

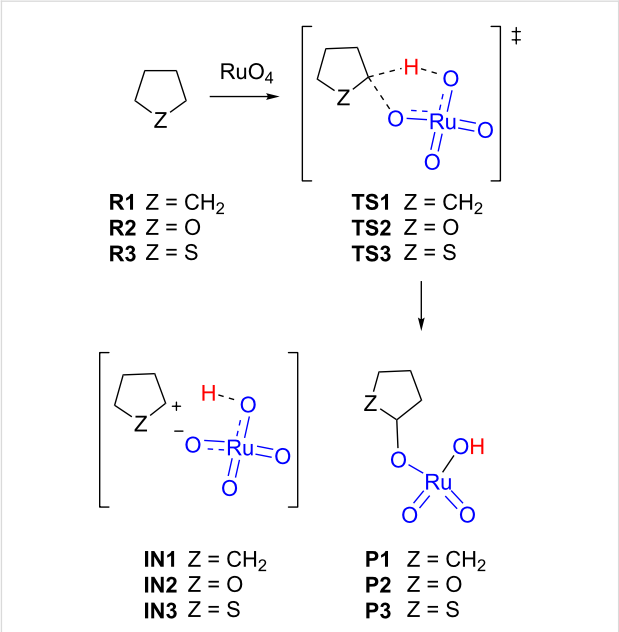

Scheme 4: Rate-limiting step for the oxidation of cyclopentane (**R1**), tetrahydrofuran (**R2**) and tetrahydrothiophene (**R3**).

B3LYP-d3bj/Def2SVP level of theory in the gas phase and considering solvent effects for acetonitrile and water and their corresponding energy values were calculated at the same level. Since the experimental conditions for the oxidation reactions usually involve a polar medium containing water, all discussions were based on data obtained considering solvent effects for water (for the results using other levels of theory see Supporting Information File 1). We located the corresponding transition structures **TS1**, **TS2** and **TS3**. Any attempt to locate (and optimize) ionic pairs **IN1**, **IN2** and **IN3** failed and, in all cases, the optimization ends at the corresponding products **P1**–**3**, clearly indicating that those ionic pairs are not stable as energy minima even in highly polar conditions (modelled using continuum water solvent).

The obtained energy barriers were 14.6, 6.0 and 7.5 kcal/mol for **TS1**, **TS2** and **TS3**, respectively, predicting an easier oxidation for the heterocyclic compounds. Similar differences between the barriers were obtained in acetonitrile (barriers of 16.6, 8.0 and 8.8 kcal/mol for **TS1**, **TS2** and **TS3**, respectively); the highest observed barriers with respect to water are in agreement with a highly polar reaction.

The corresponding transition structure for cyclopentane **TS1** showed a typical geometry for an asynchronous concerted reaction (Figure 1) in agreement with that observed in the previous study carried out at the B3LYP/6-31G(d) level of theory with implicit MeCN solvent [25]. In that study, the forming/breaking bond distances (estimated for decalines in acetonitrile and acetone) were in the following ranges: the C–H bonds were 1.37–1.41 Å, the O–H bonds were 1.19–1.22 Å, and the C–O bonds were 2.57–2.84 Å. The observed values for **TS1** in water (C–H: 1.34 Å; O–H: 1.24 Å and C–O: 2.65 Å) and acetonitrile (C–H: 1.34 Å; O–H: 1.24 Å and C–O: 2.64 Å) were similar, but placing the hydrogen atom slightly closer to the carbon atom. Similar distances for the C–H–O system were found for **TS2** (C–H: 1.30 Å and O–H: 1.30 Å) and **TS3** (C–H: 1.33 Å and O–H: 1.23 Å), corresponding to tetrahydrofuran and tetrahydrothiophene, respectively. On the other hand, the C–O distance increased to 3.00 Å in **TS2** and to 3.15 Å in **TS3** (similar data were found in acetonitrile, see Supporting Information File 1) clearly indicating a delay in the formation of the C–O bond. This situation is compatible with the stabilization of a developing positive charge at the carbon atom by a mesomeric effect of the α-heteroatom. Nevertheless, the corresponding IRCs for the three transition structures confirmed a concerted reaction connecting the corresponding encounter pairs **EP1**, **EP2** and **EP3** (see Supporting Information File 1), formed from reagents **R1**–**3** and ruthenium(IV) tetroxide, with **P1**, **P2** and **P3**, respectively. A close inspection of the IRCs revealed a shoulder characteristic of a transient carbocation [23] which is more pronounced following the sequence **R1** < **R2** < **R3**. The preliminary analysis of the evolution of bonds along those IRCs further confirmed a high asynchronicity, showing a substantial delay in the formation of the C–O bond with respect to the H transfer from the C atom to the O atom, and following the sequence **TS1** < **TS2** < **TS3** (Figure 1, red arrows).

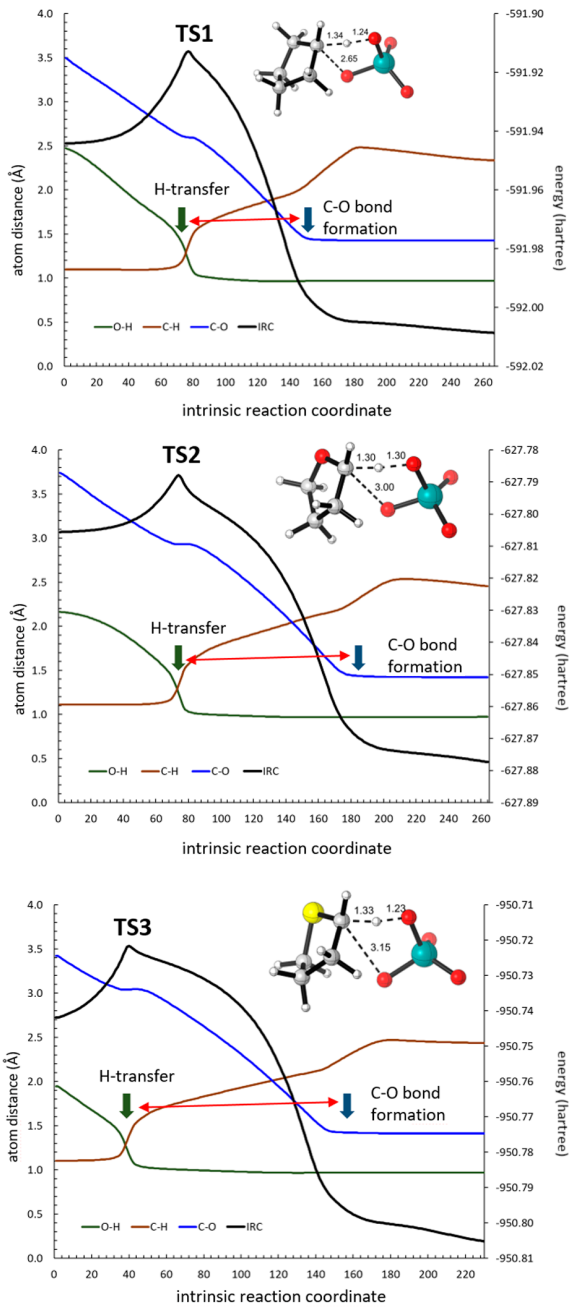

Figure 1: Optimized (B3LYP-d3bj/Def2SVP/cpcm=MeCN) geometries of transition structures corresponding to the oxidation of cyclopentane (**TS1**), tetrahydrofuran (**TS2**) and tetrahydrothiophene (**TS3**). The IRC (black trace) and O–H (green trace), C–H (brown trace), and C–O (blue trace) distances are also given. The double red arrow indicates the delay between H transfer and C–O bond formation.

Even though the above data clearly point out to a typical one-step-two-stage process [69-71] in which the bonds are broken and formed in two separate events, only a topological analysis of the ELF will provide the exact moment in which those events take place and provide evidences of the formation of a transient carbocation. The ELF analysis [39,40,72,73] allows calculation of the so-called basins of attractors [74], that are the areas in which the probability of finding an electron pair is maximal. Monosynaptic and disynaptic basins correspond to separate atoms and bonds, respectively. When a bond is formed, two monosynaptic basins merge into a new disynaptic basin.

The complete ELF analyses of the IRCs corresponding to **TS1**, **TS2** and **TS3** have allowed identifying changes in the electron distribution of atoms and bonds during the reaction coordinate and the precise moment in which bonds are broken and formed.

The ELF analysis of the oxidation of cyclopentane (Figure 2) showed an asynchronous concerted process with the transition state at point 77 (29% of IRC). Breaking of the C1–H bond is immediately followed by H transfer (point 78) and O3–H bond formation (point 81). The formation of the second C–O bond takes place at point 128 (48% of IRC). The gap between H transfer and C1–O6 bond formation (from point 81 to point 127, corresponding to 17% of IRC) is compatible with the existence of a transient carbocation at C1. Nevertheless, the reaction might also be considered just an asynchronous concerted process with a clear partial charge development during the formation of O3–H and C1–O6 bonds that takes place in two separate events.

The stabilization of the above-mentioned transient carbocation can be achieved by introducing heteroatoms. The ELF analysis corresponding to the oxidation of tetrahydrofuran (Figure 3A) again showed a typical one-step-two-stage situation. In this case, the gap between the H transfer and the formation of C1–O6 bond (from point 77 to point 157, corresponding to a 30% of the IRC) is larger than that of cyclopentane (corresponding to a 17% of IRC) as a consequence of the stabilizing effect of the incipient positive charge exerted by the oxygen atom. The effective existence of a transient carbocation is supported by the disappearance of V(C1) and the trigonal planar geometry observed for C1 in the above indicated gap. The evolution of the electron population is in clear agreement with the development of a partial positive charge at C1 (+0.25 at point 100). The oxidation of tetrahydrothiophene reflects the same situation, but to a greater degree (Figure 3B).

Interestingly, the ELF analyses evidence the high polarity of Ru–O bonds by assigning about 7e to the oxygen atoms. Because of this, during the reaction coordinate an increase of only 1e is assigned to Ru for which about 12e (coming from 4e of valence directly assigned plus 8e from the last layer $4s^2 4p^6$) have been initially assigned (Figure 4). Although this assignment does not correlate with the classical valence concept of 8e for Ru(VIII) it actually reflects a more real situation.

As stated above, attempts of locating the corresponding ion pairs failed, ending at the final **P1**–**3** products and confirming that they are not stationary points. However, this does not mean

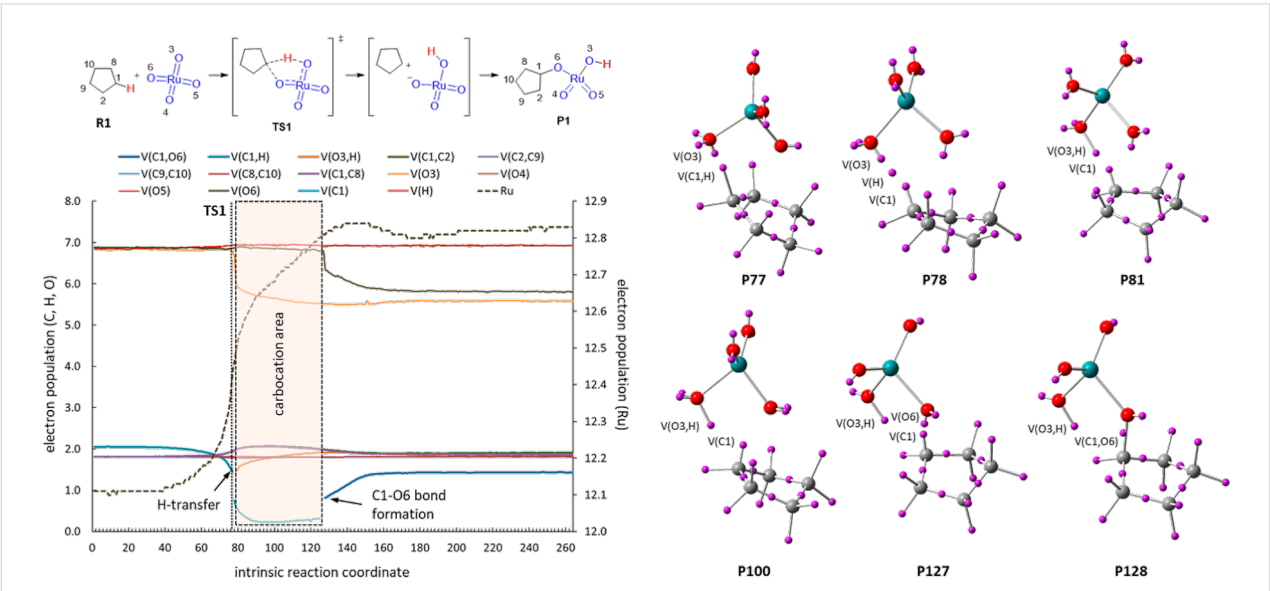

Figure 2: ELF analysis for the oxidation of cyclopentane (**R1**). Left: evolution of the electron population along the IRC. Right: Descriptors of basins at selected points of the IRC.

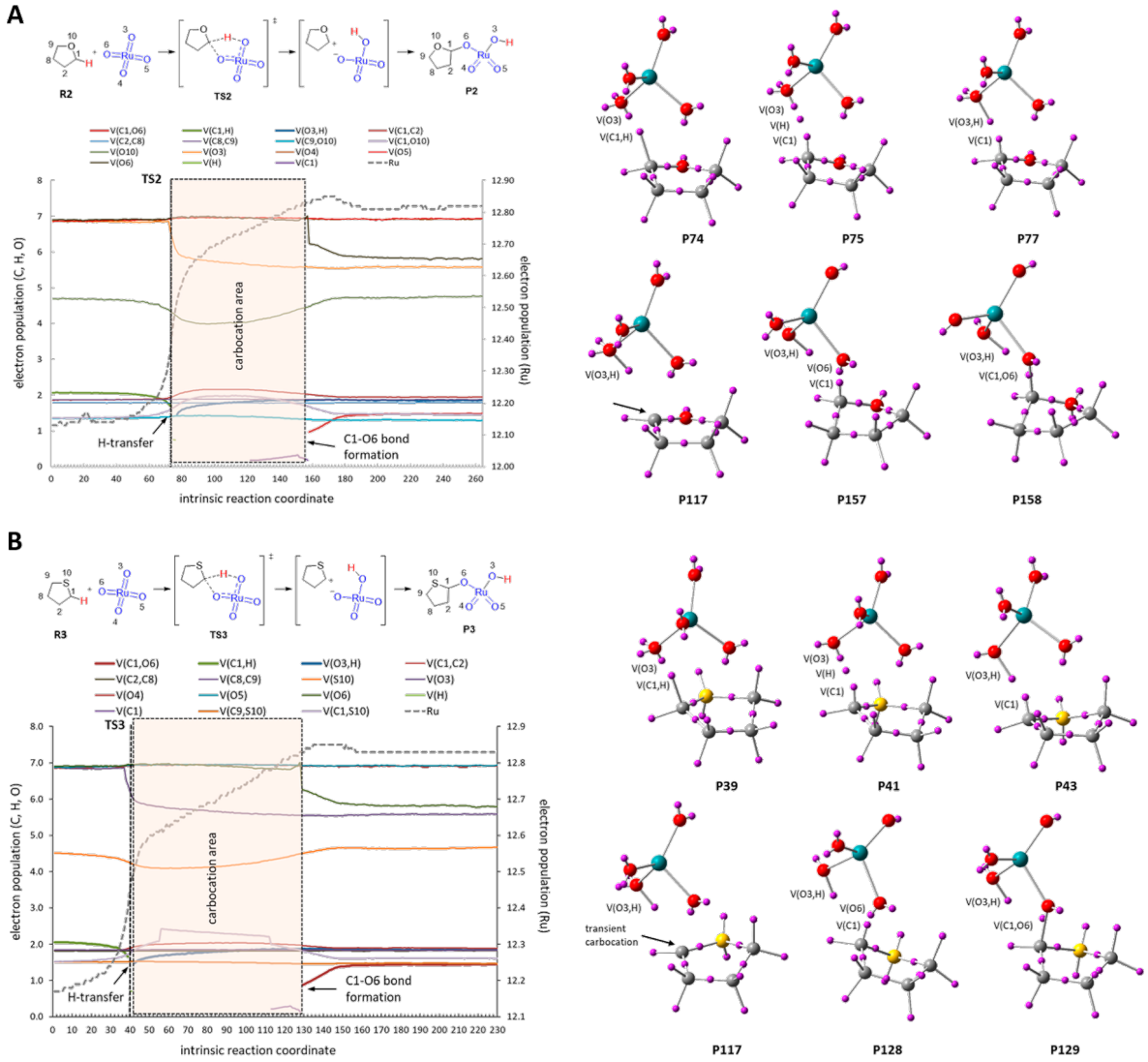

Figure 3: ELF analysis for the oxidation of tetrahydrofuran (**R2**, A) and tetrahydrothiophene (**R3**, B). Left: evolution of the electron population along the IRC. Right: Descriptors of basins at selected points of the IRC.

that they cannot exist in the form of transient species as we have recently demonstrated [38].

A completely different situation was found with the oxidation of *N*-methylpyrrolidine (**R4**) and *N*-benzylpyrrolidine **R5** (Scheme 5). In the case of *N*-alkylpyrrolidines two regiosiomeric oxidations can take place at *endo* (cycle) and *exo* (*N*-chain) positions. We located the four transition structures **TS4a** and **TS5a**, corresponding to the *endo* series, and **TS4b** and **TS5b**, corresponding to the *exo* series.

In all cases, the observed barriers were below the reagents illustrating a favorable reaction (see Figure 5). For *N*-methylpyrrolidine (**R4**), the *endo* oxidation was preferred over the *exo* oxidation by 1.3 kcal/mol whereas for *N*-benzylpyrrolidine **R5** the difference in favor of the *endo* oxidation was only 0.3 kcal/mol suggesting a directing effect of the *p*-methoxyphenyl group. Notably, the IRC analyses of the transition structures revealed as end points of the reactions the ion pairs **IN4**,**5**. Indeed, optimization of those points led to **IN4a**, **IN5a** and **IN5b** as energy minima; only **IN4b** could not be located, the optimization of which led to **P4b**. Transformation of ion pairs into the corresponding products **P4a** and **P5a**,**b** was found to be essentially barrierless. As expected, the ion pairs identified as minima adopt the form of an iminium ion, the most stable being **IN5b**, corresponding to that conjugated with the *p*-methoxyphenyl group, which stabilizes the positive charge. These results are in agreement with the experimental findings of Petride and co-workers, who demonstrated the existence of iminium ions as intermediates in this sort of oxidation [26].

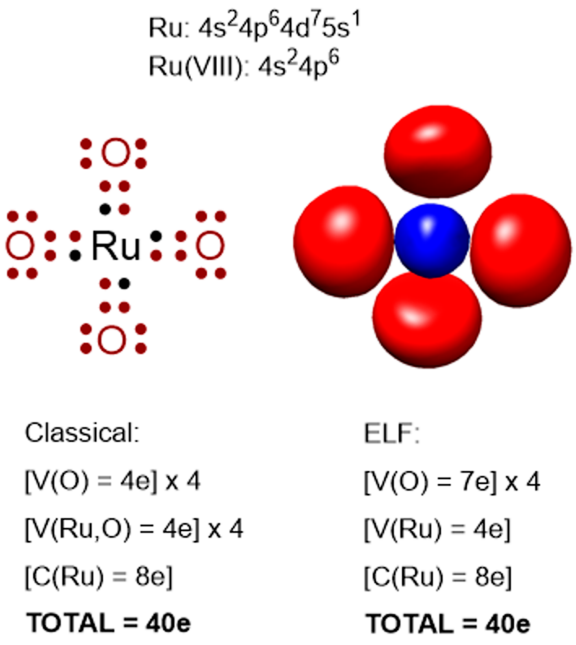

Figure 4: ELF assignment of electrons to the Ru environment. C(Ru) corresponds to a monosynaptic core basin assigned to ruthenium. V(Ru) and V(O) correspond to monosynaptic valence basins assigned to ruthenium and oxygen atoms, respectively. V(Ru,O) corresponds to a disynaptic valence basin assigned to a Ru–O bond (not present in ELF analysis).

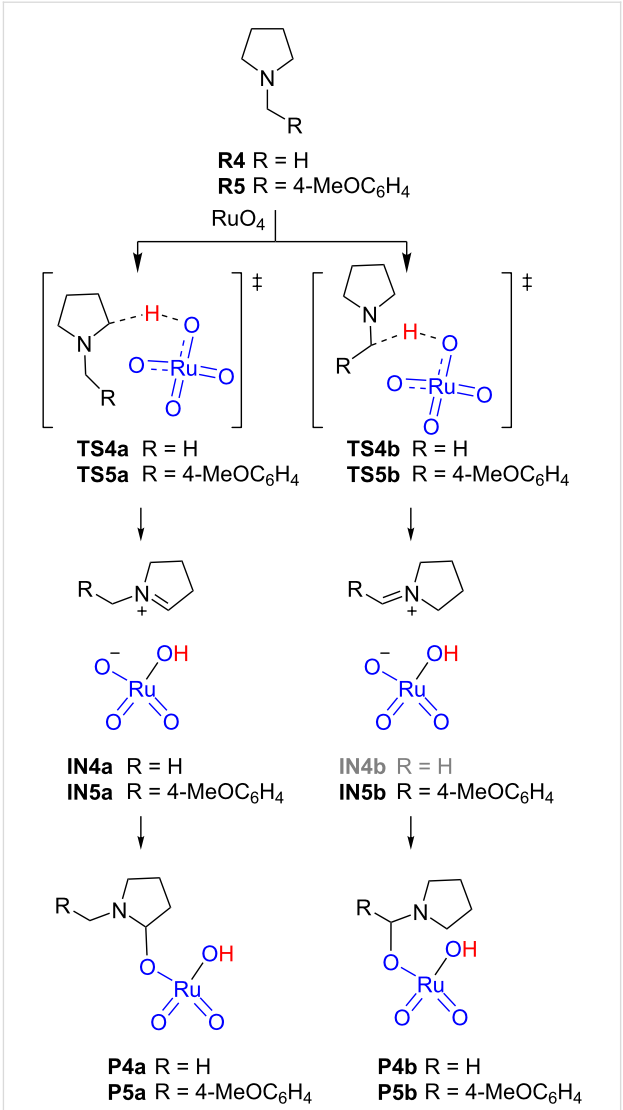

Scheme 5: Rate-limiting step for the oxidation of *N*-methyl- and *N*-benzylpyrrolidines **R4** and **R5**, respectively.

The geometries of the transition structures showed large distances between the carbon to be oxidized and the ruthenium oxygen indicating that, in fact, they do not correspond to forming bonds (Figure 6). The largest distances correspond to the formation of *endo* iminium ions (3.61 Å and 3.63 Å for **TS4a** and **TS5a**, respectively). The shortest distance (3.24 Å) was observed for **TS4b** in agreement with the direct formation of **P4b** as mentioned above.

We performed the ELF analysis for the *endo* oxidation reaction of **R4** (see Supporting Information File 1) and, as expected, we only observed the H transfer corresponding to the concomitant breaking of the C–H bond and formation of the O–H bond but the resulting iminium ion was stable enough to be considered a real intermediate according to IUPAC definition of 1994, which is: "*A molecular entity with a lifetime appreciably longer than a molecular vibration – **corresponding to a local potential energy minimum** of depth greater than R T – that is formed (directly or indirectly) from the reactants and reacts further to give (either directly or indirectly) the products of a chemical reaction*" [75].

Although, according to the IUPAC definition a transient carbocation cannot be considered an intermediate (since it is required to be a local energy minimum), this transient carbocation does in fact exist, as we have demonstrated experimentally in a reaction in which the chiral information is lost as a consequence of the presence of a transient carbocation [38]. The stability of the transient carbocation can be enhanced by the presence of heteroatoms that stabilize the developing positive charge by resonance, as in the case of tetrahydrofuran and tetrahydrothiophene. Moreover, the presence of a nitrogen atom provides enough stabilization to be located as an energy minimum and to be captured experimentally [26]. Table 1 summarizes the differences observed in the studied cases.

The presence of a heteroatom contributes to lower the energy barrier of the oxidation reaction, and in the case of the pyrrolidine, it is below the reactant, demonstrating the stabilizing effect of the heteroatom in the transition structure. The asyn-

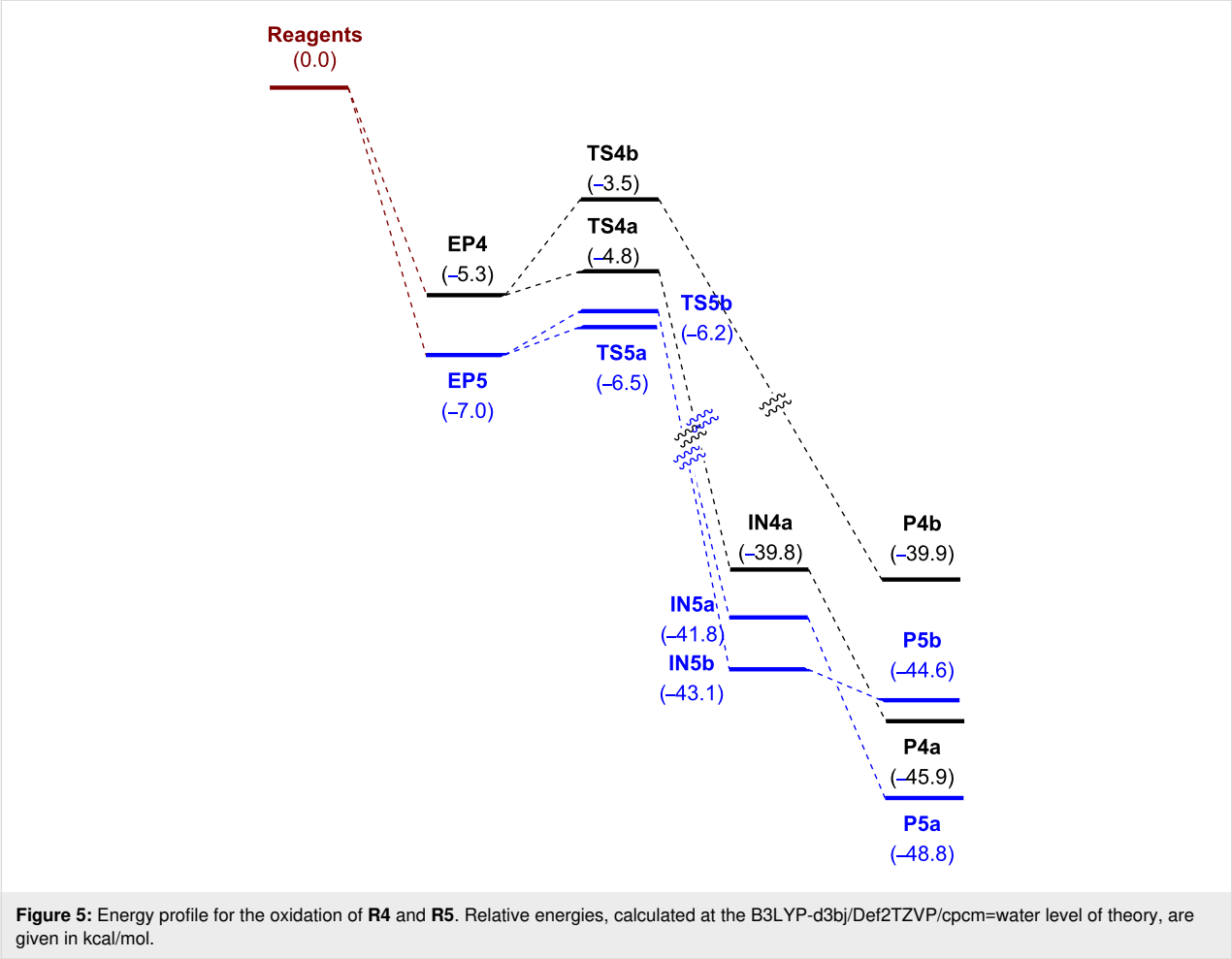

Figure 5: Energy profile for the oxidation of **R4** and **R5**. Relative energies, calculated at the B3LYP-d3bj/Def2TZVP/cpcm=water level of theory, are given in kcal/mol.

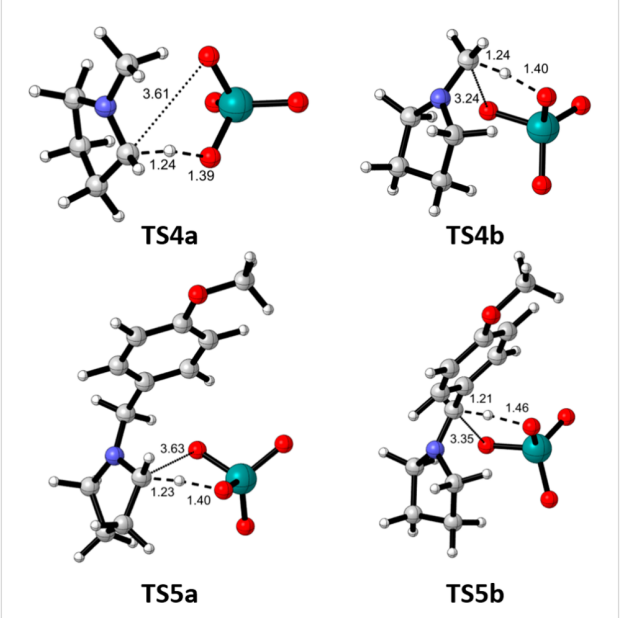

Figure 6: Optimized (B3LYP-d3bj/Def2SVP/cpcm=water) transition structures for the oxidation of **R4** and **R5**.

Table 1: Summary of results.

	barrier[a]	H transfer[b]	C–O formation[b]	% carbocation[c]
R1	14.6	30	49	17
R2	6.0	29	60	30
R3	7.5	17	56	40
R4	–3.5[d]	20	–[e]	80

[a]Given in kcal/mol relative to separate reagents. [b]Given in % with respect to the total number of points of the IRC. [c]Calculated on the number of points between the H transfer and C–O bond formation with respect to the total number of points of the IRC. [d]The corresponding encounter pair is 8.5 kcal/mol below the reagents. [e]The product of the reaction is the iminium cation therefore the C–O bond is not formed.

chronicity of the reaction can be measured on the basis of the lapse between breaking of the C–H bond and formation of the C–O bond. Whereas H transfer takes places at similar moments (30% and 29% of the IRC, for the representative cases of cyclopentane (**R1**) and tetrahydrofuran (**R2**), respectively) after starting the reaction, the formation of the C–O bond takes more

time for **R2** (60% of the IRC) than for **R1** (49% of the IRC), giving more chance to the transient carbocation for the former (30% of the IRC vs 17% of the IRC for the latter).

Conclusion

The oxidation of cyclopentane with ruthenium tetroxide is a highly polar asynchronous concerted process that during a brief lapse of time develops a transient carbocation. This result does not contradict previous calculations [25], but does point out the necessity of analyzing the full reaction coordinate to detect species that might explain some chemical behavior. Indeed, further theoretical studies on MD simulations would be needed to elucidate the lifetime of the transient carbocation [34,35]. These results demonstrate the one-step-two-stage character [42] of the ruthenium oxidations of alkanes in which H transfer and O–C bond formation take place in two separate events within the same reaction coordinate. We suggest a more adequate use of the IUPAC definition of intermediate given in 1996 [76] (*any reaction species that is neither an initial reactant nor a final product is referred to as an intermediate*) rather than that of 1994 [75], since it is in this case not strictly necessary for the transient carbocations described above to be local energy minima.

Supporting Information

Supporting Information File 1

Energy data, optimized geometries, full data of ELF analysis and Cartesian coordinates.
[https://www.beilstein-journals.org/bjoc/content/supplementary/1860-5397-15-158-S1.pdf]

Acknowledgements

This work was supported by the Spanish Ministerio de Economía y Competitividad (MINECO) (project number CTQ2016-76155-R), by the Fondos Europeos para el Desarrollo Regional (FEDER) and the Gobierno de Aragon (Zaragoza, Spain, Groups E34-R17). The authors acknowledge the Institute of Biocomputation and Physics of Complex Systems (BIFI) at the University of Zaragoza for computer time at clusters Terminus and Memento. St. Francis-Prof. Thyagarajan Foundation (San Antonio, TX, USA) is gratefully acknowledged for a donation for software acquisition. M.-A. C. and L. L. thank Universities of Catania and Pavia for partial financial support.

ORCID® iDs

Tomás Tejero - https://orcid.org/0000-0003-3433-6701
Pedro Merino - https://orcid.org/0000-0002-2202-3460

References

1. Murahashi, S.-I.; Komiya, N. Ruthenium-catalyzed oxidation for organic synthesis. In *Modern Oxidation Methods,* 2nd ed.; Bäckvall, J.-E., Ed.; Wiley-VCH: Weinheim, Germany, 2010; pp 241–275. doi:10.1002/9783527632039.ch7
2. Arends, I. W. C. E.; Kodama, T.; Sheldon, R. A. Oxidation Using Ruthenium Catalysts. In *Ruthenium Catalysts and Fine Chemistry;* Bruneau, C.; Dixneuf, P. H., Eds.; Topics in Organometallic Chemistry, Vol. 11; Springer: Berlin, Heidelberg, 2004; pp 277–320. doi:10.1007/b94652
3. Martín, V. S.; Palazón, J. M.; Rodríguez, C. M.; Nevill, C. R., Jr.; Hutchinson, D. K. Ruthenium(VIII) Oxide. *Encyclopedia of Reagents for Organic Synthesis;* John Wiley and Sons, Ltd.: Chichester, UK, 2013. doi:10.1002/047084289x.rr009.pub3
4. Courtney, J. L. Ruthenium Tetroxide Oxidations. In *Organic Syntheses by Oxidation with Metal Compounds;* Mijs, W. J.; de Jonge, C. R. H. I., Eds.; Plenum Press: New York, U.S.A., 1986; pp 445–467. doi:10.1007/978-1-4613-2109-5_8
5. Murahashi, S.-I.; Komiya, N. Ruthenium-Catalyzed Oxidation of Alkenes, Alcohols, Amines, Amides, β-Lactams, Phenols, and Hydrocarbons. In *Modern Oxidation Methods;* Bäckvall, J.-E., Ed.; Wiley-VCH: Weinheim, Germany, 2004; pp 165–191. doi:10.1002/3527603689.ch6
6. Pombeiro, A. J. L.; da Silva, M. F. C. G., Eds. *Alkane Functionalization;* John Wiley & Sons, Ltd: Chichester, United Kingdom, 2019. doi:10.1002/9781119379256
7. Plietker, B. *Synthesis* **2005,** 2453–2472. doi:10.1055/s-2005-872172
8. Carlsen, P. H. J.; Katsuki, T.; Martin, V. S.; Sharpless, K. B. *J. Org. Chem.* **1981,** *46,* 3936–3938. doi:10.1021/jo00332a045
9. Dragojlović, V.; Bajc, S.; Amblès, A.; Vitorović, D. *Org. Geochem.* **2005,** *36,* 1–12. doi:10.1016/j.orggeochem.2004.07.011
10. Tanaka, K.; Yoshifuji, S.; Nitta, Y. *Chem. Pharm. Bull.* **1988,** *36,* 3125–3129. doi:10.1248/cpb.36.3125
11. Kaname, M.; Yoshifuji, S.; Sashida, H. *Tetrahedron Lett.* **2008,** *49,* 2786–2788. doi:10.1016/j.tetlet.2008.02.127
12. Tenaglia, A.; Terranova, E.; Waegell, B. *Tetrahedron Lett.* **1989,** *30,* 5271–5274. doi:10.1016/s0040-4039(01)93761-x
13. Lee, D. G.; van den Engh, M. *Can. J. Chem.* **1972,** *50,* 2000–2009. doi:10.1139/v72-322
14. Coudret, J. L.; Zöllner, S.; Ravoo, B. J.; Malara, L.; Hanisch, C.; Dörre, K.; de Meijere, A.; Waegell, B. *Tetrahedron Lett.* **1996,** *37,* 2425–2428. doi:10.1016/0040-4039(96)00325-5
15. Bakke, J. M.; Lundquist, M. *Acta Chem. Scand., Ser. B* **1986,** *40,* 430–433. doi:10.3891/acta.chem.scand.40b-0430
16. Tenaglia, A.; Terranova, E.; Waegell, B. *J. Chem. Soc., Chem. Commun.* **1990,** 1344–1345. doi:10.1039/c39900001344
17. Bakke, J. M.; Bethell, D. *Acta Chem. Scand.* **1992,** *46,* 644–649. doi:10.3891/acta.chem.scand.46-0644
18. Bakke, J. M.; Braenden, J. E. *Acta Chem. Scand.* **1991,** *45,* 418–423. doi:10.3891/acta.chem.scand.45-0418
19. Tenaglia, A.; Terranova, E.; Waegell, B. *J. Org. Chem.* **1992,** *57,* 5523–5528. doi:10.1021/jo00046a040
20. Coudret, J.-L.; Waegell, B. *Inorg. Chim. Acta* **1994,** *222,* 115–122. doi:10.1016/0020-1693(94)03900-3
21. Bakke, J. M.; Frøhaug, A. E. *Acta Chem. Scand.* **1994,** *48,* 160–164. doi:10.3891/acta.chem.scand.48-0160
22. Bakke, J. M.; Frøhaug, A. E. *J. Phys. Org. Chem.* **1996,** *9,* 507–513. doi:10.1002/(sici)1099-1395(199607)9:7<507::aid-poc811>3.0.co;2-l

23. Bakke, J. M.; Frøhaug, A. E. *Acta Chem. Scand.* **1995,** *49,* 615–622. doi:10.3891/acta.chem.scand.49-0615
24. Bakke, J. M.; Frøhaug, A. E. *J. Phys. Org. Chem.* **1996,** *9,* 310–318. doi:10.1002/(sici)1099-1395(199606)9:6<310::aid-poc790>3.0.co;2-e
25. Drees, M.; Strassner, T. *J. Org. Chem.* **2006,** *71,* 1755–1760. doi:10.1021/jo051521d
26. Petride, H.; Drăghici, C.; Florea, C.; Petride, A. *Cent. Eur. J. Chem.* **2004,** *2,* 302–322. doi:10.2478/bf02475575
27. Petride, H.; Costan, O.; Drăghici, C.; Florea, C.; Petride, A. *ARKIVOC* **2005,** No. x, 18–32.
28. Petride, H.; Drăghici, C.; Florea, C.; Petride, A. *Cent. Eur. J. Chem.* **2006,** *4,* 674–694. doi:10.2478/s11532-006-0039-8
29. Yang, Z.; Houk, K. N. *Chem. – Eur. J.* **2018,** *24,* 3916–3924. doi:10.1002/chem.201706032
30. Yang, Z.; Yu, P.; Houk, K. N. *J. Am. Chem. Soc.* **2016,** *138,* 4237–4242. doi:10.1021/jacs.6b01028
31. Xue, X.-S.; Jamieson, C. S.; Garcia-Borràs, M.; Dong, X.; Yang, Z.; Houk, K. N. *J. Am. Chem. Soc.* **2019,** *141,* 1217–1221. doi:10.1021/jacs.8b12674
32. Yu, P.; Yang, Z.; Liang, Y.; Hong, X.; Li, Y.; Houk, K. N. *J. Am. Chem. Soc.* **2016,** *138,* 8247–8252. doi:10.1021/jacs.6b04113
33. Bogle, X. S.; Singleton, D. A. *Org. Lett.* **2012,** *14,* 2528–2531. doi:10.1021/ol300817a
34. Popov, S.; Shao, B.; Bagdasarian, A. L.; Benton, T. R.; Zou, L.; Yang, Z.; Houk, K. N.; Nelson, H. M. *Science* **2018,** *361,* 381–387. doi:10.1126/science.aat5440
35. Blümel, M.; Nagasawa, S.; Blackford, K.; Hare, S. R.; Tantillo, D. J.; Sarpong, R. *J. Am. Chem. Soc.* **2018,** *140,* 9291–9298. doi:10.1021/jacs.8b05804
36. Chiacchio, M. A.; Legnani, L.; Caramella, P.; Tejero, T.; Merino, P. *Eur. J. Org. Chem.* **2017,** 1952–1960. doi:10.1002/ejoc.201700127
37. Díaz, E.; Reyes, E.; Uria, U.; Carrillo, L.; Tejero, T.; Merino, P.; Vicario, J. L. *Chem. – Eur. J.* **2018,** *24,* 8764–8768. doi:10.1002/chem.201801434
38. Ortega, A.; Manzano, R.; Uria, U.; Carrillo, L.; Reyes, E.; Tejero, T.; Merino, P.; Vicario, J. L. *Angew. Chem., Int. Ed.* **2018,** *57,* 8225–8229. doi:10.1002/anie.201804614
39. Silvi, B.; Savin, A. *Nature* **1994,** *371,* 683–686. doi:10.1038/371683a0
40. Savin, A.; Nesper, R.; Wengert, S.; Fässler, T. F. *Angew. Chem., Int. Ed. Engl.* **1997,** *36,* 1808–1832. doi:10.1002/anie.199718081
41. Merino, P.; Chiacchio, M. A.; Legnani, L.; Delso, I.; Tejero, T. *Org. Chem. Front.* **2017,** *4,* 1541–1554. doi:10.1039/c7qo00233e
42. Merino, P.; Tejero, T.; Delso, I.; Matute, R. *Org. Biomol. Chem.* **2017,** *15,* 3364–3375. doi:10.1039/c7ob00429j
43. Chiacchio, M.-A.; Legnani, L.; Caramella, P.; Tejero, T.; Merino, P. *Tetrahedron* **2018,** *74,* 5627–5634. doi:10.1016/j.tet.2018.07.056
44. Spitzer, U. A.; Lee, D. G. *J. Org. Chem.* **1975,** *40,* 2539–2540. doi:10.1021/jo00905a029
45. Lee, D. G.; van den Engh, M. *Can. J. Chem.* **1972,** *50,* 3129–3134. doi:10.1139/v72-501
46. Tangari, N.; Tortorella, V. *J. Chem. Soc., Chem. Commun.* **1975,** 71b–72. doi:10.1039/c3975000071b
47. *Gaussian;* Gaussian Inc.: Wallingford, CT, 2009.
48. Becke, A. D. *J. Chem. Phys.* **1993,** *98,* 5648–5652. doi:10.1063/1.464913
49. Lee, C.; Yang, W.; Parr, R. G. *Phys. Rev. B* **1988,** *37,* 785–789. doi:10.1103/physrevb.37.785
50. Grimme, S.; Ehrlich, S.; Goerigk, L. *J. Comput. Chem.* **2011,** *32,* 1456–1465. doi:10.1002/jcc.21759
51. Grimme, S.; Antony, J.; Ehrlich, S.; Krieg, H. *J. Chem. Phys.* **2010,** *132,* 154104. doi:10.1063/1.3382344
52. Weigend, F. *Phys. Chem. Chem. Phys.* **2006,** *8,* 1057–1065. doi:10.1039/b515623h
53. Weigend, F.; Ahlrichs, R. *Phys. Chem. Chem. Phys.* **2005,** *7,* 3297–3305. doi:10.1039/b508541a
54. Barone, V.; Cossi, M. *J. Phys. Chem. A* **1998,** *102,* 1995–2001. doi:10.1021/jp9716997
55. Cossi, M.; Rega, N.; Scalmani, G.; Barone, V. *J. Comput. Chem.* **2003,** *24,* 669–681. doi:10.1002/jcc.10189
56. Schlegel, H. B. Geometry optimization on potential energy surfaces. In *Modern Electronic Structure Theory, Part I;* Yarkony, D. R., Ed.; World Scientific Publishing: Singapore, 1995; pp 459–500. doi:10.1142/9789812832108_0008
57. Fukui, K. *J. Phys. Chem.* **1970,** *74,* 4161–4163. doi:10.1021/j100717a029
58. Hratchian, H. P.; Schlegel, H. B. *J. Phys. Chem. A* **2002,** *106,* 165–169. doi:10.1021/jp012125b
59. Tanaka, R.; Yamashita, M.; Chung, L. W.; Morokuma, K.; Nozaki, K. *Organometallics* **2011,** *30,* 6742–6750. doi:10.1021/om2010172
60. Savin, A.; Becke, A. D.; Flad, J.; Nesper, R.; Preuss, H.; von Schnering, H. G. *Angew. Chem., Int. Ed. Engl.* **1991,** *30,* 409–412. doi:10.1002/anie.199104091
61. Savin, A.; Nesper, R.; Wengert, S.; Fässler, T. F. *Angew. Chem., Int. Ed. Engl.* **1997,** *36,* 1808–1832. doi:10.1002/anie.199718081
62. Savin, A.; Silvi, B.; Colonna, F. *Can. J. Chem.* **1996,** *74,* 1088–1096. doi:10.1139/v96-122
63. Silvi, B. *J. Mol. Struct.* **2002,** *614,* 3–10. doi:10.1016/s0022-2860(02)00231-4
64. Llusar, R.; Beltrán, A.; Andrés, J.; Noury, S.; Silvi, B. *J. Comput. Chem.* **1999,** *20,* 1517–1526. doi:10.1002/(sici)1096-987x(19991115)20:14<1517::aid-jcc4>3.0.co;2-#
65. Silvi, B.; Fourré, I.; Alikhani, M. E. *Monatsh. Chem.* **2005,** *136,* 855–879. doi:10.1007/s00706-005-0297-8
66. Andrés, J.; Berski, S.; Feliz, M.; Llusar, R.; Sensato, F.; Silvi, B. *C. R. Chim.* **2005,** *8,* 1400–1412. doi:10.1016/j.crci.2004.12.014
67. Noury, S.; Krokidis, X.; Fuster, F.; Silvi, B. *Comput. Chem. (Oxford, U. K.)* **1999,** *23,* 597–604. doi:10.1016/s0097-8485(99)00039-x
68. *CYLview,* 1.0b; Legault, C. Y.; Université de Sherbrooke, 2009, http://www.cylview.org.
69. Domingo, L. R.; Arno, M.; Saez, J. A. *J. Org. Chem.* **2009,** *74,* 5934–5940. doi:10.1021/jo900889q
70. Roca-López, D.; Polo, V.; Tejero, T.; Merino, P. *J. Org. Chem.* **2015,** *80,* 4076–4083. doi:10.1021/acs.joc.5b00413
71. Roca-López, D.; Polo, V.; Tejero, T.; Merino, P. *Eur. J. Org. Chem.* **2015,** 4143–4152. doi:10.1002/ejoc.201500447
72. Becke, A. D.; Edgecombe, K. E. *J. Chem. Phys.* **1990,** *92,* 5397–5403. doi:10.1063/1.458517
73. Andres, J.; Berski, S.; Domingo, L. R.; Polo, V.; Silvi, B. *Curr. Org. Chem.* **2011,** *15,* 3566–3575. doi:10.2174/138527211797636156
74. Savin, A. *J. Chem. Sci.* **2005,** *117,* 473–475. doi:10.1007/bf02708351
75. Muller, P. *Pure Appl. Chem.* **1994,** *66,* 1077–1184. doi:10.1351/pac199466051077
76. Laidler, K. J. *Pure Appl. Chem.* **1996,** *68,* 149–192. doi:10.1351/pac199668010149

BEILSTEIN JOURNAL OF ORGANIC CHEMISTRY

Enantioselective PCCP Brønsted acid-catalyzed aza-Piancatelli rearrangement

Gabrielle R. Hammersley, Meghan F. Nichol, Helena C. Steffens, Jose M. Delgado, Gesine K. Veits and Javier Read de Alaniz*

Letter

Open Access

Address:
Department of Chemistry and Biochemistry, University of California Santa Barbara, Santa Barbara, CA 93106-9510, USA

Email:
Javier Read de Alaniz* - javier@chem.ucsb.edu

* Corresponding author

Keywords:
aza-Piancatelli; Brønsted acid; cyclopentane; furylcarbinols; PCCP

Beilstein J. Org. Chem. **2019,** *15,* 1569–1574.
doi:10.3762/bjoc.15.160

Received: 05 April 2019
Accepted: 03 July 2019
Published: 12 July 2019

This article is part of the thematic issue "Reactive intermediates – carbocations".

Guest Editor: S. R. Hare

Abstract

An enantioselective aza-Piancatelli rearrangement has been developed using a chiral Brønsted acid based on pentacarboxycyclopentadiene (PCCP). This reaction provides rapid access to valuable chiral 4-amino-2-cyclopentenone building blocks from readily available starting material and is operationally simple.

Introduction

The discovery of a wide range of cyclopentane containing natural products [1,2] and biologically active molecules such as palau'amine [3,4], agelastatin A [5-7], pactamycin [8-10], and aristeromycin [11,12], has created a demand for new methodologies to construct this privileged scaffold. The aza-Piancatelli reaction has recently emerged as a particularly attractive method to access densely functionalized cyclopentene cores bearing nitrogen substituents directly from readily available 2-furylcarbinols [13-15]. Inspired by Piancatelli's original work in 1976 [16], our group has developed both the inter- and intramolecular aza-Piancatelli reaction using commercially available dysprosium trifluoromethanesulfonate ($Dy(OTf)_3$) as a catalyst with a range of nitrogen nucleophiles [17-23]. The range of catalytic systems facilitating this reaction has been extended to include other Brønsted and Lewis acids, such as phosphomolybdic acid (PMA) [24], $Ca(NTf_2)_2$ [25], $In(OTf)_3$ [26], $La(OTf)_3$ [27], and $BF_3{\cdot}OEt_2$ [28], as well as other nucleophiles [29-31].

In all cases examined, the products of the aza-Piancatelli reaction have a *trans* relationship between the C4 and C5 substituents [13-15]. It is believed that the 4π conrotatory electrocyclization step that converts the pentadienyl cation **5** into the corresponding cyclopentenone adduct **6** is responsible for control-

ling the relative diastereoselectivity in this cascade rearrangement (Figure 1). Analogous to the Nazarov cyclization, controlling the absolute stereochemistry can be achieved by governing the direction of the conrotatory electrocyclization, clockwise vs counterclockwise [32-34]. Despite the direct relationship to the asymmetric Nazarov cyclization, however, it was not until 2016 that the first asymmetric aza-Piancatelli reaction was described. To control the absolute stereochemistry of the aza-Piancatelli rearrangement, Rueping [35], Sun [36], and Patil [37] independently demonstrated that chiral phosphoric acids can be used as an enantioselectivity-inducing element capable of controlling the clockwise or counterclockwise conrotation of the key 4π electrocyclization step.

Although the utility of these asymmetric catalytic systems is unquestionable, the ability to identify the optimal catalyst is not straightforward. In each case, extensive optimization of the reaction conditions was required to achieve high enantioselectivity and good yield, with small variations to the catalyst architecture or solvent having dramatic effects on enantioselectivity or yield. Because of these challenges and our group's ongoing interest in further developing the aza-Piancatelli reaction, we sought to identify other asymmetric catalytic systems capable of controlling the absolute stereochemistry. To this end, we envisioned that the chiral pentacarboxycyclopentadiene (PCCP) Brønsted acid catalyst (**8**) recently developed by the Lambert lab might be suitable (Figure 1) [38]. First, the pK_a values measured in acetonitrile (MeCN) are lower than chiral phosphoric acids (Brønsted acid pK_a = 8.85 vs chiral phosphoric acids pK_a = 12–14) [38]. Given the enhanced acidity, we reasoned that this type of chiral Brønsted acid catalyst could facilitate the dehydration reaction of the furylcarbinol to generate the oxocarbenium intermediate. Second, by analogy to asymmetric induction in aza-Piancatelli reactions with chiral phosphoric acids,

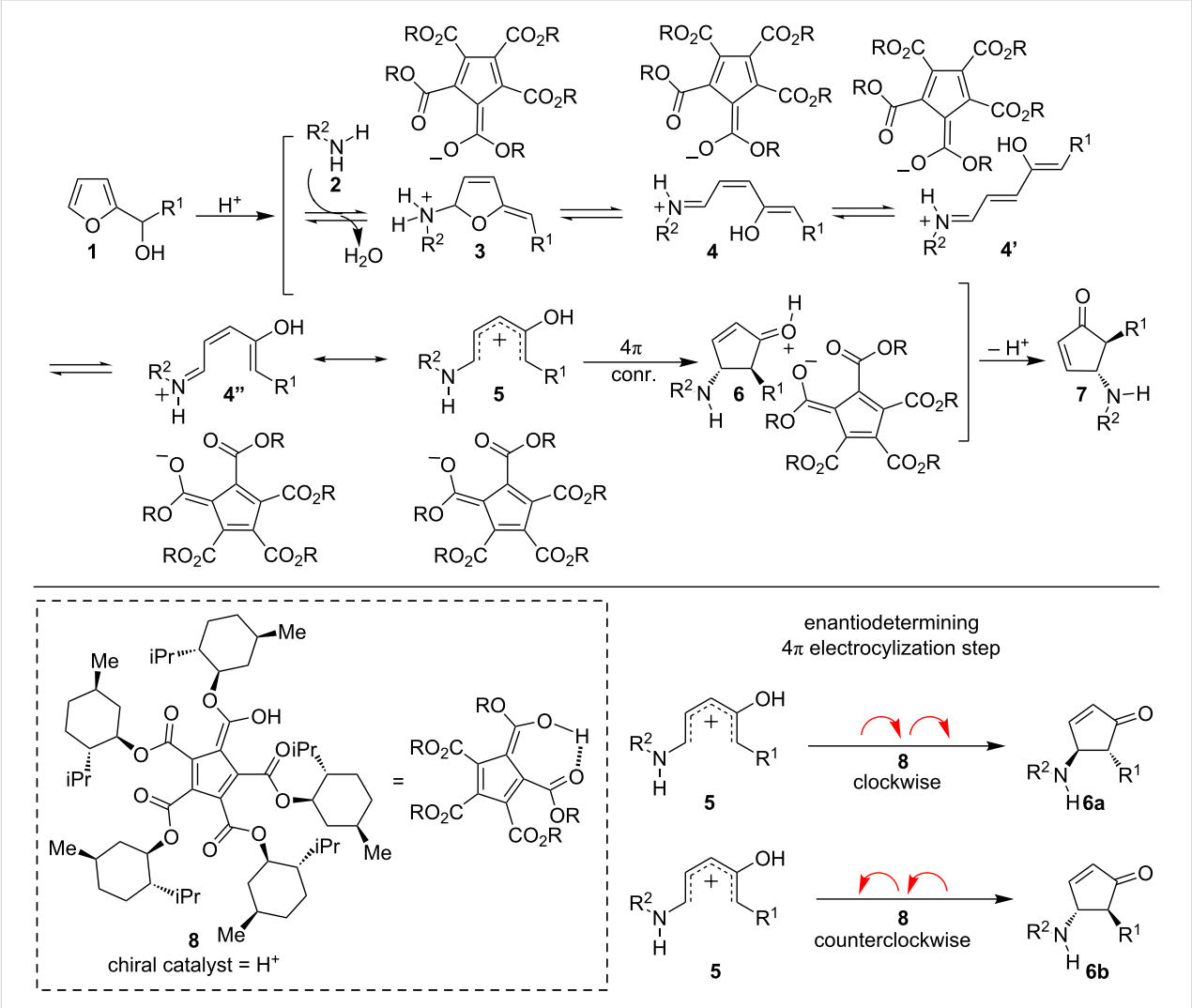

Figure 1: Proposed mechanism of the asymmetric aza-Piancatelli reaction.

where enantioselectivity has generally been achieved by strategically installing bulky groups on the hydrogen-bonding catalysts, we hypothesized that a PCCP-derived catalyst could be used. It is proposed that the chiral anion moieties serve to interact with the key intermediate **5** during the enantiodetermining electrocyclization step [35-37]. A tentative mechanistic hypothesis for the asymmetric aza-Piancatelli is shown in Figure 1. Finally, this new catalyst can be produced inexpensively and on scale, features that are attractive for developing a wide range of asymmetric transformations.

Results and Discussion

Herein, we describe our initial efforts in this area using chiral Brønsted acid catalyst **8**. Our investigations began by examining the reaction of *para*-iodoaniline (**2a**) with furylcarbinol **1a** in dichloromethane (DCM) in the presence of 5 mol % chiral Brønsted acid **8** (Table 1). We were pleased to find that **8** catalyzed the desired asymmetric transformation at 40 °C, affording 4-aminocyclopentenone **7a** in 78% yield and a moderate 65% ee. At lower temperatures (30 °C and 23 °C (rt)) the selectivity increased to 73% and 78% ee, respectively. For consistency the optimization studies were all allowed to run for 48 h with higher temperatures being more efficient (Table 1, entries 1–3). Importantly, the catalytic activity did not diminish with extended reaction time and the yield of the room temperature reaction could be increased to 70% by extending the reaction time from 48 h to 120 h (Table 1, entry 4). The asymmetric reaction was found to be most effective at 23 °C (Table 1, entries 3 and 4). Unfortunately, attempts to lower the temperature further resulted in exceedingly long reaction times, greater than 5 days, and thus were not pursued. Next the effects of aromatic and halogenated solvents were evaluated (Table 1, entries 5–7), with DCM proving optimal. We developed the reaction using 5 mol % catalyst in DCM at 23 °C as the optimized reaction conditions.

With optimized reaction conditions in hand, we set out to explore the scope and limitations of the asymmetric reaction (Scheme 1). Initially, we examined the reaction of various anilines with furylcarbinol **1a**. Scheme 1 summarizes the results obtained with *ortho-, meta-,* and *para*-substituted aniline derivatives. The reaction of anilines bearing an electron-withdrawing group at the *para*-position afforded the optimal balance between efficiency and enantioselectivity. Consistent with Rueping's work [35], *ortho*-aminobenzoic acid, which contains an additional hydrogen bond group afforded the best selectivity (**7k**). To simplify the purification process, all acid products were transformed into the corresponding methyl ester in situ using (trimethylsilyl)diazomethane. A slight drop in enantioselectivity is observed when the benzoic acid group was moved to the *meta*-position or when using the methyl ester (**7i** and **7j**). The absolute stereochemistry of the product **7k** was assigned by comparison to literature [35] and the other products were assigned by analogy.

To further expand the substrate scope, we investigated the effects on both reactivity and enantioselectivity when substituted furylcarbinols were used with either *para*-iodoaniline (**2a**)

Table 1: Initial optimization studies.

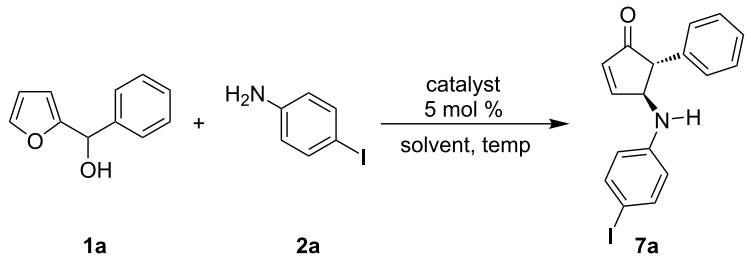

1a **2a** **7a**

Entry	Solvent	Temp (°C)	ee (%)	Yield (%)
1	DCM	40	65	78
2	DCM	30	73	46
3	DCM	rt	78	26
4[a]	DCM	rt	75	70
5	DCE	rt	68	23
6	fluorobenzene	rt	76	20
7	toluene	rt	75	12

[a]This reaction was run for 5 days whereas the rest of the reactions were run for 2 days. Dichloromethane (DCM), 1,2-dichloroethane (DCE), room temperature (rt).

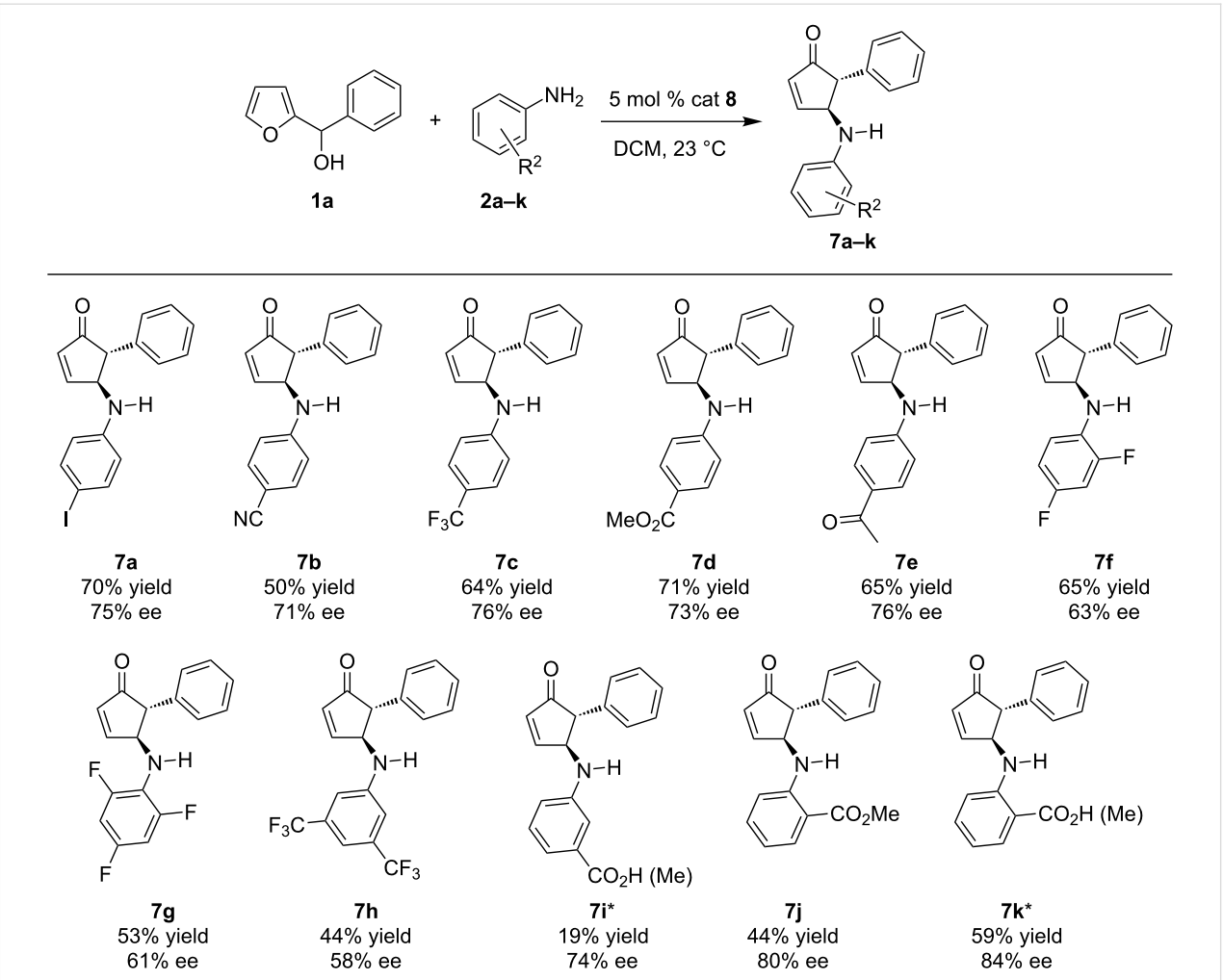

Scheme 1: Asymmetric aza-Piancatelli rearrangement with a range of substituted anilines. *To simplify the purification process, carboxylic acids were transformed in situ into the corresponding methyl ester using (trimethylsilyl)diazomethane.

or *ortho*-aminobenzoic acid (**2k**, Scheme 2). In every case examined, the *ortho*-aminobenzoic acid gave higher selectivity compared to the corresponding *para*-iodoaniline, which supports the importance of the additional hydrogen bonding capability of the carboxylic acid group. In contrast, with the exception of **7p** and **7q**, a lower yield was obtained when *ortho*-aminobenzoic acid was used. Presumably, this decrease in efficiency is due to the increased steric bulk on the aniline, which slows the initial nucleophilic attack on the furan ring required to initiate the cascade sequence. This highlights that a balance between nucleophilicity and hydrogen bond capabilities are required to obtain an efficient and selective reaction. Compared to the rearrangement of furylcarbinol **1a**, sterically bulky aryl groups attached to the furylcarbinol resulted in significantly diminished enantioselectivity (**7l** and **7m**). In contrast, placing a substituent at either the *meta*- or *para*-position showed no effect on the selectivity when compared to an unsubstituted phenyl group. For example, **1a** afforded the desired product in 75% ee, while **1n** and **1p** afforded the cyclopentenone product in 76% ee and 75% ee, respectively. In general, the enantioselectivity of the reactions with *para*-iodoaniline and *ortho*-aminobenzoic acid behaved similarly, with the selectivity being influenced most obviously by changes in the furylcarbinol. However, a dramatic difference in selectivity was observed when employing a tertiary furylcarbinol (**7r** and **7s**). In this case, *ortho*-aminobenzoic acid resulted in the desired product with good enantioselectivity (72% ee), while *para*-iodoaniline only gave a modest 41% ee. The exact nature for the decrease in enantioselectivity in this case with *para*-iodoaniline is not clear.

Conclusion

In summary, we have developed an efficient asymmetric aza-Piancatelli rearrangement that constructs a carbon–carbon bond plus a carbon–nitrogen bond and controls the absolute stereochemistry of the two stereocenters, through control of the direction of conrotation, in a single operation. This strategy offers a

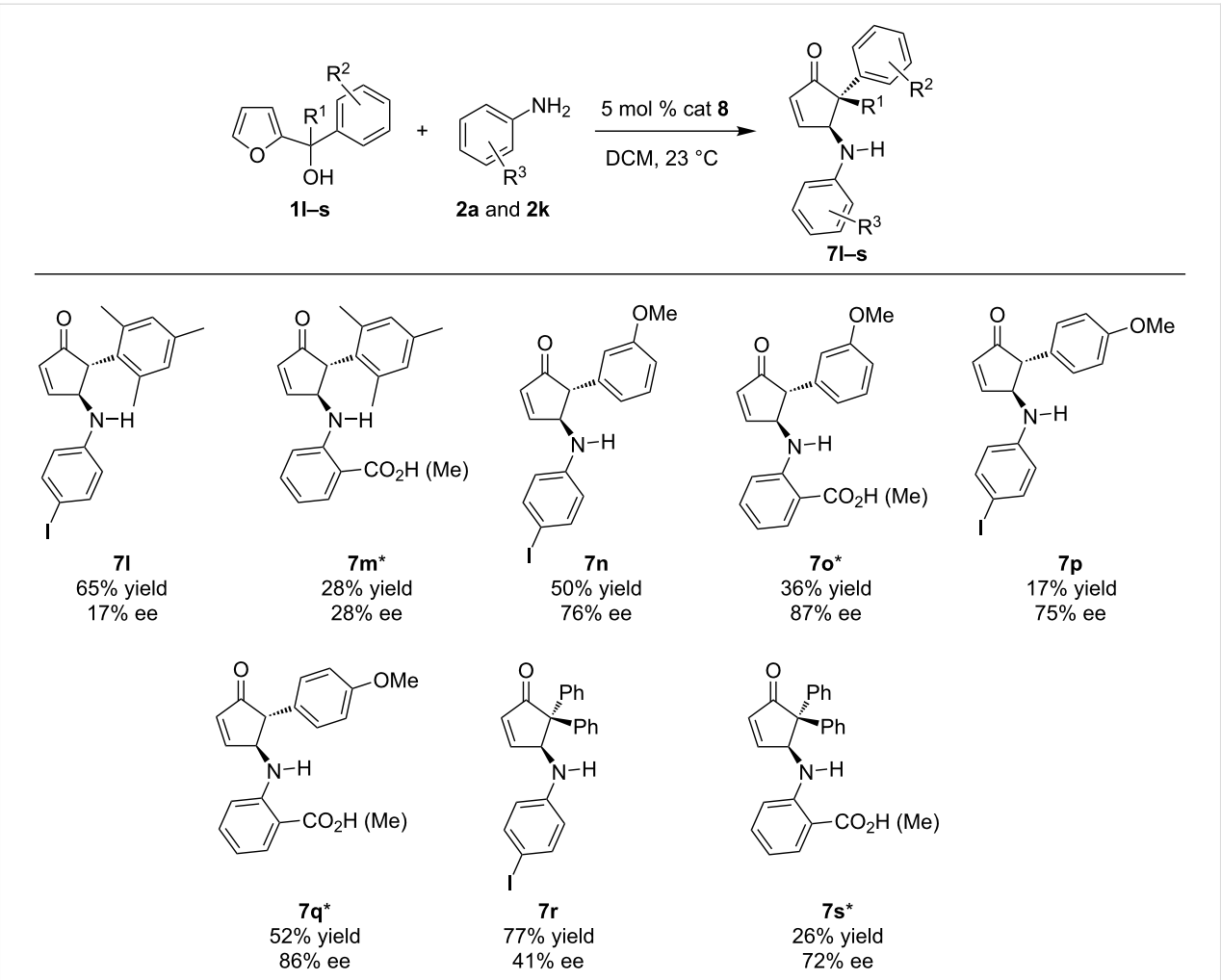

Scheme 2: Asymmetric aza-Piancatelli rearrangement with a range of substituted furylcarbinols. *To simplify the purification process, carboxylic acids were transformed in situ into the corresponding methyl ester using (trimethylsilyl)diazomethane.

practical alternative to using chiral phosphoric acids and demonstrates that chiral PCCP-based Brønsted acid catalysts can be used to control the absolute stereochemistry of the aza-Piancatelli rearrangement. The PCCP chiral Brønsted acid catalyzed reaction shows good substrate scope and proceeds well with a range of aniline and furylcarbinol derivatives. The ability to control the absolute stereochemistry of the 4π electrocyclization using an inexpensive and easy to prepare chiral Brønsted acid catalyst holds tremendous promise for the aza-Piancatelli and related rearrangements.

Experimental

General procedure for the rearrangement: Furylcarbinol **1** and aniline **2** were dissolved in DCM. At 23 °C, 5 mol % of the catalyst **8** was added to the reaction mixture and the reaction mixture was stirred for 5 days. The reaction was then quenched with saturated aqueous sodium bicarbonate and extracted with DCM (3 × 5 mL). The combined organic layers were dried over $MgSO_4$, filtered, and concentrated in vacuo. The residue was then purified by column chromatography to afford cyclopentenone **7**.

Supporting Information

Supporting Information File 1

Experimental part and copies of NMR spectra.
[https://www.beilstein-journals.org/bjoc/content/supplementary/1860-5397-15-160-S1.pdf]

Acknowledgements

This work was supported by the National Science Foundation under a Career Award CHE-1057180. The research made use of NMR instrumentation that was supported by an NIH Shared Instrumentation Grant (1S10OD012077-01A1). M. F. N. thanks the Mellichamp Academic Initiative in Sustainability for a

fellowship in support of this research. J. M. D. thanks the McNair Foundation for support.

ORCID® iDs

Gabrielle R. Hammersley - https://orcid.org/0000-0002-4391-6954
Meghan F. Nichol - https://orcid.org/0000-0002-3607-6002
Jose M. Delgado - https://orcid.org/0000-0003-3292-0584
Javier Read de Alaniz - https://orcid.org/0000-0003-2770-9477

References

1. Liu, G.; Shirley, M. E.; Van, K. N.; McFarlin, R. L.; Romo, D. *Nat. Chem.* **2013,** *5,* 1049–1057. doi:10.1038/nchem.1788
2. Heasley, B. *Curr. Org. Chem.* **2014,** *18,* 641–686. doi:10.2174/1385272813176660150
3. Köck, M.; Grube, A.; Seiple, I. B.; Baran, P. S. *Angew. Chem., Int. Ed.* **2007,** *46,* 6586–6594. doi:10.1002/anie.200701798
4. Seiple, I. B.; Su, S.; Young, I. S.; Lewis, C. A.; Yamaguchi, J.; Baran, P. S. *Angew. Chem., Int. Ed.* **2010,** *49,* 1095–1098. doi:10.1002/anie.200907112
5. Trost, B. M.; Dong, G. *J. Am. Chem. Soc.* **2006,** *128,* 6054–6055. doi:10.1021/ja061105q
6. Yoshimitsu, T.; Ino, T.; Tanaka, T. *Org. Lett.* **2008,** *10,* 5457–5460. doi:10.1021/ol802225g
7. Duspara, P. A.; Batey, R. A. *Angew. Chem., Int. Ed.* **2013,** *52,* 10862–10866. doi:10.1002/anie.201304759
8. Hanessian, S.; Vakiti, R. R.; Dorich, S.; Banerjee, S.; Lecomte, F.; DelValle, J. R.; Zhang, J.; Deschênes-Simard, B. *Angew. Chem., Int. Ed.* **2011,** *50,* 3497–3500. doi:10.1002/anie.201008079
9. Malinowski, J. T.; Sharpe, R. J.; Johnson, J. S. *Science* **2013,** *340,* 180–182. doi:10.1126/science.1234756
10. Sharpe, R. J.; Malinowski, J. T.; Johnson, J. S. *J. Am. Chem. Soc.* **2013,** *135,* 17990–17998. doi:10.1021/ja409944u
11. Trost, B. M.; Kuo, G. H.; Benneche, T. *J. Am. Chem. Soc.* **1988,** *110,* 621–622. doi:10.1021/ja00210a064
12. Mieczkowski, A.; Roy, V.; Agrofoglio, L. A. *Chem. Rev.* **2010,** *110,* 1828–1856. doi:10.1021/cr900329y
13. Piutti, C.; Quartieri, F. *Molecules* **2013,** *18,* 12290–12312. doi:10.3390/molecules181012290
14. Wenz, D. R.; Read de Alaniz, J. *Eur. J. Org. Chem.* **2015,** 23–37. doi:10.1002/ejoc.201402825
15. Gomes, R. F. A.; Coelho, J. A. S.; Afonso, C. A. M. *Chem. – Eur. J.* **2018,** *24,* 9170–9186. doi:10.1002/chem.201705851
16. Piancatelli, G.; Scettri, A.; Barbadoro, S. *Tetrahedron Lett.* **1976,** *17,* 3555–3558. doi:10.1016/s0040-4039(00)71357-8
17. Veits, G. K.; Wenz, D. R.; Read de Alaniz, J. *Angew. Chem., Int. Ed.* **2010,** *49,* 9484–9487. doi:10.1002/anie.201005131
18. Palmer, L. I.; Read de Alaniz, J. *Angew. Chem., Int. Ed.* **2011,** *50,* 7167–7170. doi:10.1002/anie.201102102
19. Palmer, L. I.; Read de Alaniz, J. *Org. Lett.* **2013,** *15,* 476–479. doi:10.1021/ol303263q
20. Yu, D.; Thai, V. T.; Palmer, L. I.; Veits, G. K.; Cook, J. E.; Read de Alaniz, J.; Hein, J. E. *J. Org. Chem.* **2013,** *78,* 12784–12789. doi:10.1021/jo402155b
21. Read de Alaniz, J.; Palmer, L. *Synlett* **2014,** *25,* 8–11. doi:10.1055/s-0033-1340157
22. Fisher, D.; Palmer, L. I.; Cook, J. E.; Davis, J. E.; Read de Alaniz, J. *Tetrahedron* **2014,** *70,* 4105–4110. doi:10.1016/j.tet.2014.03.007
23. Veits, G. K.; Wenz, D. R.; Palmer, L. I.; St. Amant, A. H.; Hein, J. E.; Read de Alaniz, J. *Org. Biomol. Chem.* **2015,** *13,* 8465–8469. doi:10.1039/c5ob00944h
24. Subba Reddy, B. V.; Narasimhulu, G.; Subba Lakshumma, P.; Vikram Reddy, Y.; Yadav, J. S. *Tetrahedron Lett.* **2012,** *53,* 1776–1779. doi:10.1016/j.tetlet.2012.01.115
25. Lebœuf, D.; Schulz, E.; Gandon, V. *Org. Lett.* **2014,** *16,* 6464–6467. doi:10.1021/ol5032987
26. Reddy, B. V. S.; Reddy, Y. V.; Lakshumma, P. S.; Narasimhulu, G.; Yadav, J. S.; Sridhar, B.; Reddy, P. P.; Kunwar, A. C. *RSC Adv.* **2012,** *2,* 10661–10666. doi:10.1039/c2ra21591h
27. Liu, J.; Shen, Q.; Yu, J.; Zhu, M.; Han, J.; Wang, L. *Eur. J. Org. Chem.* **2012,** 6933–6939. doi:10.1002/ejoc.201200962
28. Nunes, J. P. M.; Afonso, C. A. M.; Caddick, S. *RSC Adv.* **2013,** *3,* 14975. doi:10.1039/c3ra42663g
29. Yin, B.; Huang, L.; Wang, X.; Liu, J.; Jiang, H. *Adv. Synth. Catal.* **2013,** *355,* 370–376. doi:10.1002/adsc.201200850
30. Wang, C.; Dong, C.; Kong, L.; Li, Y.; Li, Y. *Chem. Commun.* **2014,** *50,* 2164–2166. doi:10.1039/c3cc49191a
31. Xu, J.; Luo, Y.; Xu, H.; Chen, Z.; Miao, M.; Ren, H. *J. Org. Chem.* **2017,** *82,* 3561–3570. doi:10.1021/acs.joc.7b00090
32. Tius, M. A. *Eur. J. Org. Chem.* **2005,** 2193–2206. doi:10.1002/ejoc.200500005
33. Frontier, A. J.; Collison, C. *Tetrahedron* **2005,** *61,* 7577–7606. doi:10.1016/j.tet.2005.05.019
34. Shimada, N.; Stewart, C.; Tius, M. A. *Tetrahedron* **2011,** *67,* 5851–5870. doi:10.1016/j.tet.2011.05.062
35. Cai, Y.; Tang, Y.; Atodiresei, I.; Rueping, M. *Angew. Chem., Int. Ed.* **2016,** *55,* 14126–14130. doi:10.1002/anie.201608023
36. Li, H.; Tong, R.; Sun, J. *Angew. Chem., Int. Ed.* **2016,** *55,* 15125–15128. doi:10.1002/anie.201607714
37. Gade, A. B.; Patil, N. T. *Synlett* **2017,** *28,* 1096–1100. doi:10.1055/s-0036-1558952
38. Gheewala, C. D.; Collins, B. E.; Lambert, T. H. *Science* **2016,** *351,* 961–965. doi:10.1126/science.aad0591

License and Terms

BEILSTEIN JOURNAL OF ORGANIC CHEMISTRY

The cyclopropylcarbinyl route to γ-silyl carbocations

Xavier Creary

Full Research Paper

Open Access

Address:
Department of Chemistry and Biochemistry, University of Notre Dame, Notre Dame, IN 45556, USA

Email:
Xavier Creary - creary.1@nd.edu

Keywords:
bicyclobutane; carbocation; cyclopropylcarbinyl; rearrangement; silicon

Beilstein J. Org. Chem. **2019,** *15,* 1769–1780.
doi:10.3762/bjoc.15.170

Received: 25 March 2019
Accepted: 03 July 2019
Published: 24 July 2019

This article is part of the thematic issue "Reactive intermediates – carbocations".

Guest Editor: S. R. Hare

Abstract

The mesylate derivative of *cis*-1-hydroxymethyl-2-trimethylsilylcyclopropane has been prepared, along with a number of related mesylates and triflates with substituents on the 1-position. These substrates all solvolyze in CD_3CO_2D to give products derived from cyclopropylcarbinyl cations that undergo further rearrangement to give 3-trimethylsilylcyclobutyl cations. These 3-trimethylsilylcyclobutyl cations are stabilized by a long-range rear lobe interaction with the γ-trimethylsilyl group. When the substituent is electron-withdrawing (CF_3, CN, or CO_2CH_3), significant amounts of bicyclobutane products are formed. The bicyclobutanes are a result of γ-trimethylsilyl elimination from the cationic intermediate that has an unusually long calculated Si–C bond. The solvolysis chemistry of mesylate and triflate derivatives of *trans*-1-hydroxymethyl-2-trimethylsilylcyclopropane and 1-substituted analogs can be quite different since these substrates do not generally lead to 3-trimethylsilylcyclobutyl cations.

Introduction

Carbocations, positively charged trivalent carbon compounds and reactive intermediates, have continued to fascinate chemists since the early discoveries of tropylium [1,2] and trityl [3-7] salts. Many of the giants of organic chemistry during the last century contributed heavily to the development of carbocation chemistry. This article will deal with three types of carbocations that have been of intense and fundamental interest over the years, i.e., cyclopropylcarbinyl cations, electron-deficient cations, and silyl substituted carbocations. A brief overview of these types of carbocations is warranted.

Cyclopropylcarbinyl cations are an extensively studied system [8,9]. Initial interest was derived from the fact that both cyclopropylcarbinyl and cyclobutyl substrates **1** and **2**, where X represents diazonium ion [10,11], chloride [10], or naphthalenesulfonate [12] leaving groups, reacted in aqueous solvents to give an identical mixture of products **3**, **4**, and **5** (Scheme 1). Additionally, solvolysis rates were far greater than expected for primary and strained secondary systems. To account for these facts, it has been suggested that there are common cationic intermediates in these solvolysis reactions of **1** and **2**. Labelling

[13-15], stable ion [16-19], and computational studies [19] implicate the involvement of three degenerate cyclopropylcarbinyl cations, **6a**, **6b**, and **6c**, in equilibrium with cyclobutyl cation **7**, as well as the homoallylic cation **8** (Scheme 2). Cations **6** are stabilized by the cyclopropyl ring and are therefore much more stable than simple primary carbocations. The cyclobutyl cation **7** is also quite stabilized relative to simple secondary carbocations. This cation has been called a "bicyclobutonium" cation, **7a**, which is a nonclassical cation (a cation containing hypercoordinated carbon) that could be derived from protonation of bicyclobutane [20]. Another potential mode of stabilization is by an interaction of the cationic center with the adjacent strained cyclobutyl bonds as in **7b**.

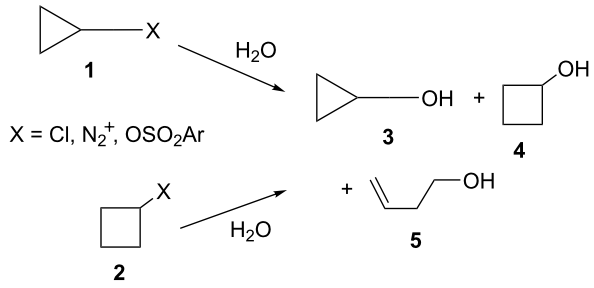

Scheme 1: Solvolyses of cyclopropylcarbinyl and cyclobutyl substrates.

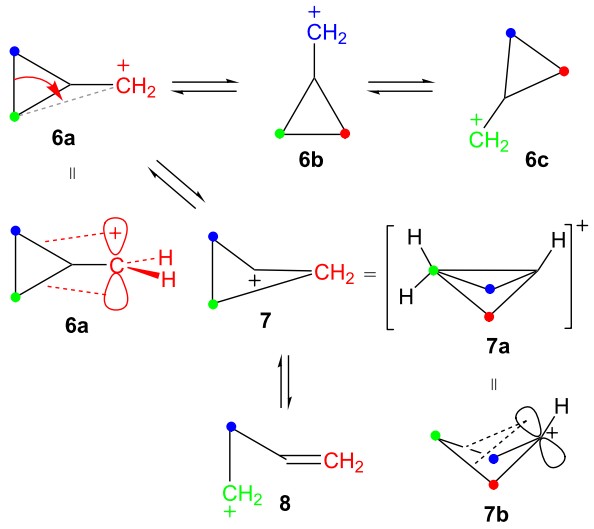

Scheme 2: The cyclopropylcarbinyl–cyclobutyl–homoallyl cation manifold.

A second class of carbocations that this article will deal with is the so-called "electron-deficient" carbocation, i.e., carbocations **9** (Figure 1) substituted with electron-withdrawing groups E [21]. Many studies have shown that such cations can indeed be generated and that they can derive stabilization by a variety of mechanisms. Chief among these cations are the α-trifluoromethyl [22-24], α-cyano [22,25-29], α-carbonyl [30-33], and α-phosphoryl [34,35] analogs of **9**. Carbocations of type **9** will be examined in conjunction with the cyclopropylcarbinyl–cyclobutyl manifold.

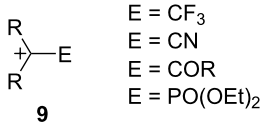

Figure 1: Electron-deficient carbocations.

The third type of carbocation that will be incorporated into this paper is the trimethylsilyl-substituted carbocation [36-44]. We have been interested in long-range interactions of silicon with both carbene [45-48] and carbocation centers [49,50]. Along these lines, γ-trimethylsilyl cations of general type **11** have been generated under stable-ion [51] as well as solvolytic conditions [52-54]. They are greatly stabilized by the "rear lobe" type of interaction shown involving the γ-trimethylsilyl group. A number of related cations are also stabilized by analogous γ-silyl interactions [55-59], which have also been termed "percaudal" interactions [56]. Certain carbenes can also be stabilized in a similar fashion [60,61]. Thus substrates of type **10** solvolyze in protic solvents with large rate enhancements (anchimeric assistance) to generate carbocations **11** as reactive intermediates (Scheme 3). These cations **11** capture solvent molecules to give exclusively products **12** with net retention of configuration, a characteristic of carbocations that are stabilized by this type of rear lobe interaction.

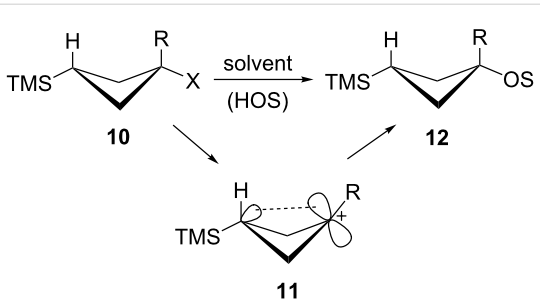

Scheme 3: Solvolyses of γ-trimethylsilylcyclobutyl substrates.

A series of cyclopropylcarbinyl substrates **13** and **14** (Figure 2), where X is a leaving group and R is an electron-donating group and E is an electron-withdrawing group, have now been examined. The goal was to evaluate the cyclopropylcarbinyl to cyclobutyl cation rearrangement. Can these substrates lead to

γ-trimethylsilyl-substituted cyclobutyl cations **11** and what are the fates of such carbocations? Answers to these questions were sought.

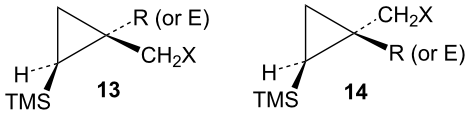

Figure 2: Substrates of interest.

Results and Discussion

Phenyl-substituted systems

The first compounds to be examined were the mesylates **19** and **20**. These substrates were prepared as shown in Scheme 4. Irradiation of ethyl 2-diazo-2-phenylacetate (**15**) in vinyltrimethylsilane as solvent gave an isomeric mixture of esters **16**. Subsequent reduction with lithium aluminum hydride gave a mixture of alcohols **17** and **18**, which could be readily separated by silica gel chromatography. The assignment of stereochemistry of these isomers was based on shielding effects in both ^{1}H and ^{13}C NMR spectra. For example, the trimethylsilyl singlet in **18** appears at δ −0.30 (shielded by the *cis*-phenyl group), while the trimethylsilyl singlet in **17** appears at δ 0.14 (deshielded by the *trans*-phenyl group). Such effects are in complete agreement with calculated shifts based on B3LYP/6-31G* calculated structures of **17** and **18**. Additionally, nOe studies on **17** confirm the stereochemical assignment. Conversion to mesylates **19** and **20** using mesyl chloride and triethylamine was straightforward.

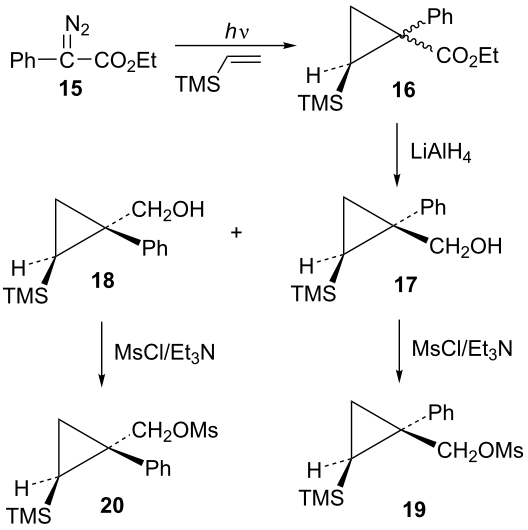

Scheme 4: Synthesis of mesylates **19** and **20**.

Mesylate **19** reacts readily in CD_3CO_2D at 20 °C (Table 1) to give the substituted cyclobutyl acetate **21** (92%) as the major product along with 8% of the alkene **22**. It is proposed (Scheme 5) that these products arise from stepwise formation of the cyclopropylcarbinyl cation **23**. This cation can rearrange via migration of bond *a* to give the cyclobutyl cation **24**. The *cis*-nature of the phenyl group and the hydrogen in cation **23** necessarily results in the formation of the γ-silyl-stabilized cation **24**. This cation is the source of the acetate **21**. Alternatively, cation **23** can rearrange by migration of the *b* bond of the cyclopropane. This leads to the β-silylcyclobutyl cation **25**, which can subsequently desilylate to give the minor product, the alkene **22**. Interestingly, formation of the γ-silyl cation **24** is preferred over the β-silyl cation **25**.

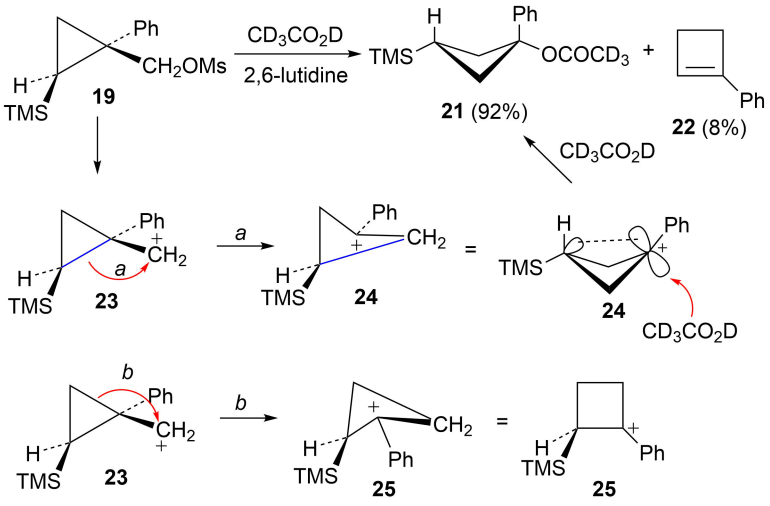

Scheme 5: Reaction of mesylate **19** in CD_3CO_2D.

Reaction of the isomeric mesylate **20** in CD_3CO_2D gives the same rearranged products **21** and **22**. These products are accounted for mechanistically in Scheme 6. The initially formed cyclopropylcarbinyl cation **26** rearranges by migration of the *a* bond of the cyclopropane to give the cyclobutyl cation **27**. This cation **27** is different from the γ-silyl-stabilized cation **24** in that the *cis*-nature of the phenyl and TMS groups in **26** requires that these groups are closer to each other in **27**. Shown in Figure 3 are M062X/6-311+G** calculated structures and energies of cations **27** and **24**, which are distinct energy minima, along with the transition state **28** which connects these two cations. Cation **27** derives most of its stabilization from the phenyl group, while

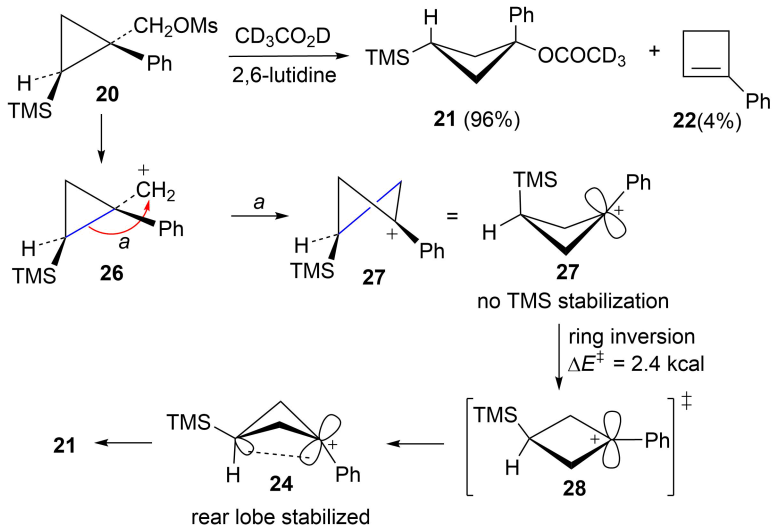

Scheme 6: Reaction of mesylate **20** in CD_3CO_2D.

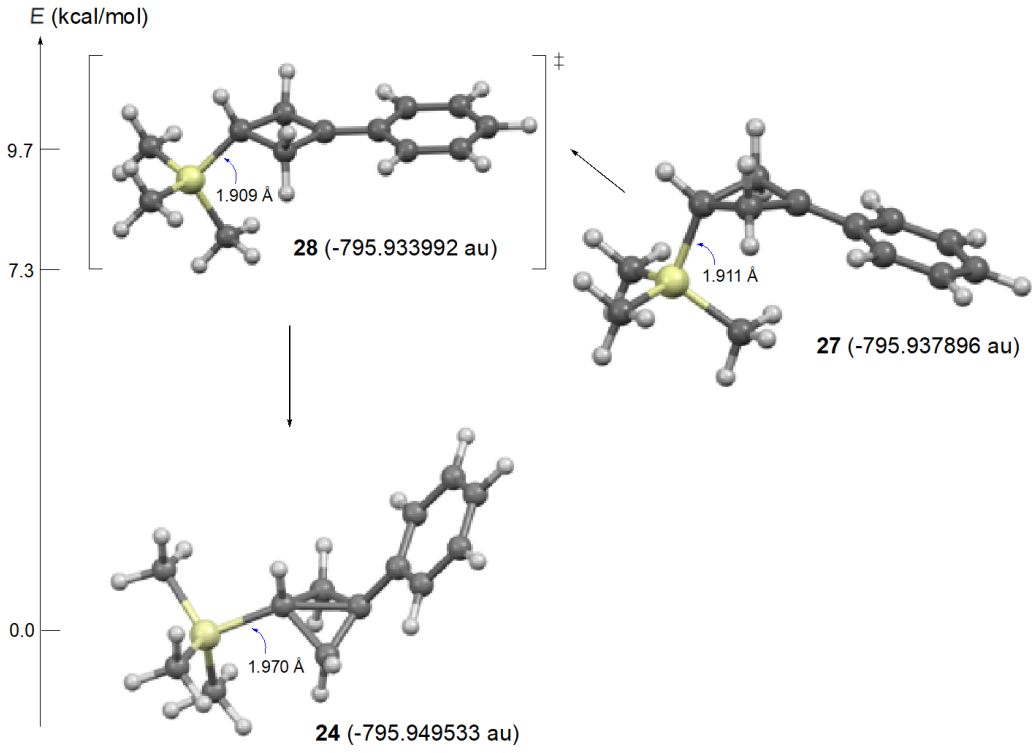

Figure 3: M062X/6-311+G** calculated structures and relative energies of cations **24**, **27**, and transition state **28**.

the TMS group in the 3-position provides no cross-ring stabilization. The calculated barrier for ring inversion of **27** to give the lower energy rear lobe stabilized γ-trimethylsilyl cation **24** is only 2.4 kcal/mol. Calculations at the B3LYP/6-31G*, B3LYP/6-311+G**, MP2/6-31G*, and the MP2/6-311+G** levels lead to the same conclusions, i.e., cations **24** and **27** are distinct energy minima with a very low barrier for conversion of **27** to **24**. Therefore, formation of **27** under solvolytic conditions should readily yield **24**, and subsequently the substitution product **21**. The small amount (4%) of elimination product **22** is a result of rearrangement of **26** to the β-trimethylsilyl cation **25** as described in Scheme 5.

Unsubstituted and methyl-substituted systems

Attention was next turned to potential γ-trimethylsilylcyclobutyl cation systems lacking phenyl stabilization. Thus pure *Z*- and *E*-alcohols **29** and **30** were each cyclopropanated under Simmons–Smith conditions, and the resultant stereochemically pure alcohols were converted to mesylates **31** and **32**, respectively (Scheme 7). For rate comparisons, cyclopropylcarbinyl mesylate **33** [62,63] was also prepared.

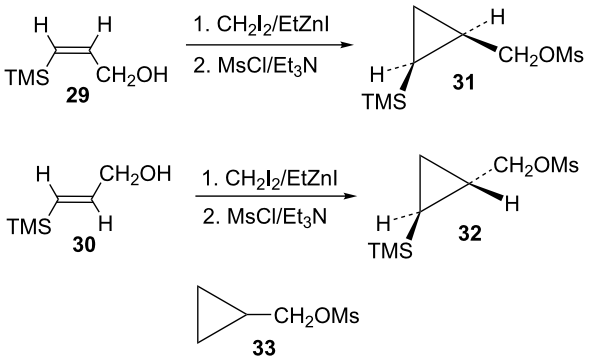

Scheme 7: Synthesis of mesylates **31** and **32**.

Mesylate **31** reacted readily in CD_3CO_2D to give the *cis*-cyclobutyl acetate **34** as the major product (Scheme 8), along with a small amount of cyclobutene (**35**). The rate of **31** (Table 1) is not substantially enhanced relative to the unsubstituted cyclopropylcarbinyl mesylate (**33**). The small rate enhancement factor of 3.56 is consistent with a small inductive stabilization of the initially formed cationic intermediate. This behavior is completely analogous to that of the phenyl analog **19** and a similar mechanistic pathway is proposed. The initially formed cyclopropylcarbinyl cation **36** rearranges to the γ-silylcyclobutyl cation **37**, the source of the major product **34**. The desilylated product **35** arises from the alternative β-trimethylsilylcyclobutyl cation.

The behavior of mesylate **32** is in contrast to that of **31** and the phenyl analog **20**. Five products, **35**, **38**, **39**, **40**, and **41**, are obtained and these products are formed in essentially the identical ratio as seen in our previous study of the *trans*-mesylate **42** [52]. The similarity of products formed from acetolysis of **32** and **42** implies that the same cation rearrangement manifold is involved. Scheme 9 gives a mechanistic rationale for these products. Capture of an unrearranged discrete cyclopropylcarbinyl cation **43** gives the major product **38**, while migration of bond *c* to the cationic center gives rearranged cation **44**, the source of the rearranged acetate **39**. Ring expansion via migration of bond *b* in **43** gives the β-trimethylsilyl-stabilized cyclobutyl cation **45**, and subsequent desilylation provides cyclobutene (**35**). Alternatively, cyclobutyl to homoallylic cation rearrangement leads to the homoallylic products **40** and **41** via internal mesylate return or solvent capture. Of interest is the fact that no product **34** (derived from γ-trimethylsilyl-stabilized cation **37**) is formed. Our previous computational study [52] provided insight into the lack of involvement of cation **37**. This study at the B3LYP/6-31G* level suggested that migration of bond *a* in **43** is not viable since the resultant cation **47** is not an energy minimum at this level, but a transition state. However, a current study at the M062X/6-311+G** level finds

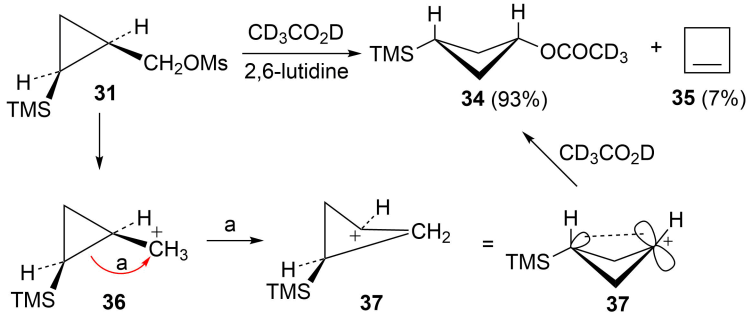

Scheme 8: Reaction of mesylate **31** in CD_3CO_2D.

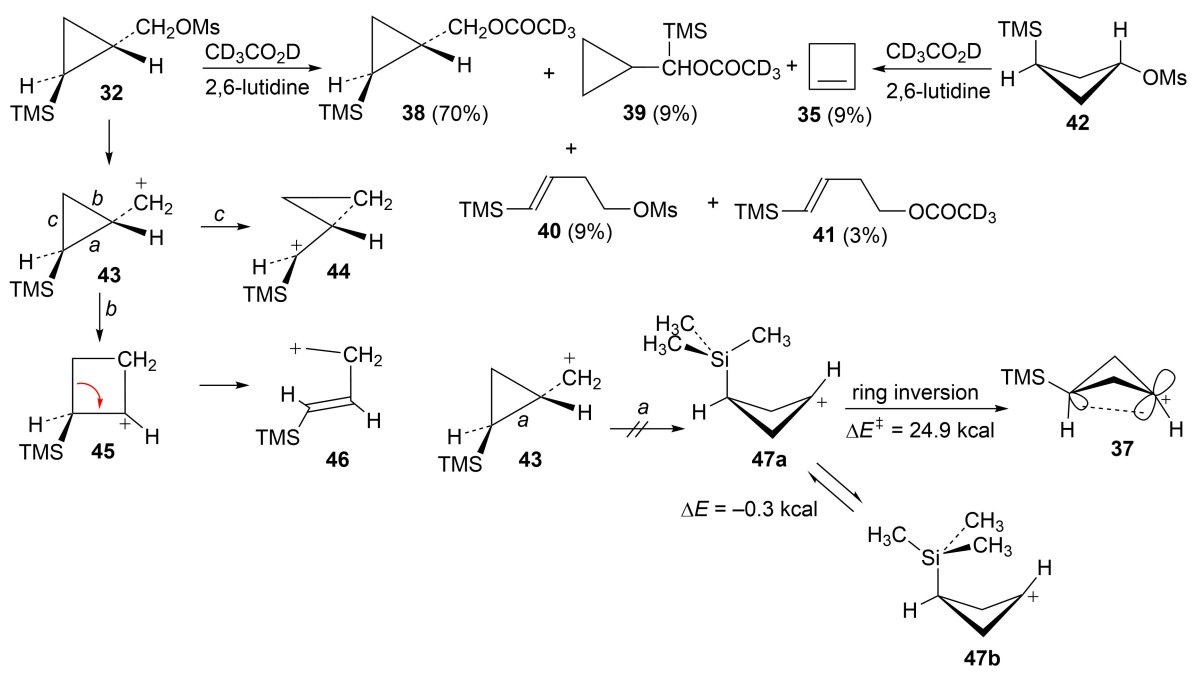

Scheme 9: Reaction of mesylate **32** in CD_3CO_2D.

that both conformations **47a** and **47b** are energy minima. While **47a** lies 10.8 kcal/mol above **37**, the barrier for inversion of **47a** to **37** is quite large (24.9 kcal/mol). Hence there is no viable route to **37**.

In order to complete the study of substrates **13** with electron-donating groups, the methyl analog **48** was prepared from the corresponding cyclopropylcarbinyl alcohol, which was available from methyl 2-diazopropanoate by a process completely analogous to the synthesis of the phenyl analog **17**. The mesylate derivative was too reactive for rates to be measured and hence the trifluoroacetate derivative **48** was studied. Acetolysis gave the acetate **50** along with a smaller amount of methylcyclobutene (**51**, Scheme 10). This reactivity is completely analogous to that seen in the phenyl and hydrogen analogs **19** and **31**, i.e., a mechanistic scheme involving the γ-trimethylsilyl-stabilized cation **52** is likely.

The isomeric trifluoroacetate **49** (shown in Table 1) gives methylcyclobutene (**51**) (68%) as the major acetolysis product, along with minor products that are identical to those previously reported [52] in solvolysis of the trifluoroacetate derivative of (1*r*,3*r*)-1-methyl-3-(trimethylsilyl)cyclobutanol. As in the case of mesylate **32**, the γ-trimethylsilyl-stabilized cation **52** is apparently not formed from trifluoroacetate **49** due to stereochemical constraints.

Systems with electron-withdrawing groups

Attention was next turned to cyclopropylcarbinyl systems substituted with electron-withdrawing groups. Previously Tilley

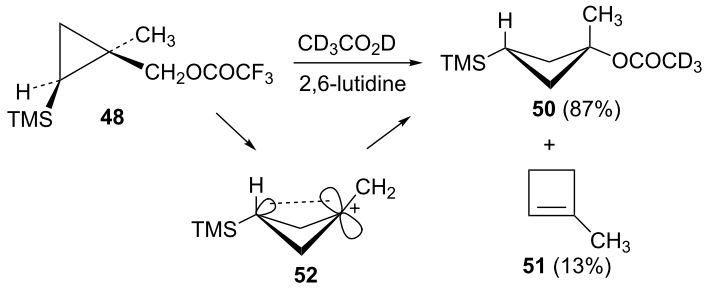

Scheme 10: Reaction of trifluoroacetate **48** in CD_3CO_2D.

Table 1: Solvolysis rates for substrates in CD_3CO_2D at 20.0 °C.

Compound	k (s^{-1})	k_{rel} (for ROMs)
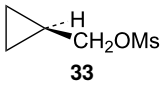 **33**	1.71×10^{-4}	1.0
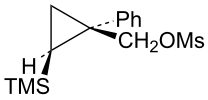 **19**	6.50×10^{-4}	3.8
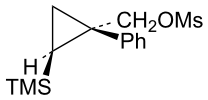 **20**	1.26×10^{-3}	7.4
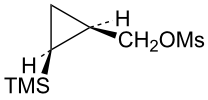 **31**	6.09×10^{-4}	3.6
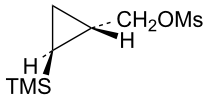 **32**	6.89×10^{-4}	4.0
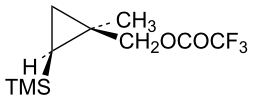 **48**	1.31×10^{-7}[a]	76[b,c]
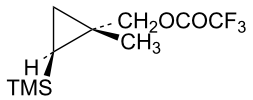 **49**	8.91×10^{-8}[a]	52[b,c]

[a]Extrapolated from data at higher temperatures. k for **48** at 60.0 °C = 2.58×10^{-5} s^{-1}; k for **48** at 80.0 °C = 2.33×10^{-4} s^{-1}; k for **49** at 60.0 °C = 1.62×10^{-5} s^{-1}; k for **49** at 80.0 °C = 1.42×10^{-4} s^{-1}. [b]Mesylate is too reactive for rate to be measured. [c]Assuming mesylate reacts 10^5 faster than trifluoroacetate.

and co-workers [55] have examined the triflate **53** and found that this system solvolyzes with rear lobe TMS participation (Scheme 11). The unusual feature in solvolysis of **53** is the formation of the highly strained bicyclobutane **55** as the sole product. It was therefore of interest to see if the cyclopropylcarbinyl to cyclobutyl rearrangement could be used to access the carbocation **54**, and subsequently, bicyclobutane **55**. It was also of interest to see if other bicyclobutanes could be formed if the CF_3 group were replaced by other electron-withdrawing groups that we have previously examined in carbocation forming reactions.

The requisite trifluoromethyl-substituted cyclopropylcarbinyl systems were prepared by addition of the carbene derived from the diazoester **56** to vinyltrimethylsilane as shown in

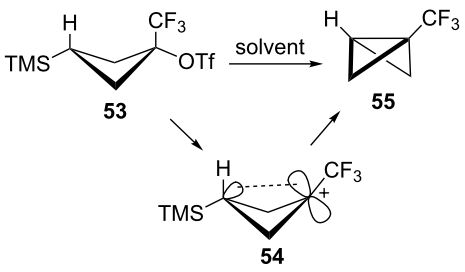

Scheme 11: Bicyclobutane formation from a γ-trimethylsilyl cation.

Scheme 12. Reduction of the ester mixture **57** with lithium aluminum hydride gave a chromatographically separable mixture of alcohols **58** and **59**. Stereochemistry of the alcohol **58** was established by long-range ^{19}F coupling to the *cis*-trimethylsilyl group hydrogens ($J_{H\text{-}F}$ = 0.9 Hz). Long-range ^{19}F coupling to the TMS methyl groups of **58** was also observed in the ^{13}C NMR spectrum ($J_{C\text{-}F}$ = 2.1 Hz) [64,65]. This long-range ^{19}F coupling is not observed when the CF_3 group is *trans* to the TMS group in the isomer **59**.

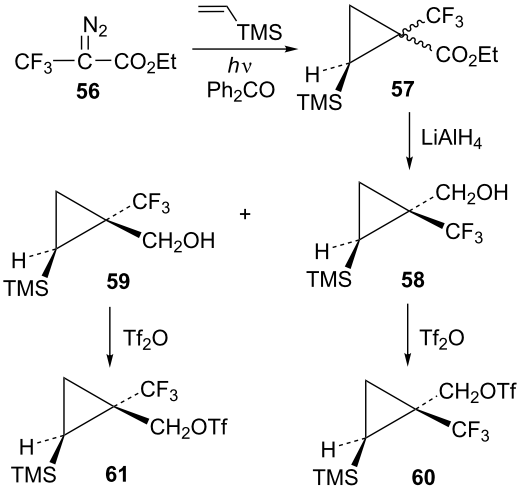

Scheme 12: Formation of triflates **60** and **61**.

Additional cyclopropylcarbinyl systems containing the electron-withdrawing cyano and carbomethoxy groups were prepared in an analogous fashion as shown in Scheme 13. Carbomethoxy-cyano carbene addition to vinyltrimethylsilane followed by lithium borohydride reduction of the ester functionality of **63** gave a separable mixture of alcohols **64** and **65**. The stereochemistry of the product **65** was established using nOe studies. Cyano to carbomethoxy conversion in **65** to give alcohol **66** was straightforward. Triflate derivatives **67** and **68** were prepared since analogous mesylate derivatives were relatively unreactive. Triflate **69** was a highly reactive substrate that could only be

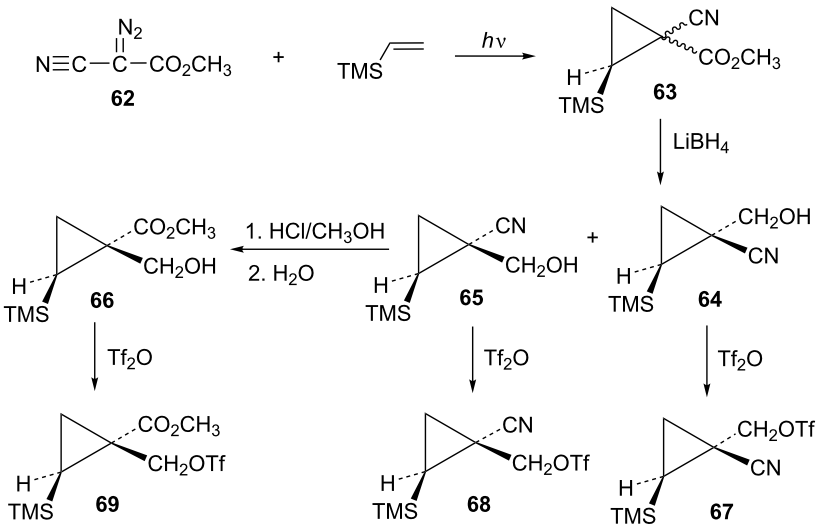

Scheme 13: Formation of triflates **67**, **68**, and **69**.

prepared in about 80% purity. The less reactive mesylate derivative **75** was therefore prepared and used for kinetic studies.

The triflates **61**, **68**, and **69** (with electron-withdrawing groups *trans* to trimethylsilyl) were all solvolyzed in CD_3CO_2D and results are shown in Scheme 14. Since the triflate **69** was highly reactive and could not be isolated in pure form, the mesylate derivative **75** was used in kinetic studies that were carried out in the 40–60 °C range. Rates of reaction of mesylate derivatives (Table 2) were all substantially slower than the parent mesylate **33** or the phenyl, methyl, or H analogs. This is attributed to a significant inductive destabilizing β-effect of the group E on the initially formed cation **73**. The triflates all produced significant amounts of bicyclobutane products **55** and **72** along with some unrearranged substitution products **70**. In the cases of **68** and **69**, some rearranged substitution products **71** were also formed. The mesylate **75** gave the same initial products as the triflate **69**. However, the bicyclobutane **72c** formed from mesylate **75** was not completely stable at 40–60 °C, but degraded slowly to a mixture of other products. The bicyclobutanes **55**, **72b**, and **72c** were quite stable in CD_3CO_2D at 20 °C, where triflate studies were carried out.

The bicyclobutane products **55** and **72** are a result of desilylation of the γ-silyl cations **54** and **74**. Why are bicylobutanes formed from cations **54** and **74** and not from cations **24**, **37**, and **52**, which do not have electron-withdrawing groups? Previous studies have shown that "electron-deficient" cations **9**, where

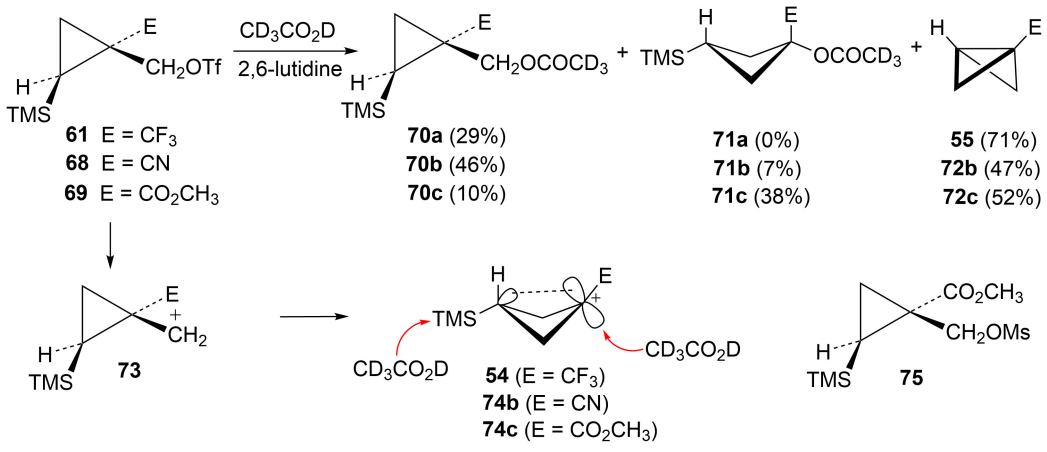

Scheme 14: Reactions of substrates with electron-withdrawing groups in CD_3CO_2D.

Table 2: Solvolysis rates for substrates in CD_3CO_2D at 20.0 °C.

Compound	k (s^{-1})	k_{rel} (for ROMs)
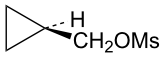 **33**	1.71×10^{-4}	1.00
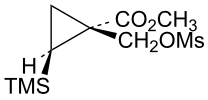 **75**	1.26×10^{-7}[a]	7.3×10^{-4}
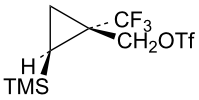 **61**	2.25×10^{-4}	1.3×10^{-5}[b]
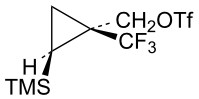 **60**	1.25×10^{-3}	7.3×10^{-5}[b]
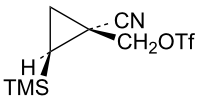 **68**	2.14×10^{-4}	1.3×10^{-5}[b]
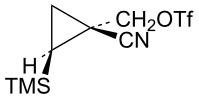 **67**	1.61×10^{-3}	9.4×10^{-5}[b]

[a]Extrapolated from data at higher temperatures. k at 40.0 °C = 2.24×10^{-6} s^{-1}; k at 50.0 °C = 8.40×10^{-6} s^{-1}; k at 60.0 °C = 2.85×10^{-5} s^{-1}. [b]Assuming triflate reacts 10^5 faster than mesylate.

E = COR [66], CN [25], CF_3 [67], and $PO(OEt)_2$ [34], readily eliminate β-hydrogens to form alkenes as major products. They do not readily capture solvent at the cationic center. It is therefore expected that nucleophilic attack at the cationic centers of **54** and **74** will be slowed. Table 3 shows results of calculations on the γ-trimethylsilylcyclobutyl cations shown in Figure 4 at different levels of theory. The presence of the electron-withdrawing group results in an increase in the Si–C3 bond length relative to the cations **24** and **52**. Also, the cross-ring C1–C3 distance is decreased. In the language of resonance theory, these features are in line with increased contributions of form **74a** to the overall structure of the cation. These features suggest more facile nucleophilic attack should occur at silicon, favoring bicyclobutane formation. Also included in Table 3 are calculated bond lengths in the phosphoryl-substituted cation **74d**, which also shows a very long Si–C bond. Preferred trimethylsilyl elimination from this intermediate is in line with the behavior of mesylate **76**, which gives exclusively the bicyclobutane **77** on solvolysis in CH_3CO_2H (Scheme 15).

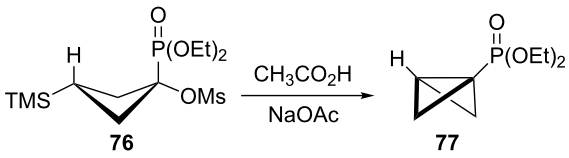

76 **77**

Scheme 15: Bicyclobutane formation from mesylate **76** in CH_3CO_2H.

The final item to be addressed is the behavior of triflates **60** and **67** with electron-withdrawing CF_3 and CN groups *cis* to the tri-

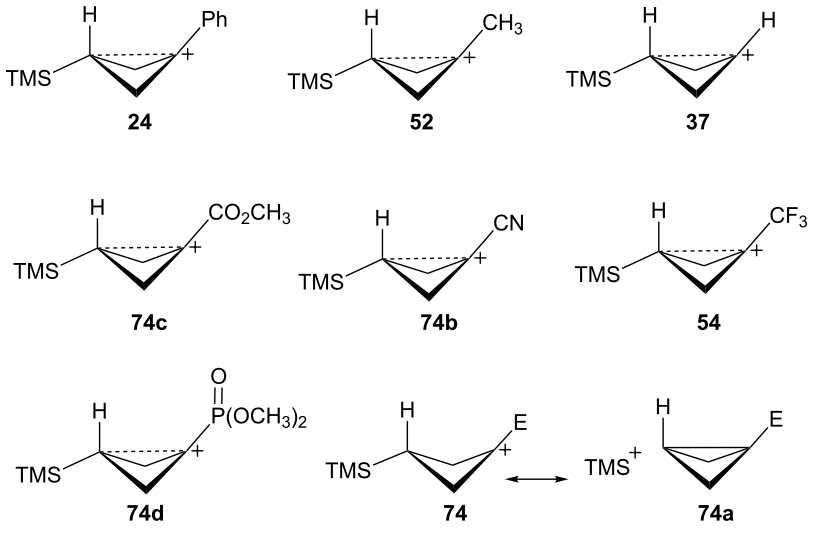

Figure 4: γ-Trimethylsilyl cations.

Table 3: Calculated bond lengths (Å) of γ-trimethylsilyl cations.

Cation	Bond	B3LYP/ 6-31G*	B3LYP/ 6-311+G**	MP2/ 6-31G*	MP2/ 6-311+G**	M062X/ 6-311+G**
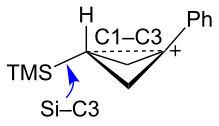 **24**	Si–C3 C1–C3	1.962 1.916	1.959 1.914	1.975 1.760	1.970 1.759	1.970 1.736
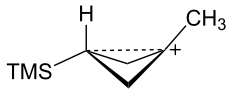 **52**	Si–C3 C1–C3	1.999 1.717	1.994 1.719	1.990 1.665	1.983 1.675	1.984 1.652
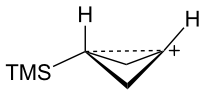 **37**	Si–C3 C1–C3	2.016 1.662	2.013 1.659	2.004 1.636	1.998 1.645	2.000 1.616
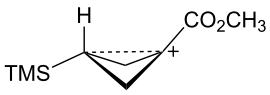 **74c**	Si–C3 C1–C3	2.018 1.658	2.018 1.655	2.009 1.625	2.002 1.632	2.007 1.601
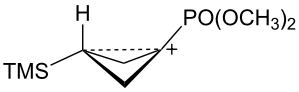 **74d**	Si–C3 C1–C3	2.013 1.663	2.012 1.659	2.008 1.624	2.003 1.630	2.004 1.602
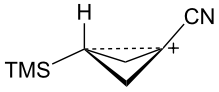 **74b**	Si–C3 C1–C3	2.046 1.694	2.045 1.688	2.037 1.652	2.028 1.663	2.031 1.623
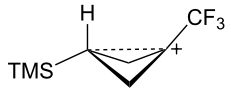 **54**	Si–C3 C1–C3	2.034 1.646	2.037 1.642	2.024 1.616	2.019 1.623	2.024 1.595

methylsilyl group. These substrates gave exclusively unrearranged substitution products **78** and **79** when reacted in CD_3CO_2D (Scheme 16). The lack of rearrangement products suggests that these potent electron-withdrawing groups make further rearrangement of cations **80** untenable. Indeed, M062X/6-311+G** calculations show that the potential rearranged cation **81** (E = CN) is not even an energy minimum, but a transition state.

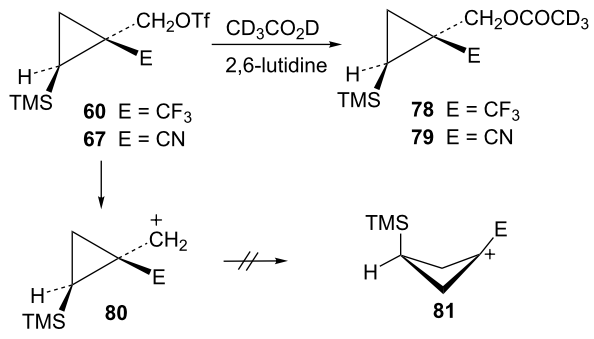

Scheme 16: Reactions of triflates **60** and **67** in CD_3CO_2D.

Conclusion

1-Substituted-*cis*-2-trimethylsilylcyclopropylcarbinyl mesylates and triflates **13** solvolyze in CD_3CO_2D to give products derived from 3-trimethylsilylcyclobutyl cations. These cationic intermediates are stabilized by a long-range rear lobe interaction with the γ-trimethylsilyl group. When the substituent is electron-withdrawing (CF_3, CN, or CO_2CH_3), significant amounts of bicyclobutane products are formed. The bicyclobutanes are a result of γ-trimethylsilyl elimination from the cationic intermediate. Computational studies support a carbocation intermediate with an unusually long Si–C bond, indicative of increased demand for Si–C hyperconjugation due to the electron-withdrawing group. With the exception of the phenyl substitution,

the chemistry of *trans*-derivatives **14** is quite different since these substrates are geometrically precluded from forming γ-trimethylsilyl-stabilized cyclobutyl cations.

Experimental

Full experimental details are given in Supporting Information File 1.

Supporting Information

Full experimental details, ^{1}H and ^{13}C NMR spectra of new compounds, and M062X/6-311+G** computational studies are presented as Supporting Information.

Supporting Information File 1

Experimental details and ^{1}H and ^{13}C NMR spectra of new compounds.
[https://www.beilstein-journals.org/bjoc/content/supplementary/1860-5397-15-170-S1.pdf]

Supporting Information File 2

M062X/6-611+G** calculated structures, energies, and Cartesian coordinates for carbocations and transition states.
[https://www.beilstein-journals.org/bjoc/content/supplementary/1860-5397-15-170-S2.pdf]

ORCID® iDs

Xavier Creary - https://orcid.org/0000-0002-1274-5769

References

1. Merling, G. *Ber. Dtsch. Chem. Ges.* **1891,** *24,* 3108–3126. doi:10.1002/cber.189102402151
2. von E. Doering, W.; Knox, L. H. *J. Am. Chem. Soc.* **1954,** *76,* 3203–3206. doi:10.1021/ja01641a027
3. Norris, J. F.; Sanders, W. W. *Am. Chem. J.* **1901,** *25,* 54–62.
4. Kehrmann, F.; Wentzel, F. *Ber. Dtsch. Chem. Ges.* **1901,** *34,* 3815–3819. doi:10.1002/cber.19010340393
5. Gomberg, M. *Ber. Dtsch. Chem. Ges.* **1907,** *40,* 1847–1888. doi:10.1002/cber.19070400289
6. Freedman, H. H. In *Carbonium Ions;* Olah, G. A.; von Ragué Schleyer, P., Eds.; Wiley Interscience: New York, U.S.A., 1973; Vol. IV, pp 1501–1578. See for a review and leading references.
7. Horn, M.; Mayr, H. *J. Phys. Org. Chem.* **2012,** *25,* 979–988. doi:10.1002/poc.2979 See for a review and leading references.
8. Richey, H. G., Jr. In *Carbonium Ions;* Olah, G. A.; von Ragué Schleyer, P., Eds.; Wiley Interscience: New York, U.S.A., 1972; Vol. III, pp 1201–1294. See for a leading review.
9. Wiberg, K. B.; Hess, B. A., Jr.; Ashe, A. J., III. In *Carbonium Ions;* Olah, G. A.; von Ragué Schleyer, P., Eds.; Wiley Interscience: New York, U.S.A., 1972; Vol. III, pp 1295–1345. See for a leading review.
10. Demjanow, N. J. *Ber. Dtsch. Chem. Ges.* **1907,** *40,* 4961–4963. doi:10.1002/cber.190704004168
11. Roberts, J. D.; Mazur, R. H. *J. Am. Chem. Soc.* **1951,** *73,* 2509–2520. doi:10.1021/ja01150a029
12. Sneen, R. A.; Lewandowski, K. M.; Taha, I. A. I.; Smith, B. R. *J. Am. Chem. Soc.* **1961,** *83,* 4843–4848. doi:10.1021/ja01484a035
13. Roberts, J. D.; Mazur, R. H. *J. Am. Chem. Soc.* **1951,** *73,* 3542–3543. doi:10.1021/ja01151a550
14. Caserio, M. C.; Graham, W. H.; Roberts, J. D. *Tetrahedron* **1960,** *11,* 171–182. doi:10.1016/0040-4020(60)80068-3
15. von Ragué Schleyer, P.; Majerski, Z. *J. Am. Chem. Soc.* **1971,** *93,* 665–671. doi:10.1021/ja00732a019
16. Olah, G. A.; Reddy, V. P.; Prakash, G. K. S. *Chem. Rev.* **1992,** *92,* 69–95. doi:10.1021/cr00009a003
17. Saunders, M.; Siehl, H. U. *J. Am. Chem. Soc.* **1980,** *102,* 6868–6869. doi:10.1021/ja00542a045
18. Staral, J. S.; Yavari, I.; Roberts, J. D.; Prakash, G. K. S.; Donovan, D. J.; Olah, G. A. *J. Am. Chem. Soc.* **1978,** *100,* 8016–8018. doi:10.1021/ja00493a045
19. Koch, W.; Liu, B.; DeFrees, D. J. *J. Am. Chem. Soc.* **1988,** *110,* 7325–7328. doi:10.1021/ja00230a008
20. Siehl, H.-U. *Adv. Phys. Org. Chem.* **2018,** *52,* 1–47. doi:10.1016/bs.apoc.2018.10.001
21. Creary, X. *Chem. Rev.* **1991,** *91,* 1625–1678. doi:10.1021/cr00008a001
22. Gassman, P. G.; Tidwell, T. T. *Acc. Chem. Res.* **1983,** *16,* 279–285. doi:10.1021/ar00092a003
23. Tidwell, T. T. *Angew. Chem., Int. Ed. Engl.* **1984,** *23,* 20–32. doi:10.1002/anie.198400201
24. Allen, A. D.; Tidwell, T. T. In *Advances in Carbocation Chemistry;* Creary, X., Ed.; Jai Press Inc.: Greenwich, CT, 1989; Vol. 1, pp 1–44.
25. Gassman, P. G.; Talley, J. J. *J. Am. Chem. Soc.* **1980,** *102,* 1214–1216. doi:10.1021/ja00523a076
26. Gassman, P. G.; Talley, J. J. *J. Am. Chem. Soc.* **1980,** *102,* 4138–4143. doi:10.1021/ja00532a026
27. Dixon, D. A.; Charlier, P. A.; Gassman, P. G. *J. Am. Chem. Soc.* **1980,** *102,* 3957–3959. doi:10.1021/ja00531a051
28. Gassman, P. G.; Saito, K. *Tetrahedron Lett.* **1981,** *22,* 1311–1314. doi:10.1016/s0040-4039(01)90304-1
29. Gassman, P. G.; Guggenheim, T. L. *J. Org. Chem.* **1982,** *47,* 3023–3026. doi:10.1021/jo00136a048
30. Begue, J. P.; Charpentier-Morize, M. *Acc. Chem. Res.* **1980,** *13,* 207–212. doi:10.1021/ar50151a003
31. Creary, X. *Acc. Chem. Res.* **1985,** *18,* 3–8. doi:10.1021/ar00109a002
32. Creary, X. In *Advances in Carbocation Chemistry;* Creary, X., Ed.; Jai Press Inc.: Greenwich, CT, 1989; Vol. 1, pp 45–92.
33. Charpentier-Morize, M.; Begue, J.-P. In *Advances in Carbocation Chemistry;* Creary, X., Ed.; Jai Press Inc.: Greenwich, CT, 1989; Vol. 1, pp 219–253.
34. Creary, X.; Geiger, C. C.; Hilton, K. *J. Am. Chem. Soc.* **1983,** *105,* 2851–2858. doi:10.1021/ja00347a054
35. Creary, X.; Underiner, T. L. *J. Org. Chem.* **1985,** *50,* 2165–2170. doi:10.1021/jo00212a033

36. Siehl, H.-U. In *Recent Developments in Carbocation and Onium Ion Chemistry;* Laali, K. K., Ed.; ACS Symposium Series No. 965; American Chemical Society: Washington, DC, 2007; pp 1–31. See for a review and leading references.
37. Siehl, H.-U.; Müller, T. In *The Chemistry of Organosilicon Compounds;* Rappoport, Z.; Apeloig, Y., Eds.; John Wiley and Sons: New York, U.S.A.; Vol. 2, pp 595–701. See for a review and leading references.
38. Lambert, J. B.; Zhao, Y.; Emblidge, R. W.; Salvador, L. A.; Liu, X.; So, J. H.; Chelius, E. C. *Acc. Chem. Res.* **1999,** *32,* 183–190. doi:10.1021/ar970296m See for a review and leading references.
39. Lambert, J. B.; Liu, X. *J. Organomet. Chem.* **1996,** *521,* 203–210. doi:10.1016/0022-328x(96)06228-6 See for a review and leading references.
40. Lambert, J. B. *Tetrahedron* **1990,** *46,* 2677–2689. doi:10.1016/s0040-4020(01)88362-9 See for a review and leading references.
41. Lambert, J. B.; Chelius, E. C. *J. Am. Chem. Soc.* **1990,** *112,* 8120–8126. doi:10.1021/ja00178a041 See for a review and leading references.
42. Lambert, J. B.; Wang, G. T.; Finzel, R. B.; Teramura, D. H. *J. Am. Chem. Soc.* **1987,** *109,* 7838–7845. doi:10.1021/ja00259a036 See for a review and leading references.
43. White, J. M. *Aust. J. Chem.* **1995,** *48,* 1227–1251. doi:10.1071/ch9951227 See for a review and leading references.
44. Sommer, L. H.; Bailey, D. L.; Whitmore, F. C. *J. Am. Chem. Soc.* **1948,** *70,* 2869–2872. doi:10.1021/ja01189a009 See for a review and leading references.
45. Creary, X.; Butchko, M. A. *J. Am. Chem. Soc.* **2001,** *123,* 1569–1578. doi:10.1021/ja002407+
46. Creary, X.; Butchko, M. A. *J. Org. Chem.* **2001,** *66,* 1115–1121. doi:10.1021/jo001112b
47. Creary, X.; Jiang, Z.; Butchko, M.; McLean, K. *Tetrahedron Lett.* **1996,** *37,* 579–582. doi:10.1016/0040-4039(95)02266-x
48. Creary, X.; Wang, Y.-X. *Tetrahedron Lett.* **1989,** *30,* 2493–2496. doi:10.1016/s0040-4039(01)80433-0
49. Creary, X.; Kochly, E. D. *J. Org. Chem.* **2009,** *74,* 2134–2144. doi:10.1021/jo802722z
50. Creary, X.; O'Donnel, B. D.; Vervaeke, M. *J. Org. Chem.* **2007,** *72,* 3360–3368. doi:10.1021/jo062668n
51. Siehl, H.-U.; Fulj, M. *Pure Appl. Chem.* **1998,** *70,* 2015–2022. doi:10.1351/pac199870102015
52. Creary, X.; Kochly, E. D. *J. Org. Chem.* **2009,** *74,* 9044–9053. doi:10.1021/jo901821f
53. Creary, X.; Heffron, A. *J. Org. Chem.* **2014,** *79,* 2547–2555. doi:10.1021/jo500007p
54. Creary, X.; Heffron, A.; Going, G.; Prado, M. *J. Org. Chem.* **2015,** *80,* 1781–1788. doi:10.1021/jo502691t
55. Mercadante, M. A.; Kelly, C. B.; Hamlin, T. A.; Delle Chiaie, K. R.; Drago, M. D.; Duffy, K. K.; Dumas, M. T.; Fager, D. C.; Glod, B. L. C.; Hansen, K. E.; Hill, C. R.; Leising, R. M.; Lynes, C. L.; MacInnis, A. E.; McGohey, M. R.; Murray, S. A.; Piquette, M. C.; Roy, S. L.; Smith, R. M.; Sullivan, K. R.; Truong, B. H.; Vailonis, K. M.; Gorbatyuk, V.; Leadbeater, N. E.; Tilley, L. J. *Chem. Sci.* **2014,** *5,* 3983–3994. doi:10.1039/c4sc01732c
56. Shiner, V. J., Jr.; Ensinger, M. W.; Kriz, G. S. *J. Am. Chem. Soc.* **1986,** *108,* 842–844. doi:10.1021/ja00264a050
57. Shiner, V. J., Jr.; Ensinger, M. W.; Huffman, J. C. *J. Am. Chem. Soc.* **1989,** *111,* 7199–7205. doi:10.1021/ja00200a045
58. Grob, C. A.; Gründel, M.; Sawlewicz, P. *Helv. Chim. Acta* **1988,** *71,* 1502–1507. doi:10.1002/hlca.19880710615
59. Adcock, W.; Clark, C. I.; Schiesser, C. H. *J. Am. Chem. Soc.* **1996,** *118,* 11541–11547. doi:10.1021/ja961870c
60. Creary, X. *J. Am. Chem. Soc.* **2013,** *135,* 6570–6578. doi:10.1021/ja400747u
61. Creary, X. *J. Org. Chem.* **2015,** *80,* 11378–11387. doi:10.1021/acs.joc.5b01955
62. Mascitti, V.; Corey, E. J. *J. Am. Chem. Soc.* **2006,** *128,* 3118–3119. doi:10.1021/ja058370g
63. Ohta, H.; Ishizaka, T.; Tatsuzuki, M.; Yoshinaga, M.; Iida, I.; Yamaguchi, T.; Tomishima, Y.; Futaki, N.; Toda, Y.; Saito, S. *Bioorg. Med. Chem.* **2008,** *16,* 1111–1124. doi:10.1016/j.bmc.2007.10.087
64. Hsee, L. C.; Sardella, D. J. *Magn. Reson. Chem.* **1990,** *28,* 688–692. doi:10.1002/mrc.1260280806
65. Chen, J.; Reibenspies, J.; Derecskei-Kovacs, A.; Burgess, K. *Chem. Commun.* **1999,** 2501–2502. doi:10.1039/a907559c
66. Creary, X. *J. Am. Chem. Soc.* **1984,** *106,* 5568–5577. doi:10.1021/ja00331a029
67. Jansen, M. P.; Koshy, K. M.; Mangru, N. N.; Tidwell, T. T. *J. Am. Chem. Soc.* **1981,** *103,* 3863–3867. doi:10.1021/ja00403a040

License and Terms

BEILSTEIN JOURNAL OF ORGANIC CHEMISTRY

Inherent atomic mobility changes in carbocation intermediates during the sesterterpene cyclization cascade

Hajime Sato*[1,2], Takaaki Mitsuhashi[3], Mami Yamazaki[1], Ikuro Abe[3] and Masanobu Uchiyama[2,3]

Letter

Open Access

Address:
[1]Graduate School of Pharmaceutical Sciences, Chiba University, 1-8-1 Inohana, Chuo-ku, Chiba 260-8675, Japan, [2]Clustering of Pioneering Research (CPR) Advanced Elements Chemistry Laboratory, RIKEN, 2-1 Hirosawa, Wako, Saitama 351-0198, Japan and [3]Graduate School of Pharmaceutical Sciences, University of Tokyo, 7-3-1 Hongo, Bunkyo-ku, Tokyo 113-0033, Japan

Email:
Hajime Sato* - hajime.sato@chiba-u.jp

* Corresponding author

Keywords:
biosynthesis; carbocation; DFT; substrate recognition; terpene cyclase

Beilstein J. Org. Chem. **2019,** *15,* 1890–1897.
doi:10.3762/bjoc.15.184

Received: 24 April 2019
Accepted: 22 July 2019
Published: 07 August 2019

This article is part of the thematic issue "Reactive intermediates – carbocations".

Guest Editor: S. R. Hare

Abstract

We previously showed that the regio- and stereoselectivity in terpene-forming reactions are determined by the conformations of the carbocation intermediates, which reflect the initial conformation of the substrate, geranylfarnesyl diphosphate (GFPP). However, it remains unclear how the initial conformation of GFPP is controlled, and which part(s) of the GFPP molecule are important for its fixation inside the substrate-binding pocket. Here, we present the first detailed analysis of the inherent atomic mobility in carbocation intermediates during sesterterpene biosynthesis. We identified two methyl groups as the least mobile of all the carbons of the carbocation intermediates in the first half of the cyclization cascade. Our analysis suggests that these two methyl groups are critical for the preorganization of GFPP in the biosynthetic pathways leading to sesterfisherol and quiannulatene.

Introduction

Terpene synthases are thought to have four main roles: (i) triggering the biosynthetic cyclization cascade by the elimination of pyrophosphate or by protonation; (ii) preorganization of the substrate to generate the reactive conformation; (iii) protection of reactive intermediates from water; and (iv) termination of the reaction by deprotonation or hydration. We previously established the importance of conformation in the carbocation cyclization cascade [1], focusing on two sesterterpenes, i.e., quiannulatene [1,2] and sesterfisherol [3-5], as representative examples. These two sesterterpenes are synthesized via a 5/12/5 tricyclic intermediate, which leads to a 5/6/8/5 tetracyclic intermediate. This, in turn, is transformed to a 4/6-membered ring in quiannulatene biosynthesis, whereas 5/5 ring formation proceeds in sesterfisherol biosynthesis (Scheme 1, Scheme 2,

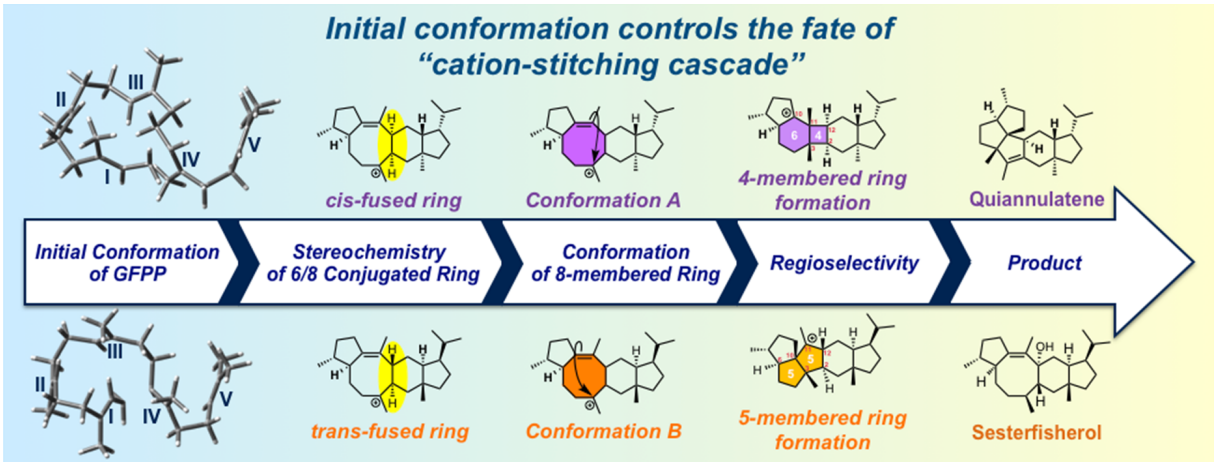

Scheme 1: The regio- and stereoselectivity in quiannulatene and sesterfisherol biosynthesis are determined by the initial conformation of GFPP.

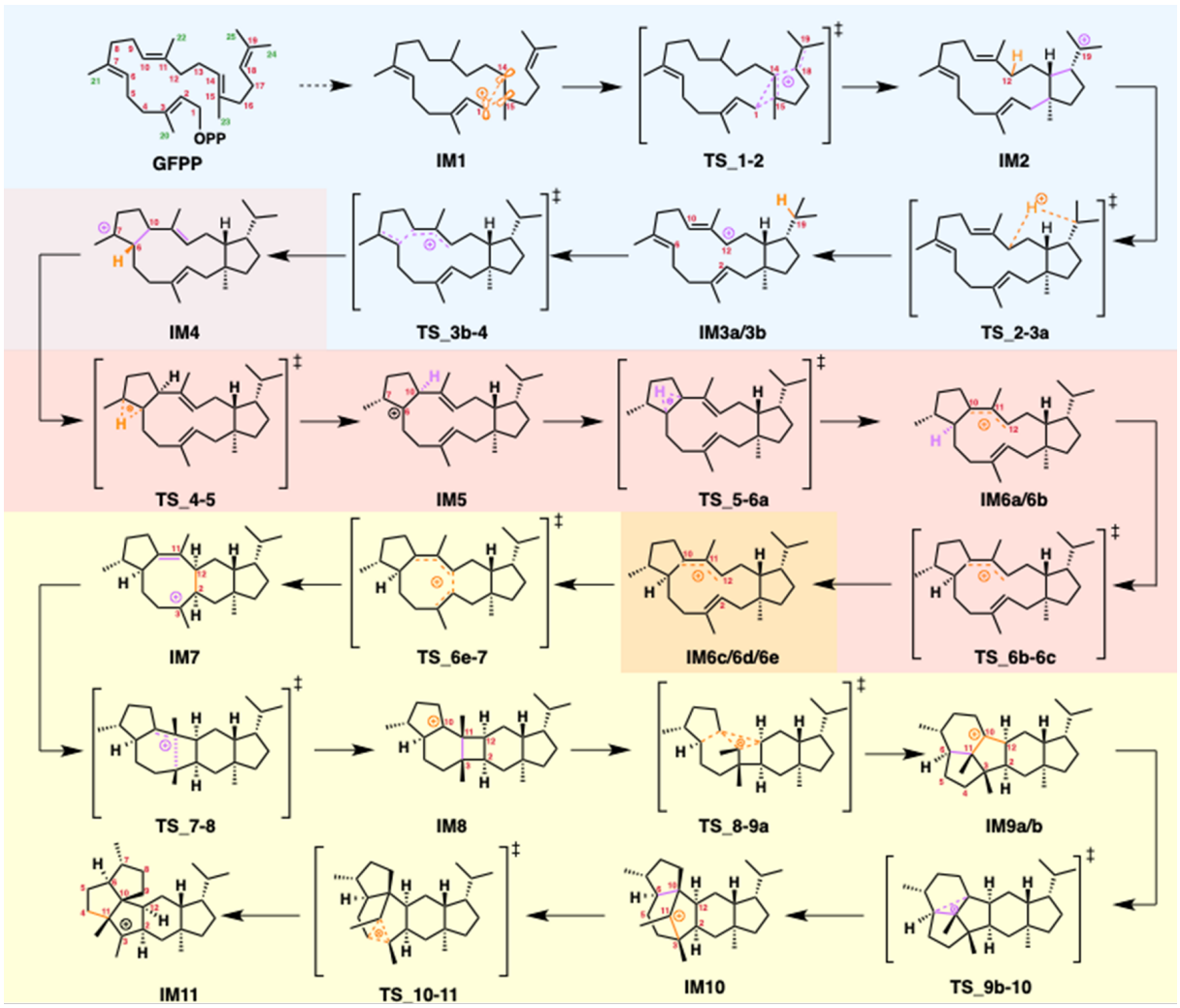

Scheme 2: Reaction mechanism of quiannulatene biosynthesis. GFPP: geranylfarnesyl diphosphate, IM: intermediate. Quiannulatene is formed by the deprotonation of **IM11**. Phase (I): 5/12/5 tricycle formation is highlighted in blue. Phase (II): conformational changes and hydrogen shifts are highlighted in orange. Phase (III): ring rearrangements are highlighted in yellow.

and Scheme 3). Based on our DFT calculations, this regioselectivity is determined by the conformation of the eight-membered ring in the 5/6/8/5 tetracyclic intermediate, which is derived from the initial conformation of GFPP. However, it remains unclear how the initial conformation of GFPP is controlled, and which part(s) of the GFPP molecule are most important for enzymatic preorganization in the terpene cyclase active site [3,5,6].

Although many terpene cyclases are known [6-10], it is still challenging to identify the precise initial conformation of the oligoprenyl diphosphate substrate in the active site, even by X-ray crystal structure determination. This is because the substrate can sometimes bind to the active site in an unreactive conformation [11]. Recently, Siegel and Tantillo reported an innovative method for predicting the docking mode of carbocation intermediates in terpene cyclase [12,13], based on QM calculation and computational docking with the Rosetta protein modeling suite [14,15]. Interestingly, probable docking modes are quite limited in the first few steps, but are much more diverse in the later part of the cyclization cascade, which may indicate that the affinity of carbocation intermediates for the terpene cyclase decreases as the reaction proceeds. Hence, we hypothesized that some part(s) of the substrate structure are less mobile (relatively fixed) in the first few steps of cyclization cascade, and thus play essential roles in the enzymatic preorganization of GFPP.

There have been many theoretical studies of terpene-forming reactions [16-18], and it appears that inherent reactivity [17] is in good accordance with the experimental outcome. This may mean that terpene cyclases do not tightly regulate the cyclization reaction steps once the carbocation is generated. Therefore, we considered that key regions of GFPP that control the fit of the substrate to the enzyme's binding site could be identified by calculating the inherent structural mobility of the carbocation intermediates. This does involve the assumption that we can neglect the influence of changes in the interior structure of the enzyme as the reaction proceeds; however, based on the above-mentioned reports, we regard this as reasonable. Nevertheless, to minimize the effects of such changes, we focused on the first half of the cyclization cascade. In this study, we report

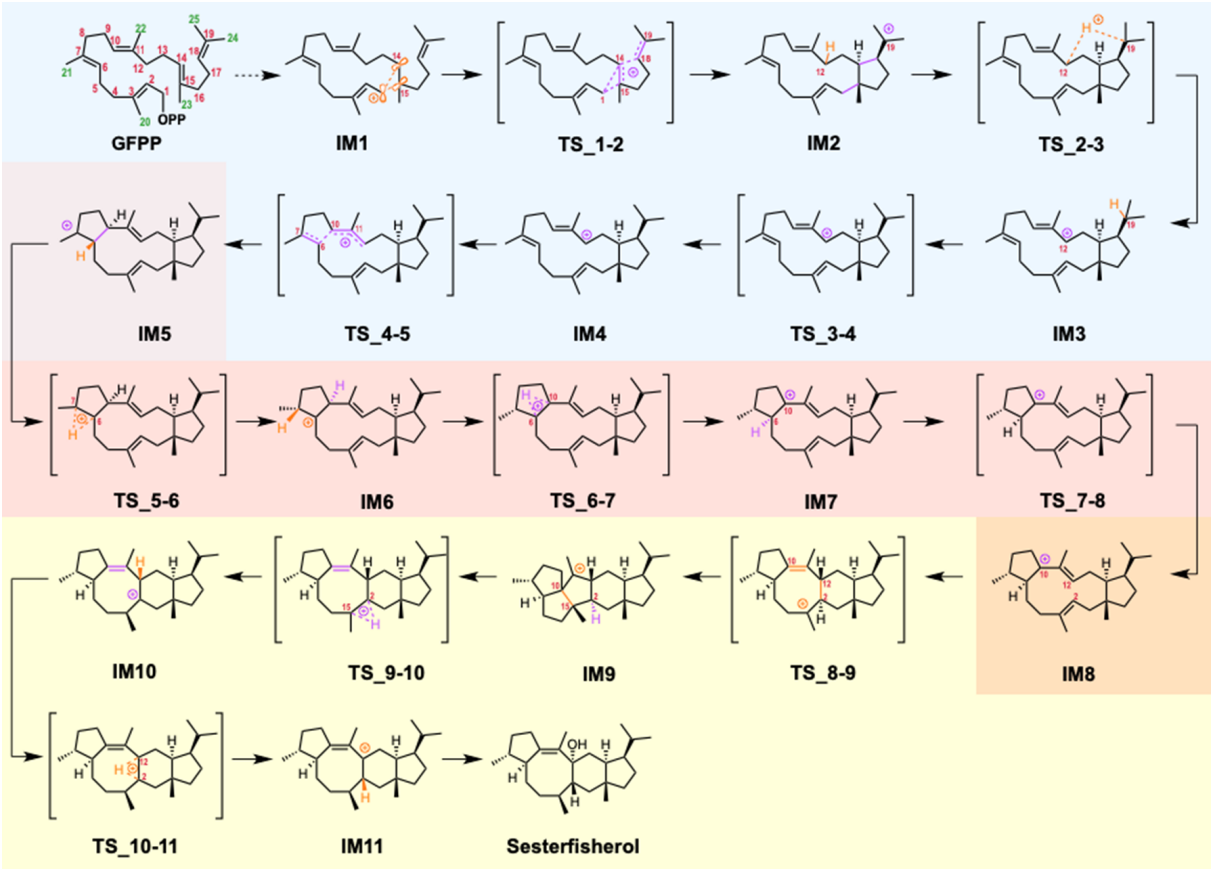

Scheme 3: Reaction mechanisms of sesterfisherol biosynthesis. Sesterfisherol is formed by the hydration of **IM11**. Phase (I): 5/12/5 tricycle formation is highlighted in blue. Phase (II): conformational changes and hydrogen shifts are highlighted in orange. Phase (III): ring rearrangements are highlighted in yellow.

the first analysis of the inherent structural mobility of carbocation intermediates in sesterterpene biosynthesis, and we discuss the implications for the mechanism of fixation (preorganization) of the substrate GFPP inside the binding pocket of the enzyme.

Results and Discussion

For the analysis of inherent structural mobility, we firstly carried out IRC calculations using GRRM11 with Gaussian 09, obtaining 2609 plots for quiannulatene formation and 2640 plots for sesterfisherol formation. We divided the whole biosynthetic process into three phases; (I) 5/12/5 tricycle formation, (II) conformational changes and hydrogen shifts, and (III) ring rearrangements (Scheme 2 and Scheme 3). Then, we computed the inherent structural mobility of the carbocation intermediates by calculating the displacements of all carbons between each plot. The results of these analyses are shown as heat maps in Figure 1, Figure 2, and Figure 3. In these heat maps, the Y axis shows the carbon number and the X axis shows the coordinate. Highly mobile carbons are shown in red, moderately mobile carbons in yellow, and static carbons in blue.

Phase I: 5/12/5 tricycle formation

Based on our inherent mobility analysis, C1–C5, C15, C16, C20, C21 and C23 are static during 5/12/5 tricyclic formation in the biosynthesis of both quiannulatene and sesterfisherol (Figure 1). Interestingly, although the conversion of **IM1** to **IM2** involves C1–C15 and C14–C18 bond formations, the displacements of C6–C12, and C22 are also large, indicating that these regions, though they are distant from the reaction centre, are relatively flexible and not tightly fixed by the enzyme. As we reported previously, the initial conformation of GFPP, in particular the orientation of six methyl groups (C20–C25), is critical. Therefore, we focused on these methyl groups. While

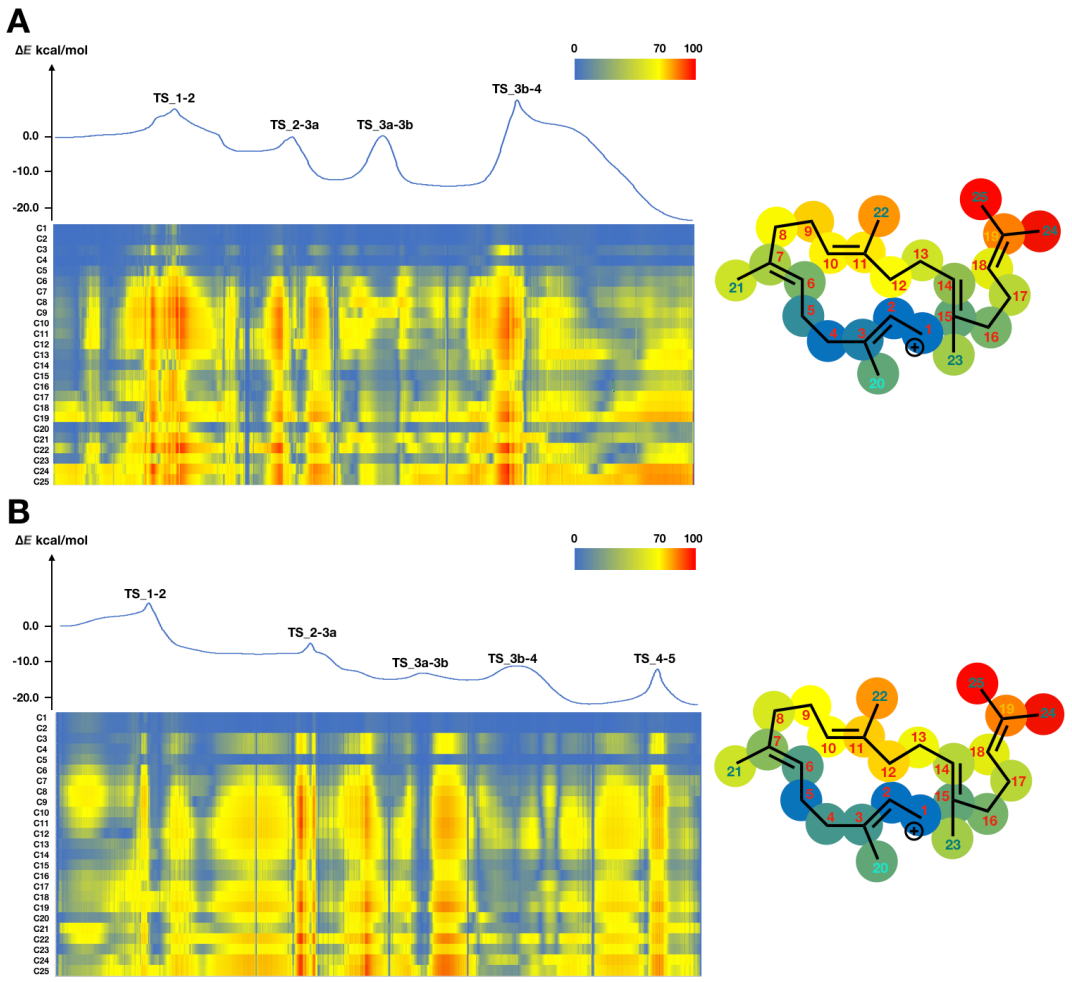

Figure 1: Energy diagram and heat map analysis of 5/12/5 tricycle formation (A) **IM1–IM4** in quiannulatene biosynthesis. (B) **IM1–IM5** in sesterfisherol biosynthesis. An energy diagram, heat map of inherent mobility and structural heat map are shown. All energies are shown in kcal/mol. The Y axis shows the carbon number and the X axis shows the coordinate in the heat map. The right structural heat map shows the total mobility in tricycle formation. Red means high mobility, yellow means moderate mobility, and blue means static. TS: transition state.

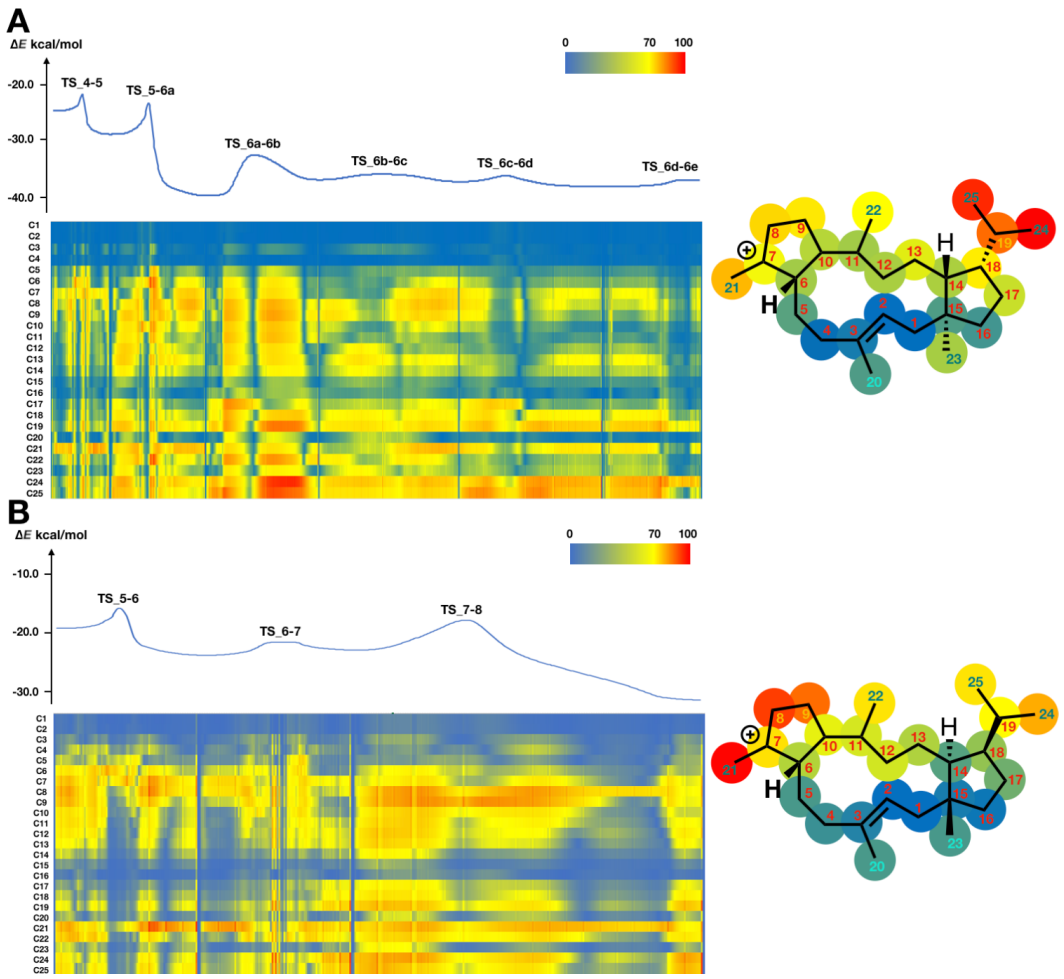

Figure 2: Energy diagram and heat map analysis of conformational change and hydrogen shift (A) **IM4–IM6e** in quiannulatene biosynthesis. (B) **IM5–IM8** in sesterfisherol biosynthesis. An energy diagram and heat map of inherent mobility are shown. All energies are shown in kcal/mol. The Y axis shows the carbon number and the X axis shows the coordinate in the heat map. The right structural heat map shows the total mobility. Red means high mobility, yellow means moderate mobility, and blue means static. TS: transition state.

the C20, C21 and C23 methyl groups are quite static in phase I, the other three methyl groups are relatively flexible, which suggests that C20, C21 and C23 could be key determinants of the affinity for the enzyme's binding pocket. The C24 and C25 methyl groups are the most mobile moieties, and the dramatic displacements of these two methyl groups are consistent with a previous report that the counterclockwise rotation of the isopropyl moiety is necessary for 1,5-hydrogen shift to occur (**TS_2-3a** in quiannulatene biosynthesis and **TS_2-3** in sesterfisherol biosynthesis) [19].

Phase II: conformational changes and hydrogen shifts

In phase II, different trends of inherent mobility are seen between quiannulatene and sesterfisherol biosynthesis. As shown in Figure 2, C1–C5, C15, C16, C20, and C23 are static, as in phase I. However, C21 is quite mobile, because the C7 carbocation becomes an sp^3 carbon due to 1,2-hydrogen shift (**TS_4-5**). After two successive 1,2-hydrogen shifts, four-step conformational changes take place in quiannulatene biosynthesis, in which C24 and C25 are highly mobile. On the other hand, C8, C9 and C21 are quite mobile in sesterfisherol biosynthesis. These different mobility trends result from the different types of conformational change required to achieve regioselectivity in the following ring rearrangement reactions.

Phase III: ring rearrangements

While C23 is still static in phase III, C20 is relatively flexible, which might serve to decrease the affinity for the enzyme's binding pocket. Interestingly, although different types of ring rearrangement reactions occur in each pathway, the same inherent mobility trends were observed. As shown in Figure 3, C4–C11, C21 and C22 appear to be quite mobile in the terpene cyclase binding pocket in both pathways, indicating that their

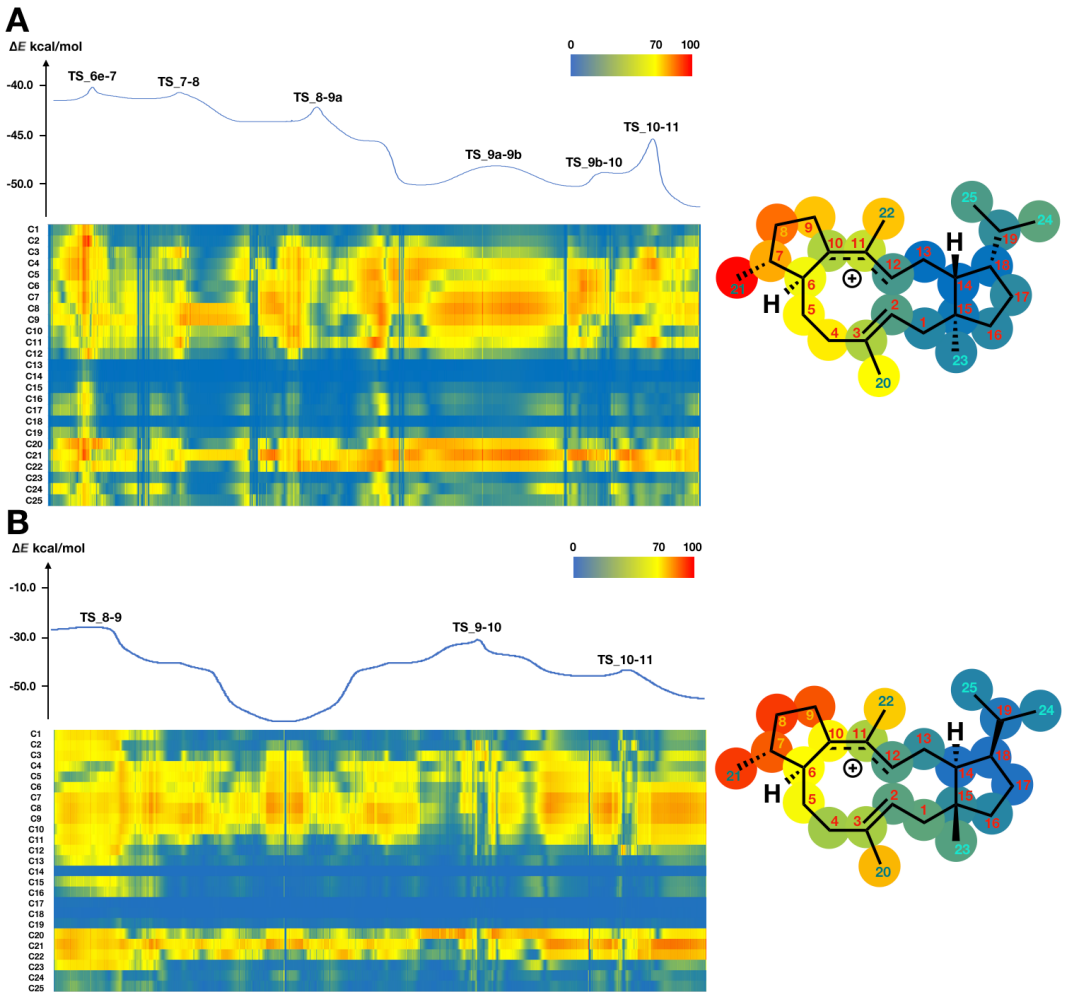

Figure 3: Energy diagram and heat map analysis of ring rearrangement (A) **IM6e–IM11** in quiannulatene biosynthesis. (B) **IM8–IM11** in sesterfisherol biosynthesis. An energy diagram and a heat map of inherent mobility are shown. All energies are shown in kcal/mol. The Y axis shows the carbon number and the X axis shows the coordinate in the heat map. The right structural heat map shows the total mobility. Red means high mobility, yellow means moderate mobility, and blue means static. TS: transition state.

steric interaction with the enzyme has little influence on this phase of the biosynthesis. Based on this analysis, it appears that the destination of the cyclization cascade is determined by the conformations of the carbocation intermediates, but not by enzymatic constraints. This insight is consistent with our previous findings [1].

Conclusion

In order to clarify the influence of the conformational preorganization [20] of GFPP bound to a sesterterpene synthase on the reaction outcome, we computed the inherent atomic mobility in the carbocation intermediates during the biosynthesis of two sesterterpenes, quiannulatene and sesterfisherol. Two methyl groups, i.e., C20 and C23, remain static during the first half of the cyclization cascade, indicating that they could be determinants of the affinity for the enzyme cavity of sesterterpene synthase. Interestingly, inherent mobility shows the same trend in phase I (5/12/5 tricycle formation) and phase III (ring rearrangement), but not in phase II (conformational changes and hydrogen shifts), of quiannulatene and sesterfisherol biosynthesis, indicating that phase II is the key process for the structural diversification, in accordance with our previous study [1]. Moreover, C20 becomes flexible in phase III, which could result in decreased affinity for the enzyme, and this might be relevant to substrate release. Few X-ray crystal structures of terpene cyclases are available [7,8], so we believe inherent mobility analysis will be useful to predict the mechanism of conformational preorganization of the substrate to achieve different biosynthetic outcomes in other terpene-forming reactions. We are currently applying this approach to sesterterpenes that are synthesized through a 5/6/11 tricyclic intermediate.

Experimental

All calculations were carried out using GRRM11 [21-25] with Gaussian 09 [26]. All TS structures were obtained from the literature [1,3]. Intrinsic reaction coordinate (IRC) calculations [27-30] were carried out with B3LYP/6-31+G(d,p) for quiannulatene and with M06-2X/6-31G(d,p) for sesterfisherol. All 3D structures were drawn by Gauss View 6. All displacement calculations were performed using in-house software written in C++ (see Supporting Information File 3).

Supporting Information

Supporting Information File 1

Coordinates and energies of quiannulatene biosynthesis.
[https://www.beilstein-journals.org/bjoc/content/supplementary/1860-5397-15-184-S1.log]

Supporting Information File 2

Coordinates and energies of sesterfisherol biosynthesis.
[https://www.beilstein-journals.org/bjoc/content/supplementary/1860-5397-15-184-S2.log]

Supporting Information File 3

Software for inherent mobility analysis.
[https://www.beilstein-journals.org/bjoc/content/supplementary/1860-5397-15-184-S3.cpp]

Supporting Information File 4

How to use in house software to calculate inherent atomic mobility.
[https://www.beilstein-journals.org/bjoc/content/supplementary/1860-5397-15-184-S4.pdf]

Acknowledgements

This work was supported by JSPS KAKENHI (S) (No. 17H06173 (M.U.)), JSPS Grant-in-Aid for Scientific Research on Innovative Areas (No. 17H05430 (M.U.), JP16H06454 (M.Y.), and JP16H06443 (I.A.)). Provision of computational resources (Project G18008) on HOKUSAI GreatWave (RIKEN) is gratefully acknowledged.

ORCID® iDs

Hajime Sato - https://orcid.org/0000-0001-5185-096X

References

1. Sato, H.; Mitsuhashi, T.; Yamazaki, M.; Abe, I.; Uchiyama, M. *Angew. Chem., Int. Ed.* **2018,** *57,* 14752–14757. doi:10.1002/anie.201807139
2. Okada, M.; Matsuda, Y.; Mitsuhashi, T.; Hoshino, S.; Mori, T.; Nakagawa, K.; Quan, Z.; Qin, B.; Zhang, H.; Hayashi, F.; Kawaide, H.; Abe, I. *J. Am. Chem. Soc.* **2016,** *138,* 10011–10018. doi:10.1021/jacs.6b05799
3. Ye, Y.; Minami, A.; Mandi, A.; Liu, C.; Taniguchi, T.; Kuzuyama, T.; Monde, K.; Gomi, K.; Oikawa, H. *J. Am. Chem. Soc.* **2015,** *137,* 11846–11853. doi:10.1021/jacs.5b08319
4. Sato, H.; Narita, K.; Minami, A.; Yamazaki, M.; Wang, C.; Suemune, H.; Nagano, S.; Tomita, T.; Oikawa, H.; Uchiyama, M. *Sci. Rep.* **2018,** *8,* 2473. doi:10.1038/s41598-018-20916-x
5. Narita, K.; Sato, H.; Minami, A.; Kudo, K.; Gao, L.; Liu, C.; Ozaki, T.; Kodama, M.; Lei, X.; Taniguchi, T.; Monde, K.; Yamazaki, M.; Uchiyama, M.; Oikawa, H. *Org. Lett.* **2017,** *19,* 6696–6699. doi:10.1021/acs.orglett.7b03418
6. Minami, A.; Ozaki, T.; Liu, C.; Oikawa, H. *Nat. Prod. Rep.* **2018,** *35,* 1330–1346. doi:10.1039/c8np00026c
7. Christianson, D. W. *Chem. Rev.* **2017,** *117,* 11570–11648. doi:10.1021/acs.chemrev.7b00287
8. Chen, M.; Harris, G. G.; Pemberton, T. A.; Christianson, D. W. *Curr. Opin. Struct. Biol.* **2016,** *41,* 27–37. doi:10.1016/j.sbi.2016.05.010
9. Mitsuhashi, T.; Abe, I. *ChemBioChem* **2018,** *19,* 1106–1114. doi:10.1002/cbic.201800120
10. Dickschat, J. S. *Nat. Prod. Rep.* **2016,** *33,* 87–110. doi:10.1039/c5np00102a
11. Major, D. T.; Freud, Y.; Weitman, M. *Curr. Opin. Chem. Biol.* **2014,** *21,* 25–33. doi:10.1016/j.cbpa.2014.03.010
12. O'Brien, T. E.; Bertolani, S. J.; Tantillo, D. J.; Siegel, J. B. *Chem. Sci.* **2016,** *7,* 4009–4015. doi:10.1039/c6sc00635c
13. O'Brien, T. E.; Bertolani, S. J.; Zhang, Y.; Siegel, J. B.; Tantillo, D. J. *ACS Catal.* **2018,** *8,* 3322–3330. doi:10.1021/acscatal.8b00342
14. Richter, F.; Leaver-Fay, A.; Khare, S. D.; Bjelic, S.; Baker, D. *PLoS One* **2011,** *6,* e19230. doi:10.1371/journal.pone.0019230
15. Meiler, J.; Baker, D. *Proteins: Struct., Funct., Bioinf.* **2006,** *65,* 538–548. doi:10.1002/prot.21086
16. Hong, Y. J.; Tantillo, D. J. *Chem. Soc. Rev.* **2014,** *43,* 5042–5050. doi:10.1039/c3cs60452g
17. Tantillo, D. J. *Angew. Chem., Int. Ed.* **2017,** *56,* 10040–10045. doi:10.1002/anie.201702363
18. Tantillo, D. J. *Nat. Prod. Rep.* **2011,** *28,* 1035–1053. doi:10.1039/c1np00006c
19. Chiba, R.; Minami, A.; Gomi, K.; Oikawa, H. *Org. Lett.* **2013,** *15,* 594–597. doi:10.1021/ol303408a
20. Tantillo, D. J. *Org. Lett.* **2016,** *18,* 4482–4484. doi:10.1021/acs.orglett.6b01919
21. Maeda, S.; Osada, Y.; Morokuma, K.; Ohno, K. *GRRM 11*, Version 11.03, 2012.
22. Maeda, S.; Ohno, K.; Morokuma, K. *Phys. Chem. Chem. Phys.* **2013,** *15,* 3683–3701. doi:10.1039/c3cp44063j
23. Ohno, K.; Maeda, S. *Chem. Phys. Lett.* **2004,** *384,* 277–282. doi:10.1016/j.cplett.2003.12.030
24. Maeda, S.; Ohno, K. *J. Phys. Chem. A* **2005,** *109,* 5742–5753. doi:10.1021/jp0513162
25. Ohno, K.; Maeda, S. *J. Phys. Chem. A* **2006,** *110,* 8933–8941. doi:10.1021/jp061149l
26. *Gaussian 09,* Revision E.01; Gaussian, Inc.: Wallingford, CT, 2009.
27. Fukui, K. *Acc. Chem. Res.* **1981,** *14,* 363–368. doi:10.1021/ar00072a001
28. Page, M.; Doubleday, C.; McIver, J. W., Jr. *J. Chem. Phys.* **1990,** *93,* 5634–5642. doi:10.1063/1.459634

29. Ishida, K.; Morokuma, K.; Komornicki, A. *J. Chem. Phys.* **1977,** *66,* 2153–2156. doi:10.1063/1.434152
30. Gonzalez, C.; Schlegel, H. B. *J. Phys. Chem.* **1990,** *94,* 5523–5527. doi:10.1021/j100377a021

License and Terms

BEILSTEIN JOURNAL OF ORGANIC CHEMISTRY

Characterization of two new degradation products of atorvastatin calcium formed upon treatment with strong acids

Jürgen Krauß[1], Monika Klimt[1], Markus Luber[1], Peter Mayer[2] and Franz Bracher[*1]

Full Research Paper

Open Access

Address:
[1]Department of Pharmacy – Center for Drug Research, Ludwig-Maximilians University Munich, Butenandtstr. 5-13, 81377 Munich, Germany and [2]Department of Chemistry, Ludwig-Maximilians University Munich, Butenandtstr. 5-13, 81377 Munich, Germany

Email:
Franz Bracher[*] - Franz.Bracher@cup.uni-muenchen.de

* Corresponding author

Keywords:
atorvastatin; crystal structure; cyclization; degradation products; fragmentation; stress test

Beilstein J. Org. Chem. **2019,** *15,* 2085–2091.
doi:10.3762/bjoc.15.206

Received: 27 May 2019
Accepted: 22 August 2019
Published: 02 September 2019

This article is part of the thematic issue "Reactive intermediates – carbocations" and is dedicated to the memory of Prof. Dr. Gerhard Rücker, Bonn.

Guest Editor: S. R. Hare

Abstract

Atorvastatin calcium (Lipitor®, Sortis®) is a well-established cholesterol synthesis enzyme (CSE) inhibitor commonly used in the therapy of hypercholesterolemia. This drug is known to be sensitive to acid treatment, but only little data has been published on the structures of the degradation products. Here we report the identification of two novel degradation products of atorvastatin, which are formed only under drastic acidic conditions. While treatment with conc. sulfuric acid led to a loss of the carboxanilide residue (accompanied by an expectable lactonization/dehydration process in the side chain), treatment with conc. aqueous hydrochloric acid gave a complex, bridged molecule under C–C-bond formation of the lactone moiety with the pyrrole, migration of the isopropyl group and loss of the carboxanilide residue. The novel degradation products were characterized by NMR spectroscopy, HRMS data and X-ray crystal structure analysis.

Introduction

Over the past decades, the general trend toward globalization of the supply chains for active pharmaceutical ingredients has created new challenges for the authorities in ensuring the safety and quality of the drug supply [1]. Unprecedented impurities can appear, most likely if limited information is available about details (or alterations) of production processes of drugs. On the one hand, it is impossible to check drug substances routinely for all imaginable impurities, on the other hand it is desirable to identify as much as possible degradation products of drugs resulting from inappropriate exposition to potentially harmful conditions during production, manufacturing and storage. For being able to provide relevant data in a manageable time frame, two kinds of stress tests have found broad application: accelerated storage conditions (higher temperatures, higher

humidity, …) typically provide reliable data on the stability of a drug, but are still time-consuming; on the other hand in "forced degradation experiments" the drug is submitted to more drastic conditions (e.g., strong acid or base, strong oxidant, very high temperature), and potential degradation products can be identified in very short time [2,3]. However, forced degradation experiments are highly artificial in nature, and thus one has to keep in mind that these extremely drastic conditions are prone to lead to results that might be out of proportion for daily quality control [3]. Nevertheless, knowledge about the outcome of stress tests under extreme conditions helps to get insight into the overall reactivity of drug substances.

Atorvastatin calcium (**1,** marketed as the trihydrate in Lipitor®, Sortis®), is a well-established drug for treatment of hypercholesterolemia [4]. This drug is monographed in the leading pharmacopoeias (Ph. Eur., USP), and a couple of impurities are listed there. Most of these impurities result from the synthesis process (stereoisomers, products resulting from impure starting materials or side reactions), and only one of these impurities, lactone **2**, is most likely a degradation product, resulting from acid-mediated lactonization of the 3,5-dihydroxyheptanoate side chain.

A couple of previous publications deal with stress tests on atorvastatin (and its salts), and an overview has been published by Sirén [5]. Hereby, atorvastatin was found to be sensitive to acidic, oxidative, photochemical and thermal stress. Acidic degradation of atorvastatin was reported to follow first order kinetics, but decomposition products were not characterized in this [6] and several other reports, which only determined the downsizing of the atorvastatin peak in HPLC after treatment with acid [7-10]. The most prominent decomposition product upon acidic treatment, compound **2**, results from lactonization of the 3,5-dihydroxyheptanoate side chain under moderately acidic conditions (0.1 M HCl) [11-14]. Shah et al. [15] identified six additional decomposition products upon treatment with 0.1 M HCl at 80 °C for 24 h, among which the dehydrated lactone **3** was dominating, accompanied by minor amounts of products arising from dehydration of the δ-hydroxy group and some epimers resulting from acid-catalyzed isomerization reactions. In contrast, Vukkum et al. [13] describe, besides lactones **2** and **3**, an α,β-unsaturated carboxylic acid **4**. Treatment under more drastic conditions (6 M HCl, reflux, 3 h) was reported to result mainly in hydrolysis of the anilide moiety to give carboxylic acid **5** [16,17] (Figure 1).

Here we report on the results of our investigations on the decomposition of atorvastatin calcium (**1**) under strongly acid conditions.

Results and Discussion

Stress tests

Since the lability of atorvastatin towards moderately acidic conditions is well-documented, we aimed at investigating the outcome of incubation with acids under more drastic conditions. Treatment of atorvastatin calcium trihydrate (**1**) with 2 M aqueous hydrochloric acid at room temperature (Table 1, entry 1) gave, in accordance with previous reports, only hydroxylactone **2** (55% yield). This outcome was confirmed by comparison with published NMR data [18,19]. At elevated temperature (reflux, 4 h; Table 1, entry 2) a mixture of lactone **2** and known unsaturated lactone **3** [15] (arising from acid-catalyzed dehydration of **2**) was obtained. Under even more drastic acidic conditions (refluxing with 6 M hydrochloric acid for 3 h, with 20% aqueous H_2SO_4 for 2 h, or with *p*-toluenesulfonic acid in toluene for 5 h; Table 1, entries 3–5) unsaturated lactone **3** was formed exclusively and in high to almost quantitative yields (Table 1).

When atorvastatin calcium trihydrate (**1**) was submitted to extremely strong acidic conditions by refluxing with concentrated (37%) aqueous hydrochloric acid (entry 6), a new product **6** was formed in almost quantitative yield. The ^{1}H NMR analysis clearly indicated that the entire carboxanilide partial structure got lost under these conditions. However, no signal was observed which could be attributed to a C–H group at the pyrrole ring. The ^{13}C NMR data showed one carbonyl resonance at 170.3 ppm, assignable to a lactone moiety. The HMBC experiment showed a cross peak between the proposed lactone carbonyl carbon and a neighboring CH-O group, confirming the lactone moiety, and the DEPT spectrum showed a new aliphatic methine resonance at 25.2 ppm. By HRESIMS mass data (found: 404.2020 for $[M + H]^+$) a molecular formula of $C_{26}H_{26}FNO_2$ was confirmed, excluding incorporation of HCl into this artefact. Finally, X-ray crystallography structure analysis (see Figure 2 and Supporting Information File 1) disclosed the structure of **6**, bearing a novel, bridged tricyclic 1,5-methanopyrrolo[1,2-*e*][1,5]oxazonin-3-one ring system (Scheme 1).

In contrast, submission of atorvastatin calcium trihydrate (**1**) to concentrated sulfuric acid for two hours at 60 °C (Table 1, entry 7) led to the degradation product **7** in low yield (18%) (Scheme 1). No further decomposition products could be isolated. Here, lactonization and dehydration steps in the side chain took place as observed before in the other acid treatments, however, under these extremely strong, virtually anhydrous acid conditions, the entire carboxanilide residue was removed to give the (*S*)-configured 4-unsubstituted pyrrole **7**, as exemplified by a typical CH resonance at 6.20 ppm in the ^{1}H NMR spectrum. This structure was further

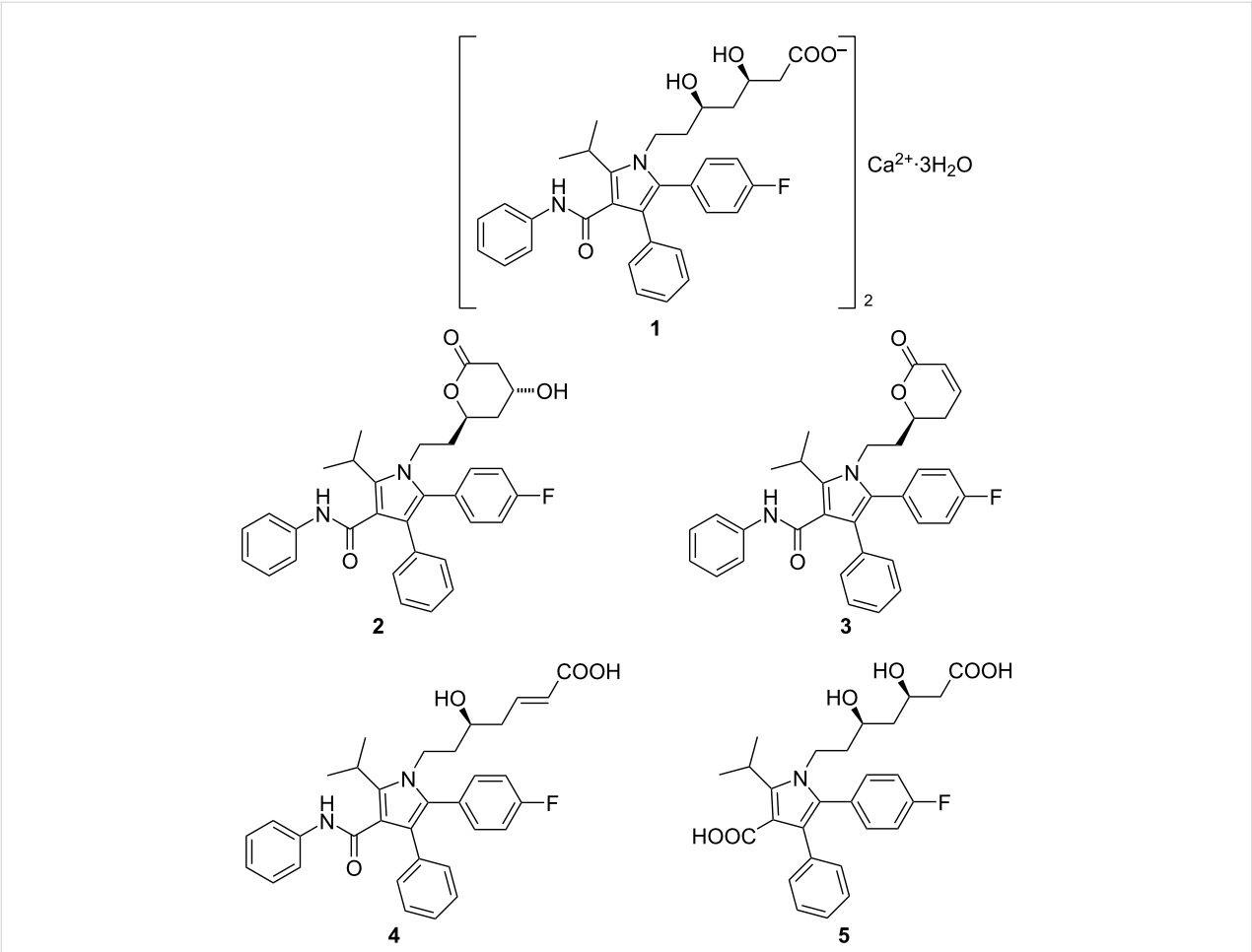

Figure 1: Atorvastatin calcium trihydrate (**1**) and previously published decomposition products arising from treatment with acids: lactone **2**, dehydrated lactone **3**, α,β-unsaturated carboxylic acid **4**, and carboxylic acid **5** (resulting from postulated anilide hydrolysis).

Table 1: Acidic stress conditions and decomposition products formed.

Entry no.	Acidic conditions	Decomposition products (yield)			
		2	**3**	**6**	**7**
1	2 M HCl, 20 °C, 2 h	55%	–	–	–
2	2 M HCl, reflux, 4 h	65%	14%	–	–
3	6 M HCl, reflux, 3 h	–	70%	–	–
4	20% H_2SO_4, reflux, 2 h	–	>98%	–	–
5	*p*-toluenesulfonic acid, toluene, reflux, 5 h	–	95%	–	–
6	37% HCl, reflux, 5 h	–	–	96%	–
7	conc. H_2SO_4, 60 °C, 2 h	–	–	–	18%

confirmed by X-ray data (see Figure 2 and Supporting Information File 1).

HPLC method for the detection of the novel impurities

In order to provide a convenient method for including our new findings into quality control of atorvastatin batches, we worked out an isocratic HPLC protocol, which prettily separates the four artefacts **2**, **3**, **6** and **7** from atorvastatin (**1**). This method uses an RP18 stationary phase (Eurospher 100–C18), isocratic elution with 0.01 M ammonium acetate buffer (pH 4)-acetonitrile 54:46 (v/v) at a flow rate of 1 mL/min at 40 °C, with UV detection at 246 nm (Figure 3).

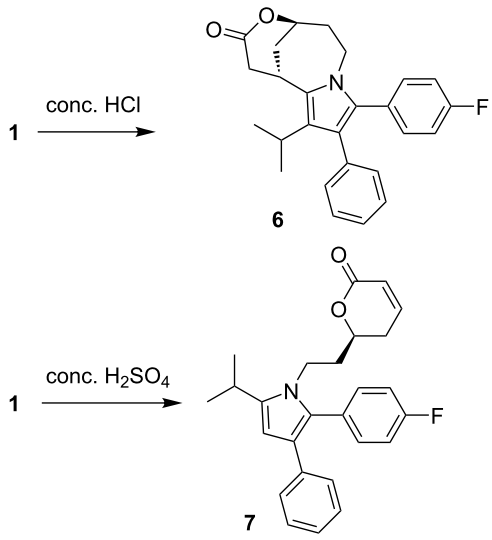

Scheme 1: Formation of novel artefacts **6** and **7** under extremely strong acidic conditions.

Discussion

In this investigation we first confirmed some pathways of decomposition of atorvastatin under acidic conditions. With dilute mineral acids at room temperature, atorvastatin is conveniently converted into the lactone **2** under retention at the C5–O bond of the aliphatic chain [13,20], whereas treatment under more drastic conditions (e.g., 6 M HCl or heating) causes expectable subsequent dehydration to give the unsaturated lactone **3** [13,15]. In contrast to previous reports [16,17] we could not find any indication for a cleavage of the carboxanilide partial structure to give free pyrrolecarboxylic acid **5** under treatment with 6 M HCl under reflux.

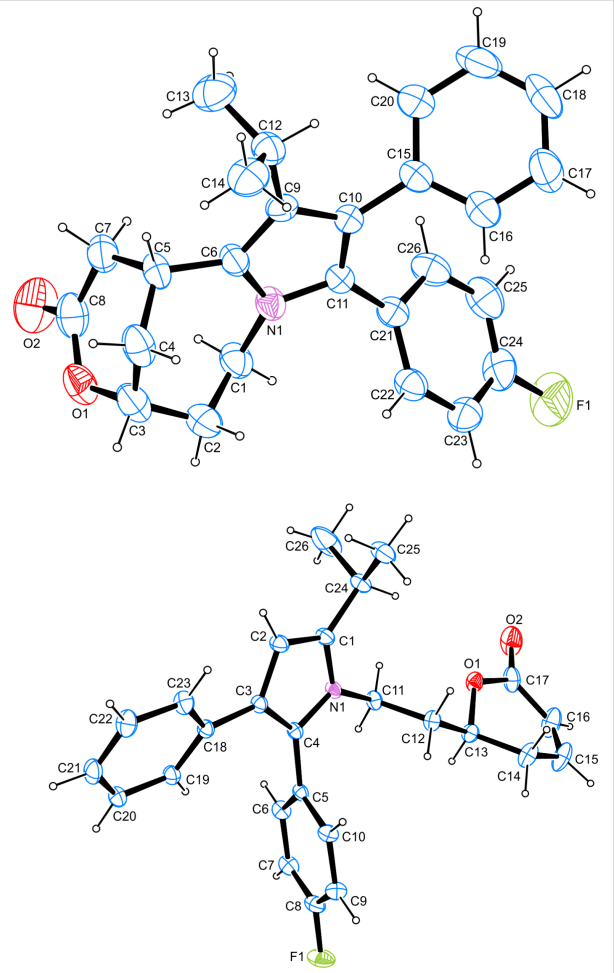

Figure 2: Top: Molecular structure of artefact **6**. Shown here is the molecular structure of one of three independent molecules in **6** drawn at the 50% ellipsoid probability level. Bottom: Molecular structure of artefact **7** (drawn at the 50% ellipsoid probability level).

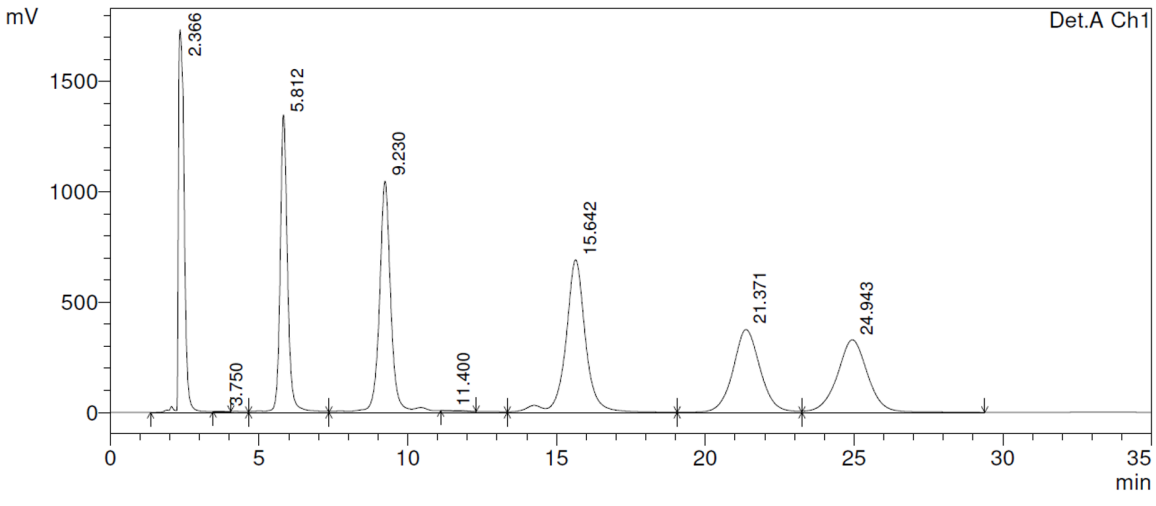

Figure 3: Separation of atorvastatin (**1**; retention time: 5.8 min) from the four decomposition products **2** (retention time: 9.2 min), **3** (retention time: 15.6 min), **6** (retention time: 21.4 min) and **7** (retention time: 24.9 min). Chromatogram obtained with a solution containing 10 mg each in 5.0 mL DMF (retention time 2.3 min), diluted 1:5 with the eluent buffer before injection.

However, upon treatment with concentrated sulfuric acid, lactonization/dehydration is accompanied by complete loss of the carboxanilide residue to give pyrrole **7**. Complete one-step removal of carboxamide residues from aromatic rings has been observed before in investigations of fragmentations of protonated species in mass spectrometry [21,22]. For benzanilides Tu [21] proposed a mechanism involving protonation of the amide oxygen, followed by 1,3 proton shift to the ring carbon next to the amide carbonyl group, followed by elimination of protonated phenyl isocyanate under re-aromatization. For the pyrrole derived substrate investigated here, even direct protonation at C-3 of the pyrrole by strong acid is most likely, due to the significant basicity of pyrroles. Delocalization of the positive charge (**A** ↔ **A'**) as shown in Scheme 2 will support the initial ring protonation step. The X-ray analysis of compound **7** revealed that the asymmetric center in the lactone ring is (*S*)-configured, indicating that once again the lactonization step took place with retention at the remaining stereocenter (the shift from (*R*) to (*S*) configuration is only a nomenclatory result of altered priorities of residues around the stereocenter upon dehydration). A comparable fragmentation has been observed in the CID (collision-induced dissociation) mass spectrum of atorvastatin, where the base peak observed at *m*/*z* 440 clearly corresponds to a loss of phenyl isocyanate [22].

In contrast, refluxing **2** with concentrated aqueous hydrochloric acid (37%) led to the formation of the complex, bridged product **6**. Most likely, this decomposition starts again with lactonization of the 3,5-dihydroxyheptanoate side chain, followed by dehydration to give the unsaturated lactone **3**. This hypothesis was confirmed by refluxing pure lactone **3** with 37% hydrochloric acid, resulting in clean conversion into **6** as well. In the following, this unsaturated lactone (Michael system) most likely performs an acid-mediated intramolecular attack at C-2 of the electron-rich pyrrole ring. In a cascade of subsequent reactions, the carboxanilide moiety at C-3 is eliminated and the isopropyl residue, originally located at C-2 of the pyrrole, is shifted to C-3, rendering the annulated, tetrasubstituted pyrrole **6**. The structure of **6** was confirmed by X-ray crystal structure analysis. However, most likely cleavage of the carboxanilide moiety (compare formation of **7** from atorvastatin with concentrated sulfuric acid) is not the initial step in the cascade of reactions leading from intermediate **3** to product **6**. In a control experiment, we treated compound **7** with 37% hydrochloric acid under the above mentioned conditions, but only a complex mixture of decomposition products was obtained, with no indication for formation of **6**. As the intermediate occurrence of a positive charge at C-2 of the pyrrole ring and a sp^3-hybridized C-3 are most likely triggering the elimination of phenyl isocyanate from the pyrrole (see postulated mechanism shown in Scheme 2), we propose the formation of an intermediate **C**, which is formed via initial acid-mediated electrophilic attack of the unsaturated lactone at C-2 of the pyrrole ring. The resulting carbenium ion should be stabilized as shown in Scheme 3 (**B** ↔ **B'**). Subsequent shift of the isopropyl group from C-2 to C-3 then would give carbenium(-iminium) ion **C**, which can eliminate protonated phenyl isocyanate under formation of bridged pyrrole **6**. A comparable shift of the isopropyl group in atorvastatin has previously been observed only under oxidative conditions, giving rise to pyrrolidone-type degradation products [23].

Conclusion

Atorvastatin calcium trihydrate (**1**) is known to be an acid-labile drug, and incubation with dilute mineral acids gives the known lactone **2**, which was further dehydrated to unsaturated lactone **3** under more drastic conditions. Treatment with very strong acids gave two hitherto unknown degradation products, whose structures were elucidated by NMR and crystal structure analysis. The bridged tricyclic product **6** was formed with concen-

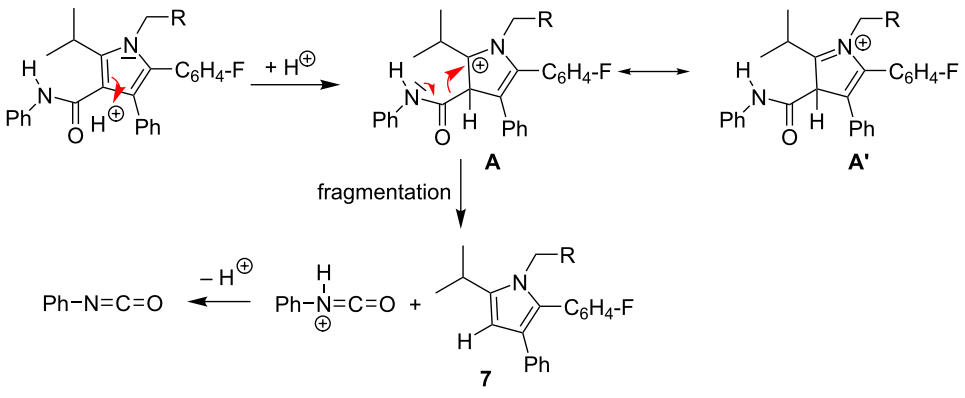

Scheme 2: Proposed mechanism for the formation of desamidated product **7**.

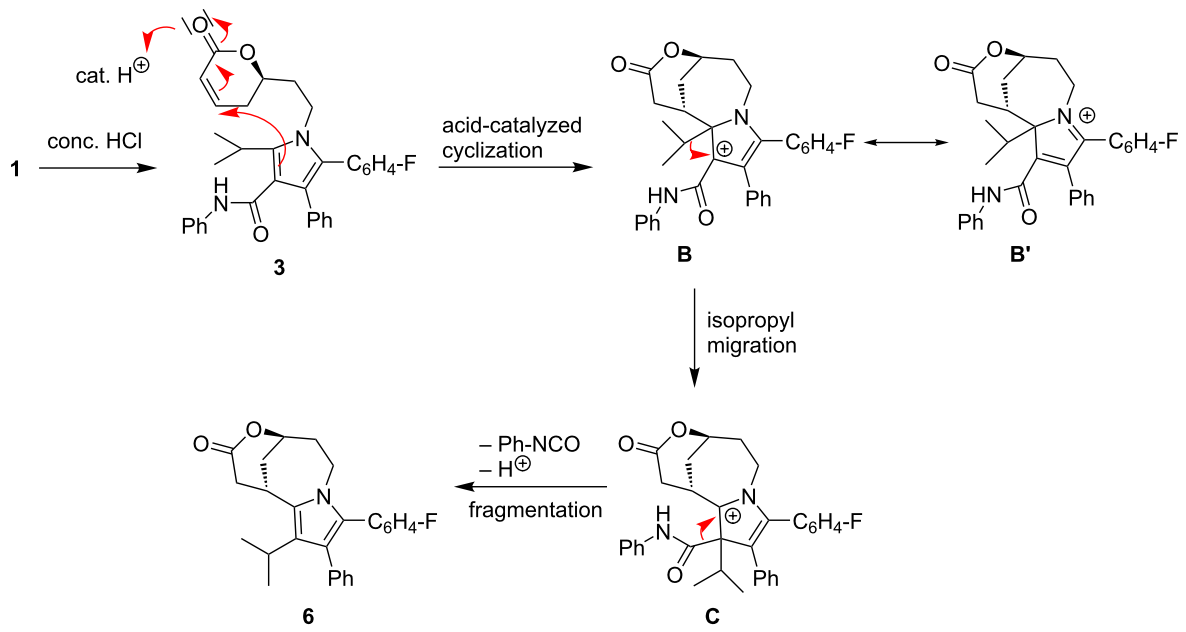

Scheme 3: Proposed mechanism for the formation of bridged product **6** under cyclization, isopropyl migration and carboxanilide fragmentation.

trated hydrochloric acid, whereas lactone **7** resulted from treatment with concentrated sulfuric acid. We propose mechanisms for the formation of the novel artefacts **6** and **7** here. But it has to be mentioned that these new artefacts, which are formed only under extremely drastic conditions, are not likely to be relevant in terms of drug safety and control of impurities in launched atorvastatin batches.

Supporting Information

Supporting Information File 1

Materials and methods; stress tests and analytical data of the products obtained thereby; details of characterization of **6** and **7** by X-ray data; crystallographic data for **6** and **7**, NMR spectra of artefacts **2**, **3**, **6**, and **7**.
[https://www.beilstein-journals.org/bjoc/content/supplementary/1860-5397-15-206-S1.pdf]

Supporting Information File 2

checkCIF/PLATON report (Structure factors for artefacts **6** (wq033) and **7** (wv633)).
[https://www.beilstein-journals.org/bjoc/content/supplementary/1860-5397-15-206-S2.pdf]

Acknowledgements

The authors thank Prof. Dr. Herbert Mayr for helpful discussions.

ORCID® iDs

Franz Bracher - https://orcid.org/0000-0003-0009-8629

Preprint

A non-peer-reviewed version of this article has been previously published as a preprint doi:10.3762/bxiv.2019.31.v1

References

1. Woo, J.; Wolfgang, S.; Batista, H. *Clin. Pharmacol. Ther. (Hoboken, NJ, U. S.)* **2008,** *83,* 494–497. doi:10.1038/sj.clpt.6100493
2. Klick, S.; Muijselaar, P. G.; Waterval, J.; Eichinger, T.; Korn, C.; Gerding, T. K.; Debets, A. J.; Vandingenen, J.; Sänger, C.; van den Beld, C.; Somsen, G.; de Jong, G. *Pharm. Technol.* **2004,** *29,* 48–66.
3. Blessy, M.; Patel, R. D.; Prajapati, P. N.; Agrawal, Y. K. *J. Pharm. Anal.* **2014,** *4,* 159–165. doi:10.1016/j.jpha.2013.09.003
4. Haque, T.; Khan, B. V. *Clin. Lipidol.* **2010,** *5,* 615–625.
5. Sirén, H. M. M. *J. Biomed. Res. Pract.* **2017,** *1,* 100003. http://hdl.handle.net/10138/236735
6. Oliveira, M. A.; Yoshida, M. I.; Belinelo, V. J.; Valotto, R. S. *Molecules* **2013,** *18,* 1447–1456. doi:10.3390/molecules18021447
7. Chowdhury, T.; Jakaria, M.; Bhuiyan, D.; Arifujjaman; Mamur, A. J. *Sci. Innovation Res.* **2014,** *3,* 598–601.
8. Zaheer, Z.; Farooqui, M.; Mangle, A. A.; Nikalje, A. *Afr. J. Pharm. Pharmacol.* **2008,** *2,* 204–210.
9. Chaudhari, B. G.; Patel, N. M.; Shah, P. B. *Chem. Pharm. Bull.* **2007,** *55,* 241–246. doi:10.1248/cpb.55.241
10. Chaudhari, B. G.; Patel, N. M.; Shah, P. B.; Patel, L. J.; Patel, V. P. *J. AOAC Int.* **2007,** *90,* 1539–1546.

11. Mohammadi, A.; Rezanour, N.; Ansari Dogaheh, M.; Ghorbani Bidkorbeh, F.; Hashem, M.; Walker, R. B. *J. Chromatogr., B* **2007,** *846,* 215–221. doi:10.1016/j.jchromb.2006.09.007
12. Seshadri, R. K.; Desai, M. M.; Raghavaraju, T. V.; Krishnan, D.; Rao, D. V.; Chakravarthy, I. E. *Sci. Pharm.* **2010,** *78,* 821–834. doi:10.3797/scipharm.1004-14
13. Vukkum, P.; Babu, J. M.; Muralikrishna, R. *Sci. Pharm.* **2013,** *81,* 93–114. doi:10.3797/scipharm.1208-06
14. Rakibe, U.; Tiwari, R.; Rane, V.; Wakte, P. *Acta Chromatogr.* **2019,** *31,* 33–44. doi:10.1556/1326.2017.00333
15. Shah, R. P.; Kumar, V.; Singh, S. *Rapid Commun. Mass Spectrom.* **2008,** *22,* 613–622. doi:10.1002/rcm.3403
16. Darwish, H. W.; Hassan, S. A.; Salem, M. Y.; El-Zeany, B. A. *Spectrochim. Acta, Part A* **2016,** *154,* 58–66. doi:10.1016/j.saa.2015.10.007
17. Hassan, S. A.; Elzanfaly, E. S.; El-Zeany, S. B. A.; Salem, M. Y. *Acta Pharm.* **2016,** *66,* 479–490. doi:10.1515/acph-2016-0040
18. Sawant, P.; Maier, M. E. *Tetrahedron* **2010,** *66,* 9738–9744. doi:10.1016/j.tet.2010.10.028
19. Stach, J.; Havlíček, J.; Plaček, L.; Rádl, S. *Collect. Czech. Chem. Commun.* **2008,** *73,* 229–246. doi:10.1135/cccc20080229
20. Kearney, A. S.; Crawford, L. F.; Mehta, S. C.; Radebaugh, G. W. *Pharm. Res.* **1993,** *10,* 1461–1465. doi:10.1023/a:1018923325359
21. Tu, Y.-P. *Rapid Commun. Mass Spectrom.* **2004,** *18,* 1345–1351. doi:10.1002/rcm.1475
22. Guo, C.; Jiang, K.; Yue, L.; Xia, Z.; Wang, X.; Pan, Y. *Org. Biomol. Chem.* **2012,** *10,* 7070–7077. doi:10.1039/c2ob26011e
23. Cermola, F.; DellaGreca, M.; Iesce, M. R.; Montanaro, S.; Previtera, L.; Temussi, F. *Tetrahedron* **2006,** *62,* 7390–7395. doi:10.1016/j.tet.2006.05.027

License and Terms

BEILSTEIN JOURNAL OF ORGANIC CHEMISTRY

Acid-catalyzed rearrangements in arenes: interconversions in the quaterphenyl series

Sarah L. Skraba-Joiner, Carter J. Holt and Richard P. Johnson*

Full Research Paper

Open Access

Address:
Department of Chemistry and Materials Science Program, University of New Hampshire, Durham, NH 03824, USA

Email:
Richard P. Johnson* - Richard.Johnson@unh.edu

* Corresponding author

Keywords:
arenium ion; carbocation; density functional theory; microwave reaction; rearrangement; superacid

Beilstein J. Org. Chem. **2019,** *15,* 2655–2663.
doi:10.3762/bjoc.15.258

Received: 20 June 2019
Accepted: 18 October 2019
Published: 06 November 2019

This article is part of the thematic issue "Reactive intermediates – carbocations".

Guest Editor: S. R. Hare

Abstract

Arenes undergo rearrangement of phenyl, alkyl, halogen and other groups through the intermediacy of *ipso* arenium ions in which a proton is attached at the same carbon as the migrating substituent. Interconversions among the six quaterphenyl isomers have been studied here as a model for rearrangements of linear polyphenyls. All reactions were carried out in 1 M CF_3SO_3H (TfOH) in dichloroethane at 150 °C in a microwave reactor for 30–60 min, with product formation assessed by high field NMR analysis. Under these reaction conditions, *m,p'*-quaterphenyl is the equilibrium product. This isomer is unchanged by the reaction conditions and all other quaterphenyl isomers rearrange to *m,p'* as the dominant or sole product. DFT computations with inclusion of implicit solvation support a complex network of phenyl and biphenyl shifts, with barriers to rearrangement in the range of 10–21 kcal/mol. Consistent with experiments, the lowest energy arenium ion located on this surface is due to protonation of *m,p'*-quaterphenyl. This supports thermodynamic control based on carbocation energies.

Introduction

Carbocations are enigmatic reactive intermediates of enduring importance in chemistry. No other reactive species displays such a complex and fascinating collection of molecular rearrangements. Building on a long history, new synthetic applications [1,2] and explanations of carbocation reaction mechanisms [3-6] continue to be discovered. Chemistry in superacid solutions has played a major role in this field [7,8].

Every student of organic chemistry is taught the importance of arenium ions in the classic two step S_EAr mechanism for electrophilic aromatic substitution. Addition of an electrophile to an arene leads to a bound species, sometimes called a σ-complex, which then loses a proton at the site of substitution to yield the product [9]. Of course challenges to this simple mechanism exist [10-15], including the recent proposal of a one-step

process [16]. Reaction dynamics of electrophile–arene π complexes may also play a role in site selectivity [17]. It is less commonly known that arenium ions, like many other types of carbocations, often rearrange by 1,2-shifts. This leads to a fascinating collection of rearrangements that can migrate hydrogen, halogens or more complex substituents around the ring and even modify the carbon skeleton. Early reports by Baddeley [18] helped to explain odd results from Friedel–Crafts reactions [19] and this type of process is sometime referred to as a Baddeley rearrangement. Many examples of alkyl group migration have been described [19]. Phenyl groups migrate easily and degenerate phenyl shifts in biphenyl were confirmed by isotopic labeling [20,21]. One classic example of arenium ion chemistry is the interconversion of terphenyl isomers **1**–**3** (Scheme 1). This rearrangement was first reported by Allen and Pingert in 1942 [22] and then independently rediscovered by Olah and Meyer twenty years later [23]. Interconversion of isomers **1**–**3** is believed to occur through the intermediacy of *ipso* arenium ions **4**–**6** which connect through 1,2-phenyl shifts.

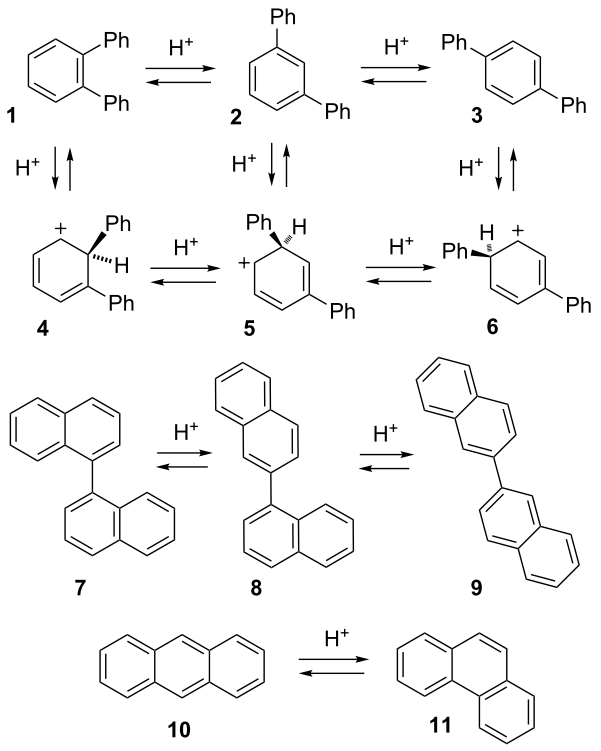

Scheme 1: Acid-catalyzed rearrangements of arenes.

The term "*ipso*" was first proposed by Perrin and Skinner to explain unusual results in electrophilic substitution reactions; this refers to protonation at the site of a substituent [24]. *Ipso* protonation is the essential step in arenium ion rearrangements. Our interest in this field arose from an accidental rediscovery of rearrangements in the terphenyl series (**1**–**3**; Scheme 1), by heating **1** with $AlCl_3$ – a reaction independently discovered twice before [22,23]! We confirmed earlier observations of facile acid-catalyzed interconversion, as well as the fact that m-terphenyl (**2**) is favored at equilibrium (observed ratio **1**:**2**:**3** is <1:69:31) and used theory to explain this product selectivity [25]. This preference is consistent with formation of the most stable arenium ion intermediate, as shown by DFT computations.

Early studies in this field used $AlCl_3$ as catalyst and it was generally assumed that adventitious traces of water generated the actual catalyst, precise identity unknown. We found these "water-promoted" reactions with catalytic $AlCl_3$ to be unreliable. To remove ambiguity about the catalyst and extend the temperature range, we developed a more reliable method for studying higher temperature carbocation rearrangements. In our method, we use 1 M (ca. 20% by volume) trifluoromethanesulfonic acid (TfOH) as catalyst with dichloroethane as our preferred solvent. Most importantly, reactions are conducted in the capped tube of a microwave reactor. With this approach, we can safely and reproducibly heat reactions to ca. 170 °C, so far without incident.

Other more complex rearrangements are easily observed. In the binaphthyl series **7**–**9**, three sequential rearrangements occur at ambient temperature favoring the 2,2'-isomer **9** (97%) at equilibrium [26]. Aryl shifts occur readily in naphthalene, with beta-substitution favored at equilibrium. Skeletal rearrangements of fused arene rings are also possible and can proceed through several mechanisms. The first example was reported by Dansi and Salvioni in 1941 in the rearrangement of benz[*a*]anthracene to chrysene [27]. We recently studied the rearrangement of anthracene (**10**) to phenanthrene (**11**) [28], finding evidence to support a complex process, suggested earlier [29], that involves initial reduction to 1,2,3,4-tetrahydroanthracene, followed by a pirouette rearrangement of the reduced ring through a spirocyclic intermediate and then re-oxidation to phenanthrene. These reactions involve a complex series of proton and hydride transfers.

Results and Discussion

Beyond terphenyls, acid-catalyzed rearrangements pose limitations in the synthesis of extended polyphenyls but the factors controlling interconversion of isomers are poorly understood [30-33]. As one recent example, Jasti and co-workers showed that cycloparaphenylenes undergo rapid acid-catalyzed rearrangement which precludes using Scholl-type chemistry in this series [30]. In the present work, we have explored rearrangements of quaterphenyls, the next homolog in the paraphenylene

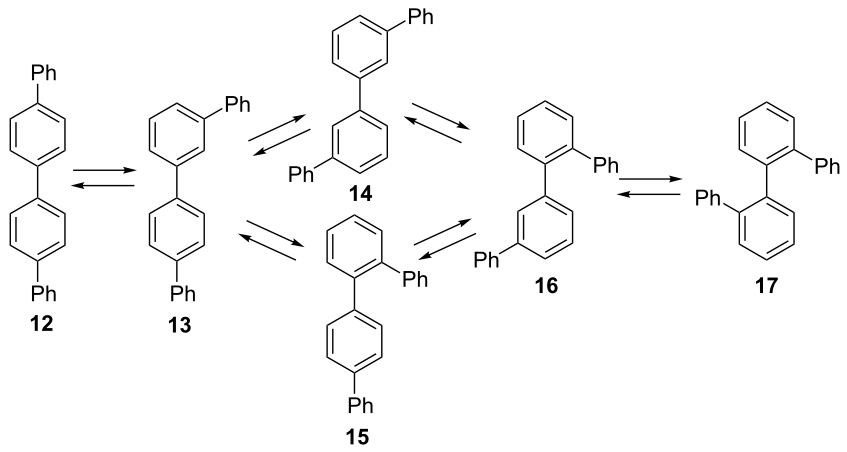

Scheme 2: Rearrangement of quaterphenyl isomers by phenyl shifts.

series, now with six structural isomers. Scheme 2 summarizes interconnections via 1,2-migration of a terminal phenyl group. As will be shown below, an internal aryl–aryl bond can also be transposed through 1,2-biphenyl migration, with a similar network of interconversions. Based on the behavior of terphenyl which favors *meta* substitution at equilibrium, we initially hypothesized that *m,m'*-quaterphenyl (**14**) would likely be the major isomer at equilibrium.

Only brief exploration of quaterphenyl rearrangements had been described previously. Isomerization of *o*,*o*'-quaterphenyl (**17**) with $SnCl_4/AlCl_3$ catalysis has been reported to yield a mixture of *p*,*p*'- (**12**), *m*,*p*'- (**13**), and *m*,*m*'-quaterphenyl (**14**) [34].

p,*p*'-Quaterphenyl (**12**) and *m*,*m*'-quaterphenyl (**14**) were available commercially. To complete the series, samples of *m*,*p*'- (**13**), *o*,*p*'- (**15**), *o*,*m*'- (**16**), and *o*,*o*'-quaterphenyl (**17**) were synthesized as shown in Scheme 3. Suzuki–Miyaura coupling was used to synthesize **13**, **15**, and **16** from the corresponding aryl bromides and boronic acids [35]. *o*,*o*'-Quaterphenyl (**17**) was synthesized by homo-coupling of 2-bromobiphenyl, as previously reported [36].

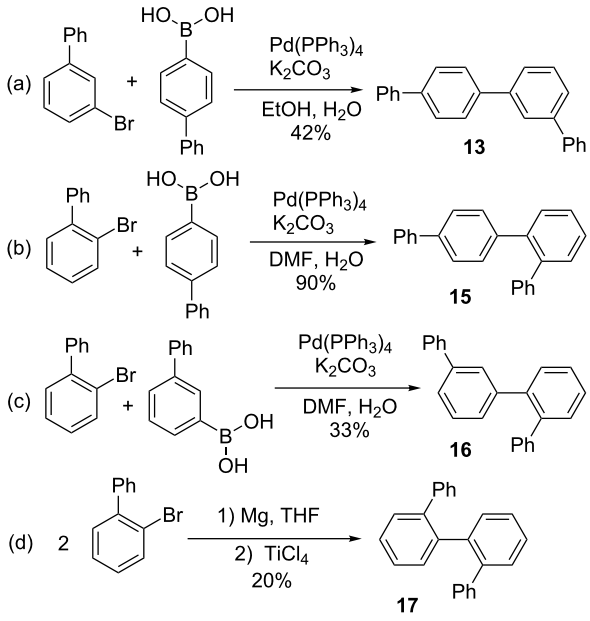

Scheme 3: Synthesis of quaterphenyl isomers.

Promoting the rearrangement of all quaterphenyl isomers at room temperature or in refluxing DCE (84 °C) proved to be difficult because *p*,*p*'-quaterphenyl (**12**) is very poorly soluble in this solvent and higher temperatures were required in some cases to reach equilibrium. In a solution of 1 M TfOH/DCE, **12** forms a colored solution more slowly (ca. 1–2 min) than previous examples we have studied. Heating these reaction mixtures in a microwave reactor allows for the substrate to dissolve in the reaction medium, resulting in a rearrangement. To provide a consistent reaction environment, the rearrangement of all isomers was studied using a microwave reactor at 150 °C, with reaction times of 30 or 60 min. After chromatographic purification to remove oligomeric material, product distributions were determined by high field ^{1}H NMR, with integration of unique resonances for each isomer. In these reactions, we attribute no special effect due to microwaves. This has been a subject of some debate in the literature [37,38]. As we have demonstrated earlier, the microwave reactor simply provides a safe and reliable way to heat samples with superacids at temperatures well above the normal solvent boiling point.

The results of quaterphenyl isomerizations are summarized in Table 1. Initially it was expected that *m*,*m*'-quaterphenyl (**14**)

Table 1: Product distributions from rearrangement of quaterphenyl isomers.[a,b].

Reactant	Time (min)	12	13	14	15	16	17	Yield
12	30	–	100	–	–	–	–	70
12	60	–	100	–	–	–	–	55
13	30	–	100	–	–	–	–	88
13	60	–	100	–	–	–	–	75
14	30	–	50	50	–	–	–	81
14	60	–	67	33	–	–	–	90
15	30	–	81	19	–	–	–	70
16	30	–	57	43	–	–	–	64
17	30	–	60	40	–	–	–	67

[a]All reactions were carried out in 1 M CF_3SO_3H in dichloroethane at 150 °C in a microwave reactor. [b]Yields are total isolated products after flash chromatography.

might be the major isomer formed at equilibrium, as previous examples have heavily favored *meta*-substitution patterns. Contrary to this expection, the major product observed in all cases was *m*,*p*'-quaterphenyl (**13**). In 30 min at 150 °C, *p*,*p*'-quaterphenyl (**12**) isomerized completely to **13**. Under the same conditions, *m*,*m*'-quaterphenyl (**14**) isomerized more slowly, yielding **13** and **14** in a 50:50 mixture in 30 min. Increased reaction time with *m,m*'-quaterphenyl (**14**) yielded **13** and **14** in a 67:33 ratio. Starting with *o*,*m*'- (**16**) or *o*,*o*'-quaterphenyl (**17**) yielded a mixture of ca. 60% **13** and ca. 40% **14** in 30 min. Similarly, *o*,*p*'-quaterphenyl (**15**) isomerized to an 81:19 mixture of **13**:**14**. When starting with *m*,*p*'-quaterphenyl, no rearrangement to **14** was observed, even at increased reaction times.

Minor products with more downfield chemical shifts were also observed *via* ^{1}H NMR of these crude product mixtures; these were easily separated from quaterphenyl isomers using flash column chromatography. Analysis of the crude product mixtures by MALDI–TOF–MS confirmed these minor products could be attributed to oligomerization (*m/z* = 344, 673).

Our conclusion from this series of experiments is that *m,p'*-quaterphenyl (**13**) is the equilibrium product from rearrangement of all of the six isomers. This is most clearly demonstrated in the rearrangement of **12** to **13** and the failure of **13** to produce other isomers. In some cases, reaction times were insufficient to fully reach equilibrium.

Computational models for quaterphenyl rearrangements

While the energy surface for the interconversion of quaterphenyl isomers initially seems straightforward, there are additional modes of rearrangement that must be considered. 1,2-Phenyl shifts are possible to interconvert isomers, occurring through protonation at the *ipso* site on the external phenyl rings (Scheme 4a). Biphenyl shifts are also possible through protonation at the internal *ipso* sites (Scheme 4b). This results in a very complex potential energy surface. Protonation of a terminal phenyl group can also lead to terphenyl migration but this process is structurally degenerate and was not explored by computations.

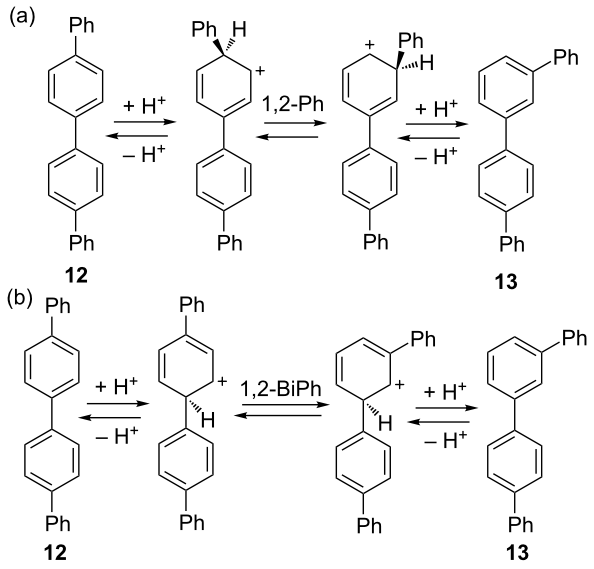

Scheme 4: Rearrangement of quaterphenyl isomers via (a) 1,2-phenyl shift and (b) 1,2-biphenyl shift.

Both phenyl and biphenyl rearrangement pathways were studied by DFT methods, with inclusion of implicit solvation by the polarizable continuum model (PCM). As in our earlier research, we employed B3LYP/6-31+G(d,p) theory with PCM solvation in dichloroethane [25,26,28]. As noted earlier by Tantillo, the B3LYP functional provides a very good description of carbocation chemistry [3].

Figure 1 shows the lowest energy pathways for 1,2-phenyl shifts, while Figure 2 shows those for a 1,2-biphenyl shifts. In each case, the energy reference is arbitrarily chosen as the linear *ipso* cation **12c** or **12d** for phenyl or biphenyl shift, respectively. Predicted barriers for rearrangements of *ipso* cations are all in the range of 9–22 kcal/mol. Common to both potential energy surfaces are the lowest energy non-*ipso* carbocations **12a**–**17a** which lie at the bottom on the energy scale. It is noteworthy that *m,p'* cation **13a** is the lowest energy species predicted by our calculations. In each diagram, double-headed vertical arrows show the energy difference between *ipso* cations and their non-*ipso* counterpart which might be formed rapidly by secondary 1,2-hydride shifts.

In principle, the equilibrium product in these complex reactions might correlate with relative energies of the neutral quaterphenyl isomers. Reliable heats of formation for quaterphenyls are unavailable in the literature but these values and other estimates for relative energies can be predicted by theory. Starting with the lowest energy conformer for each quaterphenyl, we first computed heats of formation using the T1 method [39]. Predicted values (Supporting Information File 1) are narrowly clustered in a range of ca. 2 kcal/mol, with the lowest energy isomer predicted to be *o,o'*-quaterphenyl (**17**). This low ranking for the most congested isomer may be attributed to intramolecular π stacking. Very similar results were obtained with M06-2X/6-311+G(d,p) theory, which also placed **17** as the lowest energy quaterphenyl isomer. Our results thus do not support thermodynamic control based on relative energies of the neutral quaterphenyls.

A more plausible scenario is that thermodynamic control applies to carbocation intermediates, with the equilibrium product determined by the energy of the lowest energy carbocation in solution. This is predicted to be **13a**. The speed of equilibration for different isomers is determined by the number of required steps and their barriers. Thus **12** rearranges to **13** in a phenyl or biphenyl migration, passing through **TS7** or **TS13**, respectively. This rearrangement is complete in our standard 30 min reaction time. By contrast, **17** requires three separate migration steps to arrive at **13**, passing through **16** and **14**; this rearrangement (Table 1) is incomplete during the same reaction period.

An unknown factor is the degree of protonation, especially at 150 °C. We observed earlier by NMR spectroscopy that anthracene is fully protonated at ambient temperature in 1M TfOH but 1,3,5-triphenylbenzene is not [28]. One experimental observation is that the 1M TfOH/arene reaction solutions invariably have a bright color at ambient temperature due to the

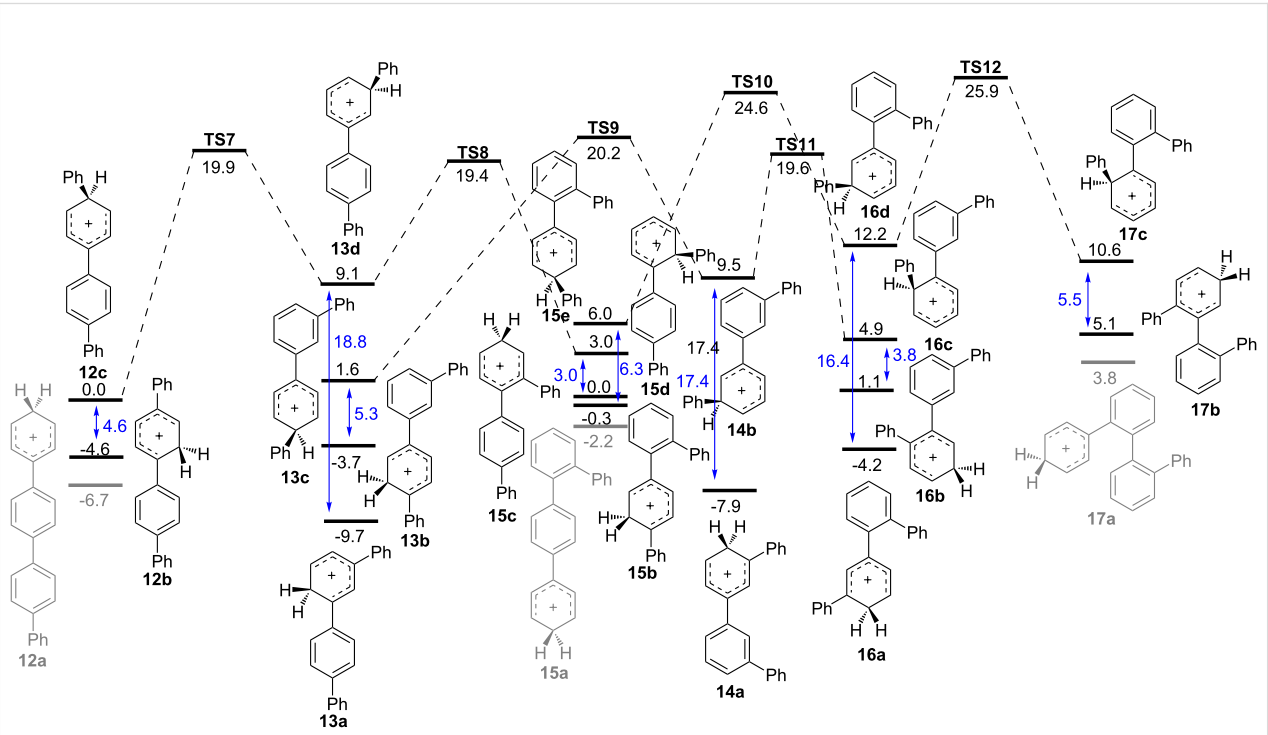

Figure 1: Pathways for terminal 1,2-phenyl shifts in quaterphenyl isomers calculated with IEFPCM(DCE)/B3LYP/6-31+G(d,p) theory. Relative free energies are given in kcal/mol.

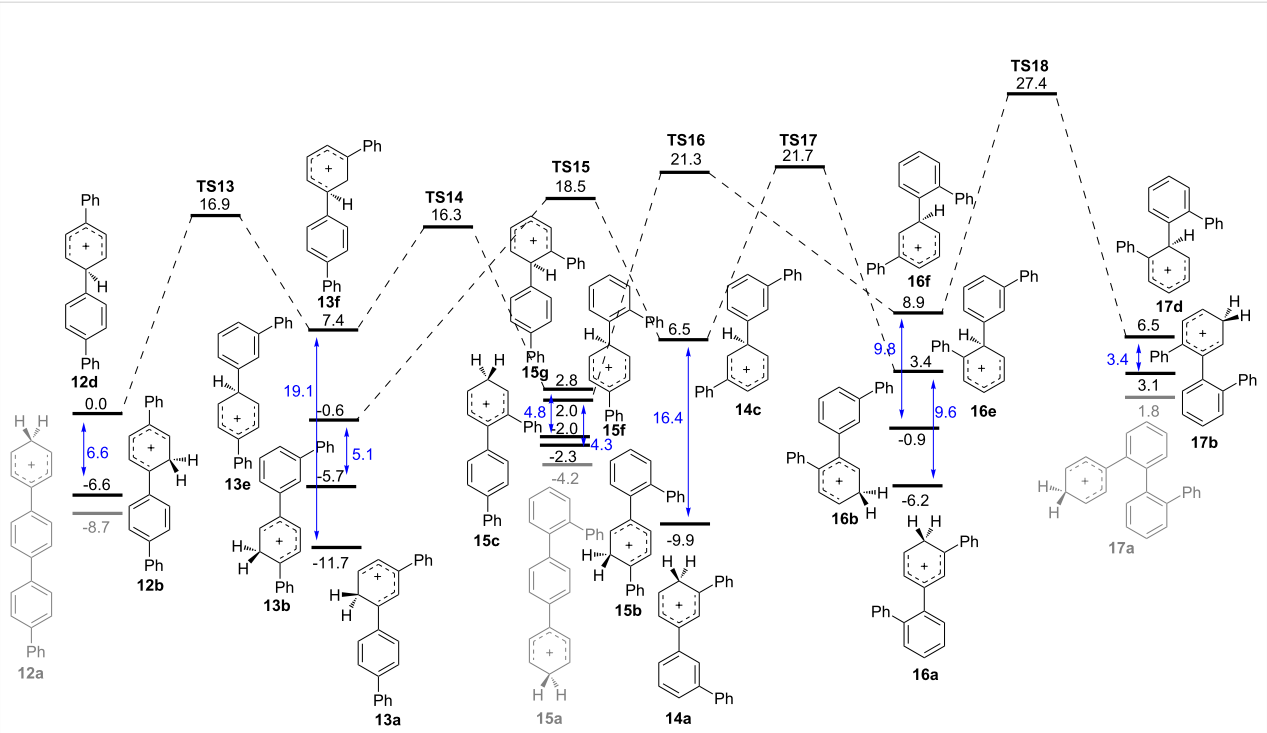

Figure 2: Pathways for 1,2-biphenyl shifts in quaterphenyl isomers calculated with IEFPCM(DCE)/B3LYP/6-31+G(d,p) theory. Relative free energies are given in kcal/mol.

carbocation [40,41]. As these solutions are heated, they become much darker in color, implying a higher level of protonation. Upon cooling, a more normal color is returned. Full protonation of **13** at 150 °C would explain thermodynamic control by cationic intermediates.

Our naïve supposition at the outset of this project that *m,m'*-quaterphenyl **14** might be favored at equilibrium was unsupported by experiment, which instead showed the *m,p'* isomer **13** to be preferred. A comparison of **5a**, the lowest energy cation from terphenyl rearrangements, with **13a**, the corresponding cation for quaterphenyls, provides a simple explanation. If a single ring is protonated, greater stability accrues from a *para* phenyl substituent with *meta* a close second. The same effect should apply to longer polyphenylene chains, resulting in a chain of aryl groups that remains mostly *para* after generating a more basic *meta* substituted site.

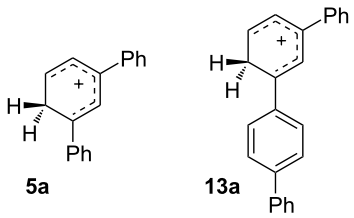

Conclusion

Acid-catalyzed interconversions among the six quaterphenyl isomers have been studied in this work as a model for rearrangements of linear polyphenyls. All reactions were carried out in 1 M CF_3SO_3H (TfOH) in dichloroethane at 150 °C in a microwave reactor for 30 or 60 min, with product formation assessed by high field NMR analysis. Under these reaction conditions, *m,p'*-quaterphenyl (**13**) is the equilibrium product. This isomer is unchanged by the reaction conditions and all other quaterphenyl isomers rearrange to *m,p'* as the dominant or sole product. DFT computations with inclusion of implicit solvation support a complex network of phenyl and biphenyl shifts, with barriers to rearrangement in the range of 10–21 kcal/mol. Consistent with experiments, the lowest energy arenium ion located on this surface is due to protonation of *m,p'*-quaterphenyl. This supports thermodynamic control based on carbocation energies. The same effect may apply to longer polyphenylene chains, resulting in a chain of aryl groups that does not fully rearrange but remains mostly *para* after generating a more basic *meta* substituted site.

Experimental

General methods. Trifluoromethanesulfonic acid (TfOH, 99% purity) and dichloroethane (DCE, 99+%) were used as received from commercial sources. Glassware was oven dried

and all reactions were run under a nitrogen atmosphere. ^{1}H NMR spectra were measured in $CDCl_3$ using a Varian XL-400 MHz spectrometer. Microwave reactions were conducted using a single-mode CEM microwave reactor in 10 mL vessels with temperature monitoring by an external sensor.

General procedure for rearrangement in the microwave (MW) reactor. In a similar manner as described in [28], under a nitrogen atmosphere, the substrate (ca. 4 – 50 mg) and 1,2-dichloroethane (DCE, 4 mL) were added to a 10 mL reaction vessel. Trifluoromethanesulfonic acid (TfOH) (0.40 mL, 4.5 mmol) was added dropwise by syringe; this typically caused formation of a bright color. The reaction mixture was purged with nitrogen, capped and heated in a microwave reactor. Reaction times represent hold times after a ramp time of ca. 10 minutes. After cooling, products were isolated by careful neutralization with saturated aqueous $NaHCO_3$ and extraction with dichloromethane. The crude product mixture was purified by flash chromatography then analyzed using ^{1}H NMR. The presence of oligomeric material was assessed on crude isolated product through time-of-flight matrix assisted laser desorption ionization (MALDI–TOF–MS) mass spectrometry, using sulfur as a matrix.

Suzuki–Miyaura coupling to form *m,p'*-quaterphenyl (13) [35]**:** 4-Biphenylboronic acid (0.18 g, 0.91 mmol) and 1 M K_2CO_3 (1.5 mL) were added to a 10 mL Pyrex microwave tube. 3-Bromobiphenyl (0.07 mL, 0.42 mmol), ethanol (2.3 mL), and $Pd(PPh_3)_4$ (28 mg, 0.24 mmol) were then added. The headspace was purged with nitrogen and the tube was capped before the reaction mixture was placed in a microwave reactor (150 °C, 30 min hold time). After the reaction, the mixture was quenched with 1 M NaOH, extracted with dichloromethane, washed with water and brine, and dried with Na_2SO_4. The organic layer was then concentrated to a brown solid and purified by chromatography with hexanes to yield *m,p'*-quaterphenyl (**13**) as a white solid (0.058 g, mp 163–166 °C, lit 167–168 °C, 42% yield); ^{1}H NMR (400 MHz, $CDCl_3$) δ 7.87–7.85 (m, 1H), 7.76–7.69 (m, 4H), 7.69–7.64 (m, 4H), 7.64–7.58 (m, 2H), 7.57–7.52 (m, 1H), 7.50–7.45 (m, 4H), 7.41–7.35 (m, 2H).

Suzuki–Miyaura coupling to form o,*p'*-quaterphenyl (15) [35]**:** K_2CO_3 (0.91 g, 6.6 mmol) and water (7.7 mL) were combined in a 25 mL round bottom flask which was purged with nitrogen, and cooled to 0 °C. Biphenyl-4-boronic acid (0.89 g, 4.5 mmol) was added, followed by 2-bromobiphenyl (0.50 g, 2.2 mmol), DMF (11.5 mL) and $Pd(PPh_3)_4$ (0.13 g, 0.1 mmol). The reaction mixture was stirred at 0 °C for 5 h. NaOH (1 M, 10 mL) was added and the product was extracted with DCM. The organic extract was washed with water and brine and dried with Na_2SO_4. The crude product was purified by flash chromatography with hexanes to yield *o,p'*-quaterphenyl as a white solid (0.55 g, mp 107–109 °C, lit 117–120 °C, 90% yield). ^{1}H NMR (400 MHz, $CDCl_3$) δ 7.61–7.57 (m, 2H), 7.50–7.40 (m, 8H), 7.35–7.29 (m, 1H), 7.26–7.17 (m, 7H).

Suzuki–Miyaura coupling to form o,*m'*-Quaterphenyl (16) [35]**:** 2-Bromobiphenyl (0.20 g, 0.80 mmol), biphenyl-3-boronic acid (0.25 g, 1.3 mmol), and $Pd(PPh_3)_4$ (0.02 g, 0.02 mmol) were dissolved in DMF (10 mL). The reaction mixture was cooled to 0 °C and purged with nitrogen. A solution of K_2CO_3 (0.20 g, 1.5 mmol) and water (5 mL) was added via syringe and the reaction mixture was stirred at 0 °C for 5 h. The product was extracted with DCM, and washed with water, NaOH, and HCl. The organic extract was then washed with water and brine and dried with Na_2SO_4. The crude product was purified by flash chromatography with hexanes to yield *o,m'*-quaterphenyl as a white solid (0.085 g, mp 84–86 °C, lit 90–91 °C, 33% yield). ^{1}H NMR (400 MHz, $CDCl_3$) δ 7.52–7.47 (m, 1H), 7.47–7.40 (m, 4H), 7.38–7.29 (m, 6H), 7.29–7.26 (m, 1H), 7.26–7.22 (m, 3H), 7.21–7.15 (m, 3H).

Synthesis of *o,o'*-quaterphenyl (17) [36]**:** A solution of 2-bromobiphenyl (0.15 g, 0.65 mmol), magnesium turnings (0.02 g, 0.69 mmol), and THF (2 mL) was stirred at ambient temperature overnight under a nitrogen atmosphere. Additional THF (4 mL) was added and the reaction mixture was cooled to −78 °C via a dry ice/acetone bath. $TiCl_4$ (0.14 g, 0.65 mmol) was added dropwise via syringe and the reaction mixture was warmed to 0 °C via an ice/water bath and stirred for 1 h. The product was extracted with ethyl acetate (3x) and dried with Na_2SO_4. The crude product was purified by chromatography with hexanes to yield *o,o'*-quaterphenyl as a white solid (0.040 g, mp 110–113 °C, *lit* 116–118 °C, 20% yield). ^{1}H NMR (400 MHz, $CDCl_3$) δ 7.4–7.40 (m, 2H), 7.38–7.29 (m, 4H), 7.18–7.14 (m, 2H), 7.10–7.05 (m, 2H), 7.03–6.96 (m, 4H), 6.62–6.59 (m, 4H).

Rearrangement of quaterphenyl isomers in a microwave reactor

***p,p'*-Quaterphenyl (12):** 150 °C, 30 min. Compound **12** (17 mg, 0.06 mmol) was heated in a MW reactor (150 °C, 30 min) according to the general rearrangement procedure. The crude product was purified via CombiFlash with hexanes to yield *m,p'*-quaterphenyl (**13**) as an off-white solid (12 mg, 70% yield).

***m,p'*-Quaterphenyl (13):** 150 °C, 30 min. Compound **13** (17 mg, 0.05 mmol) was heated in a MW reactor (150 °C, 30 minutes) according to the general rearrangement procedure.

The crude product was filtered over a silica plug with hexanes to yield **13** as an off-white solid (15 mg, 88% yield).

150 °C, 1 h. **13** (16 mg, 0.05 mmol) was heated in a MW reactor (150 °C, 1 h) according to the general rearrangement procedure. The crude product was filtered over a silica plug with hexanes to yield **13** as an off-white solid (12 mg, 75% yield).

***m*,*m*'-Quaterphenyl (14):** 150 °C, 30 min. Compound **14** (16 mg, 0.05 mmol) was heated in a MW reactor (150 °C, 30 minutes) according to the general rearrangement procedure. The crude product was purified via CombiFlash with hexanes to yield an off-white solid (13 mg, 81% yield) consisting of **13** (50%) and **14** (50%).

150 °C, 1 h. Compound **12** (10 mg, 0.03 mmol) was heated in a MW reactor (150 °C, 1 h) according to the general rearrangement procedure. The crude product was filtered over a silica plug with hexanes to yield an off-white solid (9 mg, 90% yield) consisting of **13** (67%) and **14** (33%).

***o*,*p*'-Quaterphenyl:** Compound **15** (10 mg, 0.03 mmol) was heated in a MW reactor (150 °C, 30 minutes) according to the general rearrangement procedure. The crude product was purified via CombiFlash with hexanes to yield an off-white solid (7 mg, 70% yield) consisting of **13** (81%) and **14** (19%). Minor products were eluted with ethyl acetate. MALDI–TOF–MS analysis indicated oligomerization (m/z = 344, 673).

***o*,*m*'-Quaterphenyl:** Compound **16** (28 mg, 0.09 mmol) was heated in a MW reactor (150 °C, 30 minutes) according to the general rearrangement procedure. The crude product was filtered over a silica plug with hexanes to yield an off-white solid (18 mg, 64% yield) consisting of **13** (57%) and **14** (43%).

o,o'-Quaterphenyl: Compound **17** (6 mg, 0.02 mmol) was heated in a MW reactor (150 °C, 30 minutes) according to the general rearrangement procedure. The crude product was filtered over a silica plug with hexanes to yield an off-white solid (4 mg, 67% yield) consisting of **13** (60%) and **14** (40%).

Computational methods: DFT computations on carbocation intermediates and transition states were carried out with the B3LYP functional and 6-31+G(d,p) basis set, using the polarizable continuum model in dichloroethane to model solvation [42]. Each stationary point was characterized as a minimum or transition state by vibrational frequency analysis but the large number of reaction paths precluded calculation of intrinsic reaction coordinates. Reported relative energies are from free energy calculations at 298 K.

Supporting Information

Supporting Information File 1

Selected NMR spectra, MALDI spectrum of the product mixture, Cartesian coordinates, and summary energetics for all stationary points.
[https://www.beilstein-journals.org/bjoc/content/supplementary/1860-5397-15-258-S1.pdf]

Acknowledgements

We are grateful for support from National Science Foundation award CHE-1362519. This research used the Extreme Science and Engineering Discovery Environment (XSEDE), supported by NSF Grant No. OCI-1053575.

ORCID® iDs

Sarah L. Skraba-Joiner - https://orcid.org/0000-0002-1545-0608
Carter J. Holt - https://orcid.org/0000-0001-7459-353X
Richard P. Johnson - https://orcid.org/0000-0002-1100-6235

References

1. Klumpp, D. A. Carbocations. In *Organic Reaction Mechanisms ·;* Knipe, A. C., Ed.; John Wiley & Sons, Ltd, 2016; pp 273–319. doi:10.1002/9781118707838.ch6
2. Naredla, R. R.; Klumpp, D. A. *Chem. Rev. (Washington, DC, U. S.)* **2013,** *113,* 6905–6948. doi:10.1021/cr4001385
3. Tantillo, D. J. *Angew. Chem., Int. Ed.* **2017,** *56,* 10040–10045. doi:10.1002/anie.201702363
4. Sandbeck, D. J. S.; Markewich, D. J.; East, A. L. L. *J. Org. Chem.* **2016,** *81,* 1410–1415. doi:10.1021/acs.joc.5b02553
5. Pontes, R. M. *Theor. Chem. Acc.* **2018,** *137,* 56. doi:10.1007/s00214-018-2232-1
6. Hare, S. R.; Tantillo, D. J. *Beilstein J. Org. Chem.* **2016,** *12,* 377–390. doi:10.3762/bjoc.12.41
7. Prakash, G. K. S. *J. Org. Chem.* **2006,** *71,* 3661–3676. doi:10.1021/jo052657e
8. Olah, G. A. *J. Org. Chem.* **2001,** *66,* 5943–5957. doi:10.1021/jo010438x
9. Klumpp, D. A. In *Arene Chemistry;* Mortier, J., Ed.; John Wiley & Sons, Inc: Hoboken, NJ, 2016; pp 3–31.
10. Oliveira, F. G.; Rodrigues, F. L.; de Oliveira, A. V. B.; Marçal, D. V. L. M.; Esteves, P. M. *Struct. Chem.* **2017,** *28,* 545–553. doi:10.1007/s11224-017-0915-1
11. Chen, Z.; Mo, Y. *J. Chem. Theory Comput.* **2013,** *9,* 4428–4435. doi:10.1021/ct400618k
12. Freire de Queiroz, J.; Carneiro, J. W. d. M.; Sabino, A. A.; Sparrapan, R.; Eberlin, M. N.; Esteves, P. M. *J. Org. Chem.* **2006,** *71,* 6192–6203. doi:10.1021/jo0609475
13. Esteves, P. M.; Walkimar de Carneiro, J.; Cardoso, S. P.; Barbosa, A. G. H.; Laali, K. K.; Rasul, G.; Prakash, G. K. S.; Olah, G. A. *J. Am. Chem. Soc.* **2003,** *125,* 4836–4849. doi:10.1021/ja021307w
14. Rosokha, S. V.; Kochi, J. K. *J. Org. Chem.* **2002,** *67,* 1727–1737. doi:10.1021/jo011072r

15. Kim, E. K.; Bockman, T. M.; Kochi, J. K. *J. Am. Chem. Soc.* **1993,** *115,* 3091–3104. doi:10.1021/ja00061a007
16. Galabov, B.; Nalbantova, D.; Schleyer, P. v. R.; Schaefer, H. F., III. *Acc. Chem. Res.* **2016,** *49,* 1191–1199. doi:10.1021/acs.accounts.6b00120
17. Nieves-Quinones, Y.; Singleton, D. A. *J. Am. Chem. Soc.* **2016,** *138,* 15167–15176. doi:10.1021/jacs.6b07328
18. Baddeley, G.; Kenner, J. *J. Chem. Soc.* **1935,** 303–309. doi:10.1039/jr9350000303
19. Nightingale, D. V. *Chem. Rev.* **1939,** *25,* 329–376. doi:10.1021/cr60082a001
20. Wynberg, H.; Wolf, A. P. *J. Am. Chem. Soc.* **1963,** *85,* 3308. doi:10.1021/ja00903a064
21. Necula, A.; Racoveanu-Schiketanz, A.; Gheorghiu, M. D.; Scott, L. T. *J. Org. Chem.* **1995,** *60,* 3448–3451. doi:10.1021/jo00116a035
22. Allen, C. F. H.; Pingert, F. P. *J. Am. Chem. Soc.* **1942,** *64,* 1365–1371. doi:10.1021/ja01258a038
23. Olah, G. A.; Meyer, M. W. *J. Org. Chem.* **1962,** *27,* 3682–3683. doi:10.1021/jo01057a505
24. Perrin, C. L.; Skinner, G. A. *J. Am. Chem. Soc.* **1971,** *93,* 3389–3394. doi:10.1021/ja00743a015
25. Ajaz, A.; McLaughlin, E. C.; Skraba, S. L.; Thamatam, R.; Johnson, R. P. *J. Org. Chem.* **2012,** *77,* 9487–9495. doi:10.1021/jo301848g
26. Skraba-Joiner, S. L.; McLaughlin, E. C.; Ajaz, A.; Thamatam, R.; Johnson, R. P. *J. Org. Chem.* **2015,** *80,* 9578–9583. doi:10.1021/acs.joc.5b01559
27. Dansi, A.; Salvioni, E. *Gazz. Chim. Ital.* **1941,** *71,* 549–552.
28. Skraba-Joiner, S. L.; Brulet, J. W.; Song, M. K.; Johnson, R. P. *J. Org. Chem.* **2017,** *82,* 13076–13083. doi:10.1021/acs.joc.7b02058
29. Cook, B. R.; Colgrove, S. G. *Prepr. - Am. Chem. Soc., Div. Pet. Chem.* **1994,** *39,* 372–378.
30. Sisto, T. J.; Zakharov, L. N.; White, B. M.; Jasti, R. *Chem. Sci.* **2016,** *7,* 3681–3688. doi:10.1039/c5sc04218f
31. Ormsby, J. L.; Black, T. D.; Hilton, C. L.; Bharat; King, B. T. *Tetrahedron* **2008,** *64,* 11370–11378. doi:10.1016/j.tet.2008.09.105
32. He, J.; Mathew, S.; Kinney, Z. J.; Warrell, R. M.; Molina, J. S.; Hartley, C. S. *Chem. Commun.* **2015,** *51,* 7245–7248. doi:10.1039/c5cc00826c
33. Mathew, S.; Crandall, L. A.; Ziegler, C. J.; Hartley, C. S. *J. Am. Chem. Soc.* **2014,** *136,* 16666–16675. doi:10.1021/ja509902m
34. Copeland, P. G.; Dean, R. E.; McNeil, D. *J. Chem. Soc.* **1960,** 4522–4524. doi:10.1039/jr9600004522
35. Lima, C. F. R. A. C.; Rodrigues, A. S. M. C.; Silva, V. L. M.; Silva, A. M. S.; Santos, L. M. N. B. F. *ChemCatChem* **2014,** *6,* 1291–1302. doi:10.1002/cctc.201301080
36. King, B. T.; Kroulík, J.; Robertson, C. R.; Rempala, P.; Hilton, C. L.; Korinek, J. D.; Gortari, L. M. *J. Org. Chem.* **2007,** *72,* 2279–2288. doi:10.1021/jo061515x
37. Kappe, C. O.; Pieber, B.; Dallinger, D. *Angew. Chem., Int. Ed.* **2013,** *52,* 1088–1094. doi:10.1002/anie.201204103
38. Dudley, G. B.; Stiegman, A. E. *Chem. Rec.* **2018,** *18,* 381–389. doi:10.1002/tcr.201700044
39. Ohlinger, W. S.; Klunzinger, P. E.; Deppmeier, B. J.; Hehre, W. J. *J. Phys. Chem. A* **2009,** *113,* 2165–2175. doi:10.1021/jp810144q
40. Garkusha, I.; Fulara, J.; Nagy, A.; Maier, J. P. *Astrophys. J.* **2011,** *728,* 131. doi:10.1088/0004-637x/728/2/131
41. Dallinga, G.; Mackor, E. L.; Verrijn Stuart, A. A. *Mol. Phys.* **1958,** *1,* 123–140. doi:10.1080/00268975800100151
42. Tomasi, J.; Mennucci, B.; Cammi, R. *Chem. Rev.* **2005,** *105,* 2999–3093. doi:10.1021/cr9904009

License and Terms

BEILSTEIN JOURNAL OF ORGANIC CHEMISTRY

Understanding the role of active site residues in CotB2 catalysis using a cluster model

Keren Raz[1], Ronja Driller[2,3,4], Thomas Brück[5], Bernhard Loll[2] and Dan T. Major[*1]

Full Research Paper

Open Access

Address:
[1]Department of Chemistry, Bar-Ilan University, Ramat-Gan 52900, Israel, [2]Institute of Chemistry and Biochemistry, Laboratory of Structural Biochemistry, Freie Universität Berlin, Takustr. 6, 14195 Berlin, Germany, [3]present address: Department of Molecular Biology and Genetics, Aarhus University, Gustav Wieds Vej 10, 8000 Aarhus C, Denmark, [4]present address: Danish Research Institute of Translational Neuroscience - DANDRITE, Nordic-EMBL Partnership for Molecular Medicine, Aarhus C, Denmark and [5]Werner Siemens Chair of Synthetic Biotechnology, Dept. of Chemistry, Technical University of Munich (TUM), Lichtenbergstr. 4, 85748 Garching, Germany

Email:
Dan T. Major[*] - majort@biu.ac.il

* Corresponding author

Keywords:
active site; CotB2 cyclase; diterpene; mechanism; quantum mechanics

Beilstein J. Org. Chem. **2020,** *16,* 50–59.
doi:10.3762/bjoc.16.7

Received: 25 September 2019
Accepted: 17 December 2019
Published: 08 January 2020

This article is part of the thematic issue "Reactive intermediates – carbocations".

Guest Editor: S. R. Hare

Abstract

Terpene cyclases are responsible for the initial cyclization cascade in the multistep synthesis of a large number of terpenes. CotB2 is a diterpene cyclase from *Streptomyces melanosporofaciens,* which catalyzes the formation of cycloocta-9-en-7-ol, a precursor to the next-generation anti-inflammatory drug cyclooctatin. In this work, we present evidence for the significant role of the active site's residues in CotB2 on the reaction energetics using quantum mechanical calculations in an active site cluster model. The results revealed the significant effect of the active site residues on the relative electronic energy of the intermediates and transition state structures with respect to gas phase data. A detailed understanding of the role of the enzyme environment on the CotB2 reaction cascade can provide important information towards a biosynthetic strategy for cyclooctatin and the biomanufacturing of related terpene structures.

Introduction

Enzymes catalyze numerous complex biochemical reactions in different cellular compartments [1,2]. More specifically, the enigmatic class of terpene cyclases is responsible for converting linear aliphatic oligoprenyl diphosphates into various chemically complex macrocyclic products. The resulting terpene scaffolds and their functionalized terpenoid analogues comprise the

largest and structurally most diverse family of natural products, currently representing over 80,000 reported structures from all kingdoms of life [3]. The largest diversity of terpenoids is reported for the plant kingdom where higher terpenes represent secondary metabolic products, which are responsible for, e.g., defense against biotic and abiotic stress or for attracting insects for pollination [4,5]. Industrially, terpene natural products are employed as flavoring agents [6], fragrances, pigments, cosmetics, perfumes, biofuels, and agrochemicals [5]. Additionally, terpene natural products with numerous pharmacological [7,8] and biological activities have been reported, rendering them important targets for medical and biotechnology research [9]. Chemical synthetic and sustainable biosynthetic strategies in synergy with the biological activity of different terpene natural products have been reviewed elsewhere [3,10-17].

The first crystal structure of a monoterpene cyclase [18] was reported in 2002. Subsequently, the first crystal structures of a sesquiterpene [19,20] and a triterpene [21] cyclase were published in 1997. Less than a decade ago, the first crystal structure of a diterpene cyclase was reported by Christianson and co-workers [22]. These structures, in conjunction with extensive biochemical work [10,13,14,23], have contributed to the understanding of mechanistic details of terpene cyclases and facilitated rational enzyme design [24]. Theoretical quantum mechanical (QM) investigations on the chemistry of terpenes in the gas phase have provided a detailed understanding of the carbocation mechanisms underlying terpene synthase function [25-27]. Further, we have used multiscale modeling tools to study the effects of the enzyme environment in catalyzing reactions of mono-, sesqui-, and diterpene synthases [28-36].

Diterpenes are generated from the universal aliphatic substrate geranyl geranyl pyrophosphate (GGPP) [4]. In vitro experiments demonstrated that many diterpenes have pharmaceutical applications by featuring anticancer, antibacterial, anti-inflammatory, and antiretroviral activities [37]. Moreover, they are applied in the food industry as antioxidants and sweeteners [4].

CotB2 is a bacterial diterpene cyclase from *S. melanosporofaciens,* which catalyzes the formation of cyclooctat-9-en-7-ol, representing the first committed step in the biosynthesis of the next-generation anti-inflammatory drug cyclooctatin. The intracellular target of cyclooctatin is an as of yet uncharacterized lysophospholipase, which is involved in early steps of the inflammatory signaling cascade [38-40]. In the last decade, numerous interdisciplinary studies have addressed the chemical mechanism of CotB2 catalysis utilizing different detection and analysis methods.

Meguro and co-workers [41] established the chemical mechanism for the formation of cyclooctatin using isotope labeling experiments (Scheme 1). Recently, Hong and Tantillo [38] and Sato and co-workers [39] investigated the CotB2 mechanism using QM tools. According to Meguro and co-workers [41], the cyclization process commences with the dissociation of the pyrophosphate leaving group of GGPP, forming an allylic carbocation, and two subsequent electrophilic cyclizations to

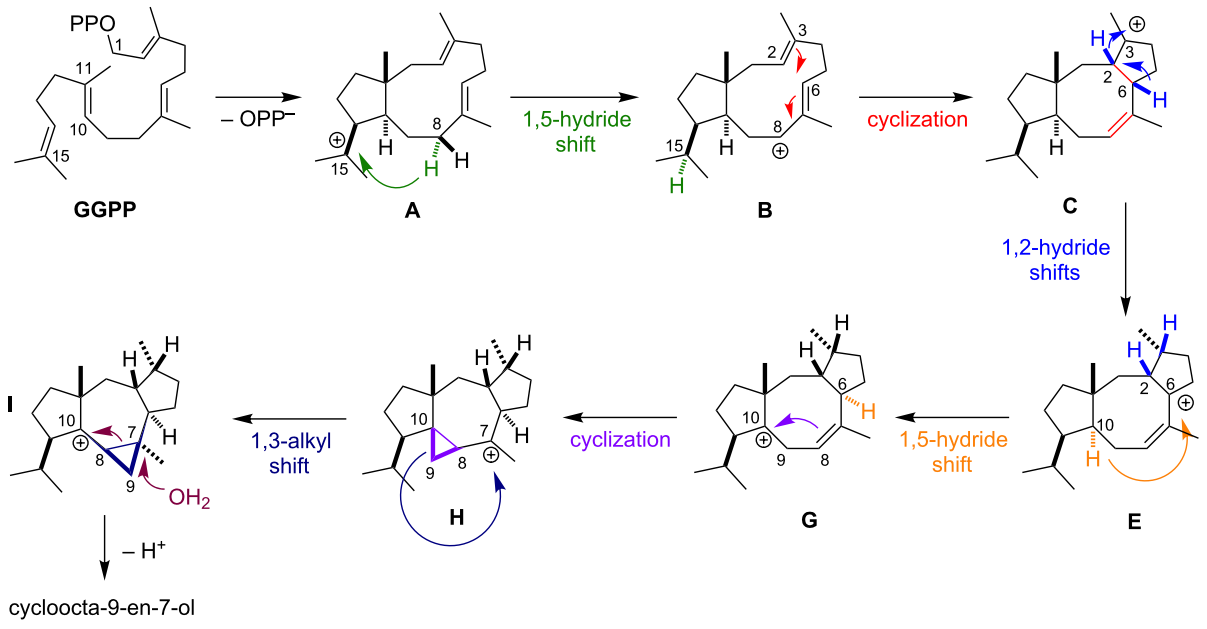

Scheme 1: Mechanism for formation of cyclooctat-9-en-7-ol, published similarly in [42].

generate intermediate **A**. Intermediate **A** undergoes a 1,5-hydride shift, forming intermediate **B**. A subsequent cyclization forms intermediate **C**. Intermediate **C** generates intermediate **E** via one of two possible pathways: either a direct 1,3-hydride shift or an indirect pathway involving two 1,2-hydride shifts. Theoretical investigations by Hong and Tantillo suggested that the indirect transformation from intermediate **C** to **E** is energetically favored and might be biosynthetically relevant [38]. This finding is in agreement with the report by Sato and co-workers [39], who performed isotope labeling experiments combined with QM calculations. Intermediate **G** forms via a 1,5-hydride shift from C6 to C10 to generate a homoallylic cation, and the formation of intermediate **H** occurs due to cyclization to yield a cyclopropyl ring. Intermediate **I** forms due to isomeric formation of a cyclopropylcarbinyl cation, as shown by isotope labeling [41]. QM calculations support this unusual 1,3-alkyl shift that interconverts **H** and **I** [38,39]. Finally, the cyclopropyl ring opens by virtue of a nucleophilic water attack, and cyclooctat-9-en-7-ol is formed.

Although gas phase calculations shed light on the reactivity of the isolated species and provided crucial mechanistic insights, the biorelevant mechanism cannot be fully understood without taking into account the enzyme–solvent environment. A common problem when studying these enzymes is the lack of high-resolution crystal structures that are biologically relevant, i.e., that have a ligand bound in a reactive configuration and have a fully closed active site. Recently, a crystal structure of the CotB2 enzyme that met these criteria was published [42]. In the current work, we describe the crucial role of the amino acids in the active site on the reaction energetics using QM calculations in an active site cluster model. The active site cluster theozyme model [43,44] was constructed from the crystal structure coordinates of active site amino acids, which were presumed to stabilize the carbocations during the reaction cascade. Each reaction step's relevant species was optimized in the active site model within a fixed enzyme approximation. The results obtained using the active site model were compared with gas phase data.

Results and Discussion

The energy profiles for both gas phase (orange) and for the active site model (blue) reactions were characterized by a sequential decreasing pattern (Figure 1). The inspection of the

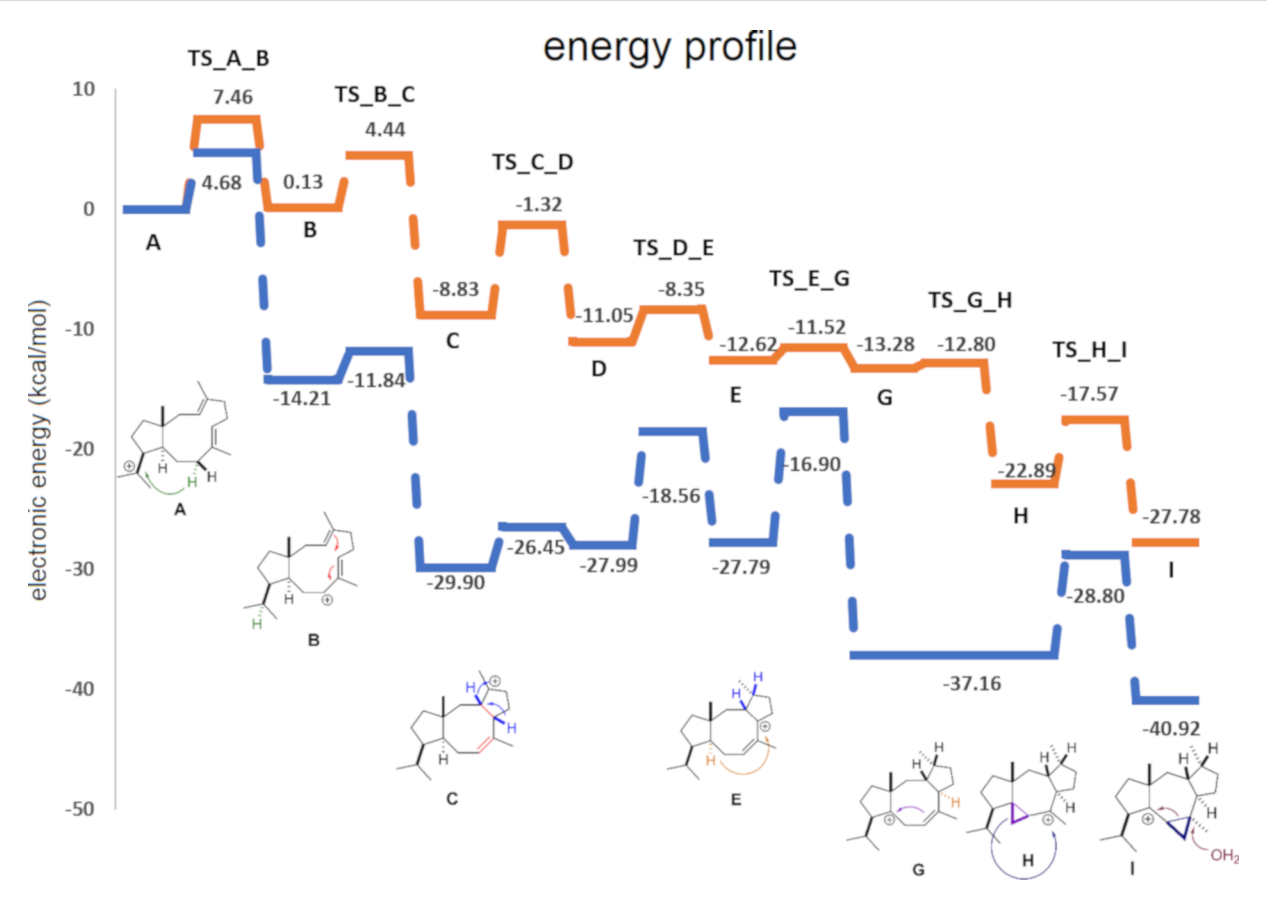

Figure 1: Computed electronic energy profiles (kcal/mol) for the CotB2 cyclase mechanism. The calculations used M062X/6-31+G(d,p).

gas phase profile revealed important information regarding the inherent reactivity [27] of the carbocation species. As the reaction proceeded, π-bonds transformed into σ-bonds, explaining the steady downhill progress of the energy profile. An additional feature was the relatively low energy barrier of less than ca. 10 kcal/mol separating the intermediates. The gas phase mechanism has been discussed extensively by Hong and Tantillo [38] and Sato and co-workers [39]. Herein, we focused on the differences between gas phase and active site model energies. All interaction distances are provided in Table 1, which provided the basis for the following categorization of interactions as π–cation, dipole–cation, and charge–cation. Note, that no attempts to quantify the individual pairwise interactions were made.

Table 1: Interactions between intermediates and TS structures with active site residues.

intermediate	interacting species		distance (Å)	interaction type
A	W186	C_{15}	4.49	π-cation
	I181	C_{15}	3.80	dipole-cation
B	N103	C_6	4.66	dipole–cation (C=O)
	N103	C_7	4.72	dipole–cation (C=O)
	N103	C_8	4.41	dipole–cation (C=O)
	T106	C_6	3.96	dipole–cation (OH)
	T106	C_7	4.15	dipole–cation (OH)
	T106	C_8	5.33	dipole–cation (OH)
	F107	C_6	4.25	π–cation
	F107	C_7	5.53	π–cation
	F107	C_8	5.88	π–cation
	I181	C_6	5.15	dipole–cation
	I181	C_7	4.45	dipole–cation
	I181	C_8	4.14	dipole–cation
C	O_3	C_3	4.20	anion–cation
	F107	C_3	3.65	π–cation
	I181	C_3	4.72	dipole–cation
D	O_3	C_2	5.03	anion–cation
	F107	C_2	4.35	π–cation
E	N103	C_6	4.74	dipole–cation (C=O)
	N103	C_7	3.81	dipole–cation (C=O)
	N103	C_8	3.04	dipole–cation (C=O)
	T106	C_6	4.43	dipole–cation (OH)
	T106	C_7	4.25	dipole–cation (OH)
	T106	C_8	5.32	dipole–cation (OH)
	F107	C_6	4.66	π–cation
	F107	C_7	5.37	π–cation
	F107	C_8	5.54	π–cation
	F149	C_6	5.84	π–cation
	F149	C_7	6.42	π–cation
	F149	C_8	7.75	π-cation
G/**H**	N103	C_7	5.91	dipole–cation
	T106	C_7	5.27	dipole–cation (OH)
	F149	C_7	5.35	π–cation
	I181	C_7	3.08	dipole–cation (C=O)
	W186	C_7	6.48	π–cation
I	N103	C_{10}	5.44	dipole–cation
	I181	C_{10}	3.31	dipole–cation (C=O)
	W186	C_{10}	5.87	π–cation

Table 1: Interactions between intermediates and TS structures with active site residues. (continued)

TS structure	interaction species		distance Å	interaction type
A_B	I181	C_{15}	3.85	dipole–cation
	I181	C_8	4.80	dipole–cation
	W186	C_{15}	4.48	π–cation
	W186	C_8	5.09	π–cation
B_C	O_3	C_2	3.78	
	O_3	C_6	5.88	anion–cation
	N103	C_2	6.26	
	N103	C_6	4.80	dipole–cation (C=O)
	T106	C_2	6.80	
	T106	C_6	4.30	dipole–cation (OH)
	F107	C_2	4.12	
	F107	C_6	4.36	π–cation
	I181	C_2	4.33	
	I181	C_6	4.80	dipole–cation
C_D	O_3	C_2	4.88	anion–cation
	O_3	C_3	4.39	anion–cation
	F107	C_2	4.42	π–cation
	F107	C_3	3.61	π–cation
	I181	C_2	4.00	dipole–cation
	I181	C_3	4.85	dipole–cation
D_E	O_3	C_2	4.66	anion–cation
	O_3	C_6	5.82	anion–cation
	F107	C_2	4.55	π–cation
	F107	C_6	5.37	π–cation
	F149	C_2	5.93	π–cation
	F149	C_6	5.05	π–cation
E_G/H	N103	C_6	6.09	dipole–cation (C=O)
	N103	C_{10}	5.20	dipole–cation (C=O)
	F107	C_6	5.07	π–cation
	F107	C_{10}	5.15	π–cation
	F149	C_6	5.42	π–cation
	I181	C_6	3.62	dipole–cation (OH)
	I181	C_{10}	3.84	dipole–cation (OH)
G/H_I	N103	C_7	5.41	dipole–cation
	N103	C_{10}	5.81	dipole–cation
	T106	C_7	5.11	dipole–cation (OH)
	T106	C_{10}	7.29	dipole–cation (OH)
	F149	C_7	5.68	π–cation
	F149	C_{10}	7.76	π–cation
	I181	C_7	3.47	dipole–cation (C=O)
	I181	C_{10}	3.03	dipole–cation (C=O)
	W186	C_7	6.09	π–cation
	W186	C_{10}	5.70	π–cation

Carbocation **A** was stabilized through π–cation interaction with W186, while **B** was stabilized due to dipole–cation interactions of the allylic carbocation at C6–C7–C8 with N103, T106, and I181. These variations in interactions resulted in an energy difference of 14.2 kcal/mol, favoring **B**, and the barrier was reduced by 2.8 kcal/mol (Figure 1). Another possible reason for

the stabilization was that C7 had a greater proximity to the pyrophosphate group than C15 (6.71 Å vs 7.54 Å, Table 1 and Figure 2). The energy difference between **B** and **C** was 15.7 kcal/mol in the active site model, compared to 8.7 kcal/mol in the gas phase. Here, the energy gain was likely due to the fact that the carbocation in intermediate **C** was located 4.21 Å away from the pyrophosphate group, which stabilized it (Table 1 and Figure 2). Moreover, π–cation interactions with F107 contributed to the stabilization as well. The activation energy for the formation of **C** was 2.4 kcal/mol in the active site model compared to 4.3 kcal/mol in the gas phase. In the active site model, **D** was less stable than **C** by almost 2 kcal/mol, while in the gas phase, **D** was more stable by ca. 2 kcal/mol. The main reason for this difference was possibly a difference in the conformation of **D** in the active site model compared to the gas phase. The dihedral angle defined by C3–C2–C6–C7 in **D** was greater by 53° in the active site model than in the gas phase, and the **D** dihedral angle C10–C9–C8–C7 in the active site was smaller by 258° than in the gas phase (Figure 4a). Moreover, the dihedral angle C2–C1–C11–C10 was greater by 281° in the active site model. The distance between C4 and C13 was significantly greater in the active site model (1.2 Å), indicating a more extended conformation. Figure 4a shows clearly that intermediate **D** was more folded in the gas phase than in the active site model. The required activation energy to form **D** was 4.1 kcal/mol lower in the active site model than the gas phase, likely due to π–cation interactions with F107 and F149 and greater proximity to the negatively charged pyrophosphate group. Another conformational difference between the gas phase and in the enzyme model was noted for **E** as well (Figure 4b). The dihedral angle C2–C3–C4–C5 was greater by 285°, and C10–C9–C8–C7 was smaller by 294° in the active site model than in the gas phase. Moreover, the angle C2–C1–C11 was greater by 5° in the active site model than in the gas phase, and the distance between C4 and C13 was smaller by 0.5 Å in the gas phase. The net result of these differences was that intermediate **E** was more folded in the gas phase, although it was not as dramatically folded as **D**. The reason for greater folding in the gas phase could have been a tendency to adopt conformations that maximized intramolecular dispersion interactions [45,46]. In the active site model of **E**, the carbocation at C6 had a greater distance from the pyrophosphate group than C2 in cation **D** (6.03 Å vs 5.03 Å) and likely contributed to a slight destabilizing effect in the active site model. This was in spite of interactions between cation **D** and N103, T106, F107, and F149. Nonetheless, the energy barrier to form **E** was higher in the active site model than in the gas phase. An elevated energy barrier was also observed for the formation of **G** (by almost 10 kcal/mol). This may be explained by the loss of interactions between **G** and the pyrophosphate moiety as the cation moved further away, deeper into the hydrophobic part of the pocket. A distinct carbocation **G** was not observed in the enzyme model. Instead, a cation resembling **H**, with a C8–C10 bond that was already partly formed, was observed. This carbocation was more stable in the active site model than **G** in the gas phase by almost 9 kcal/mol. Hence, in the enzyme model, cation **G** was not a stable species, and instead, **H** was formed spontaneously. The energy for the transformation of **E** to **H** was

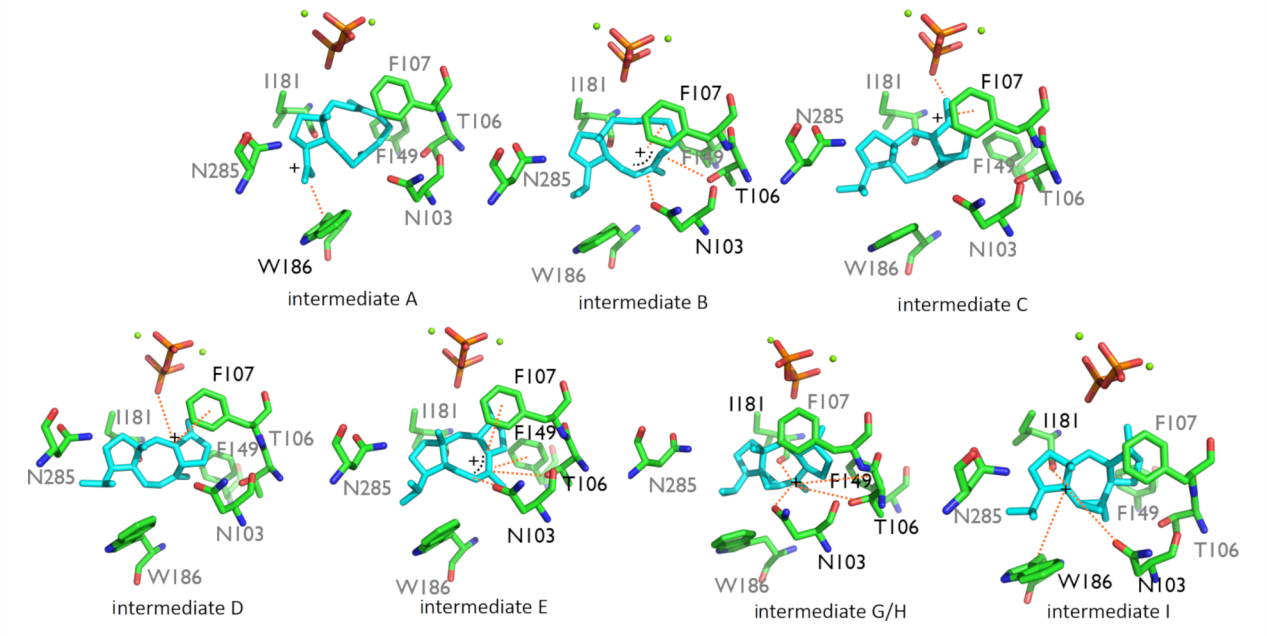

Figure 2: Intermediates **A–I** in the active site model. Interactions are marked by dashed orange lines, the interacting residues are labeled in black, the non-interacting residues are labeled in grey, and plus signs note location of the cations.

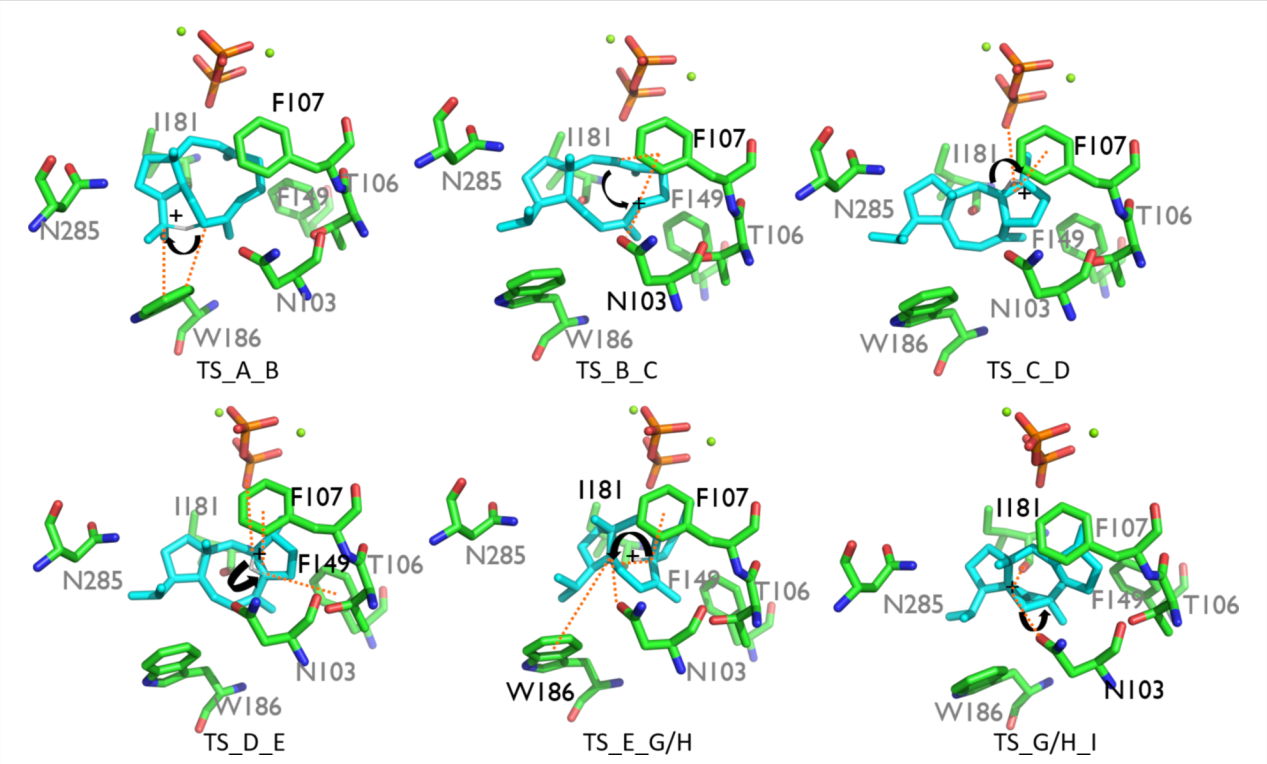

Figure 3: TS structures TS_**A**_**B**–TS_**G**/**H**_**I** in the active site model. Interactions are marked by dashed orange lines, the interacting residues are labeled in black, the non-interacting residues are labeled in grey, and the plus signs note the location of the cations.

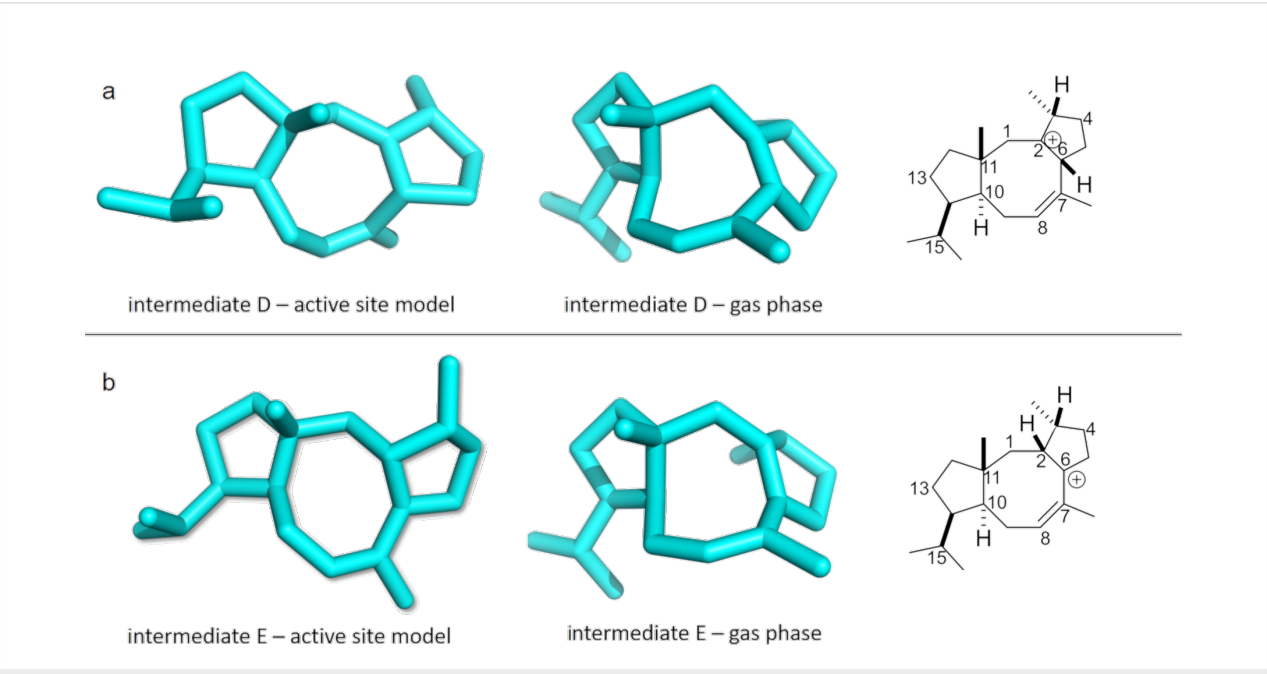

Figure 4: Comparison between gas phase and active site model conformations. A) Intermediate **D**. B) Intermediate **E**.

very similar in the gas phase and in the enzyme. Carbocation **H** formed interactions with N103, W186, and especially with I181. The relative energy difference between **H** and **I** was also similar in the gas phase and in the enzyme model. However, the activation energy was higher by 3.0 kcal/mol in the active site model, possibly due to steric effects. **I** was stabilized via inter-

actions with N103, I181, and W186, which likely made similar stabilizing contributions as in cation **H**.

It is well established that the inherent reactivity of carbocations [27], as well as correct substrate folding in the active site [3], play crucial roles in terpene synthases. The current results highlight the importance of taking into account the active site residues while modeling terpene synthase mechanisms, as we have proposed previously [28-36,42]. We found that the energy surface in the active site model was significantly perturbed compared to the gas phase potential. Additionally, structural analysis revealed that each cation was stabilized by noncovalent interactions, such as π–cation and dipole–cation interactions. A comparison of the transition state structures in the gas phase vs the active site model is shown in Table 2. These findings suggest that the rational biosynthesis of novel terpenes might be possible by careful design of CotB2 mutants. Future studies using multiscale techniques to model the enzyme reaction in a complete enzyme environment will allow careful evaluation of the usefulness of such active site theozyme models.

Conclusion

In this work, we compared the energy profiles of the terpene cyclase CotB2 reaction obtained in the gas phase and using an active site model. The calculations used identical QM methods, facilitating a direct comparison. We presented evidence for the important role played by the active site residues in CotB2 on the reaction energetics in an active site cluster model, suggesting that reaction control in terpene synthase is obtained via a combination of inherent reactivity, initial substrate folding, and enzyme environmental effects. Specifically, the results using the active site model revealed the significant effect that the active site residues have on the relative electronic energy of the intermediates and TS structures in comparison with gas phase data due to ionic, π–cation, and dipole–cation interactions. A detailed understanding of the role of the enzyme environment on the reaction cascade in CotB2 can provide important information to derive a synthetic strategy for cyclooctatin and related terpene manufacturing. Future studies using hybrid quantum mechanics and molecular mechanics techniques to model the enzyme reaction in a complete enzyme environment will allow careful evaluation of the usefulness of such active site theozyme models.

Experimental

All calculations were carried out with Gaussian 16 [47]. Geometry optimizations, frequency calculations, and intrinsic coordinate calculations were performed using the M062X/6-31+G(d,p) level of theory [48]. The gas phase structures were taken from Sato and co-workers [39]. The amino acid cage was constructed from six amino acids, which were located around the substrate and constituted part of the catalytic pocket of the enzyme (PDB-ID 6GGI) [42]. The chosen amino acids were the ones that we presumed stabilized the carbocations the most during the reaction. The coordinates of the amino acids and the substrate GGPP were taken from the corresponding X-ray structure, with a resolution of 1.8 Å [42]. In this approach, geometry optimizations with the "Modredundant" keyword were per-

Table 2: Comparison table of transition state structures in gas phase vs active site model.

TS structure	interaction species		gas phase distance (Å)	active site model distance (Å)
TS_**A_B**	C_{15}	H_{82}	1.21	1.29
	C_8	H_{82}	1.46	1.34
	C_8	C_{15}	2.58	2.52
TS_**B_C**	C_2	C_6	2.44	2.61
TS_**C_D**	C_2	H_2	1.21	1.44
	C_3	H_2	1.48	1.24
	C_3	C_2	1.41	1.41
TS_**D_E**	C_6	H_6	1.25	1.38
	C_2	H_6	1.41	1.28
	C_2	C_6	1.41	1.42
TS_**E_G/H**	C_6	H_6	1.12	1.14
	C_{10}	H_6	1.74	1.63
	C_{10}	C_6	2.63	2.49
	C_8	C_{10}	2.33	2.54
TS_**H_I**	C_9	C_7	1.71	1.66
	C_9	C_{10}	1.65	1.69
	C_{10}	C_7	2.48	2.46

formed, and the active site residues, diphosphate moiety, and magnesium ions were fixed throughout the reaction progress. The entire cage system was treated using the above-mentioned DFT method. In order to find the TS structures, complete TS optimizations using the keywords "QST2", "QST3", and “Modredundant” were performed.

A main limitation of the current cluster modeling approach was freezing of the active site residues, which did not allow any accommodation of the active site to the evolving reaction intermediates. Flexible residues were not considered due to the possible perturbation of the active site contour and the rapid fluctuation of the total electronic energy as a function of amino acid residue geometry. An additional obvious limitation were medium and long-range nonbonded interactions beyond the active site cage considered here. These effects could be considerable and will be scrutinized in future work.

The Cartesian coordinates of all species are reported in Supporting Information File 1.

Supporting Information

Supporting Information File 1

Cartesian coordinates for all species.
[https://www.beilstein-journals.org/bjoc/content/supplementary/1860-5397-16-7-S1.txt]

Funding

This work was supported by the Israeli Science Foundation (Grant no. 1683/18).

ORCID® iDs

Ronja Driller - https://orcid.org/0000-0001-8834-9087
Thomas Brück - https://orcid.org/0000-0002-2113-6957
Bernhard Loll - https://orcid.org/0000-0001-7928-4488
Dan T. Major - https://orcid.org/0000-0002-9231-0676

Preprint

A non-peer-reviewed version of this article has been previously published as a preprint doi:10.3762/bxiv.2019.108.v1

References

1. Knowles, J. R. *Nature* **1991,** *350,* 121–124. doi:10.1038/350121a0
2. Warshel, A. *Proc. Natl. Acad. Sci. U. S. A.* **1978,** *75,* 5250–5254. doi:10.1073/pnas.75.11.5250
3. Christianson, D. W. *Chem. Rev.* **2017,** *117,* 11570–11648. doi:10.1021/acs.chemrev.7b00287
4. Devappa, R. K.; Makkar, H. P. S.; Becker, K. *J. Am. Oil Chem. Soc.* **2011,** *88,* 301–322. doi:10.1007/s11746-010-1720-9
5. Singh, B.; Sharma, R. A. *3 Biotech* **2015,** *5,* 129–151. doi:10.1007/s13205-014-0220-2
6. Schwab, W.; Davidovich-Rikanati, R.; Lewinsohn, E. *Plant J.* **2008,** *54,* 712–732. doi:10.1111/j.1365-313x.2008.03446.x
7. Dewick, P. M. *Medicinal Natural Products: A Biosynthetic Approach,* 2nd ed.; John Wiley & Sons: Hoboken, NJ, 2001. doi:10.1002/0470846275
8. Radhakrishna, S.; Kumari, P. S. *Adv. Appl. Sci. Res.* **2018,** *5* (3), 94–101.
9. Rates, S. M. K. *Toxicon* **2001,** *39,* 603–613. doi:10.1016/s0041-0101(00)00154-9
10. Gershenzon, J.; Dudareva, N. *Nat. Chem. Biol.* **2007,** *3,* 408–414. doi:10.1038/nchembio.2007.5
11. Gonzalez-Burgos, E.; Gomez-Serranillos, M. P. *Curr. Med. Chem.* **2012,** *19,* 5319–5341. doi:10.2174/092986712803833335
12. Croteau, R.; Hezari, M.; Hefner, J.; Koepp, A.; Lewis, N. G. Paclitaxel Biosynthesis - The Early Steps. In *Taxane Anticancer Agents - Basic Science and Current Status;* Georg, G. I.; Chen, T. T.; Ojima, I.; Vyas, D. M., Eds.; ACS Symposium Series, Vol. 583; American Chemical Society: Washington, DC, 1994; pp 72–80. doi:10.1021/bk-1995-0583.ch005
13. Cane, D. E. *Chem. Rev.* **1990,** *90,* 1089–1103. doi:10.1021/cr00105a002
14. Christianson, D. W. *Chem. Rev.* **2006,** *106,* 3412–3442. doi:10.1021/cr050286w
15. Tholl, D. *Curr. Opin. Plant Biol.* **2006,** *9,* 297–304. doi:10.1016/j.pbi.2006.03.014
16. Zwenger, S.; Basu, C. *Biotechnol. Mol. Biol. Rev.* **2008,** *3,* 1–7.
17. Janke, R.; Görner, C.; Hirte, M.; Brück, T.; Loll, B. *Acta Crystallogr., Sect. D: Biol. Crystallogr.* **2014,** *70,* 1528–1537. doi:10.1107/s1399004714005513
18. Whittington, D. A.; Wise, M. L.; Urbansky, M.; Coates, R. M.; Croteau, R. B.; Christianson, D. W. *Proc. Natl. Acad. Sci. U. S. A.* **2002,** *99,* 15375–15380. doi:10.1073/pnas.232591099
19. Lesburg, C. A.; Zhai, G.; Cane, D. E.; Christianson, D. W. *Science* **1997,** *277,* 1820–1824. doi:10.1126/science.277.5333.1820
20. Starks, C. M.; Back, K.; Chappell, J.; Noel, J. P. *Science* **1997,** *277,* 1815–1820. doi:10.1126/science.277.5333.1815
21. Wendt, K. U.; Poralla, K.; Schulz, G. E. *Science* **1997,** *277,* 1811–1815. doi:10.1126/science.277.5333.1811
22. Köksal, M.; Jin, Y.; Coates, R. M.; Croteau, R.; Christianson, D. W. *Nature* **2011,** *469,* 116–120. doi:10.1038/nature09628
23. Croteau, R. *Chem. Rev.* **1987,** *87,* 929–954. doi:10.1021/cr00081a004
24. Brück, T.; Kourist, R.; Loll, B. *ChemCatChem* **2014,** *6,* 1142–1165. doi:10.1002/cctc.201300733
25. Tantillo, D. J. *Nat. Prod. Rep.* **2011,** *28,* 1035–1053. doi:10.1039/c1np00006c
26. Hess, B. A., Jr.; Smentek, L.; Noel, J. P.; O’Maille, P. E. *J. Am. Chem. Soc.* **2011,** *133,* 12632–12641. doi:10.1021/ja203342p
27. Tantillo, D. J. *Angew. Chem., Int. Ed.* **2017,** *56,* 10040–10045. doi:10.1002/anie.201702363
28. Dixit, M.; Weitman, M.; Gao, J.; Major, D. T. *ACS Catal.* **2017,** *7,* 812–818. doi:10.1021/acscatal.6b02584
29. Weitman, M.; Major, D. T. *J. Am. Chem. Soc.* **2010,** *132,* 6349–6360. doi:10.1021/ja910134x
30. Major, D. T.; Weitman, M. *J. Am. Chem. Soc.* **2012,** *134,* 19454–19462. doi:10.1021/ja308295p
31. Gao, J.; Ma, S.; Major, D. T.; Nam, K.; Pu, J.; Truhlar, D. G. *Chem. Rev.* **2006,** *106,* 3188–3209. doi:10.1021/cr050293k

32. Major, D. T.; Freud, Y.; Weitman, M. *Curr. Opin. Chem. Biol.* **2014,** *21,* 25–33. doi:10.1016/j.cbpa.2014.03.010
33. Ansbacher, T.; Freud, Y.; Major, D. T. *Biochemistry* **2018,** *57,* 3773–3779. doi:10.1021/acs.biochem.8b00452
34. Dixit, M.; Weitman, M.; Gao, J.; Major, D. T. *ACS Catal.* **2017,** *7,* 812–818. doi:10.1021/acscatal.6b02584
35. Freud, Y.; Ansbacher, T.; Major, D. T. *ACS Catal.* **2017,** *7,* 7653–7657. doi:10.1021/acscatal.7b02824
36. Major, D. T. *ACS Catal.* **2017,** *7,* 5461–5465. doi:10.1021/acscatal.7b01328
37. Newman, D. J.; Cragg, G. M. *J. Nat. Prod.* **2016,** *79,* 629–661. doi:10.1021/acs.jnatprod.5b01055
38. Hong, Y. J.; Tantillo, D. J. *Org. Biomol. Chem.* **2015,** *13,* 10273–10278. doi:10.1039/c5ob01785h
39. Sato, H.; Teramoto, K.; Masumoto, Y.; Tezuka, N.; Sakai, K.; Ueda, S.; Totsuka, Y.; Shinada, T.; Nishiyama, M.; Wang, C.; Kuzuyama, T.; Uchiyama, M. *Sci. Rep.* **2015,** *5,* No. 18471. doi:10.1038/srep18471
40. Kim, S.-Y.; Zhao, P.; Igarashi, M.; Sawa, R.; Tomita, T.; Nishiyama, M.; Kuzuyama, T. *Chem. Biol.* **2009,** *16,* 736–743. doi:10.1016/j.chembiol.2009.06.007
41. Meguro, A.; Motoyoshi, Y.; Teramoto, K.; Ueda, S.; Totsuka, Y.; Ando, Y.; Tomita, T.; Kim, S.-Y.; Kimura, T.; Igarashi, M.; Sawa, R.; Shinada, T.; Nishiyama, M.; Kuzuyama, T. *Angew. Chem., Int. Ed.* **2015,** *54,* 4353–4356. doi:10.1002/anie.201411923
42. Driller, R.; Janke, S.; Fuchs, M.; Warner, E.; Mhashal, A. R.; Major, D. T.; Christmann, M.; Brück, T.; Loll, B. *Nat. Commun.* **2018,** *9,* No. 3971. doi:10.1038/s41467-018-06325-8
43. Tantillo, D. J.; Jiangang, C.; Houk, K. N. *Curr. Opin. Chem. Biol.* **1998,** *2,* 743–750. doi:10.1016/s1367-5931(98)80112-9
44. Siegbahn, P. E. M.; Himo, F. *Wiley Interdiscip. Rev.: Comput. Mol. Sci.* **2011,** *1,* 323–336. doi:10.1002/wcms.13
45. Grimme, S.; Steinmetz, M. *Phys. Chem. Chem. Phys.* **2013,** *15,* 16031–16042. doi:10.1039/c3cp52293h
46. Mati, I. K.; Cockroft, S. L. *Chem. Soc. Rev.* **2010,** *39,* 4195–4205. doi:10.1039/b822665m
47. *Gaussian 16,* Revision A. 03; Gaussian, Inc.: Wallingford, CT, 2016.
48. Zhao, Y.; Truhlar, D. G. *Theor. Chem. Acc.* **2008,** *120,* 215–241. doi:10.1007/s00214-007-0310-x

License and Terms